



HAL
open science

Synthesis of novel π -conjugated functional organic semiconductors for optoelectronic applications

Shiwei Ren

► **To cite this version:**

Shiwei Ren. Synthesis of novel π -conjugated functional organic semiconductors for optoelectronic applications. Organic chemistry. Institut Polytechnique de Paris, 2021. English. NNT : 2021IP-PAX044 . tel-03934578

HAL Id: tel-03934578

<https://theses.hal.science/tel-03934578>

Submitted on 11 Jan 2023

HAL is a multi-disciplinary open access archive for the deposit and dissemination of scientific research documents, whether they are published or not. The documents may come from teaching and research institutions in France or abroad, or from public or private research centers.

L'archive ouverte pluridisciplinaire **HAL**, est destinée au dépôt et à la diffusion de documents scientifiques de niveau recherche, publiés ou non, émanant des établissements d'enseignement et de recherche français ou étrangers, des laboratoires publics ou privés.

Synthesis of novel π -conjugated functional organic semiconductors for optoelectronic applications

Thèse de doctorat de l'Institut Polytechnique de Paris
préparée à l'École Polytechnique

École doctorale n°626 Ecole Doctorale de l'Institut Polytechnique de
Paris (ED IP Paris)
Spécialité de doctorat: Chimie

Thèse présentée et soutenue à Palaiseau, le 10 Octobre 2021, par

M. Shiwei Ren

Composition du Jury :

Gilles Clavier	
Directeur de Recherche, ENS-Paris Saclay (UMR 8531- PPSM)	Président
Antonio Papagni	
Professeur des universités, Université de Milan-Bicocca (CHIM/ 06)	Rapporteur
Patrice Rannou	
Directeur de Recherche, Université Grenoble Alpes (UMR 5279- LEPMI)	Examineur
Thanh-Tuân BUI	
Maître de conférences, Université CY Cergy Paris (EA 2528- LPPI)	Examineur
Abderrahim Yaassar	
Directeur de Recherche, Ecole Polytechnique (UMR 7647- LPICM)	Directeur de thèse

Avant-Propos

Les performances des dispositifs organiques sont fortement corrélées aux structures moléculaires de la couche active du dispositif. Grâce à des modifications chimiques appropriées de la molécule, il est possible d'altérer les énergies des orbitales frontières et d'autres paramètres par ingénierie moléculaire, afin de leur conférer de nouvelles fonctionnalités ou améliorer leurs performances dans des dispositifs organiques. Le travail décrit dans ce manuscrit porte sur le développement et la synthèse de nouveaux semi-conducteurs organiques de type n (accepteurs d'électrons). Leurs propriétés optoélectroniques ont été évaluées en vue de leurs applications dans des dispositifs électroniques.

Le premier chapitre fait un état de l'art récent sur la synthèse des semi-conducteurs organiques de type N. Le second chapitre décrit la synthèse et l'étude physico-chimique de quelques dérivés 7,7' isoindigo. L'isoindigo (IID) est une molécule symétrique formée par deux cycles lactames reliés par une double liaison. Il est largement utilisé comme accepteur pour la synthèse de nouveaux systèmes donneur-accepteur, petites molécules ou copolymères. Au cours de ces dernières années, des efforts considérables ont été consacrés à la synthèse de nouveaux composés à base d'IID par ingénierie des chaînes latérales, la fusion d'hétéroatomes ou l'extension de la longueur de conjugaison. Cependant, la plupart de ces travaux ont porté uniquement les modifications chimiques en positions 6,6', et à ce jour, il n'existe aucun travail publié dans la littérature sur la modification en position 7,7'. Ainsi, ce chapitre vise à développer de nouveaux matériaux π -conjugués à base d'iosindigo à conjugaison croisée, par une étude de relation structurepropriété-morphologie. La conjugaison croisée est définie comme étant la conjugaison entre deux segments π insaturés qui, bien que non conjugués l'un à l'autre, sont conjugués à un segment insaturé intermédiaire. Les systèmes conjugués croisés sont avantageux pour la conception de nouveaux semi-conducteurs organiques, car cet arrangement conduit à une ségrégation spatiale des orbitales moléculaires frontières. L'oxindole est un élément clé et constitutif du cœur isoindigo. En effet, l'IID est formé de deux cycles benzénique fusionné avec un cycle de pyrrolone, relié par une double liaison centrale, en confirmation trans. Le troisième chapitre de ce manuscrit explore l'utilisation potentielle de l'oxindole comme unité de construction de nouvelles architectures moléculaires donneur-accepteur. Ainsi, la littérature récente recense quelques exemples décrivant l'utilisation de ce synthon pour la construction de nouveaux matériaux D-A performants, mais aucune étude systématique n'a été réalisée sur l'effet de la longueur de conjugaison du pont π -conjugué ni sur le mode de connectivité sur les propriétés photo-physiques et électrochimiques. Dans ce contexte, nous avons synthétisé un ensemble de petites molécules avec une architecture A-D-A (A : accepteur ; D : donneur) relié par un pont π -conjugué, avec différentes longueurs de conjugaison, et ayant deux segments isatylidène malononitrile comme groupes accepteurs terminaux. Notre objectif était de faire varier la longueur de conjugaison et de moduler la position de liaison du groupe isatylidène malononitrile (position 4 vs. position 6), afin d'analyser ces effets sur les propriétés structurales, photophysiques et électrochimiques. Le chapitre 4 présente une étude détaillée sur l'effet d'étendre la longueur de conjugaison π du noyau d'isoindigo, plutôt que sa modification. Cette recherche est motivée par le regain d'intérêt pour la chimie de l'indophénine. L'un des problèmes liés à la réaction de l'indophénine est la formation d'isomères. La réaction produit un mélange de tous les isomères géométriques possibles. C'est donc un défi de favoriser la formation d'une seule forme régioisomère en utilisant la réaction de l'indophénine. À cette fin, nous avons remplacé la double liaison centrale par des molécules quinoïdes, basées sur des unités EDOT. Ces ponts π -conjugués sont particulièrement adaptés, puisqu'ils fournissent un pont π espaceur, ainsi qu'une bonne capacité à agir comme des unités de verrouillage conformationnel pour favoriser la formation d'un seul

isomère. En particulier, dans ce chapitre, nous avons décrit les voies de synthèse organique, les mécanismes réactionnels, la caractérisation physique, UV-visible, et électrochimique, ainsi que les relations structure-propriété au sein de ces molécules. A l'aide de la RMN ^1H , ^1H - ^1H COSY et ^1H - ^1H NOESY, nous avons montré la formation d'un seul isomère dans ces molécules. Le dernier chapitre présente la fabrication d'une bio-interface pour la détection de bactérie, basée sur des mesures d'impédance électrochimiques. En fait, la bioélectronique est un domaine émergent à l'interface des sciences physiques et de la vie, qui cherche à connecter des éléments biologiques aux dispositifs électroniques. À l'heure actuelle, le plus grand défi auquel est confronté ce domaine, qui est en pleine expansion est la réalisation d'une interface bioélectronique souple permettant la transduction d'un signal provenant d'un élément biologique en signal électrique. Les polymères semi-conducteurs à conduction mixtes ion/électron sont récemment apparus comme des matériaux prometteurs pour la transduction des signaux à l'interface entre les éléments biologiques et les dispositifs électroniques.

Acknowledgements

First of all, I would like to express my deepest thankfulness to my supervisor, Dr. Abderrahim Yassar. It was he who gave me the opportunity to enter the prestigious Ecole Polytechnique in Paris. In fact, I started to know Dr. Yassar from my master's course and I was gradually impressed by his attitude towards teaching and education. He has strong academic skills and a passion for scientific research. I joined LPICM from my Masters internship and continued my PhD research under his supervision. I remember the first day I went to his office, he taught me the basic principles of organic semiconductor chemistry and outlining with great knowledge the research projects for the next three years. He not only gave me many helps in my research and daily life but also taught me the philosophy of life. I really appreciate everything that he did for me and it is a great honor to work as his Ph.D student. I would like to thank all the members of jury committee, Dr. Gilles Clavier, Dr. Antonio Papagni, Dr. Patrice Rannou, Dr. Thanh-Tuân BUI for their precious time to evaluate this manuscript and listen to my defense. The most important thing is that they gave me a lot of advice and recommendations for scientific research. I also wish to thank Dr. Yvan Bonnassieux, the director of LPICM, for his leadership and encouragement. The LPICM laboratory is a place with the capabilities and platform to meet all my research needs. Thanks to all members of the LPICM for their warm welcome, their amiability and their willingness to help. I would like to thank Dr. Sophie Bourcier, Dr. Louis-Joseph Alain and Dr. Cyril Colas, for helping me with mass spectroscopy and NMR analyses. Some of my material characterisation measurements were carried out by them and the results have been of great help to facilitate my PhD work. Last but not least I would like to thank the best office mates: Tinghui Zhang, Guili Zhao, for supporting me and always giving me the chance to discuss about the work. Without funding, I wouldn't have the opportunity to pursuit my dreams. I gratefully acknowledge funding from the CSC (China Scholarship Council). Lastly, I want to express my love and gratitude to my family and relatives, my parents for their support. It is with your encouragement and support that I can go through all the difficulties.

Much appreciated!

Contents

Acknowledgements	3
Abbreviations and symbols	6
Chapter 1 General Introduction	8
1.1 Introduction	8
1.2 Imide-based n-type organic semiconductor materials	11
1.3 Functional materials based on isoindigo building block	13
1.4 Purpose of this study	23
Chapter 2 Design and synthesis of 7,7'-isoindigo as a new n-type organic semiconductor..	30
2.1 Introduction	30
2.2 Results and discussion.....	38
2.2.1 Synthetic methodology.....	38
2.2.2 Crystal structure & Molecular packing 7,7'-IID based materials	40
2.2.3 UV-visible spectroscopic characterizations.....	41
2.2.4 Electrochemical studies	43
2.3 Conclusion and perspective	44
Experimental procedures and characterizations data.....	45
Chapter 3 Joint experimental and theoretical study of the optical and electrochemical properties of bis-2-(2-oxindolin-3-ylidene) malononitrile derivatives	54
3.1 Introduction	54
3.2 Results and discussion.....	57
3.2.1 Synthetic methodology.....	57
3.2.2 UV-visible spectroscopic characterizations.....	62
3.2.3 Electrochemical studies	66
3.2.4 TD-DFT studies of bis-isatin and malononitrile derivatives	68
3.3 Conclusion and perspective	74
Experimental procedures and characterization data	76

Chapter 4 Isatin as terminal group for quinoidal structures	87
4.1 Introduction	87
4.2 Results and discussion.....	90
4.2.1 Synthetic methodology.....	90
4.2.2 UV-visible spectroscopic characterizations.....	106
4.2.3 Electrochemical studies.....	108
4.3 Conclusion.....	110
Experimental precudures and characterization data	111
Chapter 5 Exploration of the utility of block conjugated copolymers as a bio-interface for sensing	127
5.1 Introduction	127
5.2 Results and discussion.....	130
5.2.1 Synthetic methodology.....	130
5.2.2 Gel permeation chromatography characterization.....	134
5.2.3 Self-assembly of P3HT- <i>b</i> -P3TEGT	134
5.2.4 UV-visible spectroscopic characterizations.....	137
5.2.5 Fabrication of biosensing surface, bacteria attachment and impedance sensing.....	138
5.3 Conclusion and perspective.....	140
Experimental procedures and characterization data	142
¹H and ¹³C NMR Spectra and Data.....	148

Abbreviations and symbols

AcOH	acetic acid
Ar	aryl
Bt	benzo thiadiazole
BPO	benzoyl peroxide
cat.	catalytic quantity
cfu	colony-forming units
DCM	dichloromethane
DMF	N, N-dimethylformamide
DMSO	dimethyl sulfoxide
dppf	bis (diphenylphosphino) ferrocene
EA	ethyl acetate
EDOT	3,4-Ethylenedioxythiophene
EtOH	ethanol
Hex	hexyl
HOMO	highest occupied molecular orbital
iPr	isopropyl
IR	infrared
LUMO	lowest unoccupied molecular orbital
Me	methyl
MeOH	methanol
MN	malononitrile
NBS	N-bromosuccinimide
<i>n</i>-BuLi	<i>n</i>-Butyllithium
NMR	nuclear magnetic resonance
PE	petroleum ether
Ph	phenyl
P3HT	poly(3-hexylthiophène)

<i>p</i>TsOH	<i>p</i>-toluenesulfonic acid
TCM	chloroform
Th	thienyl
THF	tetrahydrofuran
°C	degree Celsius
eq.	equivalent
Hz	hertz
h	hour
M	mole per liter
Min	minute
NMR	nuclear magnetic resonance
ppm	parts per million
TLC	thin layer chromatography

General introduction

1) Introduction

1.1) N-type organic semiconductors application.

Organic electronic devices have gained immense popularity in the last 30 years because they are promising in terms of their tunable electronic properties, flexibility, cost, versatile functionalization, and processability. The key components of these devices are the organic semiconductor material, which acts as an active system and determines the device performance. One of the driving forces behind the development of the field in the last decade has been the synthesis of new high-performance building blocks and the expansion of the library of organic materials suitable for various optoelectronic applications. While most of efforts have been dedicated to the development of p-type organic semiconducting materials, electron-transporting (n-type organic semiconductor materials) have been less investigated. The main reason would be the lack of π -conjugated building units with strong electron-deficiency that ensure sufficiently deep lowest unoccupied molecular orbital (LUMO) energy levels for electron transport, chemical stability issues and the large electron barrier injection. Although there are many electrons deficient building units that function well for n-type semiconducting polymers, however, the research for new electron-acceptor groups is still less developed than the study of electron-donor groups. Requirements for n-type building blocks suited for construction semiconducting materials are: electron deficiency, i.e., low-lying energy level of lowest LUMO, selective-reaction site(s) affording handle(s) for incorporation into π -conjugated system, and compatibility with various chemical reactions.¹ The search of high-performance ambient-stable n-type OSCs is motivated by the development of large-area and low-cost organic electronic devices such as integrated circuits, non-fullerene organic solar cells, thermoelectric devices, etc. **Figure 1.**

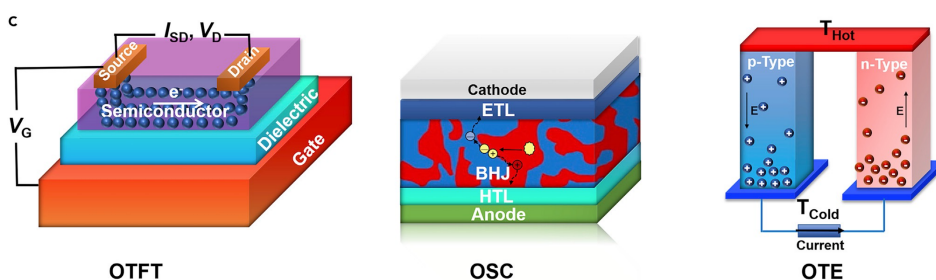
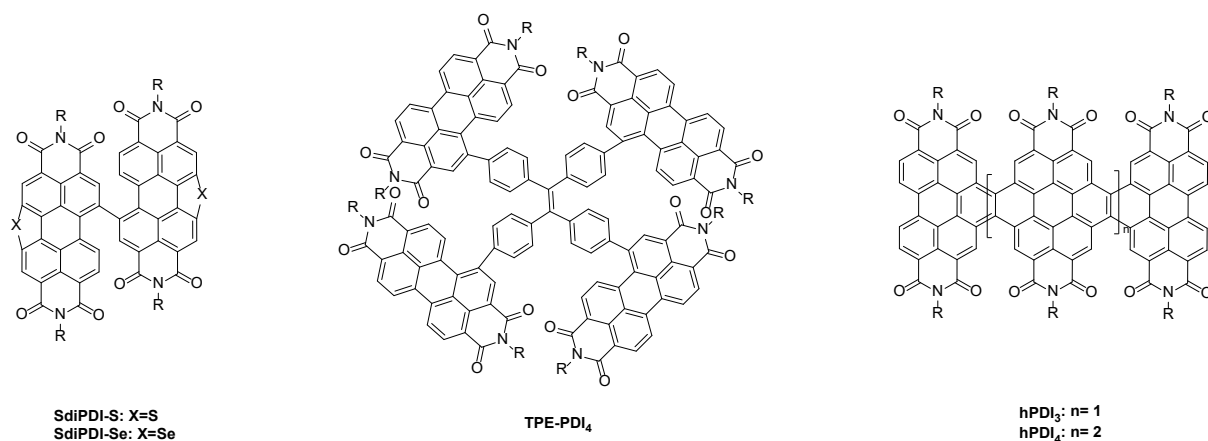


Figure 1. Example of optoelectronic device structures including a bottom-gate top-contact OFET a bulk heterojunction organic solar cell, and an organic thermoelectric device.

Regarding OFET application, in recent years, considerable progress has been made in design of n-type OSCs, and there are many review articles that summarize the recent trend in the field of n-type

OSCs for OTFT from a viewpoint of molecular design. A huge number of n-type OSCs, small molecules and polymers, have been reported and some of which exhibited high electron mobility up to $0.5\text{-}1.0\text{ cm}^2\text{V}^{-1}\text{s}^{-1}$. Chemical modification methods have been shown to be an effective strategy for the synthesis of high-performance ambient-stable n-type OSCs for OFETs, where energetic and kinetic factors were considered for the fabrication of ambient-stable electron injection and transport.²

Besides OFET applications, n-type organic semiconductors have attracted substantial interest as alternative acceptors in organic solar cells, non-fullerene solar cells.³ It should be noted that until 2015, most OSCs were based on fullerene-based receptors (PC₆₁BM, PC₇₁BM, ICBA, etc.) with some limitations, such as, narrow and weak absorption, and difficult to tune properties.⁴ A key consideration in the design of high-performance OSCs for solar cell applications is enhancing the crystallinity and thus the charge-transport ability of the acceptor material. Nevertheless, the development of highly mobile semiconductors for solution-processed solar cells is a challenging task since both p- and n- type semiconductors must form a bicontinuous and interpenetrating network with reasonably small domain sizes (~20 nm). This morphological characteristic is essential for the manufacture of efficient solar cell devices. Till now, two promising classes of non-fullerene acceptors have been developed: rylene diimide-based materials and materials based on fused aromatic cores with strong electron-accepting end groups, **Figure 2**. Recent developments have led to a power conversion efficiency up to 13%, demonstrating the potential use of non-fullerene acceptors to replace fullerene derivatives in next-generation of high-performance organic solar cells.



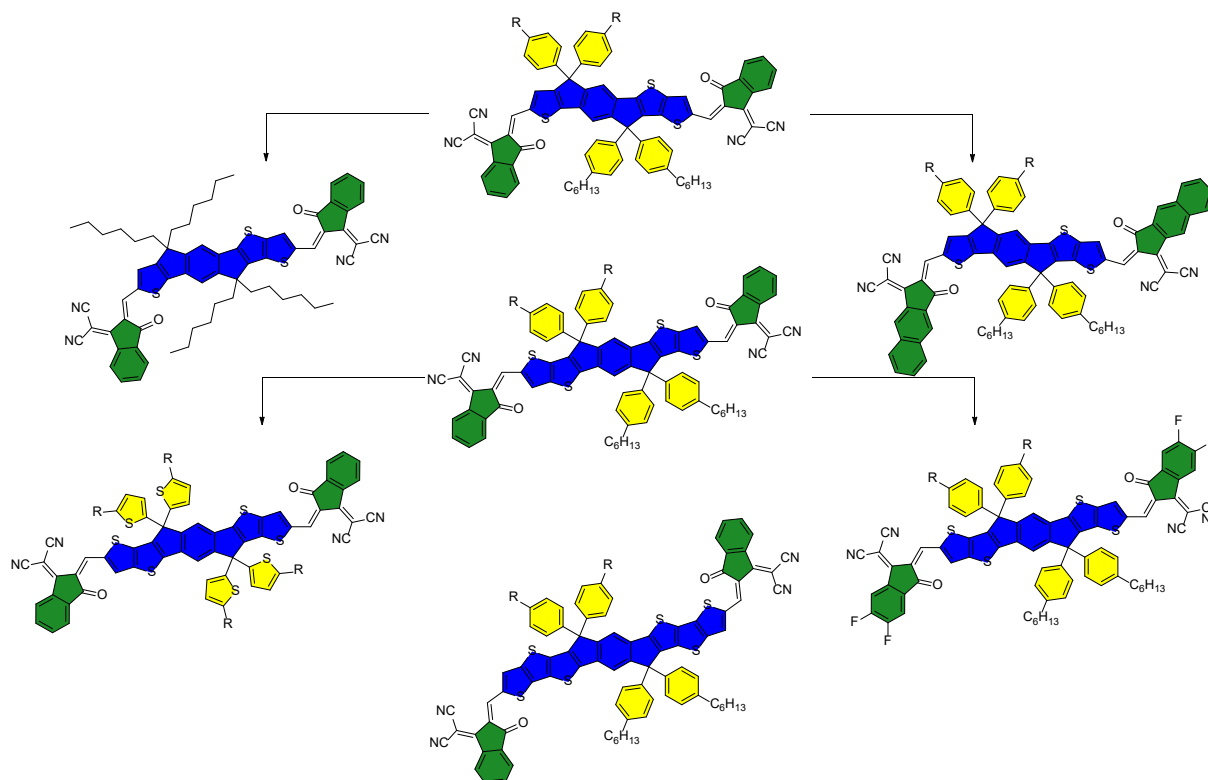


Figure 2. Top: chemical structure of PDI-based acceptor with different geometry: a ‘twisting’ strategy, including: ‘twisted dimer’ and ‘four-ring propeller’ and ‘fused-ring structure’. Bottom: representative chemical structures of linear indacenodithiophene-based acceptors. Taken from reference.³

Thermoelectric (TE) effect is the direct conversion of temperature differences to electric voltages and vice versa. Research attention is focused on novel TE-materials due to: (i) increasing in energy requirement and (ii) pollutions linked to human activities. It should be pointed out that about two-thirds of all industrial energy consumption is lost as waste heat.⁵ Consequently, it becomes urgent to promote the recovery of this huge waste heat into electrical energy. However, the efficiency of the used materials is rather low. TE performance is typically indicated by the TE figure of merit, $ZT = S^2\sigma T/k$, where σ , S , T and k are the electrical conductivity, Seebeck coefficient, absolute temperature, and thermal conductivity, respectively.⁶ An ideal TE material is expected to have a high Seebeck coefficient to improve energy conversion, a high electrical conductivity to reduce joule heating, and a low thermal conductivity to maintain a temperature gradient. One of the challenges facing in TE is the strong interdependence between the three thermoelectric properties σ , S and κ , with optimization of any one property having a detrimental effect on at least one of the others. Organic-TE materials, both conjugated polymers and small molecules, are gaining huge interest as materials in future energy conversion, because they are light weight, flexible, printable, and suitable for large area applications like wearable technologies. Both p-type and n-type organic TE materials are required for practical applications. As shown in **Figure 3** below, PEDOT: PSS is a benchmark p-type conducting polymer for TE applications, with a promising power factor of $47 \mu\text{W}/(\text{m K}^2)$, a higher electrical conductivity of

900 S/cm, and a Seebeck coefficient of 20 $\mu\text{V}/\text{K}$. In contrast, very few n-type polymer TE materials exhibited moderate TE properties with a σ of 10 S cm^{-1} and power factors of 10 $\mu\text{W m}^{-1} \text{K}^{-2}$. The reason why n-type organic TE materials are less developed compared to their p-doped counterparts, lies of the lack of materials with deeper LUMO energy level for efficient electron injection and stable charge transport as well as an efficient n-type-doping process.

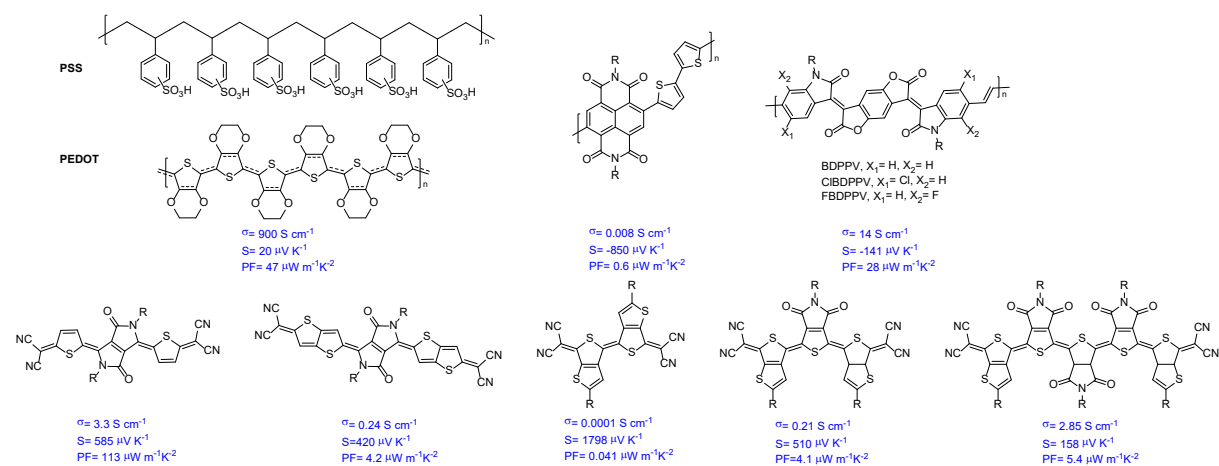


Figure 3: Chemical structures of the most performing p-, n-type and ambipolar organic semiconductors developed for TE application.

Within the lactam-based electron acceptors library, such as diketopyrrolopyrrole (DPP), perylene diimide (PDI), naphthalene diimide (NDI), and benzodipyrrolidone (BDP) are some of the most representative amide/imide-based acceptor units employed to date.

1.2) Imide-based n-type organic semiconductor materials.

Imide-functionalized electron-deficient units have been studied as one of the most promising candidates for synthesizing high-performance materials, because of its strong electron-withdrawing nature, which results in deep LUMO energy levels, thereby enabling stable electron transport. Among them rylene diimides such as perylene diimide (PDI) and naphthalene diimide (NDI) are widely used as electron acceptors in organic solar cells, and n-type organic semiconductors. This research has been reviewed recently.^{1,7} This family of molecules attracted attention because of their facile synthesis, good solubility, and deep-positioned LUMO levels. N,N'-dialkyl perylene diimide-dithiophene (P(PDI₂OD-T₂)) and N,N' dialkyl naphthalene diimide-dithiophene (P(NDI₂OD-T₂)) were among the first relevant n-channel polymers.⁸ They were obtained by Stille coupling of N, N'-dialkyl-1,7-dibromo-3,4,9,10-(PDI) or with a distannyl derivative of bithiophene. Initial electron mobility (μ_e) values in OFETs of this polymer ranged between 0.1 and 0.85 $\text{cm}^2\text{V}^{-1}\text{s}^{-1}$ depending on the film processing and device architecture. An intensive research effort by optimizing polymer molecular weight, N-alkyl chain engineering, semiconductor film processing, and device engineering, have been devoted to enhance the performance of NDI polymers in various optoelectronic devices.⁹ For instance, uniaxial orientation of

P(NDI₂OD-T₂) polymer-chain by natural brush and bar coating deposition technique enables fabrication of OFET devices with μ_e values as high as $2.3 \text{ cm}^2 \text{ V}^{-1} \text{ s}^{-1}$ and $6.4 \text{ cm}^2 \text{ V}^{-1} \text{ s}^{-1}$, respectively.^{10,11} To reduce steric hindrance, while maintaining strong electron withdrawing ability, electron-deficient building blocks, where the imide function is located between bithiophene, have been designed and synthesized. Bithiophene imide (BTI), **Figure 4**, where the imide group bridges bithiophene is a representative example of this family.¹⁰ A homopolymer of BTI has been reported to show relatively high electron mobilities of up to $0.038 \text{ cm}^2 \text{ V}^{-1} \text{ s}^{-1}$ in OFETs. Other imide-bridged units such as thiazolylthiophene imide (TTZI), bithiazole imide (BTZI) and fluorinated BTI (F-BTI), which have higher electron-deficiency than BTI, have been synthesized. Replacement of thiophenes at the end of the BTI molecular structure by thiazole units led to the construction of materials (TzBI) with higher electron-deficiency and thus providing deeper LUMO and highest occupied molecular orbital (HOMO) energy levels relative to BTI¹². Electronic structures of the resulting polymers were investigated by cyclic voltammetry and UV-vis absorption spectroscopy. While E_{LUMO} of PTzBIT and PTzBITT was similar (-3.51 eV), E_{HOMO} of PTzBIT (-6.26 eV) was deeper than that of PTzBITT (-6.14 eV). It is also noted that E_{LUMO} and E_{HOMO} of PTzBITT were deeper than those of PTBITT, a BTI-based polymer with the same thienothiophene co-unit, by 0.35 and 0.52 eV, respectively. This is most likely because only HOMO is located at the β -position of the thiophene rings in BTI and the nitrogen atoms of the thiazole rings in TzBI, and thus the electronic effect of the nitrogen atom is more pronounced on HOMO than LUMO in this system. The TzBI-based polymers showed n-type material behavior, as they provided electron mobilities up to $0.04 \text{ cm}^2 \text{ V}^{-1} \text{ s}^{-1}$ in OFET devices, indicating that TzBI is a promising building unit for construction n-type semiconducting polymers.

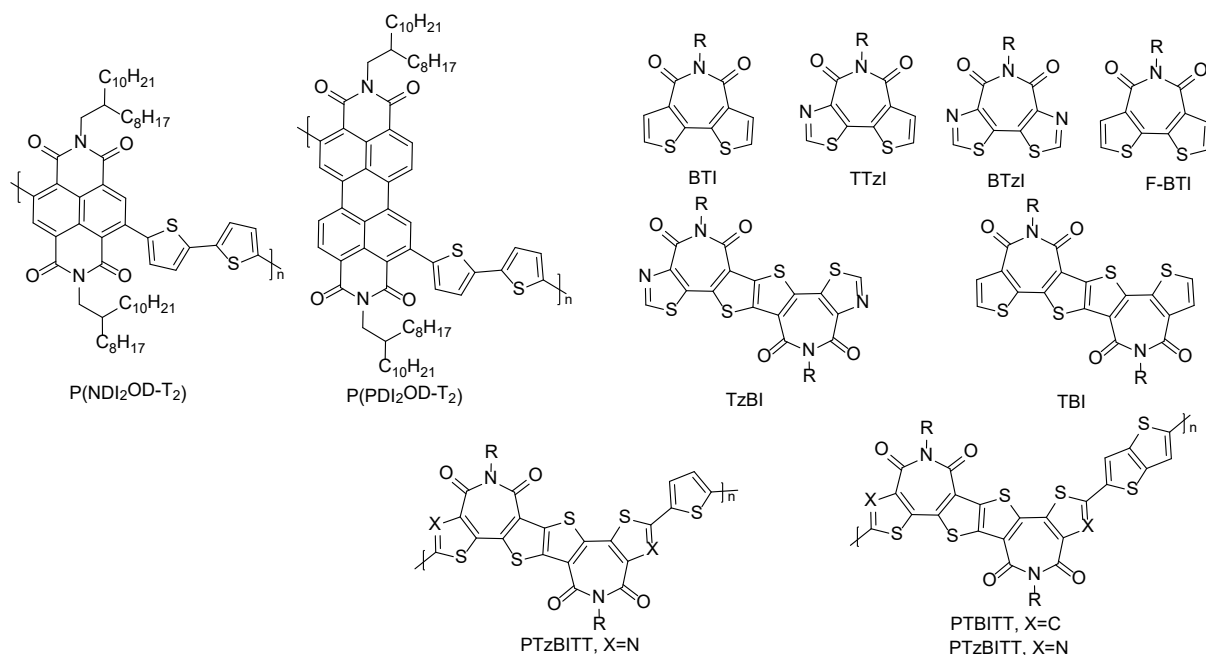


Figure 4. Chemical structures of some representative Imide-based n-type semiconducting copolymers.

1.3) Functional materials based on isoindigo building block

One of the most recently reported amide-based receptors for organic electrons is isoindigo (IID), an isomer of the widely known dye indigo. Isoindigo is one of the most used building blocks to construct organic semiconductors and donor-acceptor materials for both OPV and OFET applications. It has two lactam rings fused to a benzene ring, joined by an exocyclic double bond at the 3 and 3' positions; and exhibits strong electron-withdrawing ability. This electron deficiency gives isoindigo-based polymers intriguing properties, such as broad absorption and high open circuit voltage in OSCs, as well as high mobility and good ambient stability in FETs. These characteristics have encouraged several research groups to actively pursue the preparation of IID-based materials, and many recent and comprehensive reviews of IID-based materials have been presented.¹³⁻¹⁶ Pioneering works on the isoindigo-based materials have focused on combining this new acceptor unit with a suite of readily available donors.¹³ In most cases, changing the donor part of isoindigo-based materials does not affect the LUMO levels of resulting materials, because the LUMO levels are mostly localized on isoindigo cores. To fine tune both energy levels, researchers proposed chemical functionalization of isoindigo core. Several approaches have been reported to prepare derivatives of core substituted isoindigo. These include: halogenation of the core, heterocycle-substituted, peripherally-expanded, and core-expanded structures, **Figure 5**.

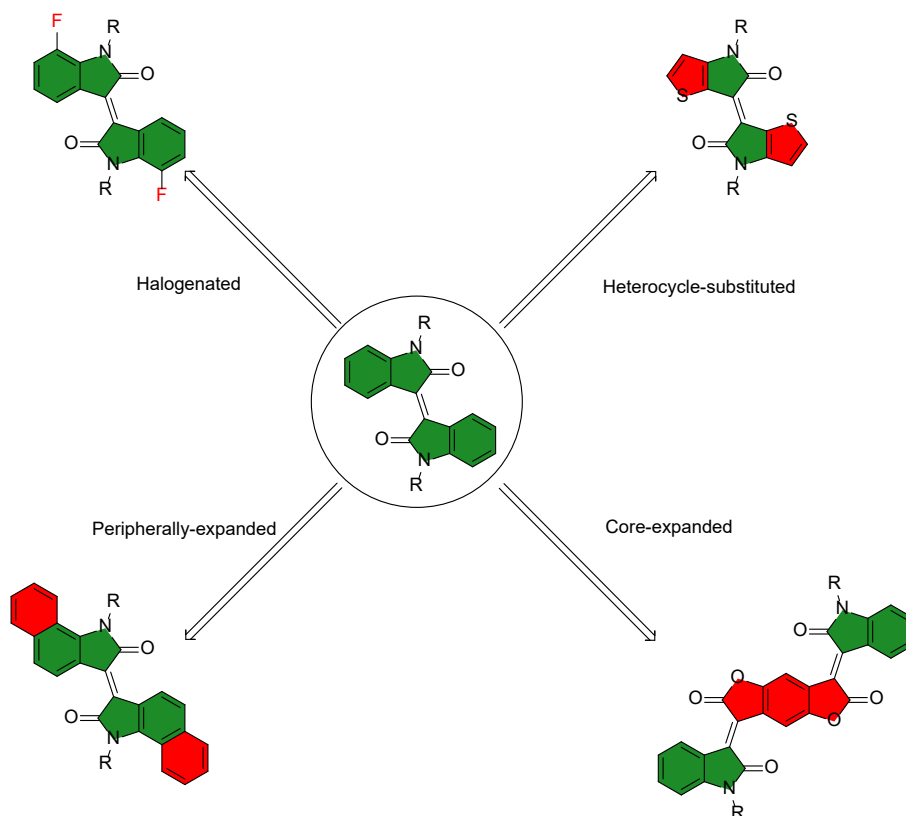


Figure 5. Schematic representation of chemical modification of IID-based materials. Adapted from ref.¹⁴

1.3.1) Core modification to realize n-type and ambipolar materials

Even though isoindigo is an electron-withdrawing unit, polymers based on this unit exhibited p-type behavior with very low electron mobilities, $3.7 \times 10^{-7} \text{ cm}^2 \text{ V}^{-1} \text{ s}^{-1}$. To enhance electron transport, and thus n-type or ambipolar behavior, one effective way is to lower LUMO energy levels of the materials. This can be achieved by introducing strong electron-withdrawing groups (EWGs), such as fluorine, chlorine, diimide moieties and cyano groups, which typically are small EWGs with weaker steric hindrance effect. EWG can effectively lower the LUMO energy level of the π -conjugated polymer. Due to its strong electronegativity, it can pull electrons out of the π -conjugated backbone. Fluorine substitution is one of the useful modifications in organic semiconductor synthesis because: (1) F substitution does not induce steric hindrance because F atom shows a small van der Waals radius of 1.35 Å, which is slightly larger than that of H ($r = 1.20 \text{ Å}$); (2) Fluorination lower both the HOMO and LUMO energy levels; (3) F atoms can induce intramolecular intermolecular F...H and F...S interactions, which may enhance the backbone coplanarity and promote better molecular crystallization.¹⁷

A molecular design strategy to achieve highly balanced ambipolar charge transport for donor-acceptor isoindigo-based copolymer through fluorination of isoindigo core was reported by Lei *et al.*¹⁸ To investigate the effect of fluorination of isoindigo units on electronic and structural properties, a fluorinated copolymer containing fluorine atoms on the isoindigo core was synthesized and compared with a non-fluorinated copolymer as a reference polymer (**Figure 6a**). The LUMO energy level of the fluoropolymer (II-i-1a, LUMO=3.88 eV) was significantly lower by 0.18 eV compared to its non-fluorinated analog (II-i-1b). Intramolecular F...H interactions led to a decreased dihedral angle between the isoindigo core and flanked thiophene; thus, affording copolymer with a more planar backbone. Fluorination effectively increases the electron mobility from 10^{-2} for II-i-1b to $0.43 \text{ cm}^2 \text{ V}^{-1} \text{ s}^{-1}$ for fluorinated II-i-1a while maintaining high hole mobility up to $1.85 \text{ cm}^2 \text{ V}^{-1} \text{ s}^{-1}$ for FET devices fabricated under ambient atmosphere. Thus, carrier transport was unbalanced because of the relatively low electron mobility. GIXRD results indicated that the fluorination promotes edge-on orientation with a stronger crystalline tendency. The same authors also reported the effect of the introduction of Cl atoms on the materials properties.¹⁹ The LUMO level of II-I-1c (3.86 eV) is lower than that of the non-chlorinated analogue and close to that of the fluorinated II-I-1a, suggesting that the chlorine atom has similar electronic effects to the fluorine atom. II-I-1c showed balanced hole and electron transport of $0.54 \text{ cm}^2 \text{ V}^{-1} \text{ s}^{-1}$ and $0.48 \text{ cm}^2 \text{ V}^{-1} \text{ s}^{-1}$, respectively, under ambient conditions. The sulfur atoms in the polymer are further replaced by selenium atoms, which are electron-rich donors. HOMO level of II-i-1d is increased to 5.57 eV, while the donor unit hardly affects the LUMO level. Unlike the enhanced

hole mobility after the introduction of fluorine atoms, the introduction of chlorine atoms significantly enhanced the electron mobility, which was $0.66 \text{ cm}^2 \text{ V}^{-1} \text{ s}^{-1}$ for II-i-1d under ambient conditions. However, the potentially negative effects of steric hindrance due to the large chlorine atomic size and thus is a non-negligible problem. Dong *et al.* found that the low film crystallinity and chain orientation of the polymer could be improved by introducing a flexible chain segment which maximizes the thermal annealing effect.²⁰ The rigid di-thiophene chain segment of II-i-1e shows a coplanar structure because the conjugated vinyl bond between two adjacent thiophenes inhibits the bond rotation of the single bond. Therefore, II-i-1c has a higher degree of rotational freedom. Because of the high degree of rotational freedom, significantly enhanced molecular ordering, and shorter π - π stacking distances are obtained by the thermal annealing process. This results in an average mobility of charge carriers ranging from 0.12 to $1.23 \text{ cm}^2 \text{ V}^{-1} \text{ s}^{-1}$. However, the rotational freedom of II-i-1d is limited and annealing at 250°C has less influenced on the crystallinity or charge carrier mobility.

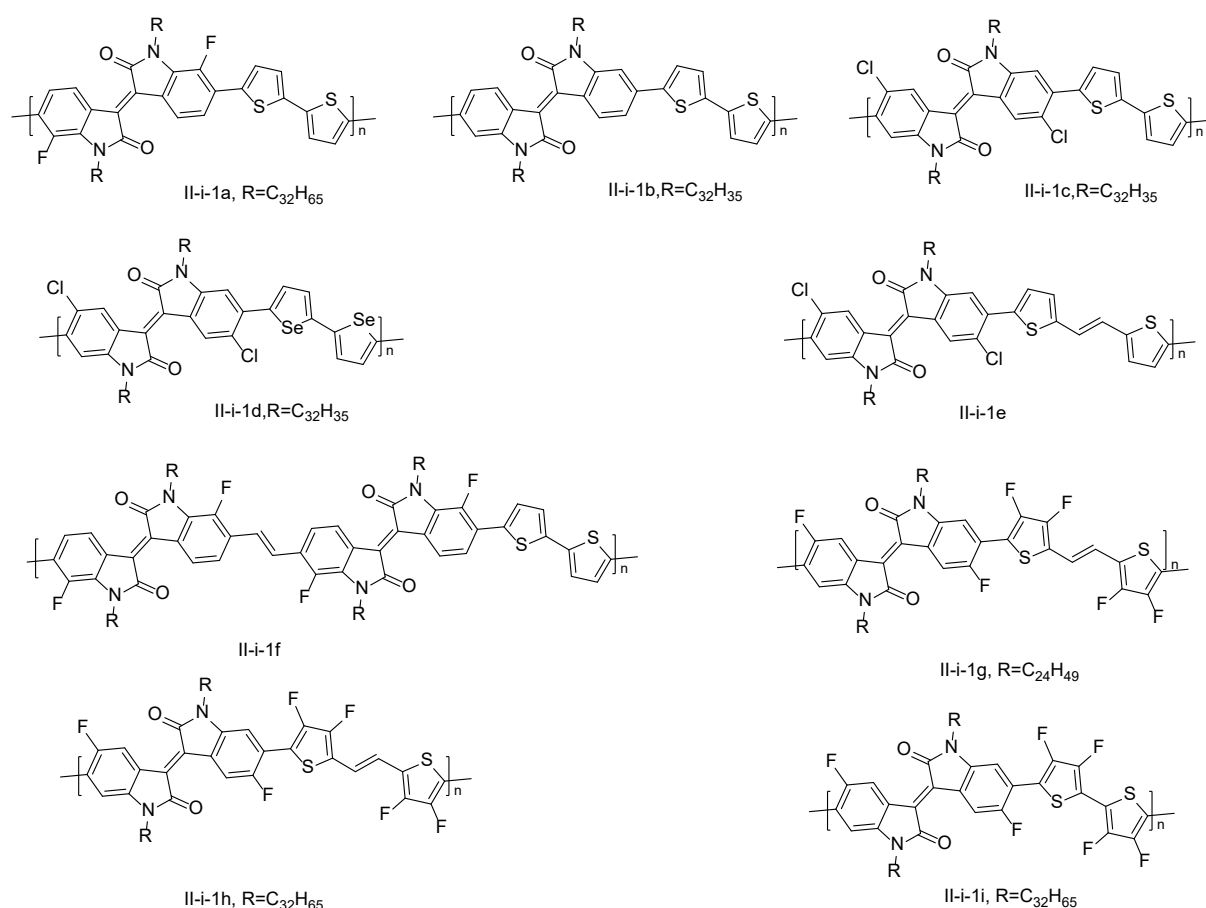


Figure 6a. Chemical structures of some representative core modification IID-based materials.

A vinyl unit was also used as a bridge to connect IID units. The increased conjugation length of the rigid skeleton had a higher electron absorption capacity, which helps to reduce the energy levels of HOMO and LUMO, thereby stabilizing the charge-carrier transport of the corresponding copolymer.²¹ To further enhance the electron-deficient ability, electron-withdrawing fluorine atoms were introduced into isoindigo core II-i-1f (Figure 6a), which can provide enhanced intermolecular interactions and

lower HOMO and LUMO energy levels. At the same time, the introduced fluorine atoms can "lock" the vinyl and adjacent units to form more intramolecular hydrogen bonds, resulting in enhanced planarity of the polymer backbone for efficient intra-chain charge migration. Non-fluorinated copolymer showed a p-type transport behavior with a hole mobility of $0.43 \text{ cm}^2\text{V}^{-1}\text{s}^{-1}$, whereas fluorinated one showed a typical ambipolar transporting behavior under ambient conditions with a high electron mobility of up to $1.82 \text{ cm}^2\text{V}^{-1}\text{s}^{-1}$ and a significantly enhanced hole mobility of up to $1.03 \text{ cm}^2\text{V}^{-1}\text{s}^{-1}$.

In a recent publication, Gao *et al.* used a multi-fluorination strategy, which introducing F atoms onto both D and A units to lower the electronic levels of the resulting copolymer and obtained an ambipolar copolymer II-i-1g with an hole and electron mobility (μ_{h} and μ_{e}) up to 3.94 and $3.50 \text{ cm}^2\text{V}^{-1}\text{s}^{-1}$, respectively.²² Unlike II-i-1g, unipolar n-type transport behavior was observed for II-i-1h and II-i-1i, with μ_{e} up to $4.97 \text{ cm}^2\text{V}^{-1}\text{s}^{-1}$ of II-i-1h. Compared to II-i-1g, the N-alkylation side-chain of II-i-1h is swapped. Shifting the branching point of the alkyl chain leads to a significant reduction of the HOMO energy level (5.82 eV vs. 5.95 eV). The authors inferred that this could be caused by the different stacking behavior of the conjugated backbone induced by polyfluorination. Polymer II-i-1i showed the lowest HOMO and LUMO energy levels of -6.09 and -3.92 eV, respectively. This can be attributed to the lower electron-donating ability of fluorinated thiophenes (without electron-rich vinylene group). These copolymers show excellent device air stability and no change in transfer properties after 40 days of storage in air. The good device stability is attributed to the presence of a large number of F atoms that resist electron trapping by oxygen or water in the air.

A series of isoindigo polymer-based organic semiconductor materials were studied along with the development of small-molecule-based organic semiconductor materials (**Figure 6b**). Yue *et al.* reported that the electron mobility of organic thin film transistors based on dicyanided II-i-1k is $0.044 \text{ cm}^2\text{V}^{-1}\text{s}^{-1}$.²³ II-i-1j or II-i-1k is formed from the corresponding mono or dibromo-isoindigo with copper cyanide in the presence of palladium catalysis. The number of cyano on the IID core has a significant effect on the LUMO energy level. The LUMO level of II-i-1j drops to 3.66 eV, while II-i-1k drops further to 3.88 eV. II-i-1k shows stacked packings with π - π face-to-face contact along the a-axis with a minimum planar spacing of only 3.22 Å and hydrogen bonding between the cyano and aromatic C-H units. A microwave heating synthesis of tetracyano isoindigo II-i-1l with moderate yields is also reported.²⁴

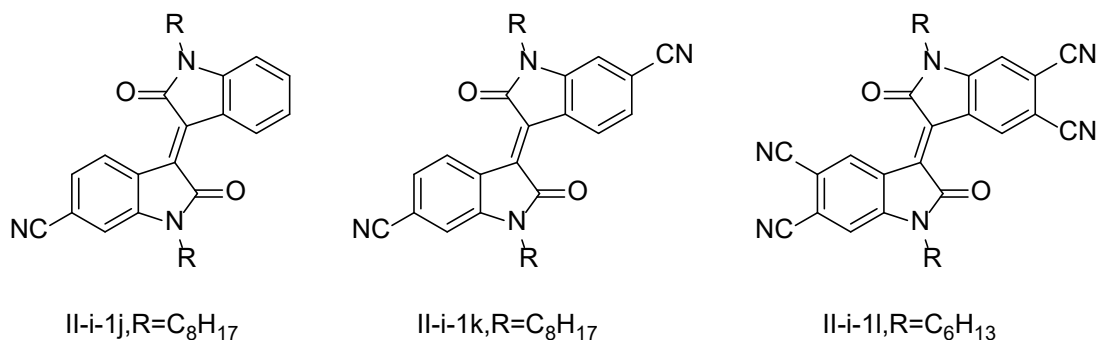


Figure 6b. Chemical structures of some representative core modification IID-based materials.

1.3.2) Heterocycle-substituted IID

Recent studies have shown that the structure of isoindigo is slightly distorted due to the steric repulsion between the proton at the position 4 on the benzene ring and the carbonyl oxygen of the lactam. Substitution of the benzene ring of isoindigo with thiophene yields thienoisindigo (TIIG, II-i-1m, **Figure 7**). The steric repulsion was mitigated and the intramolecular oxygen-sulfur (S...O) interactions stabilize the molecular planarity. In addition, due to the presence of sulfur atoms, intermolecular sulfur-sulfur (S...S) interactions are expected to lead to efficient carrier transport. Odajima *et al.* investigated the effect of molecular planarity on the performance of field-effect transistors using thioisatin derivatives.²⁵ The same electron donor is used in the D-A system, which have very similar chemical structures but slightly different cores. The LUMO of II-i-1 was almost the same as that of II-i-1o. The HOMO energy level of II-i-1n (5.06eV) is 0.6 eV lower than that of II-i-1o, 5.66 eV, which is caused by the relatively electron-rich thiophene ring. The LUMO energy level of II-i-1o was mainly concentrated in the isoindigo core, while the HOMO, LUMO energy level of II-i-1n was in the whole molecular system, as calculated by DFT. This was in contrast to many other donor-acceptor structures where the LUMO was located on the electron acceptor core. II-i-1n had a planar structure while the benzothiophene ring of II-i-1o was twisted from the isoindigo unit at a dihedral angle of 23.9°. Planar structure significantly changed the molecular stacking and film morphology thus improving the material properties and the charge carrier energy mobilities of II-i-1n-based OFETs were an order of magnitude higher than those of II-i-1o. A similar phenomenon was also obtained in polymers II-i-1p. The copolymer synthesized by Dutta *et al.* had a very low optical band gap with main absorption up to 1000 nm.²⁶ The energy levels of both HOMO and LUMO were influenced by the altered electronic structure of the donor unit. The DFT results showed that the electron density of both HOMO and LUMO are well-delocalized on the conjugate repeating unit of donor and acceptor. II-i-1p based OFETs with gold electrodes led to unipolar hole mobilities exceeding 0.1 cm²V⁻¹s⁻¹, while OFETs based on polymers II-i-1p with Al as the functional electrode could modulate the polarity of the charge carriers to produce ambipolar transport properties capable of conducting holes and electrons.

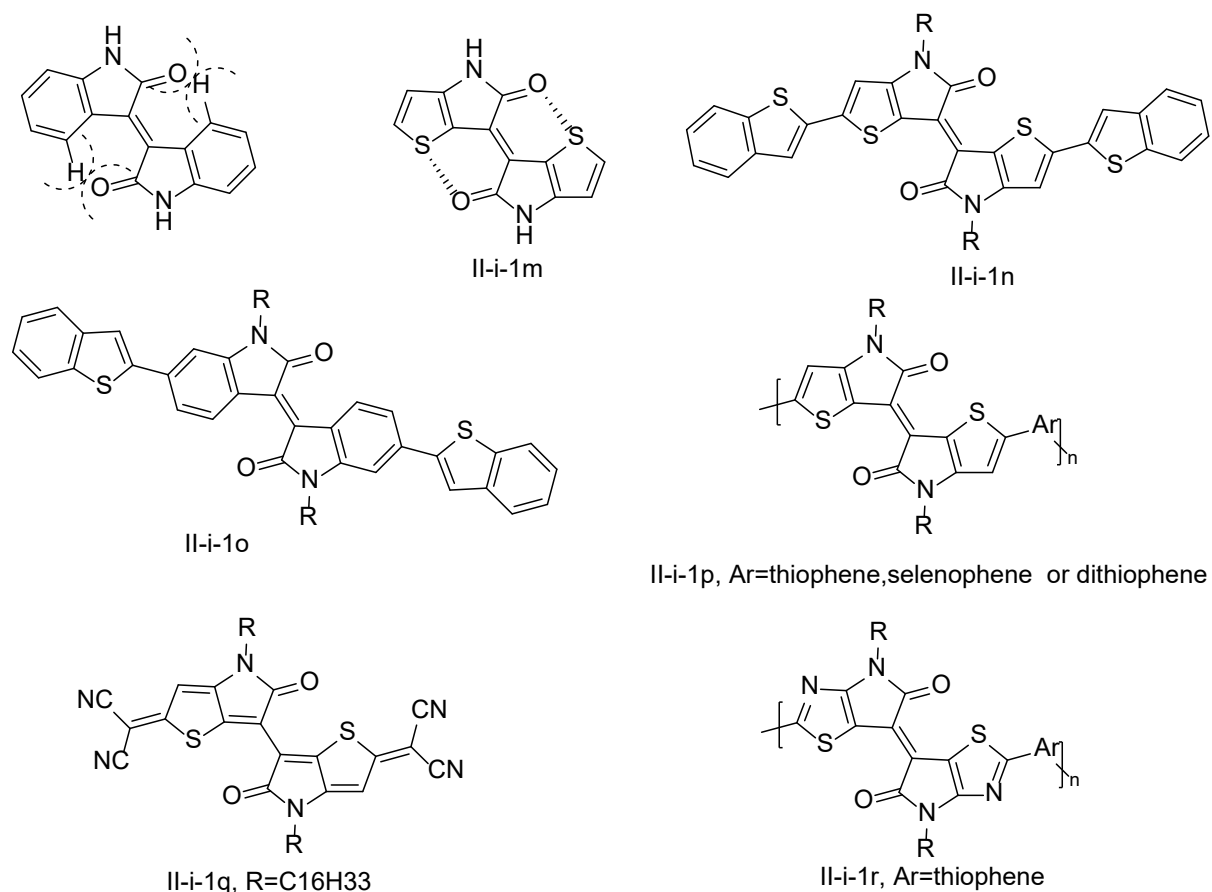


Figure 7. Chemical structures of some representative heterocycle substituted IID-based materials.

The fused planar aromatic structures can enhance π - π stacking and thus induce higher molecular order. Arulmozhi and co-workers designed TIIG as a quinoidal structure II-i-1q (**Figure 7**), thus providing n-type semiconductors with a maximum electron mobility of $2.54 \text{ cm}^2\text{V}^{-1}\text{s}^{-1}$. Due to the thiophene-thiophene linkage along the backbone, the TIIG core and the corresponding structure were almost planar with a C-C single bond distance of 1.42 \AA between the two monomers, and the non-bonded interaction between sulfur and oxygen arises due to the S...O distance of just 2.80 \AA . The intermolecular N...H distance based on the CN group is 2.52 \AA . The ability of cyano to interact with aromatic CH groups has been recognized as an important supramolecular motif to introduce organic semiconductor molecules into the desired layer arrangement.²⁷ Thiazoloisindigo II-i-1r, another structural variant of IID, was first synthesized by Li *et al.* and applied in OFETs, showing excellent bipolar mobility (hole: $3.93 \text{ cm}^2\text{V}^{-1}\text{s}^{-1}$, electron: $1.07 \text{ cm}^2\text{V}^{-1}\text{s}^{-1}$).²⁸ The decrease in LUMO of thiazoloisindigo compared with TIIG is due to the strong electron-withdrawing ability of the C=N bond.

Another variation of the core structure of IID is 7-azaisindigo, which has been investigated for optoelectronic applications. The higher electronegativity of N compared to the C led to a partial positive charge on the C atom in pyridine groups. Thus, the proton attached to the C atom at position 4 has a higher positive potential compared to IID (**Figure 8**). The additional positive charge creates an

electrostatic attraction with the negative charge of the carbonyl group favoring the planarization of the molecule.²⁹ To further reduce the LUMO energy level, strong EWG groups were introduced into II-i-1t by Wei *et al.*³⁰ More importantly, F atoms could generate intramolecular non-covalent Coulomb interactions. The distances between the F and the hydrogen of the vinylidene unit were 2.53 and 2.47 Å. The hydrogen bonding interactions formed by the F atoms and C-H bonds contributed to the intermolecular interactions and further promote the ordered stacking pattern. Compared to the reference material II-i-1u, the LUMO energy level of II-i-1t drop to 3.69 (vs. 3.47 eV) while its HOMO energy level also reduced to 6.23 eV (vs. 5.73). That was, both an enlarged energy gap and a reduced frontier orbital energy level were achieved. Thus, the II-i-1u based transistor exhibits a typical p-type transport hole mobility of $0.14 \text{ cm}^2\text{V}^{-1}\text{s}^{-1}$, while the II-i-1t based device exhibits n-type transport performance with electron mobility of $0.11 \text{ cm}^2\text{V}^{-1}\text{s}^{-1}$. As mentioned before, the strong electron-withdrawing group ability of the cyano group also made the LUMO energy level of the copolymer much lower (3.81 eV of II-i-1v).³¹ The introduction of cyano did not adversely affect the molecular planarity and there were three non-covalent interactions in the molecule. These weak interactions, S...N, C-H...N, π - π interaction, led to a good coplanar π -conjugated skeleton. The thermal annealing treatment also facilitated the grain growth, and II-i-1v- based devices had a high mobility of $1.58 \text{ cm}^2\text{V}^{-1}\text{s}^{-1}$ after a thermal annealing performed at 300°C .

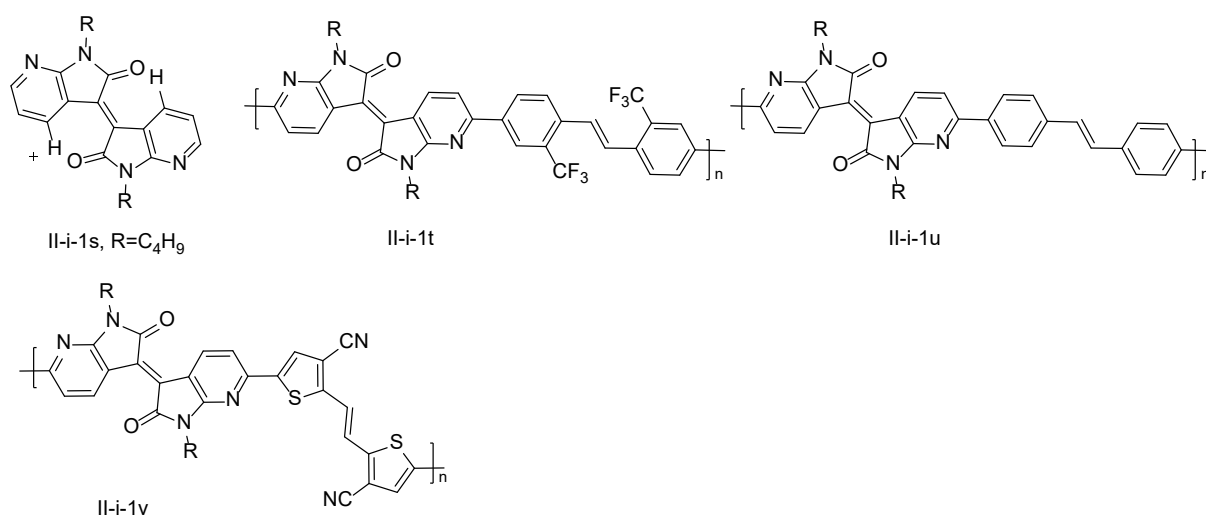


Figure 8. Chemical structures of some representative heterocycle-substituted IID-based materials.

1.3.3) Core-expanded IID

As discussed above, it is possible to modulate the electronic properties of isoindigo by inserting electron deficient functional π -conjugated bridge in the middle of the two lactam rings. As a representative structure, isoindigo benzodifurandione, in which a benzodifurandione moiety is inserted between the two lactam rings of isoindigo. Two synthetic routes were reported to synthesize BDOPV using a simple basic or acidic condensation between 1 and 2. The acidic condensation is similar to aldol

reaction used to prepare isoindigo from isatin and oxindole monomers by refluxing in toluene using *p*-TsOH as a catalyst; to eliminate one molecule of water and to form a new exocyclic carbon-carbon double bond, as shown in **Figure 9**.

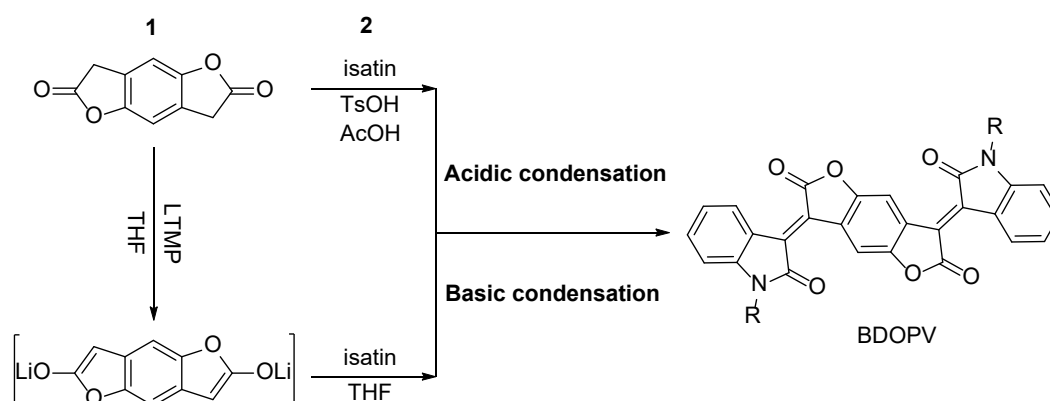


Figure 9. Synthetic route to BDOPV building block.

Pei and coworkers extended the π -conjugated motif by inserting a benzodifurandione unit as a bridge between the two oxindole fragments abbreviated as BDOPV, **Figure 10**.³² BDOPV (II-ii-1a, **Figure 10**) has four strong electron-withdrawing carbonyl groups into the BDOPV backbone affording a deep LUMO level down to -4.24 eV, significantly lower than many other electron-withdrawing units. As it has been demonstrated in IID derivatives, a π -electron donating group affects mainly the HOMO, while the LUMO is being determined by the isoindigo acceptor³³. Thus, fusing isoindigo with benzodifurandione unit affects the LUMO energy. The electronic structures of the BDOPV and its derivative AzaBDOPV with a nitrogen atom, building blocks were evaluated and compared with isoindigo by means of cyclic voltammetry and UV-vis absorption spectra³⁴. The redox properties of isoindigo, BDOPV and AzaBDOPV were characterized in solution by cyclic voltammetry measurements and data referenced against the Fc/Fc^+ redox couple. The reduction waves of isoindigo, BDOPV and AzaBDOPV were clearly observed as reversible two-step reduction processes. For the first process, the BDOPV is easier to reduce than the isoindigo. BDOPV has a first reduction potential of -0.7 V vs. Fc/Fc^+ , 0.7 mV higher than that of isoindigo (-1.4 V vs. Fc/Fc^+). From the onset potential of the first reduction wave, the E_{LUMO} were estimated to be 4.35, 4.24 and 3.65 eV below the vacuum level for AzaBDOPV, BDOPV and isoindigo, respectively. This means that replacing the carbon-carbon double-bond in isoindigo with benzodifurandione moiety lowers the E_{LUMO} by ca. 0.6 eV. Replacing a carbon atom with a nitrogen atom further lower the E_{LUMO} by 0.11 eV. From the inspections of electronic structures of BDOPV, it is clear that this building block is useful in developing n-type and ambipolar organic semiconductors. Thus, Lei *et al.* were the first to propose the benzodifurandione unit to extend isoindigo core³². They reported a novel electron-deficient PPV derivative, benzodifurandione-based PPV, II-ii-1c. This new copolymer displays high electron mobilities up to $1.1 \text{ cm}^2 \text{ V}^{-1} \text{ s}^{-1}$ under ambient conditions thanks to its locked skeleton. The carbonyl oxygen atom forms four intramolecular hydrogen bonds with the hydrogen atom of the benzene ring, thus providing a large locked aromatic ring that gives

the copolymer excellent UV and visible light stability. In addition, the use of 4-octadecyldocosyl groups as side-chains helps to enhance π - π stacking and further improve carrier mobility. Stronger aggregation tendency, better crystallinity, lower LUMO levels and above all higher electron mobilities. Considering the important effect of symmetric donor effect,³⁵ they also introduced 2,2'-bithiophene in the II-ii-1a or II-ii-1b based copolymer.^{34, 36} The HOMO levels of the two copolymers are almost identical, while the LUMO level of II-ii-1d2 (4.37 eV) was significantly lower than that of II-ii-1d1 (4.15 eV). Also, typical S...N interactions "lock" the polymer conformation. For devices fabricated in a glove box, both II-ii-1d1 and II-ii-1d2, exhibit n-type transport behavior with electron mobility up to 1.74 and 3.22 $\text{cm}^2 \text{V}^{-1} \text{s}^{-1}$, respectively. The increase in electron mobility is attributed to the lower LUMO energy level and the shortened π - π stacking distance of 3.44 Å after the introduction of nitrogen atoms, which is shorter than that of BDOPV-2T (II-ii-1d1, 3.55 Å). The introduction of F atoms into the BDOPV backbone further improves its air stability and further reduces the LUMO energy level of the polymer,³⁷ which is -4.26 and -4.30 eV for II-ii-1e and II-ii-1f, respectively. The intermolecular forces induced by the F atoms lead to a more ordered arrangement within the film. In addition, the different fluorination positions of the polymers lead to a change in the backbone conformation, which ultimately leads to a difference in device performance. The electron mobility of II-ii-1e reaches 1.70 $\text{cm}^2 \text{V}^{-1} \text{s}^{-1}$ while the highest electron mobility of II-ii-1f is 0.81 $\text{cm}^2 \text{V}^{-1} \text{s}^{-1}$. A well-balanced ambipolar transport can be achieved by introducing a strong electron withdrawing BDF (bithiophene-alkoxy).³⁸ The hole and electron mobilities of 0.27 and 0.3 $\text{cm}^2 \text{V}^{-1} \text{s}^{-1}$, respectively, for II-ii-1g. BDF units provide greater molecular planarity and S...O intermolecular interactions, resulting in better crystallinity and connectivity of π -conjugated polymers in thin films

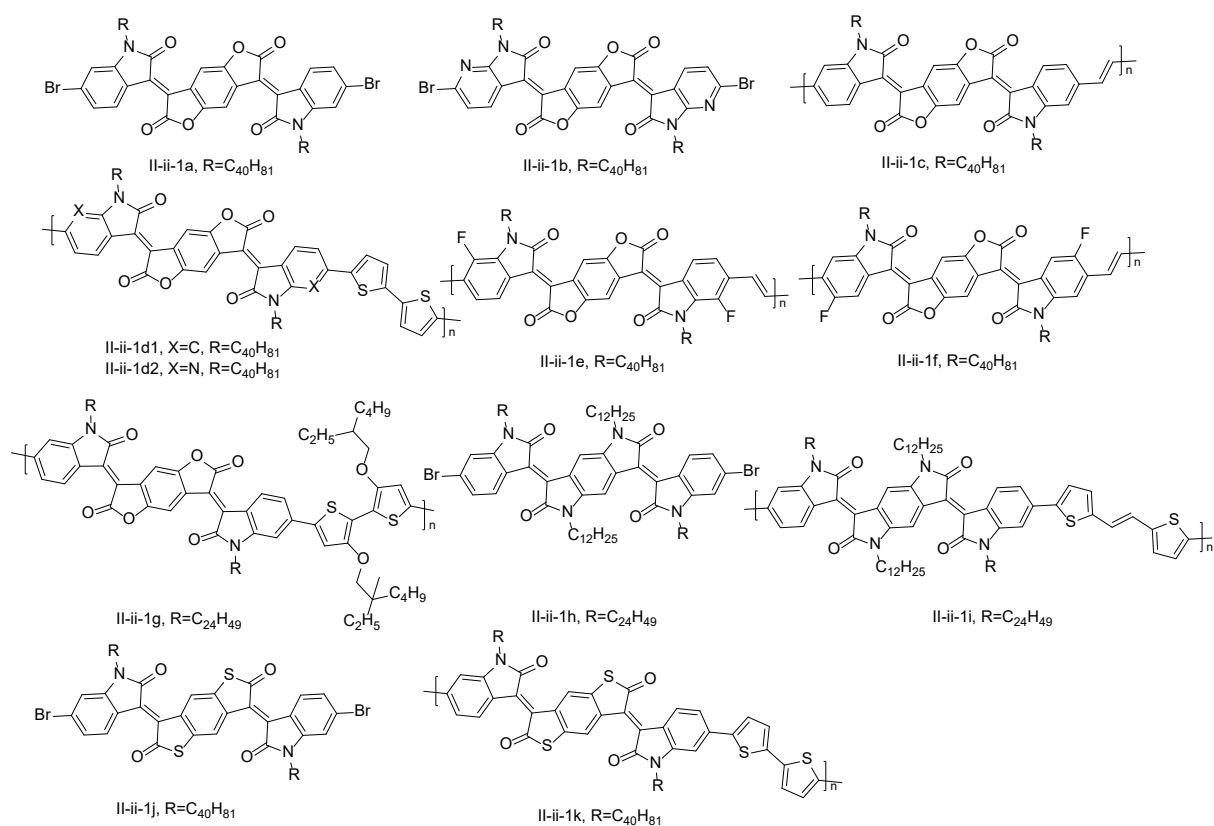


Figure 10. Chemical structures of some representative core-expanded IID-based materials.

By changing the bridging group, tetra-lactam II-ii-1h can be obtained by combining benzodipyrrolidone units, which maintain the skeleton rigidity.³⁹ The DFT calculations showed that the LUMO of II-ii-1h was well delocalized on the conjugated backbone, while the HOMO was mainly located on the benzodipyrrolidone core. In contrast, the HOMO and LUMO of II-ii-1a were uniformly distributed throughout the skeleton. The introduction of conjugated lone nitrogen pairs raises the LUMO energy level while raising the HOMO energy level, compared to II-ii-1a (-5.55/-3.74 eV vs. -6.08/-4.24 eV). II-ii-1i-based material achieved a hole mobility up to $1.92 \text{ cm}^2\text{V}^{-1}\text{s}^{-1}$. Li *et al.* replaced the structure of benzodifurandione with that of benzodithiophene dione to obtain II-ii-1j, which was polymerized with 2,2'-biothiophene to obtain ambipolar polymer II-ii-1k with $\mu_{\text{h}}/\mu_{\text{e}}$ of $0.1/0.14 \text{ cm}^2\text{V}^{-1}\text{s}^{-1}$.⁴⁰

1.3.4) Peripherally-expand IID

The fusion of PDI with strong electron withdrawing moieties is an ideal strategy to develop versatile n-type organic materials. Fusing PDI with isoindigo and DBPVP afford novel building blocks with larger π -conjugation skeletons. Yu and coworkers reported a series of four fused perylene diimides and isoindigos with different effective conjugation lengths⁴¹. Of these four building blocks, PDI-IID and PDI-IID-PDI differ from each other in the PDI/IID ratio (**Figure 11**). PDI-IID exhibits the smallest conjugation length with one PDI fused with one IID. For PDI-IID-PDI, the conjugation length was

extended with two PDIs fused with one IID. For PDI-IID-PDI, PDI-BDOPV-PDI, and PDI-DPN-PDI, which can be considered as two PDIs with fused additional different conjugation length and electron-effect IIDs into the central of PDIs.

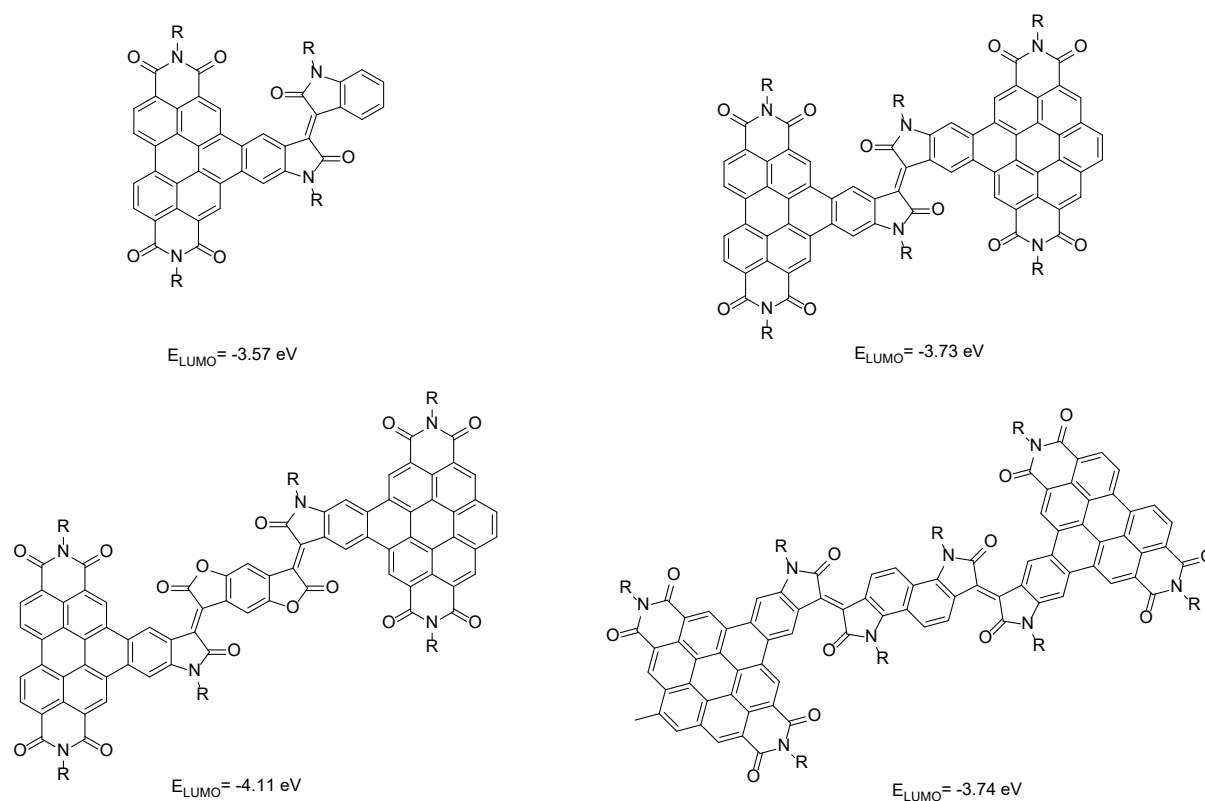


Figure 11. Chemical structures of some representative peripherally-expand IID-based materials.

Cyclic voltammetry was carried out to estimate the redox properties and energy levels of these molecules. The onset of the first reduction potentials is -1.08 eV for PDI; -1.35 eV for isoindigo (IID); -1.23 eV for PDI-IID; -1.07 eV for hybrid PDI-IID-PDI; -0.69 eV for PDI-BDOPV-PDI, and -1.06 eV for PDI-DPN-PDI. The energy of LUMO level is -3.57 eV for PDI-IID, -3.73 eV for PDI-IID-PDI, -4.11 eV for PDI-BDOPV-PDI, and -3.74 eV for PDI-DPN-PDI. The conclusions that we can draw are: i) the fusion of one PDI with isoindigo core lowers the E_{LUMO} by ca. 0.12 eV, ii) fusion of both sides of isoindigo further lowers the E_{LUMO} by 0.28 eV, and iii) extending the conjugation length of the isoindigo core results in a deeper LUMO energy, a shift of 0.66 eV was observed.

1.4) Purpose of this study

As discussed above, the performances of organic electronic devices are strongly related to the molecular structures of the active material. Through the chemical modifications one can generate tailor-made molecular structures to alter the frontier orbital energy levels, geometries, solubility and so forth to add novel functionality to enhance the devices performance. In this regard, the research described in this work aims at designing and synthesizing of new acceptor materials with the aid of contemporary

synthetic protocols. Furthermore, the properties of the obtained acceptors are evaluated in the view of their potential electronic applications.

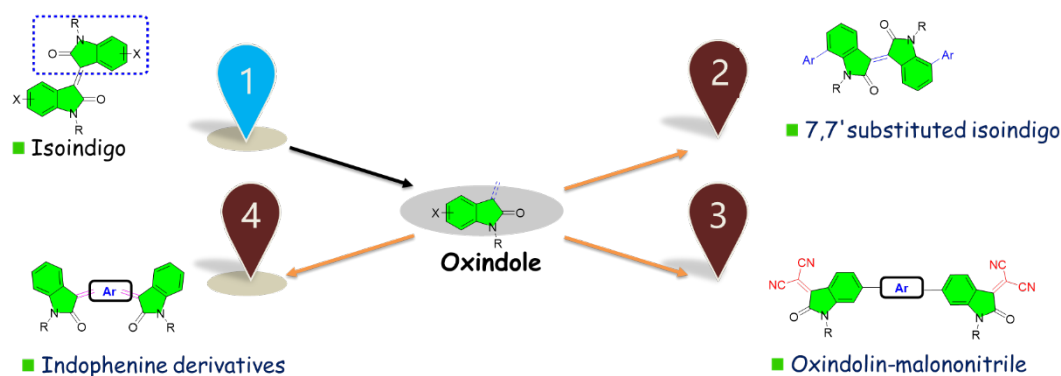
The chapter 2 of the present work focusses on the modification of the isoindigo core. Isoindigo (IID) is a symmetrical molecule consisting of two electron-deficient lactam rings fused together. It is widely used as an electron acceptor in D-A small molecules and polymers, thanks in large part to its electron withdrawing lactam groups, planar and rigid backbone, and also to its straightforward synthesis. Over the past few years, considerable effort has been devoted to the synthesis of new IID-compounds through side-chain engineering, heteroatom fusion, and conjugation length extension to tune their optoelectronic properties and morphologies. Most of works has focused on the conjugation extension of positions 6 and 5. To the best of our knowledge, there is no known report on the open literature on the positions 7. This chapter aims to further advance the synthesis of organic semiconductors through a study of structure-property-morphology relationships in cross-conjugated isoindigo materials. The cross-conjugation is defined as the conjugation between two unsaturated π -segments that, although not conjugated to each other, are conjugated to an intervening unsaturated segment. Cross-conjugated systems are advantageous for the design of new organic semiconductors, as this arrangement leads to spatial segregation of the frontier molecular orbitals.

Oxindole is a key building block for the construction of isoindigo. In fact, IID consists of two oxindole rings linked to each other at their 3-carbons by a central double bond that binds two electron-withdrawing carbonyls and two electron-rich benzene rings in trans configuration. Chapter 3 explores the potential use of oxindole as material building blocks for the preparation of new oxindole-bridged acceptors. Recent literature witnesses the interest of using this building block and its derivatives in the design of new performance materials, but no systematic study has been performed on the effect of the conjugation length and the mode of connectivity on their photophysical and electrochemical properties. In this context we have designed, and synthesized, a set of small molecules with A-D-A architecture (A: acceptor; D: donor) based on π -conjugated bridge, with different bridge lengths, as a donor unit, and two isatylidene malononitrile segments as terminal acceptor groups. Our objective was to vary the conjugation length by different spacer groups and to alter the linkage position of the isatylidene malononitrile group (position 4 vs. position 6), to analyze the effect on its structural, photophysical and electrochemical properties.

Chapter 4 aims to extend π -conjugation length of the isoindigo core, rather than its core-modification. This research is inspired by the renewed interest in the indophenine chemistry. One issue related to the indophenine reaction is isomer formation. The reaction produces a mixture of all possible geometric isomers. So, it is a challenge to prepare a single regioisomer form using indophenine reaction. To this end we replaced the central double bond with quinoidal molecules based on EDOT units. These

π -bridges are particularly suited since they provide a π -spacer bridge together with good ability to act as conformational locking units to drive the formation of single isomer. In particular, in this chapter we describe the organic synthesis routes, the mechanisms of synthesis of products, physical characterization, UV-visible, electrochemistry, the structure property relationships within these molecules. With the help of ^1H NMR experiments, ^1H - ^1H COSY and ^1H - ^1H NOESY analyses we showed a single isomer formation of these molecules.

The last chapter demonstrates the fabrication of bio-interface for sensing. In fact, bioelectronics is an emergent field at the interface of the life and physical sciences, seeking to connect biological elements with electronic devices. At present, the greatest challenge faced in this growing field is the realization of soft bioelectronic interfaces enabling the transduce between the ionic signals of biology and the electronic signals of electronic devices. Mixed ion/electron semiconducting polymers have recently emerged as promising materials for transducing signals at the interface between the biological elements and electronic devices. This chapter describes a study on a new bio-interface based on amphiphilic poly(3-hexylthiophene)-*b*-poly(3-triethylene-glycol-thiophene), P3HT-*b*-P3TEGT, for label-free impedimetric detection of Escherichia coli (E. coli). A set of amphiphilic π -conjugated random and block polythiophene that contain tetraethylene glycol side-chains and possess mixed ionic and electronic conductivities have been synthesized, and characterized. A bio-interface is fabricated by self-assembly of P3HT-*b*-P3TEGT into core-shell nanoparticles which further decorated with mannose for selective capturing of foodborne pathogens, such as E. coli. The hydrophilic block, P3TEGT promotes the antifouling property and prevents non-specific interactions while improving ionic and electronic transport properties, thus enhancing electrochemical sensing capability in aqueous solution. The self-assembly and micelle formation of P3HT-*b*-P3TEGT were analyzed through 2D-NMR, FT-IR, DLS, contact angle and microscopy characterizations. Detection of E. coli was characterized and evaluated by electrochemical impedance spectroscopy, optical and scanning electron microscopy techniques. Sensing layer based on mannose functionalized P3HT-*b*-P3TEGT nanoparticles demonstrates targeting ability toward E. coli pili protein with detection range from 10^3 cfu/ml to 10^7 cfu/ml and selectivity studied with gram positive bacteria.



Reference

- (1) Takimiya, K.; Nakano, M. Thiophene-Fused Naphthalene Diimides: New Building Blocks for Electron Deficient π -Functional Materials. *Bulletin of the Chemical Society of Japan* **2018**, *91* (1), 121-140, DOI: 10.1246/bcsj.20170298.
- (2) Gao, X.; Hu, Y. Development of n-type organic semiconductors for thin film transistors: a viewpoint of molecular design. *Journal of Materials Chemistry C* **2014**, *2* (17), 3099-3117, DOI: 10.1039/C3TC32046D.
- (3) Zhang, J.; Tan, H. S.; Guo, X.; Facchetti, A.; Yan, H. Material insights and challenges for non-fullerene organic solar cells based on small molecular acceptors. *Nature Energy* **2018**, *3* (9), 720-731, DOI: 10.1038/s41560-018-0181-5.
- (4) Sun, Y.; Liu, T.; Kan, Y.; Gao, K.; Tang, B.; Li, Y. Flexible Organic Solar Cells: Progress and Challenges. *Small Science*, 2100001, DOI: 10.1002/smsc.202100001.
- (5) Choi, J.; Gordon, M. P.; Yuan, P.; Kang, H.; Zaia, E. W.; Urban, J. J. CHAPTER 1 Introduction. In *Organic Thermoelectric Materials*; The Royal Society of Chemistry: 2020; pp 1-20.
- (6) Russ, B.; Glauddell, A.; Urban, J. J.; Chabinyc, M. L.; Segalman, R. A. Organic thermoelectric materials for energy harvesting and temperature control. *Nature Reviews Materials* **2016**, *1* (10), 16050, DOI: 10.1038/natrevmats.2016.50.
- (7) Sakai, N.; Mareda, J.; Vauthey, E.; Matile, S. Core-substituted naphthalenediimides. *Chemical Communications* **2010**, *46* (24), 4225-4237, DOI: 10.1039/C0CC00078G.
- (8) Usta, H.; Facchetti, A. Polymeric and Small-Molecule Semiconductors for Organic Field-Effect Transistors. In *Large Area and Flexible Electronics*; 2015; pp 1-100.
- (9) Sun, H.; Guo, X.; Facchetti, A. High-performance n-type polymer semiconductors: applications, recent development, and challenges. *Chem* **2020**, *6* (6), 1310-1326, DOI: 10.1016/j.chempr.2020.05.012.
- (10) Bucella, S. G.; Luzio, A.; Gann, E.; Thomsen, L.; McNeill, C. R.; Pace, G.; Perinot, A.; Chen, Z.; Facchetti, A.; Caironi, M. Macroscopic and high-throughput printing of aligned nanostructured polymer semiconductors for MHz large-area electronics. *Nature Communications* **2015**, *6* (1), 8394, DOI: 10.1038/ncomms9394.
- (11) Wang, G.; Huang, W.; Eastham, N. D.; Fabiano, S.; Manley, E. F.; Zeng, L.; Wang, B.; Zhang, X.; Chen, Z.; Li, R.; Chang, R. P. H.; Chen, L. X.; Bedzyk, M. J.; Melkonyan, F. S.; Facchetti, A.; Marks, T. J. Aggregation control in natural brush-printed conjugated polymer films and implications for enhancing charge transport. *Proceedings of the National Academy of Sciences* **2017**, *114* (47), E10066-E10073, DOI: 10.1073/pnas.1713634114.
- (12) Teshima, Y.; Saito, M.; Fukuhara, T.; Mikie, T.; Komeyama, K.; Yoshida, H.; Ohkita, H.; Osaka, I. Dithiazolylthienothiophene bisimide: a novel electron-deficient building unit for n-type

- semiconducting polymers. *ACS applied materials & interfaces* **2019**, *11* (26), 23410-23416, DOI: 10.1021/acsami.9b05361.
- (13) Stalder, R.; Mei, J.; Graham, K. R.; Estrada, L. A.; Reynolds, J. R. Isoindigo, a Versatile Electron-Deficient Unit For High-Performance Organic Electronics. *Chemistry of Materials* **2014**, *26* (1), 664-678, DOI: 10.1021/cm402219v.
- (14) Randell, N. M.; Kelly, T. L. Recent advances in isoindigo-inspired organic semiconductors. *The Chemical Record* **2019**, *19* (6), 973-988, DOI: 10.1002/tcr.201800135.
- (15) Li, J. L.; Cao, J. J.; Duan, L. L.; Zhang, H. L. Evolution of Isoindigo-Based Electron-Deficient Units for Organic Electronics: From Natural Dyes to Organic Semiconductors. *Asian Journal of Organic Chemistry* **2018**, *7* (11), 2147-2160, DOI: 10.1002/ajoc.201800198.
- (16) Lei, T.; Wang, J.-Y.; Pei, J. Design, synthesis, and structure–property relationships of isoindigo-based conjugated polymers. *Accounts of chemical research* **2014**, *47* (4), 1117-1126, DOI: 10.1021/ar400254j.
- (17) Yang, J.; Zhao, Z.; Wang, S.; Guo, Y.; Liu, Y. Insight into high-performance conjugated polymers for organic field-effect transistors. *Chem* **2018**, *4* (12), 2748-2785, DOI: 10.1016/j.chempr.2018.08.005.
- (18) Lei, T.; Dou, J.-H.; Ma, Z.-J.; Yao, C.-H.; Liu, C.-J.; Wang, J.-Y.; Pei, J. Ambipolar Polymer Field-Effect Transistors Based on Fluorinated Isoindigo: High Performance and Improved Ambient Stability. *Journal of the American Chemical Society* **2012**, *134* (49), 20025-20028, DOI: 10.1021/ja310283f.
- (19) Lei, T.; Dou, J.-H.; Ma, Z.-J.; Liu, C.-J.; Wang, J.-Y.; Pei, J. Chlorination as a useful method to modulate conjugated polymers: balanced and ambient-stable ambipolar high-performance field-effect transistors and inverters based on chlorinated isoindigo polymers. *Chemical Science* **2013**, *4* (6), 2447-2452, DOI: 10.1039/C3SC50245G.
- (20) Park, J.-J.; Kim, Y.-A.; Lee, S.-H.; Kim, J.; Kim, Y.; Lim, D.-H.; Kim, D.-Y. Chlorinated Isoindigo-Based Conjugated Polymers: Effect of Rotational Freedom of Conjugated Segment on Crystallinity and Charge-Transport Characteristics. *ACS Applied Polymer Materials* **2018**, *1* (1), 27-35, DOI: 10.1021/acsapm.8b00019.
- (21) Xu, L.; Zhao, Z.; Xiao, M.; Yang, J.; Xiao, J.; Yi, Z.; Wang, S.; Liu, Y. π -Extended Isoindigo-Based Derivative: A Promising Electron-Deficient Building Block for Polymer Semiconductors. *ACS Applied Materials & Interfaces* **2017**, *9* (46), 40549-40555, DOI: 10.1021/acsami.7b13570.
- (22) Gao, Y.; Deng, Y.; Tian, H.; Zhang, J.; Yan, D.; Geng, Y.; Wang, F. Multifluorination toward high-mobility ambipolar and unipolar n-type donor–acceptor conjugated polymers based on isoindigo. *Advanced Materials* **2017**, *29* (13), 1606217, DOI: 10.1002/adma.201606217.
- (23) Yue, W.; He, T.; Stolte, M.; Gsanger, M.; Wurthner, F. Cyanated isoindigos for n-type and ambipolar organic thin film transistors. *Chem Commun (Camb)* **2014**, *50* (5), 545-7, DOI: 10.1039/c3cc48037b.
- (24) Dasari, R. R.; Dindar, A.; Lo, C. K.; Wang, C. Y.; Quinton, C.; Singh, S.; Barlow, S.; Fuentes-Hernandez, C.; Reynolds, J. R.; Kippelen, B.; Marder, S. R. Tetracyano isoindigo small molecules and

their use in n-channel organic field-effect transistors. *Phys Chem Chem Phys* **2014**, *16* (36), 19345-50, DOI: 10.1039/c4cp02427c.

(25) Odajima, T.; Ashizawa, M.; Konosu, Y.; Matsumoto, H.; Mori, T. The impact of molecular planarity on electronic devices in thienoisindigo-based organic semiconductors. *Journal of Materials Chemistry C* **2014**, *2* (48), 10455-10467, DOI: 10.1039/C4TC02170C.

(26) Dutta, G. K.; Han, A. R.; Lee, J.; Kim, Y.; Oh, J. H.; Yang, C. Visible-Near Infrared Absorbing Polymers Containing Thienoisindigo and Electron-Rich Units for Organic Transistors with Tunable Polarity. *Advanced Functional Materials* **2013**, *23* (42), 5317-5325, DOI: 10.1002/adfm.201300536.

(27) Velusamy, A.; Yu, C. H.; Afraj, S. N.; Lin, C. C.; Lo, W. Y.; Yeh, C. J.; Wu, Y. W.; Hsieh, H. C.; Chen, J.; Lee, G. H.; Tung, S. H.; Liu, C. L.; Chen, M. C.; Facchetti, A. Thienoisindigo (TII)-Based Quinoidal Small Molecules for High-Performance n-Type Organic Field Effect Transistors. *Adv Sci (Weinh)* **2020**, *8* (1), 2002930, DOI: 10.1002/advs.202002930.

(28) Li, C.; Un, H. I.; Peng, J.; Cai, M.; Wang, X.; Wang, J.; Lan, Z.; Pei, J.; Wan, X. Thiazoloisindigo: A Building Block that Merges the Merits of Thienoisindigo and Diazaisindigo for Conjugated Polymers. *Chemistry* **2018**, *24* (39), 9807-9811, DOI: 10.1002/chem.201801432.

(29) de Miguel, G.; Camacho, L.; García-Frutos, E. M. 7, 7'-Diazaisindigo: a novel building block for organic electronics. *Journal of Materials Chemistry C* **2016**, *4* (6), 1208-1214, DOI: 10.1039/C5TC03464G.

(30) Wei, C.; Zhang, W.; Huang, J.; Li, H.; Zhou, Y.; Yu, G. Realizing n-Type Field-Effect Performance via Introducing Trifluoromethyl Groups into the Donor-Acceptor Copolymer Backbone. *Macromolecules* **2019**, *52* (7), 2911-2921, DOI: 10.1021/acs.macromol.9b00022.

(31) Wei, C.; Tang, Z.; Zhang, W.; Huang, J.; Zhou, Y.; Wang, L.; Yu, G. Molecular engineering of (E)-1, 2-bis (3-cyanothiophene-2-yl) ethene-based polymeric semiconductors for unipolar n-channel field-effect transistors. *Polymer Chemistry* **2020**, *11* (46), 7340-7348, DOI: 10.1039/D0PY01399D.

(32) Lei, T.; Dou, J.-H.; Cao, X.-Y.; Wang, J.-Y.; Pei, J. Electron-Deficient Poly(p-phenylene vinylene) Provides Electron Mobility over $1 \text{ cm}^2 \text{ V}^{-1} \text{ s}^{-1}$ under Ambient Conditions. *Journal of the American Chemical Society* **2013**, *135* (33), 12168-12171, DOI: 10.1021/ja403624a.

(33) Estrada, L. A.; Stalder, R.; Abboud, K. A.; Risko, C.; Brédas, J.-L.; Reynolds, J. R. Understanding the Electronic Structure of Isoindigo in Conjugated Systems: A Combined Theoretical and Experimental Approach. *Macromolecules* **2013**, *46* (22), 8832-8844, DOI: 10.1021/ma4013829.

(34) Dai, Y.-Z.; Ai, N.; Lu, Y.; Zheng, Y.-Q.; Dou, J.-H.; Shi, K.; Lei, T.; Wang, J.-Y.; Pei, J. Embedding electron-deficient nitrogen atoms in polymer backbone towards high performance n-type polymer field-effect transistors. *Chemical science* **2016**, *7* (9), 5753-5757, DOI: 10.1039/c6sc01380e.

(35) Lei, T.; Cao, Y.; Zhou, X.; Peng, Y.; Bian, J.; Pei, J. Systematic investigation of isoindigo-based polymeric field-effect transistors: design strategy and impact of polymer symmetry and backbone curvature. *Chemistry of Materials* **2012**, *24* (10), 1762-1770, DOI: 10.1021/cm300117x.

- (36) Lei, T.; Dou, J. H.; Cao, X. Y.; Wang, J. Y.; Pei, J. A BDOPV-Based Donor–Acceptor Polymer for High-Performance n-Type and Oxygen-Doped Ambipolar Field-Effect Transistors. *Advanced Materials* **2013**, *25* (45), 6589-6593, DOI: 10.1002/adma.201302278
- (37) Lei, T.; Xia, X.; Wang, J.-Y.; Liu, C.-J.; Pei, J. “Conformation locked” strong electron-deficient poly (p-phenylene vinylene) derivatives for ambient-stable n-type field-effect transistors: synthesis, properties, and effects of fluorine substitution position. *Journal of the American Chemical Society* **2014**, *136* (5), 2135-2141, DOI: 10.1021/ja412533d.
- (38) Takaya, T.; Mamo, M. D.; Karakawa, M.; Noh, Y.-Y. Isoindigo benzodifurandione based conjugated polymers for high performance organic field-effect transistors. *Journal of Materials Chemistry C* **2018**, *6* (29), 7822-7829, DOI: 10.1039/C8TC02348D.
- (39) Cao, Y.; Yuan, J.-S.; Zhou, X.; Wang, X.-Y.; Zhuang, F.-D.; Wang, J.-Y.; Pei, J. N-Fused BDOPV: a tetralactam derivative as a building block for polymer field-effect transistors. *Chemical Communications* **2015**, *51* (52), 10514-10516, DOI: 10.1039/C5CC02026C.
- (40) He, Y.; Quinn, J.; Deng, Y.; Li, Y. 3, 7-Bis ((E)-2-oxoindolin-3-ylidene)-3, 7-dihydrobenzo [1, 2-b: 4, 5-b'] dithiophene-2, 6-dione (IBDT) based polymer with balanced ambipolar charge transport performance. *Organic Electronics* **2016**, *35*, 41-46, DOI: 10.1016/j.orgel.2016.05.003.
- (41) Yu, Y.; Xue, N.; Xiao, C.; Ravva, M. K.; Guo, Y.; Wu, L.; Zhang, L.; Li, Z.; Yue, W.; Wang, Z. Effect of conjugation length on the properties of fused perylene diimides with variable isoindigos. *Journal of Materials Chemistry C* **2019**, *7* (39), 12263-12269, DOI: 10.1039/C9TC04078A.

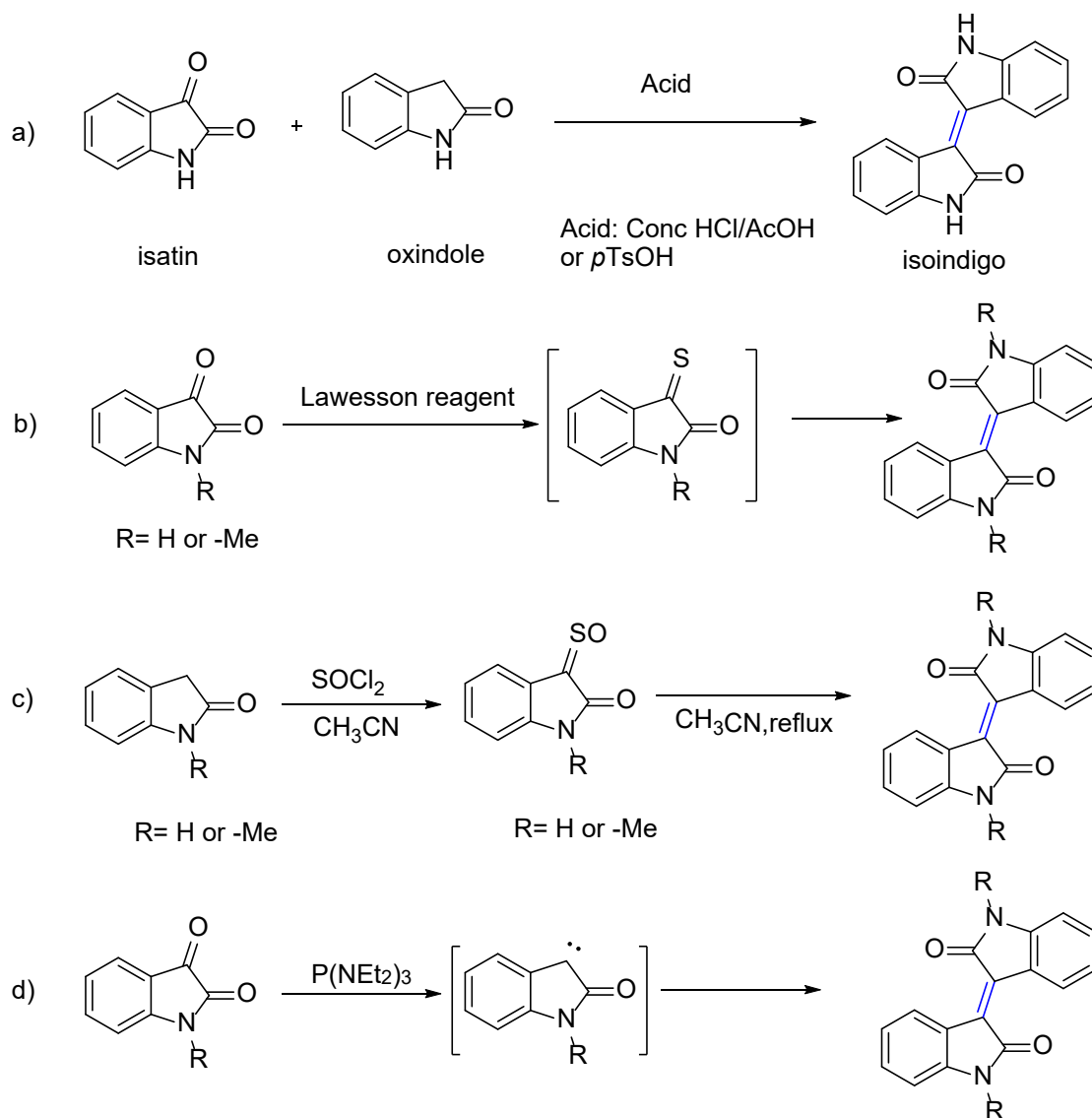
Design and synthesis of 7,7'-isoindigo as a new n-type organic semiconductor

2.1) Introduction

Isoindigo (IID) is an electron-deficient building block that has been intensely developed in solar cells and organic field effect transistors applications. For instance, donor-acceptor (D-A) conjugated polymers based on IID-derived showed hole and electron mobilities up to 14.4 and 14.9 $\text{cm}^2 \text{V}^{-1} \text{s}^{-1}$, respectively, and some ambipolar IID-materials exhibited high hole/electron mobilities of up to 5.97/7.07 $\text{cm}^2 \text{V}^{-1} \text{s}^{-1}$.¹⁻³ The power conversion efficiencies of solar cells based on all-polymer solar cells and IID-based materials have exceeded 10% and 7%, respectively,^{4,5}. Furthermore, various IID-based polymers have been used for other applications such as chemical sensors,⁶ organic electrochemical transistors,⁷ organic phototransistors,⁸ organic thermoelectrics,⁹ etc. There are numerous reviews of IID-materials covering organic transistors and organic solar cells applications.¹⁰⁻¹⁴

2.1.1) Synthesis approach to an IID family.

IID is a symmetric molecule consisting of two electron-deficient lactam rings fused together with a carbon-carbon double bond in the center having an E configuration.¹⁵ It is widely utilized as an electron acceptor for D-A (A: acceptor, D: donor) small molecules and macromolecules, owing in large part to its electron withdrawing lactam groups, planar and rigid backbones, and its straightforward synthesis. The most common synthetic route for IID derivatives is the acid-catalyzed condensation reaction of isatin and oxindole in the presence of a catalytic amount of concentrated hydrochloric acid/acetic acid¹⁶⁻¹⁷ or p-toluenesulfonic acid (**Scheme 1-a**).¹⁸⁻¹⁹ Unsubstituted IID derivatives show a low solubility, the alkylation of nitrogen atom is often used to overcome the solubility issue. An alternative synthesis route based on Lawesson's reagent was also reported for the synthesis of IID (**Scheme 1-b**).²⁰ The authors claimed that the thiation of isatin at C3 carbon takes place to form 3-thioisatin, which undergoes sulfur elimination to form IID. The treatment of oxindole with thionyl chloride afforded to sulfoxide intermediate which generate IID, when heated in acetonitrile (**Scheme 1-c**).²¹ The deoxygenation of isatin at 3 position using tris(diethylamino)phosphides form isatin ketocarbenes derivative that selectively dimerizes to afford IID (**Scheme 1-d**).²²



Scheme 1. Synthetic methods for the preparation of IID units.

Although there are a variety of methods for the preparation of IID derivatives, the acid-catalyzed condensation of isatin with oxindole is the most commonly used strategy due to its high yield and purity of final products with almost no purification step.

2.1.2) Functionalization strategy.

As shown in **Figure 1**, IID can be structurally tuned to achieve the desired properties. The phenyl rings of the IID permit access to various structural modification possibilities, including replacing the phenyl rings with aromatic heterocycles, extending the conjugation length on the periphery of the phenyl rings, and substituting with different groups, which not only change the molecular planarity but also modulate the electronic structures. Besides, modification of nitrogen atom with different side-chains endow materials with different solubility and packing motifs.

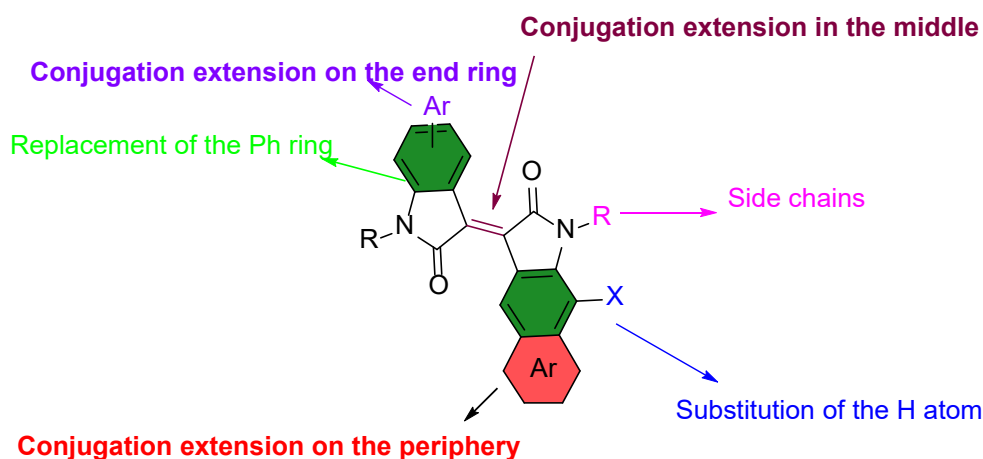


Figure 1. Functionalization strategy of isoindigo derivatives.¹⁴

Regarding the substitution pattern on the phenyl ring, there are four positions available for functional group substitution: 4,4'-; 5,5'-; 6,6'- and 7,7'-positions. The 4,4'-substitution is restricted due to the unfavorable steric hindrance between the substituents and carbonyl groups. The 6,6' substitutions lead to linearly π -conjugated chromophores, while 5,5' and 7,7'-substitutions to cross-conjugated materials. Therefore, most of the reported works use 6,6'-substitution to construct IID-materials. Stille and Suzuki-Miyaura coupling reactions are the most used methods for the functionalization of IID materials.^{23,10} More recently direct arylation has been explored as a novel coupling method that does not require organotin or borate precursors.²⁴ The dibromo-IID derivatives used in these reactions for the construction of IID-based conjugated materials are usually alkylated with selected alkyl halides under basic conditions.

Many examples of IID-derivatives involve modifying the functionality of the flanking phenyl rings with electron-rich heterocycles such as furan or thiophene have proven successful in the design of polymers and small molecules for organic electronics applications. For instance, Elsway *et al.* designed a series of D-A-D (A: acceptor, D: donor) small molecules based on different numbers of thiophene as electron-donating groups, as shown compound **1a-1d** in **Figure 2**.²⁵ With increasing the number of thiophene moieties (from Compound **I-1a**, **1c** to **1d**), the absorption spectrum in solution was gradually red-shifted. It is clear that the enhancement of intramolecular charge transfer with increasing donor strength is responsible for the red shift. The optical band gap is consequently gradually reduced from 1.81 to 1.70 and 1.61 eV, respectively. On the other hand, Compound **I-1a** and **I-1b** exhibit almost the same optical properties, while the HOMO and LUMO energy levels of both compounds are very close, which indicates that the introduction of alkyl chains on the donor does not have a significant effect. The HOMO energy level of the compound varies with the number of thiophenes, and the HOMO energy level of **I-1a** is -5.47 eV while that of the molecule **I-1d** with three thiophenes is only -5.10 eV. The photovoltaic device based on **1d** achieves the best power conversion efficiency (PCE) of ~3.2 %. Similar

oligothiophenes have also been used in solar cell devices. Compound **I-2** synthesized by Mei *et al.* achieved an energy conversion of 1.76%.²⁶ Further extended conjugation provided derivatives with a smaller optical band gap as well as increased absorptivity, and Compound **I-3** with benzothiophene as an end group had an optical band gap of 1.60.²⁷ Devices containing **I-3** and PC₆₁BM showed power conversion efficiencies of up to 3.4%.

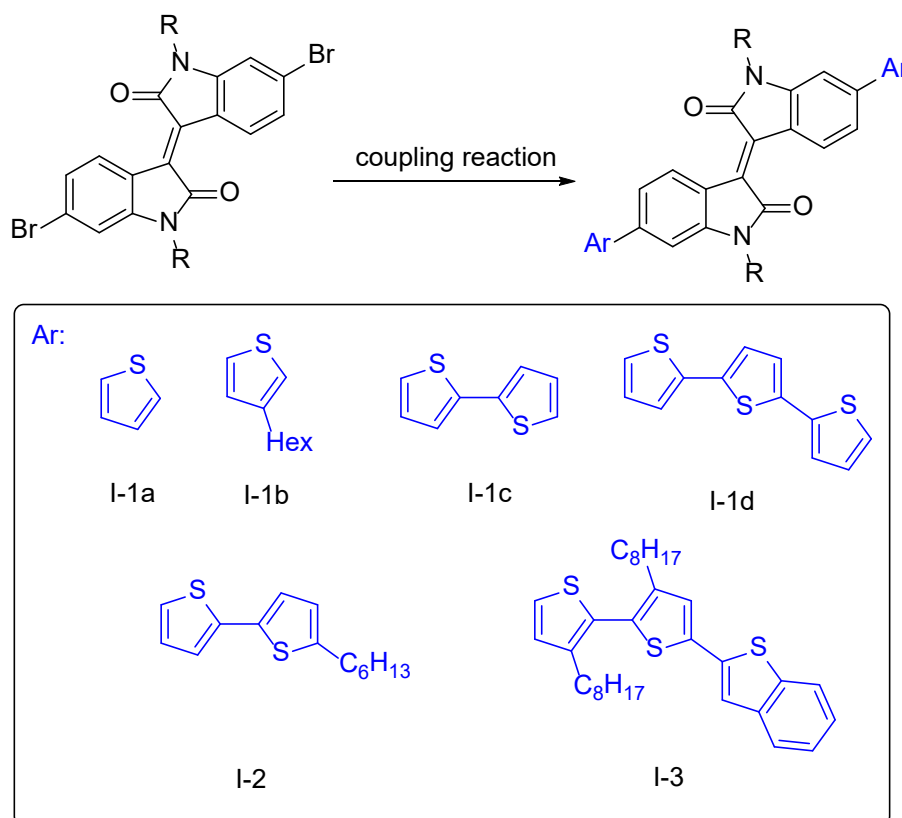


Figure 2. Molecular structures of IID-based small molecular with 6,6' conjugation

There are also various representative works of polymer-based IIDs, Wang *et al.* were among the first to demonstrate the potential of IID-polymers for solar cells with state-of-the-art cells reaching a PCE of 6.3%.^{28,29} The polymer with alternating thiophene has a broad absorption spectrum and absorption onset in the near infrared region. The polymer solar cell achieves a PCE of 3.0% and a high open-circuit voltage of 0.89 V. Although **P1** (**Figure 3**) shows a low band gap of 1.60 eV, it shows a low absorption intensity in the high energy band. While replacing thiophene ring with terthiophene enhances the UV-Vis absorption in the high energy region compared to **P1**. Due to the high aggregation of **P2**, the absorption spectrum is broad in the solid-state because the terthiophene unit is quite planar and well-suited for π - π stacking of the polymer backbone. Lei *et al.* designed and synthesized **P3** with a high yield.³⁰ The polymer has good environmental stability due to its low-lying of HOMO levels (-5.80 eV). **P3** exhibits excellent OFET performance with a hole mobility of up to 0.79 cm² V⁻¹ s⁻¹. Grenier *et al.* reports on polymers with all receptor units for n-type OFETs applications.³¹ **P4** features a particularly low LUMO energy level of -4.20 V and exhibits a moderate electron mobility.

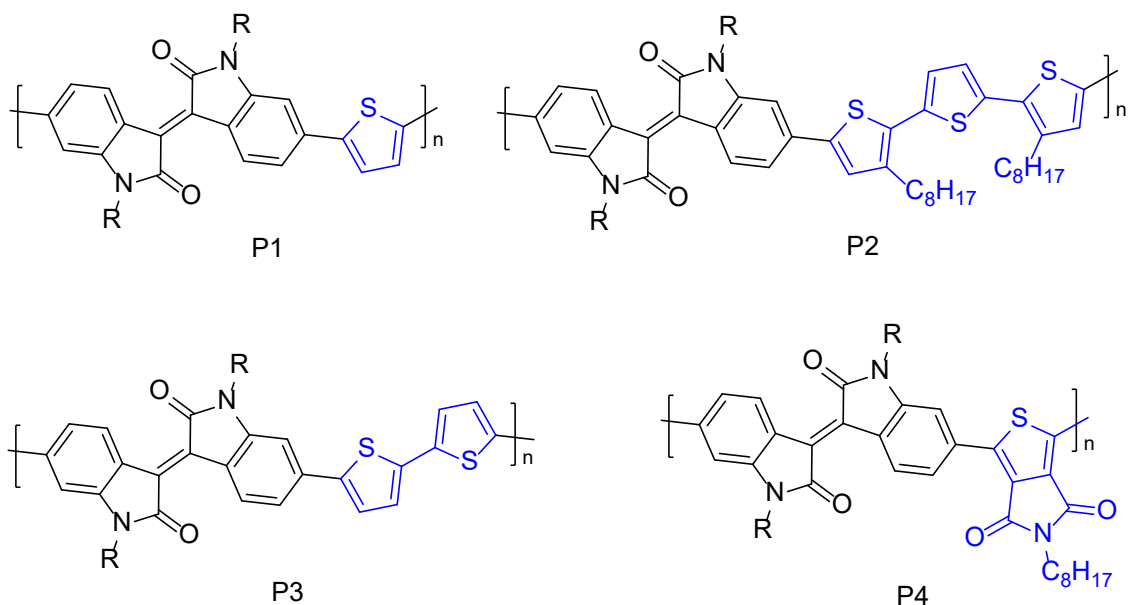


Figure 3. Macromolecular structures of IID-based polymers for OPV and OFET applications

2.1.3) The effect of substitution pattern on the electronic properties of IIDs.

There are four position that can be further substituted with functional groups. As previously discussed, most of the works were focused on 6,6'-positions, and few groups investigated the impact of the substitution at 5,5'-positions. Broadly speaking, the substitution at 6,6'-positions lead to linearly π -conjugated materials, the conjugation occurs over the entire molecule, which makes the π -electrons more delocalized (**Figure 4** left). While the 5,5'-disubstituted IID derivatives are cross-conjugated (**Figure 4** right). The cross-conjugation is defined as the π -conjugation between two unsaturated π -segments that, although not conjugated to each other, are conjugated to an intervening unsaturated segment.³²⁻³³

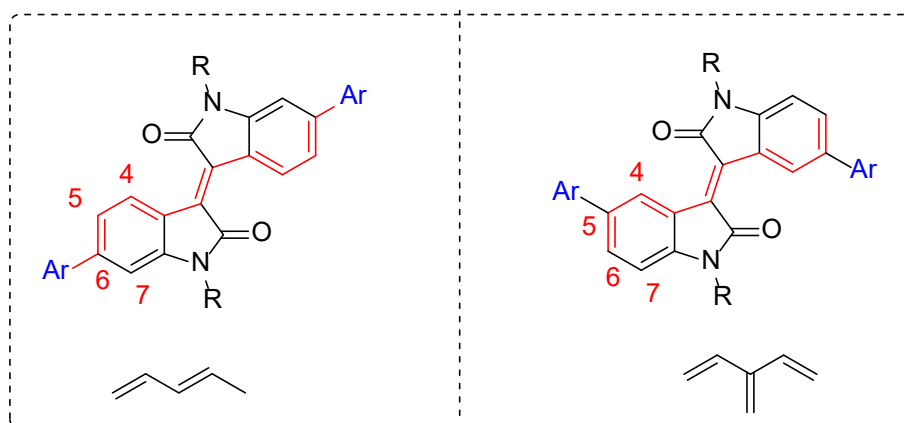


Figure 4. Effect of pattern substitution with two linking styles of IID-based π -conjugated compounds.

Kelly's group reported a comparison of the optoelectronic properties of linearly- and cross-conjugated IID-based materials (**I-4**, **I-5**, **Figure 5**).³⁴ They found that neither the orbital isosurfaces nor the optical band gap was changed. It was found, however, that the experimentally and theoretically

determined by DFT calculations, the oscillator strength of linearly conjugated **I-4** is much higher than that of cross-conjugated one. The same trend is also observed when we compare between compound **I-6** and **I-7**. The theoretical oscillator strength of **I-6** is 1.17, which is 15 times larger than that of **I-6** (0.08). On the other hand, the HOMO and LUMO energy levels of cross- and linearly conjugated materials are at the same energy level. As shown in **Table I-1**, The calculated DFT values for the LUMO energy levels of compounds **I-4** and **I-5** show 2.93 and 2.94 eV, respectively, and their HOMO energy levels are almost the same. This situation is also the same when comparing the compound, **I-6** and **I-7**, which indicates that the position of the substitution pattern on IID appears to have little impact. Janssen *et al.* noticed by DFT calculations that the HOMO and LUMO energy levels of compounds **I-8** and **I-9** are extremely close to each other (**Table I-1**).³⁵ The first electron transition of **I-8** with higher oscillator strength, $f=0.59$, compared to **I-9** with a much weaker first electron transition of 0.03. As obtained from **Table I-1**, DFT calculations for the six IID- based molecules (compound **I-10** to **15**) demonstrate that the cross-conjugation of IID strongly reduces the oscillator strength, but that their frontier orbital levels are comparable.³⁶ Regardless of the substitution pattern, the EDOT derivative shows a slightly higher LUMO energy relative to the Ph derivative, but the overall change is small. The dependence of HOMO on the substituent is greater than that of LUMO, while it is independent of the position of the substituent. Ren and his colleagues presented the effects of electron-rich and electron-poor groups at the 6- and 5- positions, respectively (**I-16**, **17**, **18**, **19**), and they revealed that the 6,6'- substitution on the core leads to a stronger intramolecular charge transfer band, while the 5,5'- substitution induces a weaker CT band.³⁷ This is due to the strong electronic coupling between the 6,6'- substituent and the core, while the electronic communication between the substituent and the IID core is restricted in the 5,5'-substituted compounds. The energy of the CT bands of these compounds depends on the electronic nature of the substituents, and substitutions with more electron-rich substituents (**I-16** and **I-17**) are more effective in reducing the energy of the CT bands. More recently Ashizawa and coworkers investigated the influence of the connecting positions of the flanking thiophene on the optoelectronic properties, crystal structures, and charge transport properties. Similarly, the substitution pattern in the diazoindigo unit has a significant effect on the oscillation strength, but not on the optical bandgap.³⁸ The optical band gaps of both compounds **I-20** and **21** are within the range of 1.84-1.90 eV, but the oscillation strength of compound **I-21** is significantly lower. The 5,5'-substitution weakens the π -delocalization of the central lactam part along the conjugated backbone, which leads to a slightly deeper HOMO in 5,5'-diazoindigo than in 6,6'-diazoindigo, although the difference is small. Both isomers adopt co-facial slipped π - π stacking in crystal. Devices made from **I-20** or **21** show an ambipolar charge transport. Their hole and electron mobility are in the same order of magnitude, **I-21** shows a higher hole mobility and its electron mobility is four times higher than that of linearly conjugated **I-20**. In other words, the extended backbone on the 5,5'-substitution positions of the diazoindigo core has a rather positive impact on charge transport, which suggests that cross-conjugation can be designed to improve the carrier mobility characteristics of transistor applications.

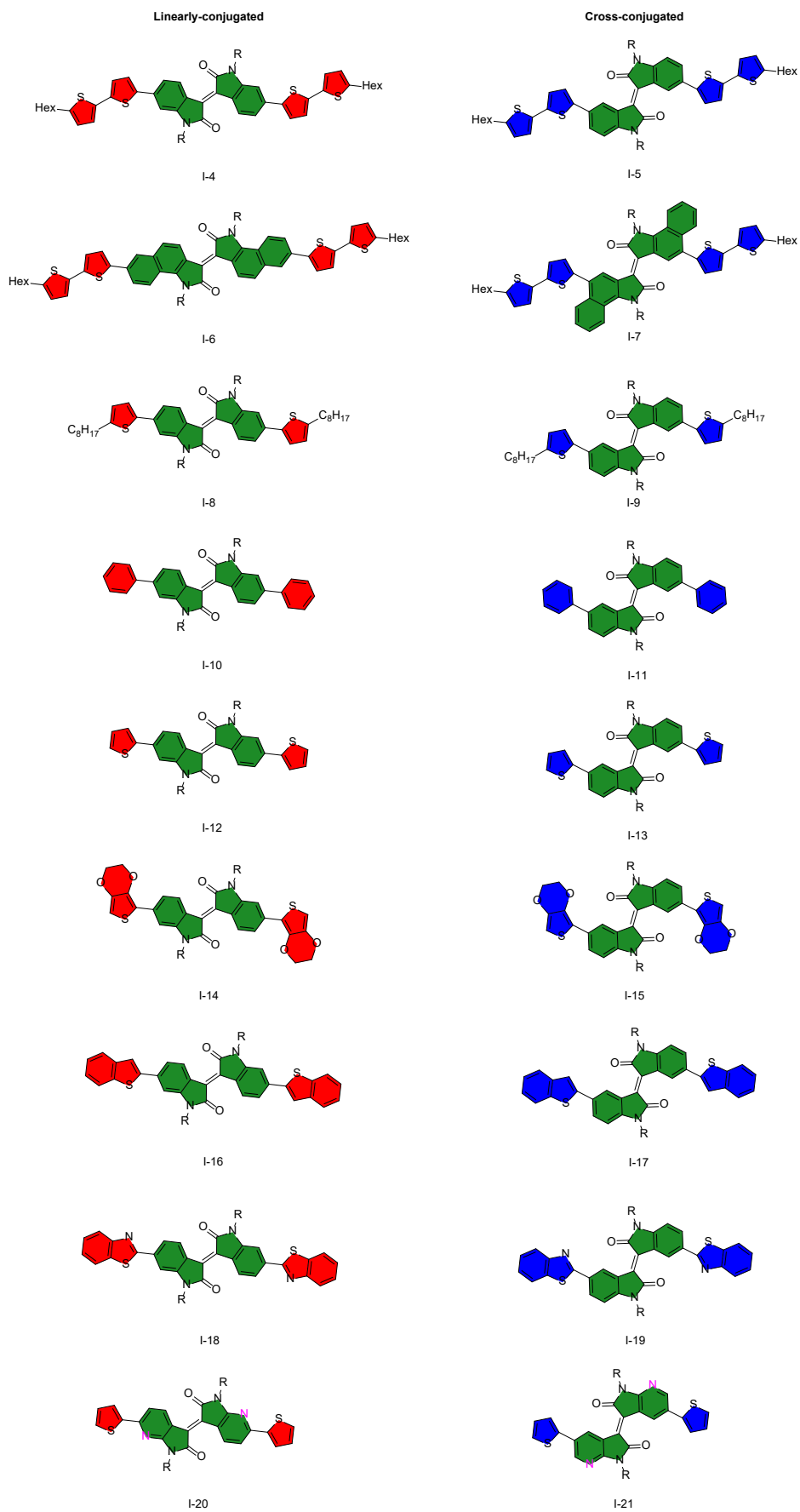


Figure 5. Molecular structures of IIDs with linearly and cross-conjugated.

Table I-1. DFT calculated optical transitions and frontier orbital energy levels.

Materials	HOMO (calcd)	LUMO (calcd)	f_{osc} (calcd)	ΔE_c (calcd)
I-4	-5.12	-2.94	1.55	2.18
I-5	-5.11	-2.93	0.02	2.18
I-6	-5.03	-3.07	1.17	1.96
I-7	-5.06	-3.10	0.08	1.96
I-8	-5.24	-2.72	0.59	2.52
I-9	-5.28	-2.74	0.03	2.54
I-10	-5.71	-3.06	0.38	2.65
I-11	-5.76	-3.12	0.04	2.64
I-12	-5.59	-3.12	0.61	2.47
I-13	-5.61	-3.15	0.03	2.46
I-14	-5.29	-2.92	0.77	2.37
I-15	-5.39	-3.04	0.02	2.35
I-16	-5.35	-2.86	0.86	2.49
I-17	-5.34	-2.86	0.025	2.48
I-18	-5.59	-3.04	0.65	2.55
I-19	-5.59	-2.99	0.039-	2.60
I-20	-7.53	-1.66	0.84	5.87
I-21	-7.80	-1.70	0.14	6.10

In summary, cross-conjugated organic semiconductors materials are less-developed, because it is generally considered to result in poor orbital overlap, less electron delocalization and poor intermolecular couplings. Consequently, it is not considered as promising approach to develop high performance materials. However, playing with the connection pattern is an important factor to govern the topology of the molecule and the molecular packing which control the carrier-transport. Concerning the IID family only the effect of 5,5'-substitution position on the optoelectronic properties has been reported, no report on the effect of 7,7'-position.

Objectives of this study

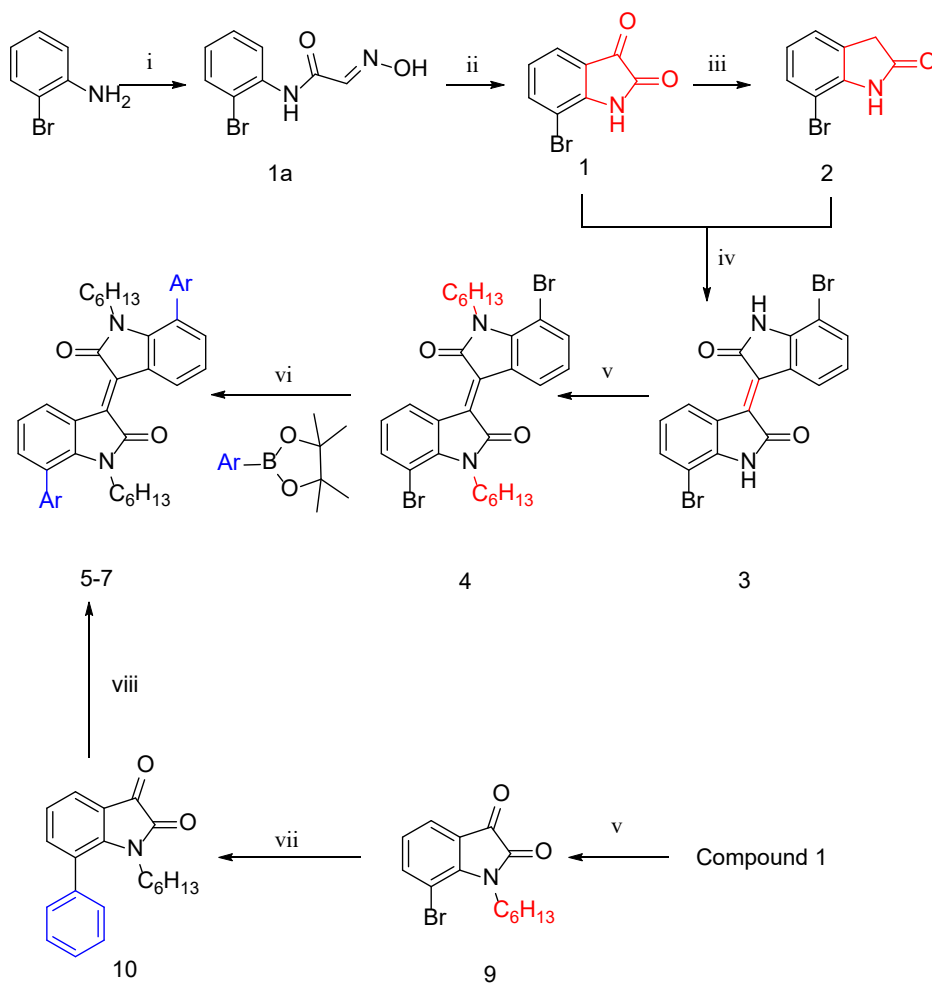
Most of the work on IID derivatives, to the best of our knowledge, has focused on the substitution at 6,6'-position to extend the conjugation length and few examples of 5,5'-substituted to study the effect of cross-conjugation on the optoelectronic properties. No known report on the open literature on the 7,7'-substitution. This chapter aims to further advances the synthesis of novel organic semiconductors

through a study of structure-property-morphology relationships in 7,7' cross-conjugated IID-materials. Cross-conjugated systems are useful materials for optoelectronic devices, as this substitution leads to spatial segregation of the frontier molecular orbitals.

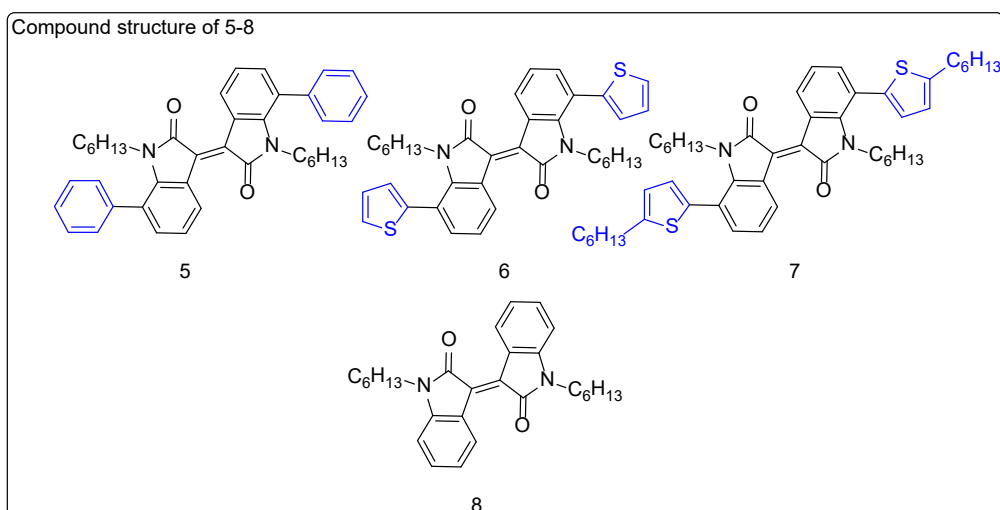
2.2) Results and discussion.

2.2.1) Synthetic methodology.

The 7,7'-isoindigo based materials were synthesized as shown in **Scheme 2**. Commercially available 2-bromoaniline was used as a precursor to obtain 7-bromo-isatin, compound **1**, through a two-step reaction, involving the reaction of chloral hydrate and hydroxylamine afforded α -isonitrosoacetanilide and subsequent electrophilic cyclization in the presence of a strong acid such as concentrated sulfuric acid. Hydrazine hydrate was used to reduce isatin to oxindole **2**. The dimerization reaction was carried out by acid-catalyzed aldol condensation of isatin with oxindole precursors. 7-bromoistain and 7-bromooxindole were heated under reflux in acetic acid to produce 7,7'-dibrominated IID in 85% yield, followed by alkylation to ensure the solubility. The strong π - π interactions and hydrogen bonding of IID result in a poor solubility of dibromo- IID in common organic solvents. The hexyl chains were introduced to both lactam nitrogen atoms in the presence of potassium carbonate in DMF, in 90% yield. Subsequent Suzuki-Miyaura coupling with a variety of borate compounds, using $\text{Pd}_2(\text{dba})_3$ as the catalyst, K_3PO_4 as the base and $\text{P}(\text{o-tyl})_3$ as the ligand, gives access to the desired 7,7' diaryl IIDs (**5-7**) with excellent yields. Product **7**, which further introduces another alkyl chain on the thiophene ring compared to product **6**, can be envisioned as a way to further improve the solubility of the materials. An alternative solution to the solubility problem is to pre-alkylate compound **1** and subsequently introduce phenyl or other aromatic rings to compound **9** via the Suzuki coupling reaction. Finally, Lawesson's reagent was successfully used to generate product **5** in 82% yield. These D-A-D compounds exhibit good solubility in organic solvents such as THF, TCM and DCM. The experimental part describes in detail the synthetic procedures and characterizations.



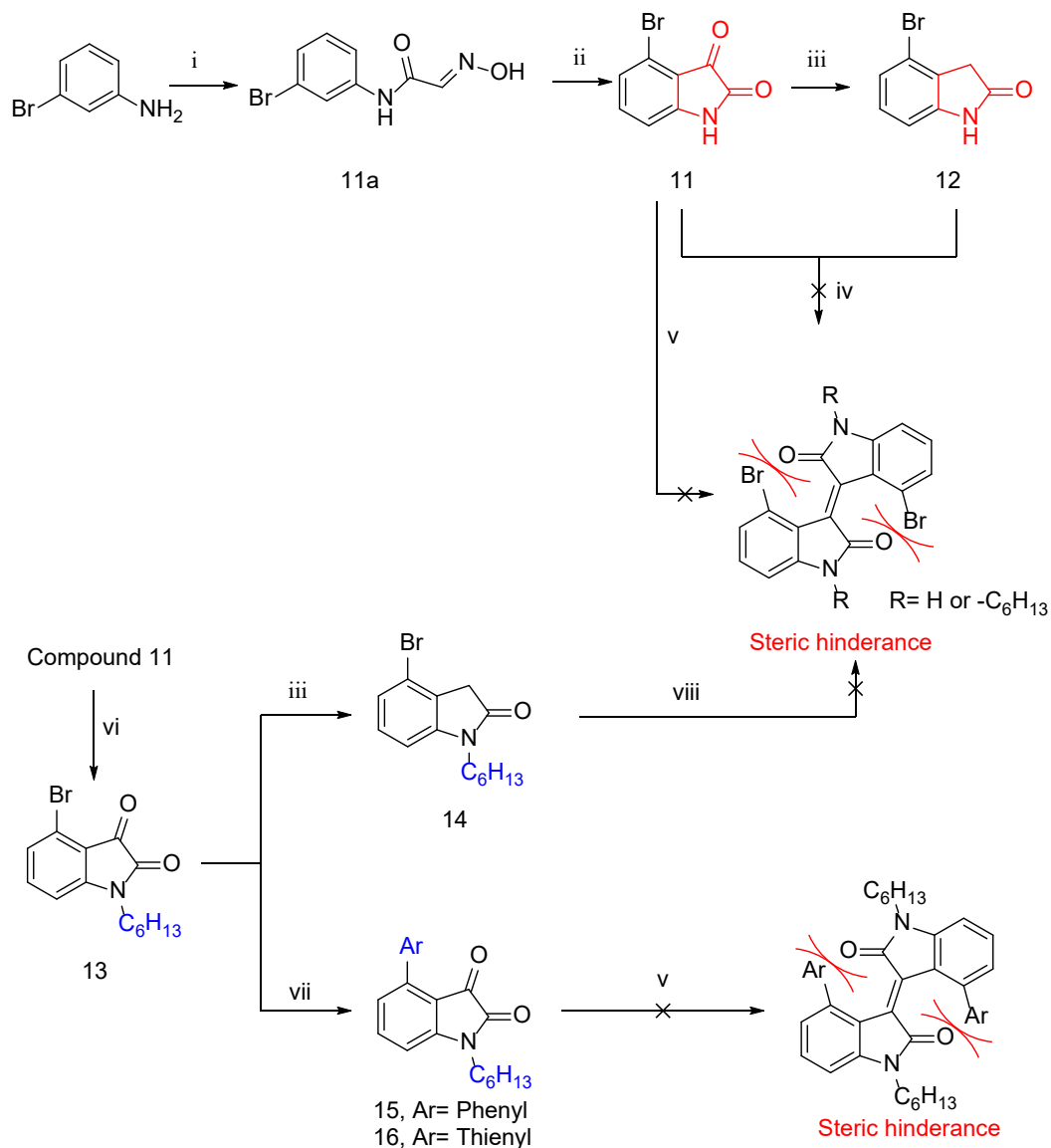
^aReagents and conditions: (i) chloral hydrate, Na₂SO₄, H₂NOH·HCl; (ii) H₂SO₄, 46% over two steps; (iii) NH₂NH₂·H₂O, reflux, CH₃CH₂ONa, Ethanol, 67%; (iv) HCl, AcOH, reflux, 85%; (v) K₂CO₃, 1-bromohexane, DMF, reflux, 90%; (vi) Pd₂(dba)₃, P(o-tyl)₃, K₃PO₄, toluene, H₂O, 65%-85%; (vii) KF, Pd(OAc)₂, MeOH, 67%; (viii) Lawesson's reagent, toluene, reflux, 82%.



Scheme 2. Synthesis of 7,7' IID-Ph (**5**), 7,7' IID-Th (**6**), 7,7' IID-Th-hex (**7**) and IID (**8**).

Using the same synthesis method, 4-bromoisatin (compound **11**) was obtained from 3-bromoaniline. Compound **11** was easily reduced with hydrazine monohydrate in EtOH to form the

desired oxindole **12**. Using hydrochloric acid and acetic acid to catalyze the condensation of **11** with **12**, however, this was not successful. Other reagents have also been tested for the dimerization of 4-bromo-isatin, such as Lawesson's reagent or SOCl_2 , but all of them did not produce the target product (**Scheme 3**). The steric hindrance between the bromine atom on the phenyl ring and the oxygen of the carbonyl of the oxindole is the main reason for the failure of the reaction.



*Reagents and conditions: (i) chloral hydrate, Na_2SO_4 , $\text{H}_2\text{NOH}\cdot\text{HCl}$; (ii) H_2SO_4 , 43% over two steps; (iii) $\text{NH}_2\text{NH}_2\cdot\text{H}_2\text{O}$, reflux, $\text{R} = \text{H}$ or *n*-hexyl, 67%- 89%; (iv) HCl , AcOH , reflux; (v) Lawesson reagent; (vi) K_2CO_3 , 1-bromohexane, DMF, reflux, 90%; (vii) Suzuki coupling: Phenylboronic acid, KF , $\text{Pd}(\text{OAc})_2$, 74%; Stille coupling: tributyl(thiophen-2-yl)stannane, $\text{Pd}(\text{dppf})\text{Cl}_2$, MeOH , 67%, (viii): SOCl_2 , CH_3CN

Scheme 3. Synthesis of 4,4'-dibromo-IID.

2.2.2) Crystal structure & Molecular packing 7,7'-IID-based materials.

We have succeeded in solving the single crystal structures of some of the products (**Figure 6**). The crystal structures of compounds **4** and **5** are shown below. The 7,7'-IID geometry obtained from X-

ray diffraction shows a completely planar and trans configuration. The two lactam blocks are in the same plane, the torsion angle between the phenyl group of **5** and the lactam plane is 65° . A similar phenomenon is observed for the substituted IID at position 6, where the crystal structure of the compound shows a dihedral angle of 39° between the phenyl and lactam when using the phenyl ring as a substituent at 6,6'-position. In contrast, the dihedral angle is only 6° using thienyl as the substituent at position 6.¹⁰ The molecules **4** formed one-dimensional π - π stacking with a distance of 3.53 Å. The molecules **5** stack into two-dimensional slipped stacks with strong intermolecular interactions, which are good and favorable for charge transport.

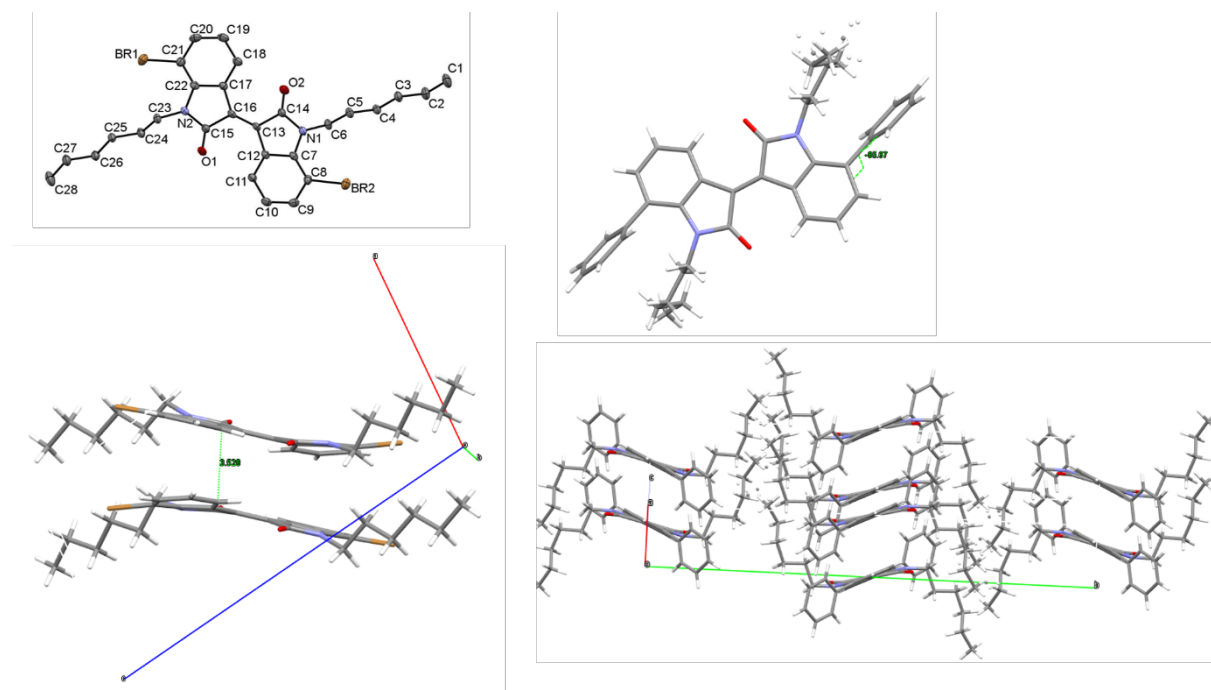


Figure 6. Left: ORTEP representation of compound **4** structure with labeling of atoms (hydrogens are omitted for clarity); molecular packing of compound **4** in the solid-state. Right: ORTEP representation of compound **5**; molecular packing of compound **5** in the solid-state.

2.2.3) UV-visible spectroscopic characterizations.

The photophysical properties of 7,7'-IID derivatives were investigated by UV-Vis spectroscopy. The UV-Vis absorption spectra were recorded in a dilute tetrahydrofuran solution, and the corresponding absorption data of these materials are listed in **Table 1**. All of the investigated D-A-D materials exhibit broad absorptions in the visible spectral region with two distinct absorption bands in the 330–450 nm region and 470–650 nm region. The bands in the high-energy area (330–450 nm) is caused by the π - π^* transition of the donor segments (phenyl and thienyl derivatives) and the bands in the low-energy area (470–650 nm) is caused by the intramolecular charge transfer transition between the donor and acceptor (**Table 1**). Compared to the IID, compound **8**, the introduction of the donor group resulted in a significant red shift of approximately 50 nm for both absorption bands. The corresponding

gap also decreased from 2.03 to 1.88 eV. A bathochromic shift of the low energy absorption is seen when increasing the strength of the donor. Approximately 20-25 nm bathochromic shift of the low energy absorption of the 7,7'-IID with the thienyl donor compared with the phenyl (**Figure 7a**). The high energy absorption band is less affected by the substitution. The absorption spectra of compound **6** and **7** reveal almost identical absorptions in the visible range, indicating that the variation of the alkyl groups on the thiophene has almost no effect on the electronic structure for this series of 7,7'-IID derivatives (**Figure 7b**). These results are similar to the absorption bands of the derivatives substituted at position 5,5' or 6,6', both of them have two absorption bands and their ranges are extremely similar.³⁶ The optical band gap of compound **7** is 1.88 eV, which is very close to the optical band gap of the materials of methyl-thiophene substituted at 6,6' position of IID.³⁹ This again shows that the substitution pattern does not have a significant effect on the absorption bands and the optical band gaps of the materials.

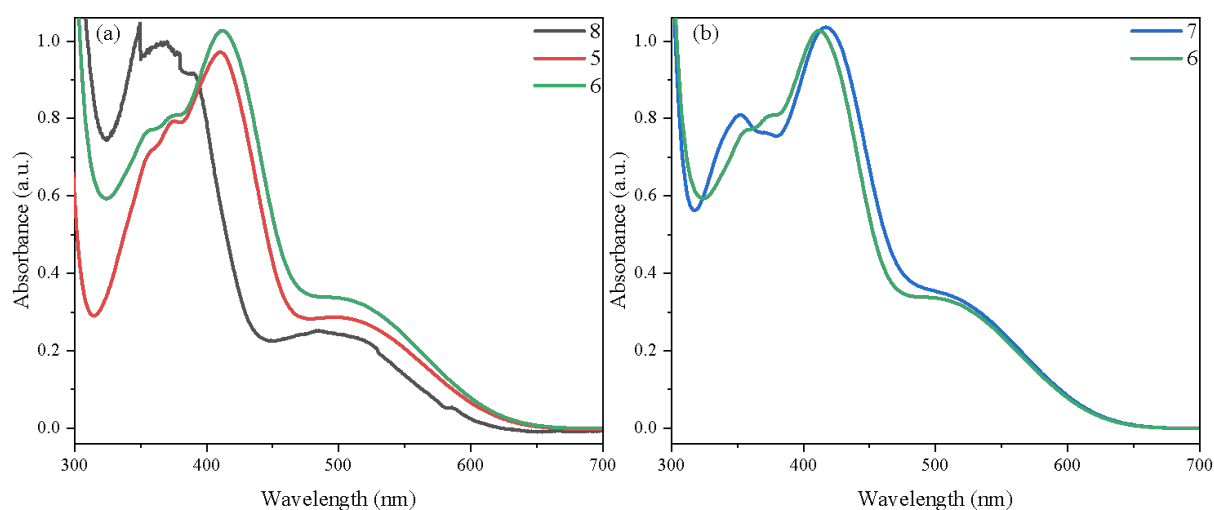


Figure 7. a) Solution UV-vis absorption spectra of **8** (black), **5** (red) and **6** (green). b) Solution UV-vis absorption spectra of **7** (blue) and **6** (green).

Materials	Low energy	High energy	λ_{onset} (nm)	E_g^{opt} (eV)	ϵ ($\text{M}^{-1} \text{cm}^{-1}$)
	$\lambda_{\text{max soln}}$ (nm)	$\lambda_{\text{max soln}}$ (nm)			
Compound 8	484	365	610	2.03	1515
Compound 5	505	408	636	1.95	9353
Compound 6	528	411	655	1.89	4810
Compound 7	530	415	660	1.88	

Table 1. Optical Characteristics of 7,7'-IID-based materials **5-8**.

2.2.4) Electrochemistry study

The redox properties of the synthesized molecules **5-8** were studied by cyclic-voltammetry (CV). CV experiments were performed in the dried DCM solutions of compounds **5-8** (~ 5 mM) and TBAPF₆ as a supporting electrolyte using three electrodes system: glassy carbon electrode as working electrode, Pt electrode as counter electrode and Ag/Ag⁺ as a reference electrode. All molecules showed irreversible oxidation waves in cyclic voltammogram and reversible reduction waves in cathodic region (**Figure 8**). Both compounds show much stronger oxidative peaks than their reductive peaks. The onset oxidation potentials, measured from the CVs were utilized to calculate the Highest Occupied Molecular Orbital (HOMO) levels and the onset reduction potentials to calculate the Low Unoccupied Molecular Orbital of the synthesized molecules. For instance, the introduction of phenyl substituents into the IID scaffold lower the HOMO levels by 0.06 eV, while the energy level of the LUMO does not change significantly. The introduction of thiophene has the most pronounced effect on the HOMO energy level. The energy level of the HOMO was further lower to 5.62 eV by using thiophene substituent. The 7,7'-isoidindigo D-A-D small molecule exhibits a low lying LUMO energy level (3.65 eV) with little change in energy level due to variation in donor strength. In contrast, the HOMO energy level is variable and strongly depends on the electron donor strength of the donor moiety (**Table 2**).

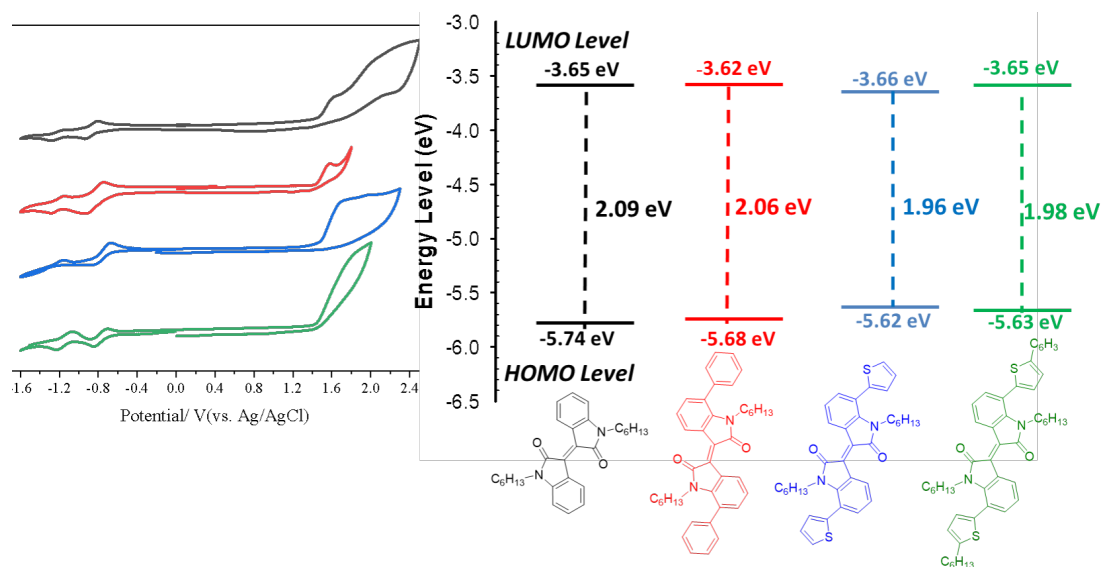


Figure 8. Cyclic voltammograms of 7,7'-IID compounds **8** (black), **5** (red), **6** (blue), **7** (green) in DCM.

Materials	$E_{\text{oxi}}^{\text{onset}}$	HOMO (eV)	E_{red} (eV)	$E_{\text{red}}^{\text{onset}}$ (eV)	LUMO (eV)	E_{g}^{cv} (eV)
Compound 8	1.47	-5.74	-0.96	-0.62	-3.65	2.09
Compound 5	1.41	-5.68	-0.87	-0.64	-3.62	2.06
Compound 6	1.35	-5.62	-0.84	-0.61	-3.66	1.96
Compound 7	1.36	-5.63	-0.85	-0.62	-3.65	1.98

Table 2. Electrochemical and Optical Characteristics of 7,7'-IID based materials **5-8**.

2.3) Conclusion and perspective

In summary, the successful synthesis of three new series of 7,7'-bifunctionalized isoindigo compounds with different electron donor groups has enabled a systematic study of the structure-electron property relationships of this class of materials. Our studies show that the optical and electrochemical properties of these materials can be modulated by peripheral substituents. The introduction of a stronger donor substituent than phenyl (e.g., thiophene) leads to a significant red-shift in absorption. The 7,7'-IID based D-A-D molecule exhibits a low-lying LUMO energy level (3.62-3.66 eV) and little change in energy level due to variation in donor strength. In contrast, the HOMO energy level is variable and strongly depends on the electron donor strength of the donor moiety.

Experimental procedures and Characterization data

7-bromoindoline-2,3-dione (1): Chloral hydrate (2.9 g, 18 mmol, 1.1eq) and Na₂SO₄ (7.4 g, 52 mmol, 3eq) were dissolved in water (40 ml) in a 250 ml round-bottomed flask and warmed to 35 °C. To a warm solution of the 2-bromoaniline (3.0 g, 17.4 mmol, 1eq) in 10 ml water, and an aqueous solution of concentrated HCl (2 ml, 37%) was added: a white precipitate of the amine sulfate was formed, a warm solution of hydroxylamine hydrochloride (3.6 g, 52 mmol, 3 eq) in 60 ml water was ultimately added. The mixture was stirred and heated at 80-85 °C for 2 h and then allowed to cool to room temperature. The suspension was filtered to afford the intermediate isonitrosoacetanilide (compound 1a). Sulfuric acid (50 ml) was heated in a 100 ml flask at 60 °C. The dry isonitrosoacetanilide was added in small portion with stirring over 30 mins so that temperature did not exceed 65 °C. The mixture was then heated to 80 °C for 15 mins, allowed to cool to room temperature. The solid was filtered and dried under vacuum to give **1** as an orange-red solid (1.84 g, 46% yield over two steps). ¹H NMR (300 MHz, DMSO, ppm) δ 11.31 (br, 1H), 7.77 (dd, *J* = 8.5, 3.8 Hz, 1H), 7.50 (d, *J* = 6.9 Hz, 1H), 7.00 (td, *J* = 7.7, 3.7 Hz, 1H). ¹H NMR (300 MHz, CDCl₃, ppm) δ 7.92-7.80 (br, 1H), 7.71 (dt, *J* = 8.2, 1.8 Hz, 1H), 7.59 (d, 1H), 7.06 (td, *J* = 7.8, 2.8 Hz, 1H).

7-bromoindolin-2-one (2): 7-Bromoisatin (2.31 g, 10.2 mmol, 1eq) was suspended in 12 mL methanol, followed by 2.30 g of hydrazine hydrate (25.5 mmol, 35% hydrazine content, 2.5eq) added in one portion. The solution was reflux for 1h. The solution was then cooled in an ice bath and the yellow crystals were filtered. (2.0 g, 84% yields). 0.54g of sodium was dissolved in 13ml of fresh anhydrous ethanol, 2 g of the above hydrazone derivative was added in small portions, with shaking, at 60-70°C. The solution was heated to reflux until the evolution of nitrogen gas has ceased. The brown solution was then poured on ice and acidified to pH = 1 with 10% HCl solution. Filtered and dried under vacuum afforded **2** as a yellow solid (1.4 g, 67% yield over two steps). ¹H NMR (300 MHz, DMSO, ppm) δ 10.61 (s, 1H), 7.33 (d, *J* = 8.3 Hz, 1H), 7.18 (d, *J* = 7.3 Hz, 1H), 6.86 (t, *J* = 7.7 Hz, 1H), 3.60 (s, 2H).

(E)-7,7'-dibromo-[3,3'-biindolinylidene]-2,2'-dione (3): 7-Bromooxindole (1.36 g, 6.4 mmol, 1eq) and 7-bromoisatin (1.45 g, 2.36 mmol, 1eq) were diluted in 40 ml acetic acid. Then the hydrochloric acid (0.25mL) was added to the mixture under argon. The mixture was reflux and stirred overnight. After cooling to room temperature, the solid was filtered and washed with water, ethanol and ethyl acetate. A deep red solid **3** was collected (2.17 g, 85% yield). ¹H NMR (300 MHz, DMSO, ppm) δ 11.22 (s, 2H), 9.02 (d, *J* = 8.1 Hz, 2H), 7.56 (d, *J* = 8.0 Hz, 2H), 6.94 (t, *J* = 8.1 Hz, 2H).

(E)-7,7'-dibromo-1,1'-dihexyl-[3,3'-biindolinylidene]-2,2'-dione (4): Under argon, potassium carbonate (0.08 g, 0.63 mmol, 2.4eq) was dissolved in 5 ml of anhydrous DMF, followed by adding 7,7-

bromoisindigo (0.11 g, 0.26 mmol, 1eq). The mixture was stirred for 20 min at 90 °C before the addition of 1-bromohexane (0.1 g, 0.63 mmol, 2.4eq). The mixture was stirred for 2 h at 100 °C. After the mixture was cooled to room temperature, ethyl acetate was added to extract the product. Then the combined organic layers were concentrated under vacuum and finally purified through column chromatography (chloroform/hexane = 1:3). The product **4** was obtained as a deep red solid (0.15 g, 90% yield). ¹H NMR (300 MHz, CDCl₃, ppm) δ 9.02 (d, *J* = 8.3 Hz, 2H), 7.47 (d, *J* = 7.5 Hz, 2H), 6.88 (t, *J* = 9.0 Hz, 2H), 4.18 (t, *J* = 7.6 Hz, 4H), 1.77-1.64 (m, 4H), 1.42-1.26 (m, 12H), 0.88 (t, 6H). ¹³C NMR (75 MHz, CDCl₃, ppm) δ 167.92, 141.82, 138.50, 133.24, 128.61, 124.87, 123.16, 101.80, 41.73, 31.51, 29.47, 26.34, 22.59, 14.04. HRMS (ESI) calculated for C₂₈H₃₂Br₂N₂O₂: 586.0831; Found: 586.0829.

(E)-1,1'-dihexyl-7,7'-diphenyl-[3,3'-biindolinylidene]-2,2'-dione (**5**): The compound **2** (270 mg, 0.46 mmol), phenylboronic acid (223 mg, 1.82 mmol, 4eq), P(o-tyl)₃ (21 mg, 0.07 mmol) and K₃PO₄ (488 mg, 2.30 mmol, 5eq) were loaded under argon. Toluene (5 mL) and water (0.5 ml) was then added to the flask. After stirring at room temperature for 0.5 h, Pd₂(dba)₃ (40 mg, 0.04 mmol) was added to the flask. The mixture was stirred at reflux for 20 h. The resulting mixture was extracted with ethyl acetate. The organic phase was then washed 3 times with brine and dried with Na₂SO₄. After removal of the solvent, the crude product was purified by column chromatography (chloroform/hexane = 1:1) to afford **5** as a yellow-red solid (220 mg, 82% yield). ¹H NMR (CDCl₃, 400 MHz, ppm) δ 9.09 (dd, *J* = 7.9, 1.3 Hz, 2H), 7.47-7.34 (m, 10H), 7.14 (dd, *J* = 7.7, 1.3 Hz, 2H), 7.03 (t, *J* = 7.8 Hz, 2H), 3.33 (t, 2H). ¹³C NMR (CDCl₃, 100 MHz, ppm) δ 168.85, 141.22, 139.08, 135.83, 133.55, 129.61, 128.55, 128.04, 127.77, 124.98, 123.13, 121.44, 41.92, 31.31, 27.67, 26.09, 22.44, 13.99. HRMS (ESI) calculated for C₄₀H₄₂N₂O₂: 582.3246; Found: 582.3244.

(E)-1,1'-dihexyl-7,7'-di(thiophen-2-yl)-[3,3'-biindolinylidene]-2,2'-dione (**6**): The compound **4** (180 mg, 0.30 mmol), 4,4,5,5-tetramethyl-2-(thiophen-2-yl)-1,3-dioxolane (257 mg, 1.22 mmol, 4eq), P(o-tyl)₃ (14 mg, 0.05 mmol) and K₃PO₄ (324 mg, 1.53 mmol, 5eq) were loaded under argon. Toluene (6 mL) and water (0.5 ml) was then added to the flask. After stirring at room temperature for 0.5 h, Pd₂(dba)₃ (30 mg, 0.03 mmol) was added to the flask. The mixture was stirred at reflux for 20 h. The resulting mixture was extracted with ethyl acetate. The organic phase was then washed 3 times with brine and dried with Na₂SO₄. After removal of the solvent, the crude product was purified by column chromatography (chloroform/hexane = 1:3) to afford **6** as a yellow-red solid (140 mg, 79% yield). ¹H NMR (CDCl₃, 400 MHz, ppm) δ 9.04 (dd, *J* = 8.0, 1.3 Hz, 2H), 7.33 (dd, *J* = 5.1, 1.2 Hz, 2H), 7.17 (dd, *J* = 7.7, 1.3 Hz, 2H), 7.03-7.00 (m, 2H), 6.98-6.97 (m, 2H), 6.94 (t, 2H), 3.37 (t, 4H). ¹³C NMR (CDCl₃, 100 MHz, ppm) δ 168.69, 139.12, 137.16, 129.58, 128.19, 126.75, 126.22, 123.14, 121.22, 116.74, 42.11, 31.37, 28.26, 26.34, 22.48, 14.00.

(E)-1,1'-dihexyl-7,7'-bis (5-hexylthiophen-2-yl)-[3,3'-biindolinylidene]-2,2'-dione (**7**): The compound **4** (110 mg, 0.18 mmol), 2-(5-hexylthiophen-2-yl)-4,4,5,5-tetramethyl-1,3-dioxolane (0.22 mg, 0.75 mmol, 4eq), P(o-tyl)₃ (8 mg, 0.03 mmol) and K₃PO₄ (200 mg, 0.93 mmol, 5eq) were loaded under argon. Toluene (6 mL) and water (0.3 ml) was then added to the flask. After stirring at room temperature for 0.5 h, Pd₂(dba)₃ (16 mg, 0.02 mmol) was added to the flask. The mixture was stirred at reflux for 24 h. The resulting mixture was extracted with ethyl acetate. The organic phase was then washed 3 times with brine and dried with Na₂SO₄. After removal of the solvent, the crude product was purified by column chromatography (chloroform/hexane = 1:4) to afford **7** as a yellow-red solid (93 mg, 68% yield). ¹H NMR (CDCl₃, 400 MHz, ppm) δ 9.01 (dd, *J* = 8.0, 1.3 Hz, 2H), 7.17 (dd, *J* = 7.7, 1.3 Hz, 2H), 6.92 (t, *J* = 7.9 Hz, 2H), 6.75 (d, *J* = 3.4 Hz, 2H), 6.66 (dt, *J* = 3.4, 0.9 Hz, 2H), 3.43 (t, 4H), 2.77 (t, *J* = 7.6 Hz, 4H). ¹³C NMR (CDCl₃, 100 MHz, ppm) δ 168.71, 146.98, 137.19, 136.25, 133.40, 129.36, 127.82, 123.60, 123.12, 121.15, 117.36, 42.12, 31.82, 31.57, 31.43, 30.11, 28.82, 28.31, 26.44, 22.60, 22.55, 14.10, 14.02.

7-bromo-1-hexylindoline-2,3-dione (**9**): To an oven-dried flask, compound **1** (0.92 g, 4.10 mmol, 1eq) and K₂CO₃ (0.68 g, 4.90 mmol, 1.2eq) were dissolved in 15 ml of anhydrous dimethylformamide. The mixture was heated for 20 mins to reflux and 0.70 ml (4.90 mmol, 1.2eq) of 1-bromohexane was added via syringe. The mixture was stirred at reflux for 24 h. After the mixture was cooled to room temperature, ethyl acetate was added to extract the product. Then the combined organic layers were concentrated under vacuum and finally purified through column chromatography (chloroform/hexane = 1:2) to afford **9** as orange-red oil. (77% yield). ¹H NMR (CDCl₃, 300 MHz, ppm) δ 7.70 (dd, *J* = 8.1, 1.3 Hz, 1H), 7.58 (dd, *J* = 7.3, 1.3 Hz, 1H), 6.98 (t, 1H), 4.16 – 4.09 (t, 2H), 1.73-1.62 (m, 2H), 1.46-1.27 (m, 6H), 0.90 (t, 3H).

1-hexyl-7-phenylindoline-2,3-dione (**10**): The compound **9** (330 mg, 1.06 mmol), phenylboronic acid (160 mg, 1.28 mmol, 1.2eq) and KF (290 mg, 5.0 mmol, 4.8 eq) were loaded under argon. MeOH (6 mL) was then added via syringe. After stirring at room temperature for 0.5 h, Pd(OAc)₂ (4%) was added to the flask. The mixture was stirred at reflux overnight. The resulting mixture was extracted with ethyl acetate. The organic phase was then washed 3 times with brine and dried with Na₂SO₄. After removal of the solvent, the crude product was passed through a short pad of silica gel to afford **10** as orange-red oil. (67% yield). ¹H NMR (CDCl₃, 300 MHz, ppm) δ 7.63 (dd, *J* = 7.4, 1.5 Hz, 1H), 7.45 (m, 3H), 7.41 – 7.33 (m, 3H), 7.12 (t, *J* = 7.6 Hz, 1H), 3.34 – 3.25 (t, 2H).

4-bromoindoline-2,3-dione (**11**): Procedure a) synthesis of isonitrosoacetanilide: Chloral hydrate (4.5 g, 27 mmol) and Na₂SO₄ (12 g, 84 mmol) were dissolved in water (60 ml) in a 250ml three-neck flask and warmed to 35 °C. To a warm solution of the 3-bromoaniline (4.2 g, 24 mmol) in 15 ml water, an aqueous solution of concentrated HCl (3.0 ml) was added: a white precipitate of the amine sulfate was formed,

a warm solution of hydroxylamine hydrochloride (5.5g, 79 mmol) in 25ml water was ultimately added. The mixture was stirred and heated at 80-85 °C for 2 h and then allowed to cool to room temperature. The suspension was filtered to afford the intermediate isonitrosoacetanilide (compound 11a). The crude product was directly used in the next step without further purification. Procedure b) synthesis of 4-bromoindoline-2,3-dione. Sulfuric acid (50 ml) was heated in a 100 ml flask at 60 °C. The dry isonitrosoacetanilide was added in small portion with stirring over 30 mins so that temperature did not exceed 65 °C. The mixture was then heated to 80 °C for 15 mins, allowed to cool to room temperature. The solid was filtered and dried under vacuum to give a mixture of 4-bromoisatin and 6-bromoisatin. Dissolved the mixture in a solution of NaOH (0.72 g) in 7.2 ml water at 60 °C and then acidified with acetic acid (15 ml). The solid was filtered and dried under vacuum to give **11** as an orange solid (43% yields over two step). ¹H NMR (DMSO-d₆, 300 MHz, ppm) δ 7.46 (t, J = 8.0 Hz, 1H), 7.23 (d, J = 8.0 Hz, 1H), 6.89 (d, J = 7.8 Hz, 1H).

4-bromoindolin-2-one (12): 4-Bromoisatin (0.5 g, 2.2 mmol) was suspended in 10 mL methanol, followed by 0.94 g of hydrazine hydrate (18 mmol, 35% hydrazine content) added in one portion. The solution was reflux for one hour. The solution was then cooled in an ice bath and the yellow crystals were filtered. (0.47 g, 90% yield). 0.54g of sodium was completely dissolved in 10ml of fresh anhydrous ethanol, 2 g of the above hydrazone derivative was added in small portions, with shaking, at 60-70°C. The solution was heated to reflux until the evolution of nitrogen gas has ceased. The brown solution was then carefully poured on ice and acidified to pH = 1 with 10% HCl solution. The solid was filtered and dried under vacuum to give **12** as a yellow solid (0.22 g, 48% yields over two steps). ¹H NMR (δ, ppm) (300 MHz, DMSO, ppm) δ 10.61 (s, 1H), 7.10 (m, 2H), 6.81 (m, 1H), 3.39 (s, 2H), 2.59 (s, 2H). ¹³C NMR (75 MHz, DMSO, ppm) δ 175.30, 145.33, 130.08, 126.94, 124.20, 118.49, 108.79, 37.48.

4-bromo-1-hexylindoline-2,3-dione (13): To an oven-dried flask, compound 11 (1.0 g, 4.42 mmol) and K₂CO₃ (0.73 g, 5.28 mmol) were dissolved in 15 ml of anhydrous dimethylformamide. The mixture was heated for 30 mins to reflux and 0.74 ml (5.27 mmol) of 1-bromohexane was added via syringe. The mixture was stirred at reflux for 24 h. After the mixture was cooled to room temperature, ethyl acetate was added to extract the product. Then the combined organic layers were concentrated under vacuum and finally purified through column chromatography to give **13** as an orange-red solid. (89% yield). ¹H NMR (CDCl₃, 300 MHz, ppm) δ 7.40 (t, J = 8.0, 1H), 7.26-7.24 (m, 1H), 6.84 (d, J = 7.9, 1H), 3.72 (t, J = 7.4, 2H), 1.74-1.61 (m, 2H), 1.45-1.25 (m, 6H), 0.90 (t, 3H). ¹³C NMR (CDCl₃, 75 MHz, ppm) δ 180.77, 156.95, 152.39, 138.78, 127.95, 120.93, 115.76, 109.41, 40.19, 31.22, 27.05, 26.39, 22.41, 13.92.

4-bromo-1-hexylindolin-2-one (14): 4-bromo-1-hexylindoline-2,3-dione (0.91 g, 2.93 mmol) was suspended in 15 mL methanol, followed by hydrazine hydrate added in one portion. The solution was heated to reflux until the evolution of nitrogen gas has ceased. The brown solution was then poured on

ice and acidified to pH = 1 with 10% HCl solution. The solid was filtered and dried under vacuum to give **14** as a yellow solid (0.7 g, 82% yield over two steps). ¹H NMR (CDCl₃, 300 MHz, ppm) δ 7.20-7.07 (m, 2H), 6.76 (m, 1H), 3.66 (t, 2H), 3.47 (s, 1H), 1.68-1.58 (m, 2H), 1.34-1.26 (m, 6H), 0.88 (s, 3H).

1-hexyl-4-phenylindoline-2,3-dione (15): The compound 13 (156 mg, 0.50 mmol), phenylboronic acid (73 mg, 0.60 mmol, 1.2eq) and KF (139 mg, 2.4 mmol, 4.8 eq) were loaded under argon. MeOH (6 mL) was then added via syringe. After stirring at room temperature for 0.5 h, Pd(OAc)₂ (4%) was added to the flask. The mixture was stirred at reflux overnight. The resulting mixture was extracted with ethyl acetate. The organic phase was then washed 3 times with brine and dried with Na₂SO₄. After removal of the solvent, the crude product was passed through a short pad of silica gel to afford **15** as an orange solid (74% yield). ¹H NMR (CDCl₃, 300 MHz, ppm) δ 7.58 (t, *J* = 7.9 Hz, 1H), 7.55 – 7.48 (m, 2H), 7.48 – 7.41 (m, 3H), 7.07 (d, *J* = 7.9 Hz, 1H), 6.86 (d, *J* = 7.9 Hz, 1H), 3.75 (t, *J* = 7.4 Hz, 2H), 1.77-1.67 (m, 2H), 1.40-1.31 (m, 6H), 0.91 (t, 3H).

1-hexyl-4-phenylindoline-2,3-dione (16): The compound 13 (390 mg, 1.25 mmol), trihexyl(thiophen-2-yl) stannane (446 mg, 1.25 mmol) were loaded under argon. 10 ml of DMF was then added via syringe.. Using 4% of the catalyst Pd(dppf)Cl₂. The mixture was stirred at reflux for 24 h. The resulting mixture was extracted with ethyl acetate. The organic phase was then washed 3 times with brine and dried with Na₂SO₄. After removal of the solvent, the crude product was purified by column chromatography (chloroform/hexane = 1:2) to afford **16** as an orange-red solid (67% yield). ¹H NMR (CDCl₃, 300 MHz, ppm) δ 8.12 (d, *J* = 3.7 Hz, 1H), 7.55 (t, *J* = 8.0 Hz, 1H), 7.48 (d, *J* = 5.1 Hz, 1H), 7.32 (d, *J* = 8.2 Hz, 1H), 7.20 (t, *J* = 4.5 Hz, 1H), 6.80 (d, *J* = 7.8 Hz, 1H), 3.78 (d, *J* = 7.4 Hz, 2H), 1.73 (t, *J* = 7.4 Hz, 2H), 1.37 – 1.27 (m, 6H), 0.92 (d, *J* = 6.5 Hz, 3H). ¹³C NMR (CDCl₃, 75 MHz, ppm) δ 181.80, 157.67, 152.07, 138.23, 137.66, 135.75, 130.34, 128.27, 128.09, 124.68, 108.34, 40.29, 31.40, 27.26, 26.57, 22.51, 13.98.

Reference

- (1) Kim, G.; Kang, S.-J.; Dutta, G. K.; Han, Y.-K.; Shin, T. J.; Noh, Y.-Y.; Yang, C. A thienoisindigo-naphthalene polymer with ultrahigh mobility of $14.4 \text{ cm}^2/\text{V} \cdot \text{s}$ that substantially exceeds benchmark values for amorphous silicon semiconductors. *Journal of the American Chemical Society* **2014**, *136* (26), 9477-9483, DOI: 10.1021/ja504537v.
- (2) Gao, Y.; Zhang, X.; Tian, H.; Zhang, J.; Yan, D.; Geng, Y.; Wang, F. High Mobility Ambipolar Diketopyrrolopyrrole-Based Conjugated Polymer Synthesized Via Direct Arylation Polycondensation. *Advanced Materials* **2015**, *27* (42), 6753-6759, DOI: 10.1002/adma.201606217.
- (3) Shi, K.; Zhang, W.; Gao, D.; Zhang, S.; Lin, Z.; Zou, Y.; Wang, L.; Yu, G. Well-balanced ambipolar conjugated polymers featuring mild glass transition temperatures toward high-performance flexible field-effect transistors. *Advanced Materials* **2018**, *30* (9), 1705286, DOI: 10.1002/adma.201705286.
- (4) Liao, S.-F.; Lu, C.-F.; Fenta, A. D.; Chen, C.-T.; Chao, C.-Y.; Su, W.-F. High face-on ratio isoindigo copolymers with extended nano-fibrillar networks in fullerene-based thick ($>300 \text{ nm}$) photovoltaics achieving a high efficiency of 10.7%. *Journal of Materials Chemistry A* **2019**, *7* (37), 21309-21320, DOI: 10.1039/C9TA06719A.
- (5) Liu, S.; Firdaus, Y.; Thomas, S.; Kan, Z.; Cruciani, F.; Lopatin, S.; Bredas, J. L.; Beaujuge, P. M. Isoindigo-3,4-Difluorothiophene Polymer Acceptors Yield "All-Polymer" Bulk-Heterojunction Solar Cells with over 7% Efficiency. *Angew Chem Int Ed Engl* **2018**, *57* (2), 531-535, DOI: 10.1002/anie.201709509.
- (6) Lu, C.-F.; Liao, S.-F.; Chen, I.-F.; Chen, C.-T.; Chao, C.-Y.; Su, W.-F. Detecting Minute Chemical Vapors via Chemical Interactions between Analyte and Fluorinated Thiophene-Isoindigo Conjugated Polymer Transistor. *ACS Applied Electronic Materials* **2019**, *1* (9), 1873-1880, DOI: 10.1021/acsaelm.9b00396.
- (7) Wang, Y.; Zeglio, E.; Liao, H.; Xu, J.; Liu, F.; Li, Z.; Maria, I. P.; Mawad, D.; Herland, A.; McCulloch, I.; Yue, W. Hybrid Alkyl-Ethylene Glycol Side Chains Enhance Substrate Adhesion and Operational Stability in Accumulation Mode Organic Electrochemical Transistors. *Chemistry of Materials* **2019**, *31* (23), 9797-9806, DOI: 10.1021/acs.chemmater.9b03798.
- (8) Wang, X.; Zhao, F.; Xue, Z.; Yuan, Y.; Huang, M.; Zhang, G.; Ding, Y.; Qiu, L. Highly Sensitive Polymer Phototransistor Based on the Synergistic Effect of Chemical and Physical Blending in D (Donor)-A (Acceptor) Copolymers. *Advanced Electronic Materials* **2019**, *5* (6), 1900174, DOI: 10.1002/aelm.201900174.
- (9) Zhao, X.; Madan, D.; Cheng, Y.; Zhou, J.; Li, H.; Thon, S. M.; Bragg, A. E.; DeCoster, M. E.; Hopkins, P. E.; Katz, H. E. High conductivity and electron-transfer validation in an n-type fluoride-anion-doped polymer for thermoelectrics in air. *Advanced Materials* **2017**, *29* (34), 1606928, DOI: 10.1002/adma.201606928.

- (10) Stalder, R.; Mei, J.; Graham, K. R.; Estrada, L. A.; Reynolds, J. R. Isoindigo, a versatile electron-deficient unit for high-performance organic electronics. *Chemistry of Materials* **2014**, *26* (1), 664-678, DOI: 10.1021/cm402219v.
- (11) Wang, E.; Mammo, W.; Andersson, M. R. 25th Anniversary Article: Isoindigo-Based Polymers and Small Molecules for Bulk Heterojunction Solar Cells and Field Effect Transistors. *Advanced Materials* **2014**, *26* (12), 1801-1826, DOI: 10.1002/adma.201304945.
- (12) Li, J. L.; Cao, J. J.; Duan, L. L.; Zhang, H. L. Evolution of Isoindigo-Based Electron-Deficient Units for Organic Electronics: From Natural Dyes to Organic Semiconductors. *Asian Journal of Organic Chemistry* **2018**, *7* (11), 2147-2160, DOI: 10.1002/ajoc.201800198.
- (13) Randell, N. M.; Kelly, T. L. Recent advances in isoindigo-inspired organic semiconductors. *The Chemical Record* **2019**, *19* (6), 973-988, DOI: 10.1002/tcr.201800135.
- (14) Wei, X.; Zhang, W.; Yu, G. Semiconducting Polymers Based on Isoindigo and Its Derivatives: Synthetic Tactics, Structural Modifications, and Applications. *Advanced Functional Materials* **2021**, 2010979, DOI: 10.1002/adfm.202010979.
- (15) Sonar, P.; Tan, H.-S.; Sun, S.; Lam, Y. M.; Dodabalapur, A. Isoindigo dye incorporated copolymers with naphthalene and anthracene: promising materials for stable organic field effect transistors. *Polymer Chemistry* **2013**, *4* (6), DOI: 10.1039/c2py20942j.
- (16) Gang, W.; Haijun, T.; Yiping, Z.; Yingying, W.; Zhubin, H.; Guipeng, Y.; Chunyue, P. Series of D- π -A system based on isoindigo dyes for DSSC: Synthesis, electrochemical and photovoltaic properties. *Synthetic Metals* **2014**, *187*, 17-23, DOI: 10.1016/j.synthmet.2013.09.039.
- (17) Sassatelli, M.; Saab, E.; Anizon, F.; Prudhomme, M.; Moreau, P. Synthesis of glycosyl-isoindigo derivatives. *Tetrahedron Letters* **2004**, *45* (25), 4827-4830, DOI: 10.1016/j.tetlet.2004.04.167.
- (18) Bouchikhi, F.; Anizon, F.; Moreau, P. Synthesis and antiproliferative activities of isoindigo and azaisoindigo derivatives. *Eur J Med Chem* **2008**, *43* (4), 755-62, DOI: 10.1016/j.ejmech.2007.05.012.
- (19) Liao, H.; Xiao, C.; Ravva, M. K.; Wang, Y.; Little, M.; Jenart, M. V.; Onwubiko, A.; Li, Z.; Wang, Z.; Brédas, J.-L. Synthesis and properties of isoindigo and benzo [1, 2-b: 4, 5-b'] bis [b] benzothiophene oligomers. *Chemical Communications* **2018**, *54* (79), 11152-11155, DOI: 10.1039/C8CC05608K.
- (20) El-Kateb, A.; Hennawy, I.; Shabana, R.; Osman, F. Thiation reactions. III. Thiation of certain dicarbonyl compounds. *Phosphorus and sulfur and the related elements* **1984**, *20* (3), 329-332, DOI: 10.1080/03086648408077642.
- (21) Bergman, J.; Romero, I. Synthesis of α -oxo-sulfines in the indole series. *Journal of Heterocyclic Chemistry* **2010**, *47* (5), 1215-1220, DOI: 10.1002/jhet.453.
- (22) Bogdanov, A. V.; Mironov, V. F.; Musin, L. I.; Buzykin, B. I.; Konovalov, A. I. Isatin derivatives in the reaction with phosphorous hexaethyltriamide. A new approach to the synthesis of isoindigo derivatives. *Russian Journal of General Chemistry* **2008**, *78* (10), 1977-1979, DOI: 10.1134/s1070363208100277.

- (23) Stalder, R.; Mei, J.; Reynolds, J. R. Isoindigo-Based Donor–Acceptor Conjugated Polymers. *Macromolecules* **2010**, *43* (20), 8348-8352, DOI: 10.1021/ma1018445.
- (24) Pouliot, J.-R.; Grenier, F.; Blaskovits, J. T.; Beaupré, S.; Leclerc, M. Direct (Hetero)arylation Polymerization: Simplicity for Conjugated Polymer Synthesis. *Chemical Reviews* **2016**, *116* (22), 14225-14274, DOI: 10.1021/acs.chemrev.6b00498.
- (25) Elsway, W.; Lee, C. L.; Cho, S.; Oh, S. H.; Moon, S. H.; Elbarbary, A.; Lee, J. S. Isoindigo-based small molecules for high-performance solution-processed organic photovoltaic devices: the electron donating effect of the donor group on photo-physical properties and device performance. *Phys Chem Chem Phys* **2013**, *15* (36), 15193-203, DOI: 10.1039/c3cp52151f.
- (26) Mei, J.; Graham, K. R.; Stalder, R.; Reynolds, J. R. Synthesis of isoindigo-based oligothiophenes for molecular bulk heterojunction solar cells. *Organic Letters* **2010**, *12* (4), 660-663, DOI: 10.1021/ol902512x.
- (27) Ren, Y.; Hailey, A. K.; Hiszpanski, A. M.; Loo, Y.-L. Isoindigo-containing molecular semiconductors: effect of backbone extension on molecular organization and organic solar cell performance. *Chemistry of Materials* **2014**, *26* (22), 6570-6577, DOI: 10.1021/cm503312c.
- (28) Wang, E.; Ma, Z.; Zhang, Z.; Henriksson, P.; Inganäs, O.; Zhang, F.; Andersson, M. R. An isoindigo-based low band gap polymer for efficient polymer solar cells with high photo-voltage. *Chemical Communications* **2011**, *47* (17), 4908-4910, DOI: 10.1039/C1CC11053E.
- (29) Wang, E.; Ma, Z.; Zhang, Z.; Vandewal, K.; Henriksson, P.; Inganäs, O.; Zhang, F.; Andersson, M. R. An Easily Accessible Isoindigo-Based Polymer for High-Performance Polymer Solar Cells. *Journal of the American Chemical Society* **2011**, *133* (36), 14244-14247, DOI: 10.1021/ja206610u.
- (30) Lei, T.; Cao, Y.; Fan, Y.; Liu, C.-J.; Yuan, S.-C.; Pei, J. High-performance air-stable organic field-effect transistors: isoindigo-based conjugated polymers. *Journal of the American Chemical Society* **2011**, *133* (16), 6099-6101, DOI: 10.1021/ja111066r.
- (31) Grenier, F.; Berrouard, P.; Pouliot, J.-R.; Tseng, H.-R.; Heeger, A. J.; Leclerc, M. Synthesis of new n-type isoindigo copolymers. *Polymer Chemistry* **2013**, *4* (6), 1836-1841, DOI: 10.1039/c2py20986a.
- (32) Phelan, N. F.; Orchin, M. Cross conjugation. *Journal of Chemical Education* **1968**, *45* (10), 633, DOI: 10.1021/ed045p633.
- (33) Limacher, P. A.; Lüthi, H. P. Cross-conjugation. *Wiley Interdisciplinary Reviews: Computational Molecular Science* **2011**, *1* (4), 477-486, DOI: 10.1002/wcms.16.
- (34) Ganguly, A.; Zhu, J.; Kelly, T. L. Effect of Cross-Conjugation on Derivatives of Benzoisoindigo, an Isoindigo Analogue with an Extended π -System. *The Journal of Physical Chemistry C* **2017**, *121* (17), 9110-9119, DOI: 10.1021/acs.jpcc.7b00742.
- (35) van Pruissen, G. W.; Brebels, J.; Hendriks, K. H.; Wienk, M. M.; Janssen, R. A. Effects of Cross-Conjugation on the Optical Absorption and Frontier Orbital Levels of Donor–Acceptor Polymers. *Macromolecules* **2015**, *48* (8), 2435-2443, DOI: 10.1021/acs.macromol.5b00046.

- (36) Estrada, L. A.; Stalder, R.; Abboud, K. A.; Risko, C.; Brédas, J.-L.; Reynolds, J. R. Understanding the Electronic Structure of Isoindigo in Conjugated Systems: A Combined Theoretical and Experimental Approach. *Macromolecules* **2013**, *46* (22), 8832-8844, DOI: 10.1021/ma4013829.
- (37) Ren, Y.; Hiszpanski, A. M.; Whittaker-Brooks, L.; Loo, Y.-L. Structure–Property Relationship Study of Substitution Effects on Isoindigo-Based Model Compounds as Electron Donors in Organic Solar Cells. *ACS applied materials & interfaces* **2014**, *6* (16), 14533-14542, DOI: 10.1021/am503812f.
- (38) Ashizawa, M.; Hasegawa, T.; Kawauchi, S.; Masunaga, H.; Hikima, T.; Sato, H.; Matsumoto, H. Influence of structure–property relationships of two structural isomers of thiophene-flanked diazaisoindigo on carrier-transport properties. *RSC Advances* **2016**, *6* (111), 109434-109441, DOI: 10.1039/c6ra17424h.
- (39) Elsayy, W.; Lee, C.-L.; Cho, S.; Oh, S.-H.; Moon, S.-H.; Elbarbary, A.; Lee, J.-S. Isoindigo-based small molecules for high-performance solution-processed organic photovoltaic devices: the electron donating effect of the donor group on photo-physical properties and device performance. *Physical Chemistry Chemical Physics* **2013**, *15* (36), 15193-15203, DOI: 10.1039/c3cp52151f.

Joint experimental and theoretical study of the optical and electrochemical properties of bis-2-(2-oxindolin-3-ylidene) malononitrile derivatives

3.1) Introduction

Bis-lactam-based organic materials are of particular interest owing to their strong electron-withdrawing nature,^{1,2} which facilitates strong intermolecular interactions through the dipolar carbonyl groups. Many experimental and theoretical works have highlighted that efficient charge transport properties arose from a delocalized low lying LUMO level, which facilitates electron injection, and stabilizes injected electrons.³ Based on the bis-lactam design strategies, various novel electron-deficient building blocks for high performance organic semiconductors have recently been reported.⁴⁻⁵ Among these materials, isatin (1H-indole-2, 3- dione) and its dicyanovinyl derivatives⁶ are synthetic precursors of many natural products and promising n-type organic materials⁷⁻⁸ because of their planar framework with two electron-withdrawing carbonyl groups.⁹ However, to date only few studies have reported the use of those building blocks to construct active channel materials for transistors. Thus, Kuo and co-workers reported the synthesis and molecular design of three di-2-(2-oxindolin-3-ylidene) malononitrile derivatives (**I-1a**, **I-1b** and **I-1c**, **Figure 1a**) with various numbers of nitrogen substituents on the phenyl rings for use as OFET-materials.¹⁰ All three derivatives had a short π - π distance of 3.31 Å for face-to-face column stacking, which was favorable for charge transfer between molecules. These columns were connected by hydrogen bonds between the nitrogen in the cyano-functional group and the hydrogen on the six-membered ring. They demonstrated that through selective introduction of nitrogen atoms on phenyl moieties, the LUMO energy level can be fine-tuned from -4.02 eV for unsubstituted to -4.16 eV for disubstituted derivative. The nitration of the benzene ring on these derivatives not only reduced the LUMO level but also enhanced the coplanarity of the molecule, which resulted in a moderate electron mobility of 0.059 cm² V⁻¹ s⁻¹ under ambient conditions. However, the replacement of a phenyl ring with a pyridine had a slightly effect on the absorption spectrum. These derivatives exhibited three main bands in their solution UV-visible spectrum at 280–290, 360–402, and 530–548 nm, respectively.

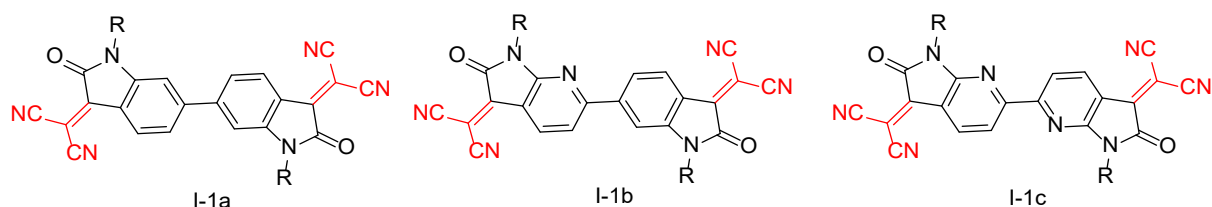


Figure 1a. Chemical structures of bis-lactam-based organic materials reported in the literature.

The same group reported the synthesis, characterization, and OFET performance of two derivatives of angular-shaped naphthalene bisisatin (**I-2**, **Figure 1b**) core, using the Martinet isatin synthesis.¹¹⁻¹² These new derivatives had a low-lying LUMO level, lower than that of previously

reported, which made them suitable for air-stable n-type OFETs. A single crystal was grown by the solvent vapor diffusion method. Molecules exhibited one-dimensional face-to-face stacking with a short π - π distance of 3.4 Å. Under ambient conditions, the maximum of electron mobility of vapor-deposited thin films was $0.63 \text{ cm}^2 \text{ V}^{-1} \text{ s}^{-1}$. OFETs measurements showed that the nature of the N-alkyl chains affects the value of the mobility of charge and the device performance. A structural analogue to angular-shaped naphthalene bis-isatin, where the naphthalene core was replaced with a phenyl group (**I-3**), was recently reported.¹³ Benzodipyrrole-2,6-dione-3,7-diylidenedimalononitrile derivatives were synthesized and tested as air-stable n-type OFET materials. The electrochemical behavior of these derivatives was investigated by cyclic voltammetry (CV). The CV spectra of all compounds showed well-defined reversible reduction waves. The LUMO levels were estimated at -4.42 eV. Both derivatives exhibited one-dimensional columnar π -stacking structures parallel to the crystallographic a-axis with very short π - π distances of 3.28 Å. OFET devices fabricated by vapor deposition, provided an electron mobility up to $0.131 \text{ cm}^2 \text{ V}^{-1} \text{ s}^{-1}$ under ambient conditions. Thienoisatin in which the phenyl ring of the isatin core was replaced by a thiophene ring, was one of the most important structural variations of isatin. It was widely used as precursor for the synthesis of thienoisindigo, which had recently emerged as a promising building unit for π -conjugated polymers, owing to strong sulfur–oxygen interactions, which induced better co-planarity of the π -conjugated backbone. Based on this assumption, Mori *et al.* synthesized bsthienoisatins and the dicyanomethylene derivatives (**I-4**) that had much stronger electron deficiency than the isatin parent.¹⁴ The crystals showed uniform stacking structures, but the packing pattern of the stacks varied depending on the alkyl chains. The resulting materials showed a low LUMO of -4.28 eV and a short π - π staking distance of 3.68 Å. These features made these materials promising for use in thin-film OFETs, with electron mobility of $0.2 \text{ cm}^2 \text{ V}^{-1} \text{ s}^{-1}$.

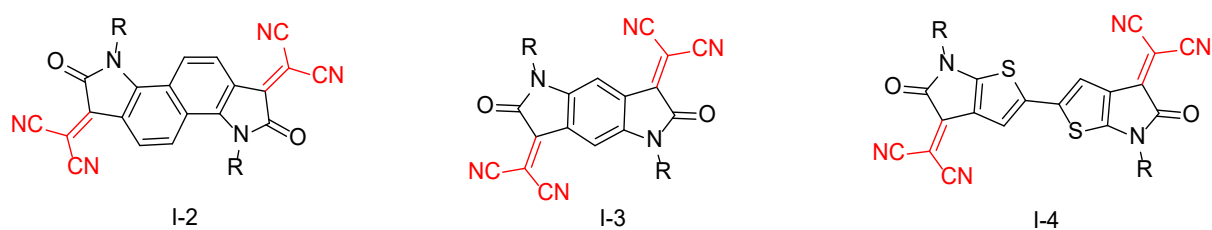


Figure 2b. Chemical structures of bis-lactam-based organic materials reported in the literature.

Fused rings derivatives as bridging groups were another research direction for this class of materials. Zhang and co-workers recently reported two series of isatin derivatives with a rigid indacenodithieno [3,2-b] thiophene moiety (IDTT) as a central bridge and both ends capped with electron-withdrawing isatin (**I-5a**, **Figure 1c**). In a second series the phenyl group was replaced by pyridine ring (**I-5b**).¹⁵ The replacement of phenyl rings with pyridine units enhanced the planarity and structural ordering by non-covalent interactions, leading to a dramatic impact on the mobility of the charge carriers. The unsubstituted molecule based on isatin did not show any field-effect behavior, whereas molecule based on azaisatin showed excellent unipolar p-type behavior with hole mobility of

$7.7 \text{ cm}^2 \text{ V}^{-1} \text{ s}^{-1}$. A series of materials based on indacenodithiophene (IDT) as a bridging group were synthesized and opto-electric properties were investigated by Zhao *et al.*¹⁶⁻¹⁷ Compound **I-5c** in chloroform solution showed a major absorption peak at 540 nm, and this absorption band was significantly red-shifted from compound **I-5c**, **I-5d** (674 nm) to **I-5e** (733 nm). The corresponding optical band gaps of **I-5c**, **I-5d** and **I-5e** were also reduced from 1.95 eV to 1.48 eV and 1.43 eV, respectively. Compared with **I-5c**, the LUMO energy level of **I-5d** was significantly lower to -4.02 eV, which was due to the fact that the LUMO energy level of the receptor varied enormously depending on the strength of the electron withdrawing moieties. On the other hand, **I-5e** exhibited an identical LUMO energy level as **I-5d**, and its thiophene analogue had a more pronounced effect on the HOMO energy level of the material. The solar cell devices based on the acceptor **I-5e** and the polymeric electron donor PTB7-Th achieved moderate performances with a maximum power conversion efficiency of 1.97%.

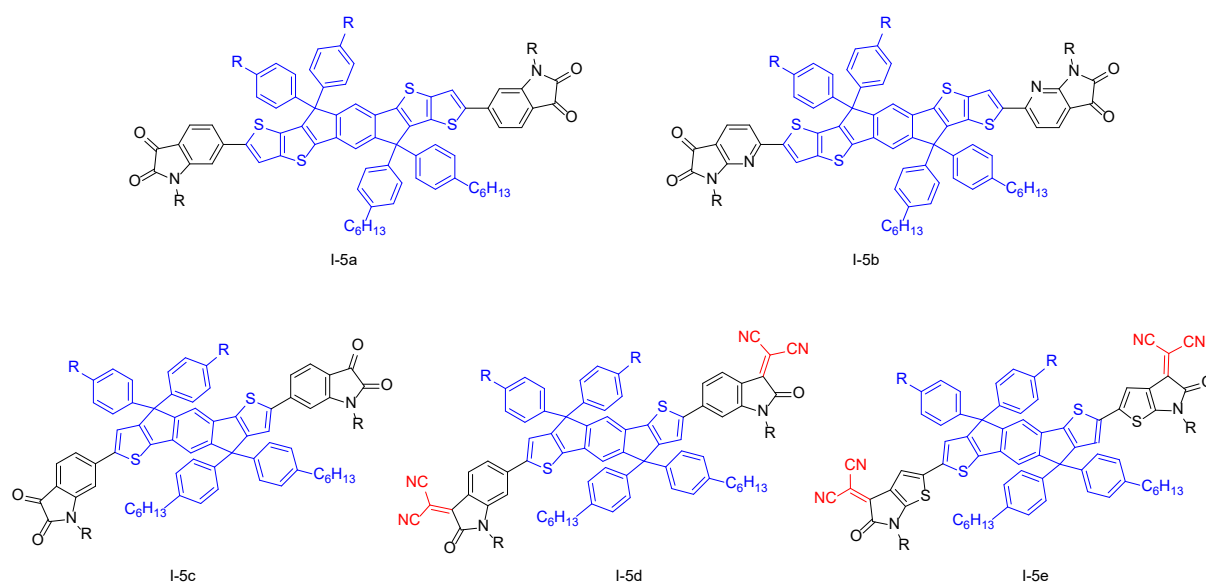


Figure 1c. Chemical structures of bis-lactam-based organic materials reported in the literature.

In summary, the literature related to the bis-isatin and dicyano derivatives, as building blocks for the design and synthesis of n-type and ambipolar organic semiconductors, has been reviewed. The early interest in this kind of molecules is related to their applications as high-performance materials for organic electronics. While there are a few examples of this family of molecules, no systematic study has been performed on the effect of the conjugation length and the mode of connectivity on their photophysical and electrochemical properties.

Objectives of this study

In this work we explore the design, and synthesis of a set of small molecules with A-D-A architecture (A: acceptor; D: donor) based on π -conjugated bridge, with different π -bridge lengths, as a donor unit, and two isatylidene malononitrile segments as terminal acceptor groups (see **Figure 2**). Our

objective is to vary the conjugation length by different spacer groups and to alter the linkage position of the isatylidene malononitrile group (position 4 vs. position 6), to analyze the effect on its structural, photophysical, and electrochemical properties.

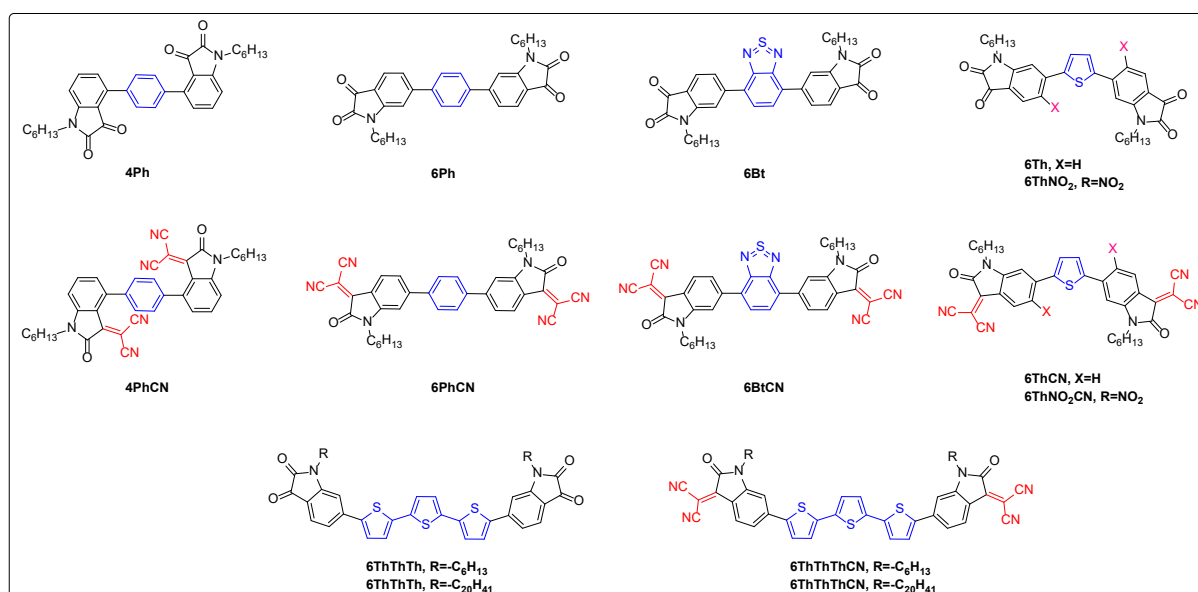


Figure 2. Chemical structures of bi-isatin and bis-isatin-CN compounds.

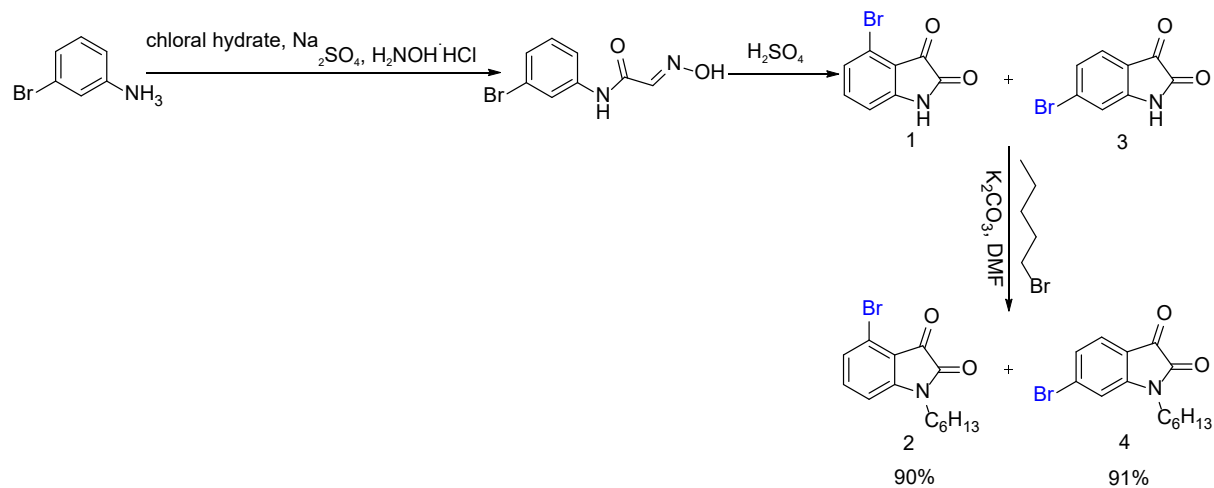
3.2) Results and discussion

We first describe the synthesis routes developed. Subsequently, we discuss the structure property relationships within these molecules, using different physical characterizations such as UV-visible spectroscopy, electrochemistry techniques, and a combination of theoretical calculation (density functional theory, TD-DFT) and energy level calculation.

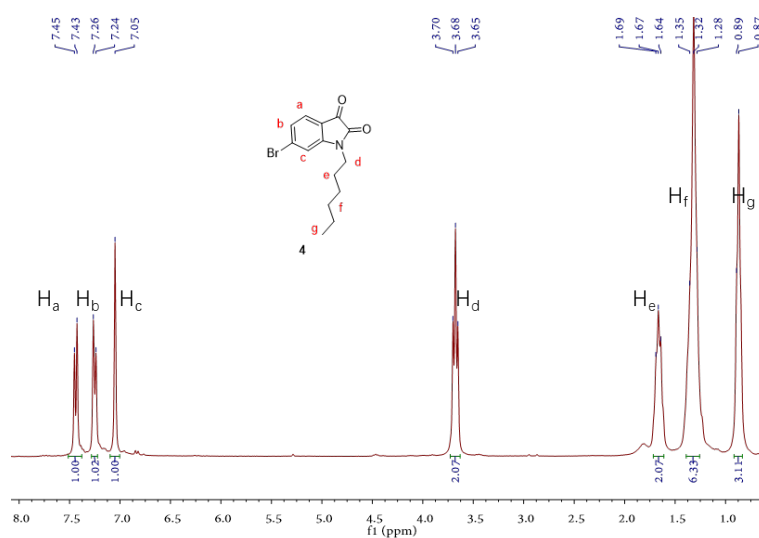
3.2.1) Synthetic methodology

Isatin molecule and its derivatives are versatile moieties that display diverse biological and pharmacological properties.¹⁸⁻¹⁹ Isatin is also as building blocks for functional organic materials.²⁰ The isatin skeleton contains an amide functional group linked to an aromatic ring via an EWG C₃ ketone functional group. The C₃ ketone is orthogonally reactive with respect to the C₂ carbonyl amide and its derivatization occurs relatively easily. The desired bromoisatins were synthesized through a two-step procedure, using the corresponding commercial 3-bromoanilines as starting materials.²¹ In the first step, bromo-aniline was reacted with chloral hydrate and hydroxylamine hydrochloride to afforded the corresponding bromo-isonitrosoacetanilide. This intermediate was then ring-closed in concentrated sulfuric acid to give a mixture of 4- and 6- bromoisatin. The separation of the two isatine-isomers have been carried out by converting them into the corresponding sodium isatinate using 0.5 mol L⁻¹ NaOH,

followed by controlled acidification of the reaction medium, leading to the regeneration of the corresponding bromisatin by cycling the two isomers at different pH values, and ultimately precipitated from the reaction medium (**Scheme 1**). Detailed synthetic procedures are elucidated in the experimental section.

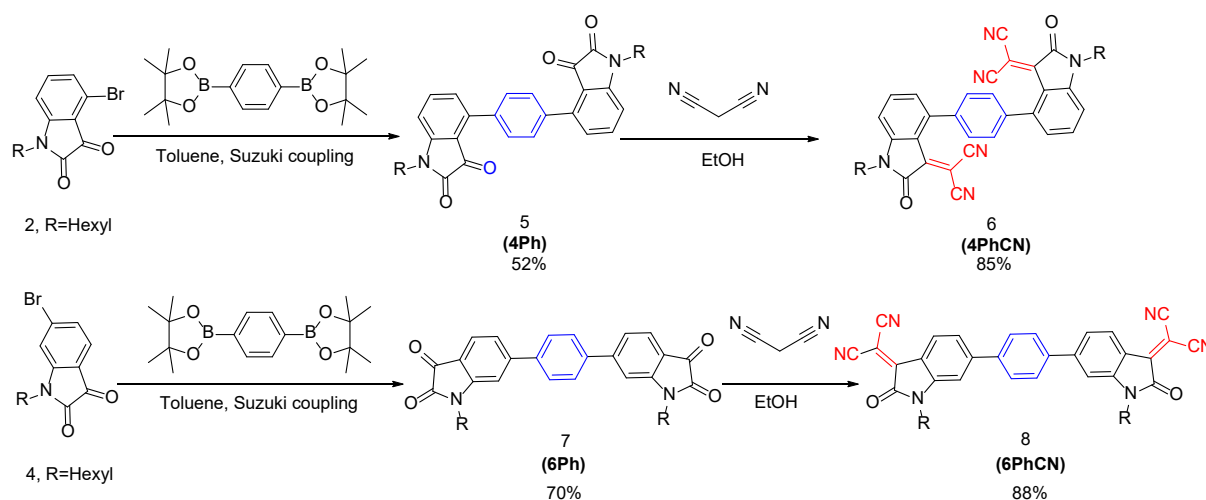


To overcome the solubility issue, we introduced alkyl side-chain, hexyl or long branched alkyl, to substitute (4 or 6) bromoisatin at the nitrogen atom. 4 or 6-Bromoisatin was reacted with 1-bromohexane in anhydrous DMF containing K_2CO_3 as a base under nitrogen atmosphere, to produce **2** or **4** in excellent yield (Scheme 1). Analysis of the 1H NMR spectra of N-hexyl 6-bromoisatin (**4**) showed a triplet peak of H_d at 3.68 ppm, assigned to the two protons on the carbon bounded to isatinic nitrogen (**Figure 3**).²²⁻²³



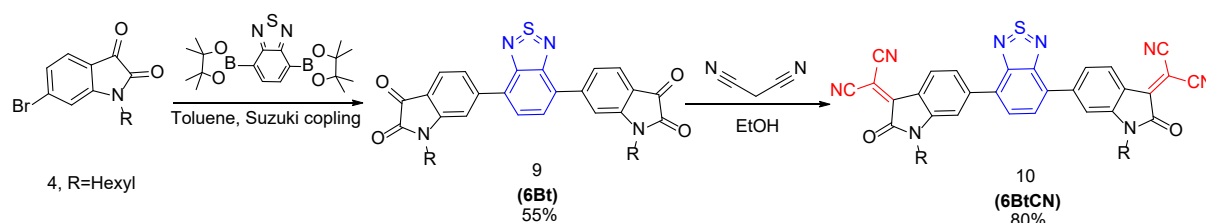
The alkylated 4 or 6-bromoisatin **2** and **4** were further reacted with 1,4-benzenediboronic acid bis(pinacol) ester, in the presence of $Pd_2(dba)_3$ as a catalyst, and K_3PO_4 as the base, to afford **5** and **7** in

52% and 70% yield, respectively. Subsequently, the bis-isatin compound **5** and **7** were treated with malononitrile via a Knoevenagel condensation reaction to generate the target products **6** and **8**, respectively (**Scheme 2**).²⁴



Scheme 2. Synthesis of bis-isatin **5**, **7** and bis-isatin-CN compounds **6**, **8**.

Replacement of phenyl with electron withdrawing benzo[*c*] [1,2,5] thiadiazole (Bt) was targeted to analyse the effect of π -bridge. The synthesis of the target compounds **9** and **10** is presented in **Scheme 3**. The Suzuki-Miyaura reaction was chosen to perform the coupling compound **4** with benzo[*c*] [1,2,5] thiadiazole²⁵ to afford **9** in a 55% yield. A similar Knoevenagel condensation reaction condition was applied to obtain the target product **10** with 80% yield.



Scheme 3. Synthesis of bis-isatin **9** and bis-isatin-CN compounds **10**.

The NMR spectra of bis-isatin **9** and bis-isatin-CN compounds **10** are compared on **Figure 4**. The H_c proton produces the most downfield signal (8.30 ppm) owing to the large deshielding effect of the neighboring -CN moiety. However, no chemical shift is observed for the other three peaks, after Knoevenagel condensation reaction.

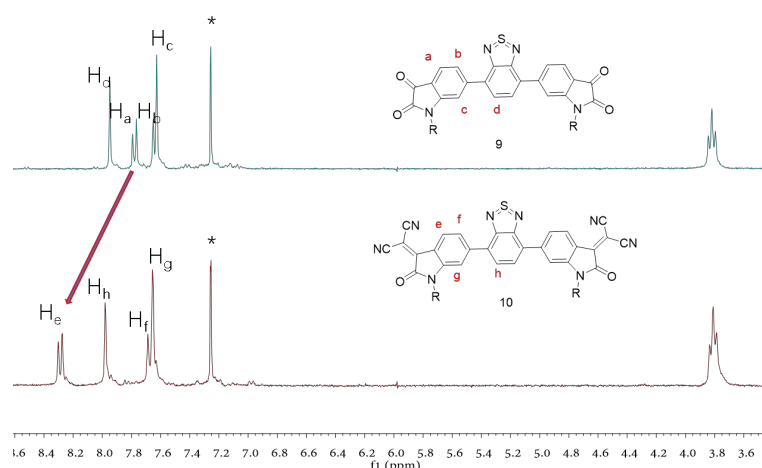
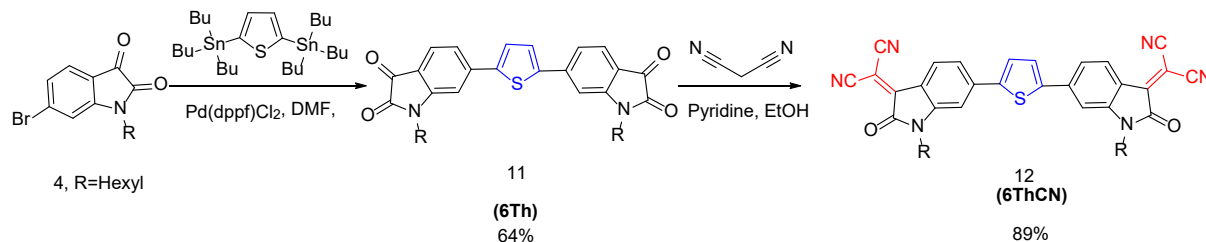


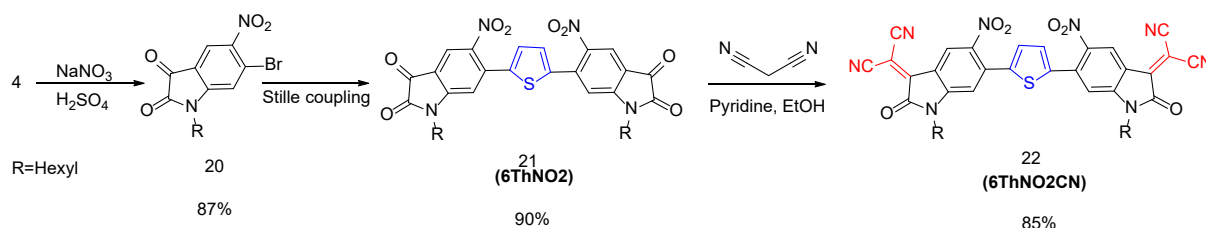
Figure 4. ^1H NMR spectrum comparison between **9** (top) and **10** (bottom), (*: solvent peak).

The choice of the π bridge is relatively limited and thiophene (Th) is one of the most used electron-rich building block for constructing semiconducting materials.²⁶ The Stille coupling reactions²⁷ between compounds **4** and 2,5-di-(tributylstannyl)-thiophene in the presence of $\text{Pd}(\text{dppf})\text{Cl}_2$ as a catalyst resulted in compound **11** with a 64% yield. Using a catalytic amount of base, such as pyridine, the Knoevenagel condensation reaction can occur at room temperature.¹⁶ The compound **12** was obtained with a yield of 89%. (**Scheme 4**).



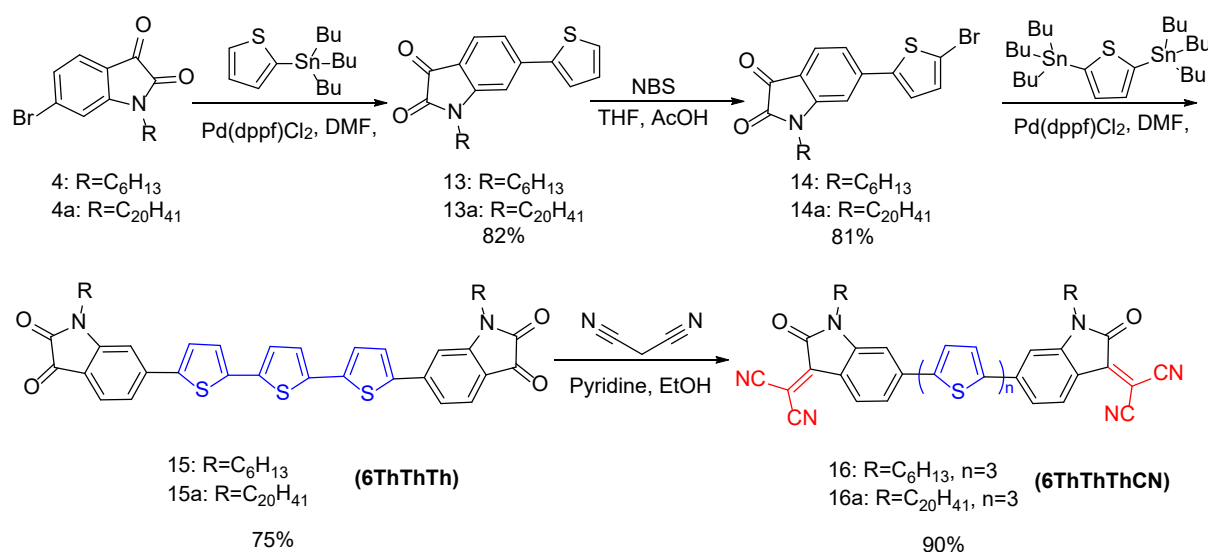
Scheme 4. Synthesis of bis-isatin **11** and bis-isatin-CNs compounds **12**.

Nitro derivatives of isatin have various medical applications²⁸ and the organic electronic application of this type of material is also worth studying. Herein, the nitro group is introduced at the position 5 of isatin, and the alkylation reaction is used to increase the solubility of compound **20**. Further Stille coupling introduced thiophene as the bridging unit of compound **21**. The synthetic target **22** was obtained through Knoevenagel condensation (**Scheme 5**).



Scheme 5. Synthesis of bis-isatin **21** and bis-isatin-CNs compounds **22**.

To extend the conjugation length between the two isatin moieties, ter-thiophene²⁹ was connected to the isatin fragment (**Scheme 6**). Reaction of 2-tributylstannylthiophene with the compound **4** under Stille coupling conditions produced the asymmetrical dye **13** in 80% yield. Selective bromination at 5-position of thiophene using the N-Bromosuccinimide, afforded the intermediate **14**.³⁰ The obtained bromo thieryl-isatin was then coupled to the 2,5-di-(tributylstannyl)-thiophene to form bis-isatin-terthienyl **15**. As previously discussed, introducing branched alkyl chains greatly improves the solubility of the final product leading to consider the synthesis of a terthiophene-isatin derivative with branched alkyl chains (Compound **15a**). NMR spectrum shows four doublet peaks and two singlet peaks in the aromatic part, plus one doublet at 3.63 ppm belonging to N-CH₂, which means that the product is highly symmetrical (Compound **16a**). The downfield shift of the Ha proton reveals the deshielding effect of the CN moiety (**Figure 5**).



Scheme 6. Synthesis of bis-isatin **15**, **15a** and bis-isatin-CN compounds **16**, **16a**.

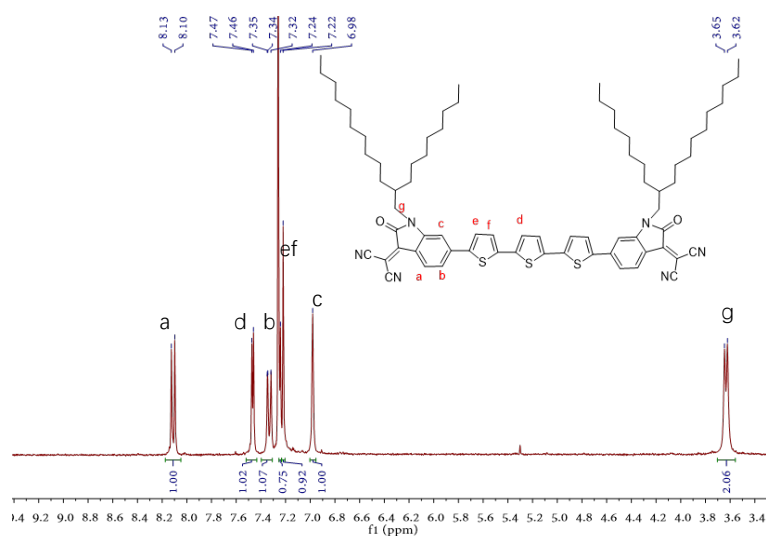


Figure 5. ¹H NMR spectrum of compound **16a**.

3.2.2) UV-visible absorption spectroscopy

The photophysical properties of bis-isatin and isatyridene malononitrile derivatives were investigated by UV-vis spectroscopy. The UV-vis absorption spectra of bis-isatin and isatyridene malononitrile derivatives were recorded in a dilute tetrahydrofuran solution (THF). The corresponding absorption data of these materials are listed in **Table 1**. For comparison purposes between bis-isatin-CNs and bis-isatin derivatives, the absorption spectra of bis-isatin and their derivatives, 4PhCN, 6PhCN, 6BtCN, 6ThCN, 6ThNO₂CN, and 6ThThThCN are also included in **Figure 6**. All these spectra share a common feature, two absorption bands in the UV-visible region, which can be assigned to a π - π^* transition of the π -conjugated backbone and charge transfer transition between the π -conjugated bridge and end-group acceptor. The position of these bands is strongly influenced by the molecular structure of the compounds, the type of π bridge and the end-group acceptor (**Table 1**). The low energy band in the visible region is attributed to the charge transfer transition arising from the acceptor moieties while the high energy band in the range of 430–650 nm is attributed to the π - π bridge. The influence of the nature of the acceptor group is demonstrated by comparison of the absorption maxima of compounds **11** and **12**, as both transitions, (i.e., the longest and lowest wavelength transitions) shifted from 440 nm and 393 nm for 6Th to 550 nm and 457 nm for 6ThCN (**Figure 6c**). A bathochromic shift of ca. 110 nm of the longest wavelength is observed when the isatin ring is replaced by an isatyridene malononitrile ring. In general, a bathochromic shift of ca. 80 nm is observed from bis-isatin to bis-isatin-CNs series because of the gradual increase in the electron-withdrawing capacity of the acceptor moieties of these molecules (see **Figure 6a-d**).

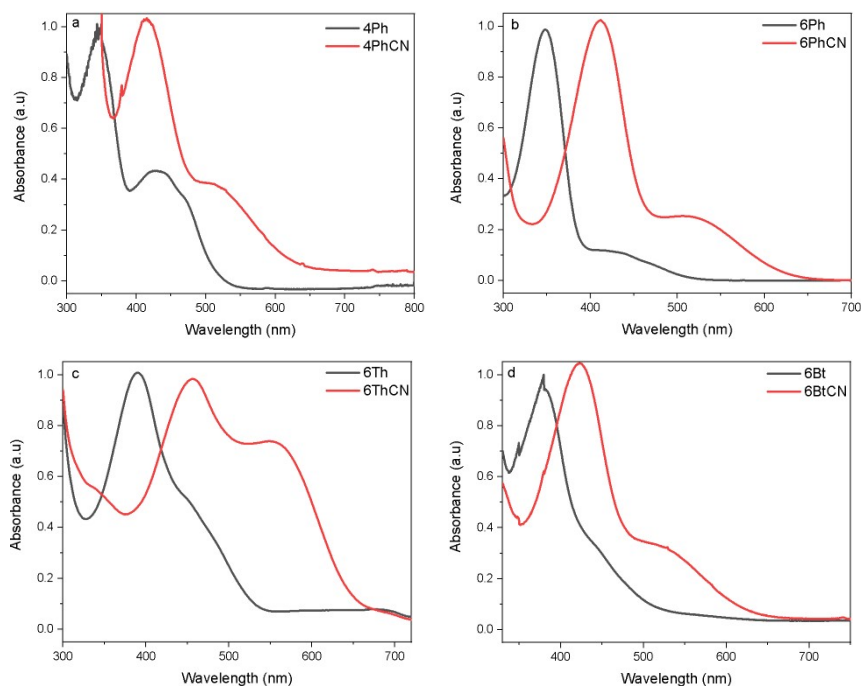


Figure 6. Bathochromic shifts observed in the solution UV-Vis spectra when comparing a series of bis-isatin to the corresponding bis-isatin-CNs ones.

There is no significant difference of the main absorption bands for the materials with phenyl rings at position 4 or 6 of the isatin core (**Figure 6e-f**), probably because they are both linearly conjugated. In addition, the possible steric hindrance of the chemical structure has always limited the introduction of a large aromatic ring at position 4 of isatin derivatives. Here, a phenyl ring was successfully introduced and a similar optical performance was achieved.

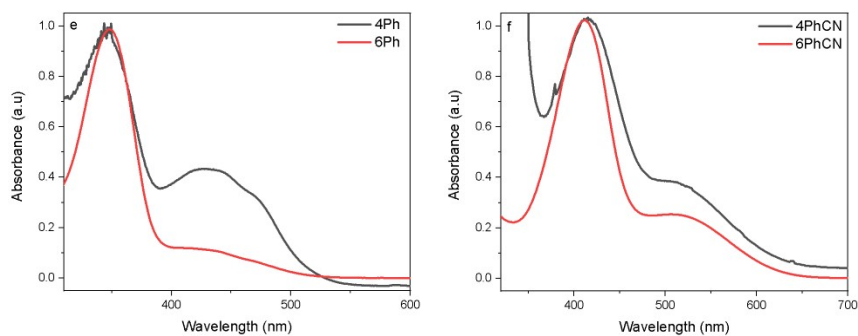


Figure 6. Solution UV-vis absorption spectra of **5** vs. **7**, and **6** vs. **8**.

Comparison of the absorption spectra of 6Ph ($\lambda_{\text{max}}=349$ nm) with 6Th ($\lambda_{\text{max}}=393$ nm) reveals that the replacement of a phenyl ring with a thiophene one causes a red shift of the high energy bands (see **Figure 6g**). This observation clearly indicates that the incorporation of a thiophene moiety in donor-acceptor structures enhances their charge-transfer properties.³¹ This trend is also pronounced in the dicyano bis-isatin, a bathochromic shift of 43 nm is observed for high energy band (see **Figure 6h**). As shown in **Figure 6g-2**, 6Th and 6Bt have very similar absorption bands, although there is a red shifted absorption of ca. 10 nm compared to 6Bt. The bathochromic shift phenomenon is more pronounced after the introduction of the dicyano group, and the red shift at both low energy and high energy is ca. 30 nm. More importantly, compared with 6PhCN and 6BtCN, the ratio of absorption bands at high wavelengths is significantly increased, that is, the peak at 550 nm is more intensive for 6ThCN in **Figure 6g-3**. This inspired us to further modify the thiophene unit and increase the number of thiophene rings to change the properties of the material.

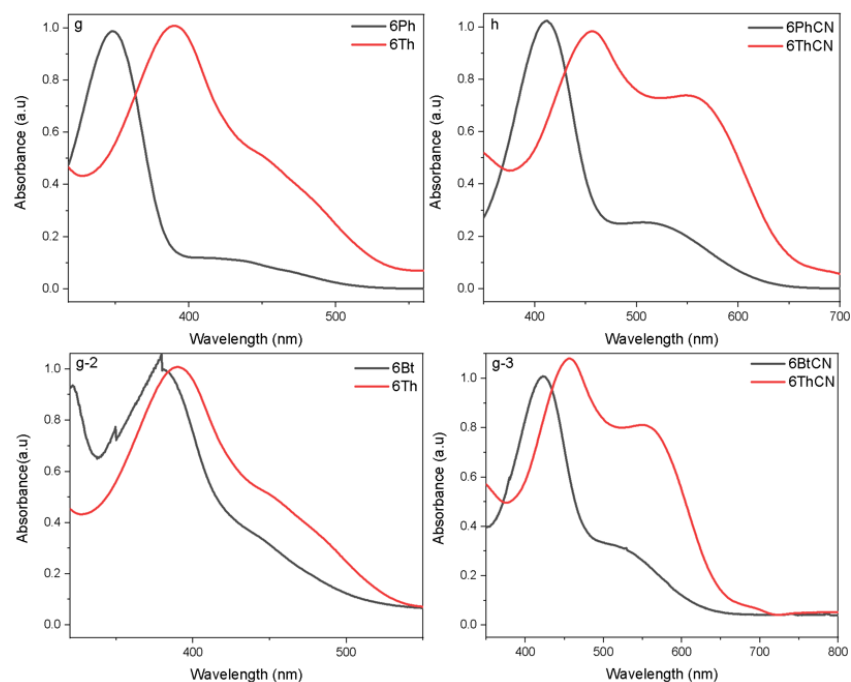


Figure 6. Solution UV-vis absorption spectra of **7** vs. **11**, **8** vs. **12**, **9** vs. **11**, and **10** vs. **12**.

The main absorption band is red-shifted to 605 nm with increasing the number of thiophene units, with an onset of absorption at 758 nm and a band gap of 1.63 eV (**Figure 6i**). The smaller band gap of 6ThThThCN compared to 6PhCN (1.97 eV for 6PhCN) suggests stronger intramolecular charge transfer properties due to the effective charge transfer from the thiophene unit to the acceptor moieties. On the other hand, the absorption spectra of compound **16** and **16a** (**Figure 6j**) display almost identical absorptions in the visible range, indicating that changes in the alkyl group on the nitrogen atom have almost no effect on the electronic structure of the isatylidene malononitrile derivatives.

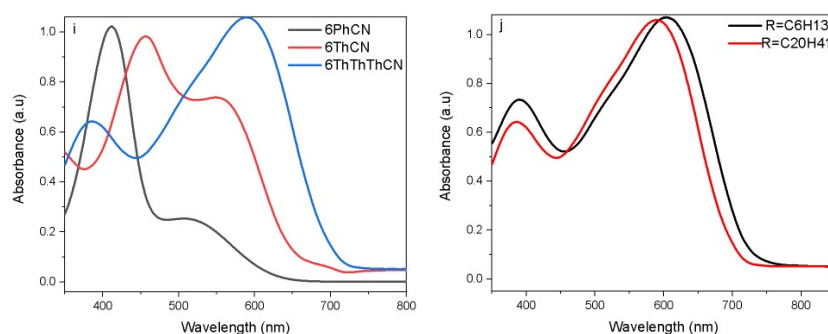


Figure 6. Solution UV-vis absorption spectra of **8** vs. **12** vs. **16**, and **16** vs. **16a**.

For both series (i.e., bis-isatin and isatylidene malononitrile derivatives), the absorption spectra show that the absorption bands originating from the aromatic bridges are gradually red-shifted to the longer wavelengths with increasing the π -conjugation length. This can be rationalized by better intramolecular π - π interactions when enlarging the π -conjugated system. In the bis-isatin series, the

lowest-energy bands have low extinction coefficients compared to that of the high-energy ones. The high energy absorption bands are associated with the π - π^* transitions of the π -bridges. Meanwhile, the lowest-energy absorption bands can be assigned to the intramolecular charge transfer (ICT) between the π -bridge donor part and the acceptor end groups. Compared with bis-isatin derivatives, isatyridene malononitrile derivatives exhibit rather large bathochromic shifts (18, 17 and 55 nm, respectively) of their absorption maxima, which is attributed to the introduction of electron-accepting dicyanovinyl end groups, leading to a π -conjugated A-D-A system. The optical gap of the bis-isatin derivative is ca. 2.20 eV, while the optical gap of the isatyridene malononitrile series is lowered to approximately 1.90 eV, with the lowest optical gap of 1.63 eV for compound **16**.

Compound **22** has an absorption maximum at 432 nm, which is 25 nm blue-shifted compared with 6ThCN (see **Figure 6k**), which can be attributed to the steric hindrance of the nitro group. The band gap of 6ThNO₂CN calculated from the onset absorption in the solution is 1.93 eV, which has a larger band gap than 6ThCN (1.85 eV for 6ThCN).

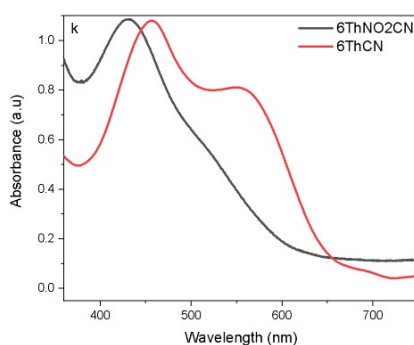


Figure 6. k) Solution UV-vis absorption spectra of **12** vs. **22**.

Table 1. Summary of optical properties of bis-isatin and isatyridene malononitrile derivatives.

Compounds	$\lambda_{\max}^{\text{sol}}$ (nm) ^a	$\lambda_{\text{onset}}^{\text{sol}}$ (nm) ^a	E_g^{opt} (eV) ^b
4Ph	430, 347	530	2.34
4PhCN	514, 415	628	1.97
6Ph	434, 349	532	2.33
6PhCN	515, 414	630	1.97
6BT	440, 380	546	2.27
6BTCN	533, 423	651	1.90
6Th	440, 393	553	2.24
6ThCN	550, 457	670	1.85
6ThNO ₂ CN	520, 432	642	1.93
6ThThTh	462	586	2.11
6ThThThCN	605, 383	758	1.63

^aIn tetrahydrofuran. ^b $E_g^{\text{opt}} = 1240 / \lambda_{\text{onset}}$ is the optical energy gap estimated from the absorption onset in THF solution.

3.2.3) Electrochemical Study

The electrochemical behavior of bis-isatin and isatylidene malononitrile derivatives was investigated by cyclic voltammetry (CV) using tetrabutylammonium perchlorate as supporting electrolyte in dichloromethane (DCM). From the onset potential of the first reduction wave, the E_{LUMO} were estimated from, $E_{\text{LUMO}} \text{ (eV)} = -4.80 - [(E_{\text{Red}}(\text{onset})) - E_{1/2}(\text{ferrocene})]$. The electrochemical data of these materials are listed in **Table 2**. The cyclic voltammograms of the bis-isatin derivatives show, one oxidation wave and two well-reversible reduction waves (**Figure 7** left). The reduction potentials were found to be dependent on the bis-isatin structure. The first reduction wave is attributed to the formation of an anion-radical specie, as has been observed previously in linear conjugated molecules and polymers. The second reduction wave is ascribed to the reduction of the anion-radical into its corresponding dianion. In the oxidation process only one oxidation wave was observed. The CV of isatylidene malononitrile derivatives under the same condition showed also two sets of reductions, but shifted to more positive values than the ones of the parent compound, bis-isatin (see the right panel of **Figure 7**). For example, compound **6** (4PhCN), $E_{\text{red1}} = -0.61 \text{ V}$ (vs. Ag/AgCl) compared compound **5** (4Ph) to $E_{\text{red1}} = -1.11 \text{ V}$ (vs Fc/Fc+), thus leading to a shift of 0.50 V. The LUMO level was determined by the nature of different type of acceptor core.

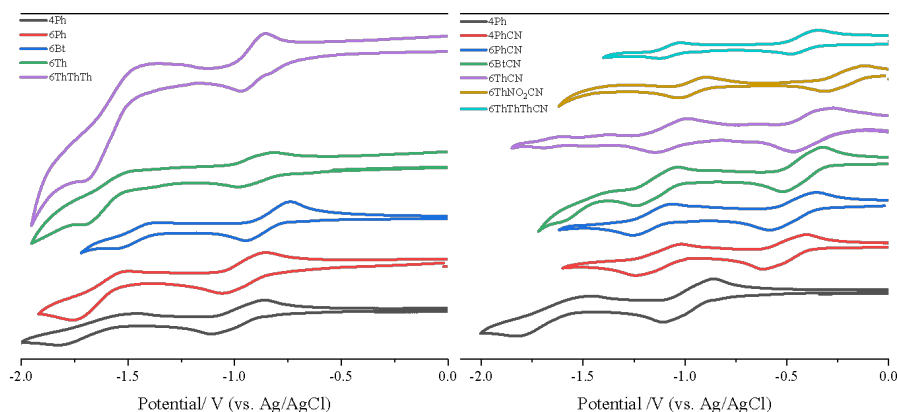


Figure 7. Cyclic voltammograms of bis-isatin to bis-isatin-CN series in DCM.

Regardless of the nature of the end-group substituents, both reduction potentials follow the trend $\text{Ph} < \text{Bt} < \text{Th}$. For instance, the first reduction process of the isatylidene malononitrile families, the thiophene or benzothiadiazole is easier to reduce than the phenyl (-0.46, -0.52 vs. -0.58 V, **Table 2**), though the difference in reduction potential is less than 0.15 V, this small change is indicative of a minor contribution of the flanking aryl groups to the LUMO (**Figure 8**). On the other hand, compounds **11** (6Th) and **15** (6ThThTh) (or compounds **12** to **16**) with one thiophene and ter-thiophene unit as bridging groups respectively have very close LUMO energy levels (**Figure 9**). Changing the π -conjugate length of the bridge or increasing donor strength has a more pronounced effect on its HOMO energy level than on the LUMO energy level. Compound **22** (6ThNO₂CN) functionalized with two nitro groups (NO₂)

and two CNs groups has a low lying LUMO energy level and the LUMO energy of this small molecule family can be easily adjusted from -3.54 eV (6Th) to -4.23 eV, apparently due to the fact that nitro is one of the strongest EWG groups.

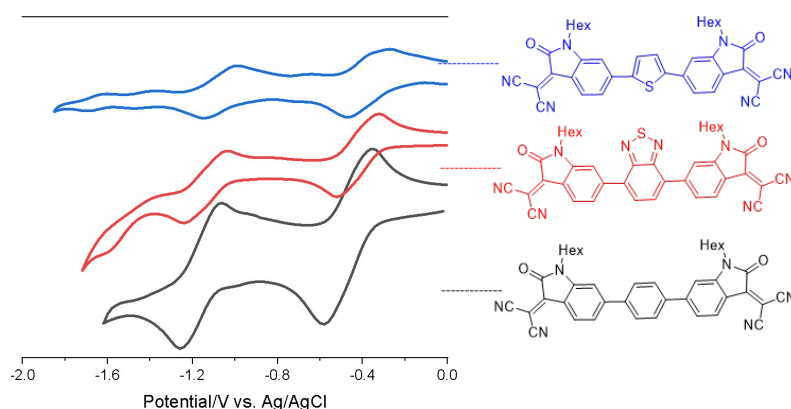


Figure 8. Cyclic voltammograms of bis-isatin-CNs series in DCM.

Table 2.

Summary of electrochemical properties of bis-isatin and isatylidene malononitrile derivatives.

Compounds	E_{red1} (eV)	E_{red}^{onset} (eV)	E_{LUMO} (eV) ^c	E_{HOMO} (eV) ^d	E_g^{cv} (eV) ^e
4Ph	-1.11	-0.87	-3.40	-5.46	2.06
4PhCN	-0.61	-0.36	-3.91	-5.92	2.01
6Ph	-1.03	-0.81	-3.46	-5.52	2.06
6PhCN	-0.58	-0.34	-3.93	-5.87	1.94
6BT	-0.93	-0.74	-3.53	-5.53	2.00
6BTCN	-0.52	-0.29	-3.98	-5.82	1.84
6Th	-0.94	-0.73	-3.54	-5.35	1.81
6ThCN	-0.46	-0.19	-4.08	-5.80	1.88
6ThNO ₂ CN	-0.30	-0.04	-4.23	-5.96	1.73
6ThThTh	-0.95	-0.71	-3.56	-5.11	1.55
6ThThThCN	-0.47	-0.24	-4.03	-5.23	1.20

^cEstimated vs vacuum level from $E_{LUMO} = -4.80 \text{ eV} - [(E_{Red}^{onset}) - E_{1/2}(\text{ferrocene})]$. ^dEstimated vs vacuum level from $E_{HOMO} = -4.80 \text{ eV} - [(E_{ox}^{onset}) - E_{1/2}(\text{ferrocene})]$. ^e E_g = electrochemical gap.

As shown in **Table 2**, the LUMO levels of bis-isatin are lying at ca. -3.50 eV and the LUMO of isatylidene malononitrile derivatives are located at ca. -4.0 eV. The deep LUMO levels of isatylidene malononitrile family can be attributed to the strong electron-withdrawing properties of the dicyanovinylene group. From the LUMO levels and the optical gaps, the highest occupied molecular orbital (HOMO) levels of bis-isatin and isatylidene malononitrile derivatives are estimated to be slightly above -5.50 and -5.90 eV, respectively (except compound 6ThNO₂CN, 6ThThTh, 6ThThThCN). Changing the linkage position of the isatylidene malononitrile group (position 4 to position 6) has a small effect on the HOMO and LUMO energy levels, with a slightly higher HOMO energy level of 0.05 eV and a slightly lower LUMO energy level of ca. 0.02 eV for 6PhCN compared to that of 4PhCN. The HOMO energy level of 6ThCN is 0.07 eV higher than that of 6PhCN, which is caused by the stronger

electron donating ability of thiophene. In addition, the HOMO energy level of 6Th is significantly higher than that of 6Bt or 6Ph (5.35 vs 5.53 or 5.52 eV, **Table 2**) within the bis-isatin series, which also indicates the strong electron donor properties of thiophene. The HOMO level of compound **16** or **16a** were much higher than one thiophene or one phenyl unit bridged compounds. The resulted HOMO-LUMO gaps decrease to 1.20 eV.

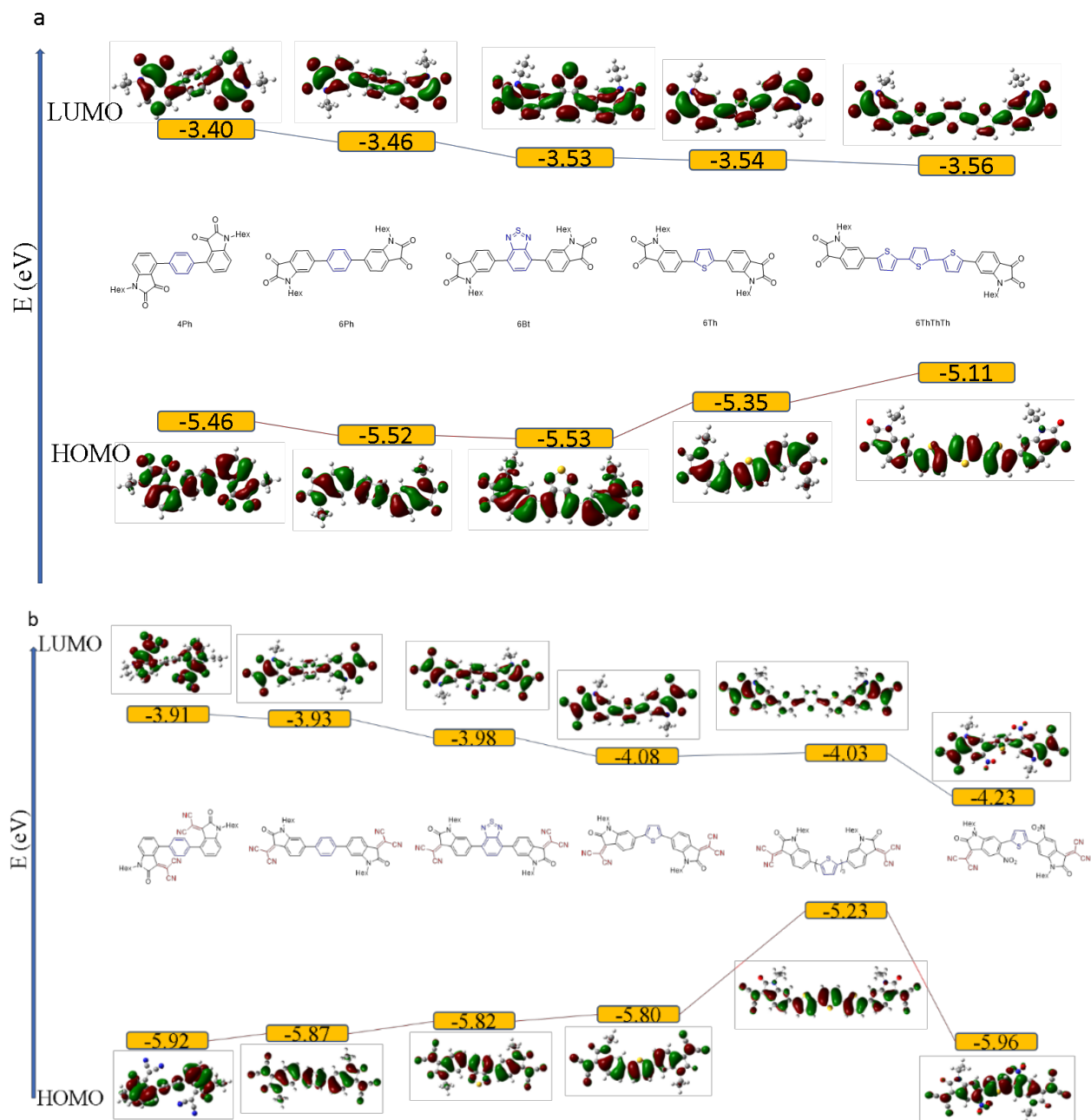


Figure 9. HOMO/LUMO energy diagram for a) bis-isatin and b) bis-isatin CNs.

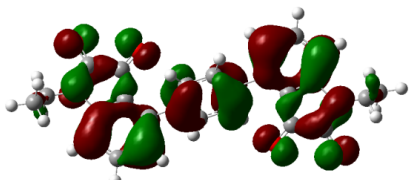
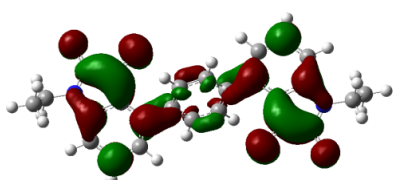
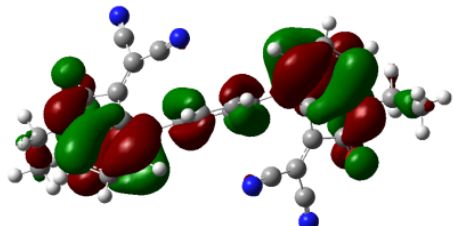
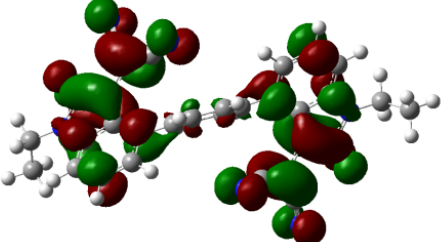
3.2.4) TD-DFT studies of bis-isatin and malononitrile derivatives.

1) Methodology and computational details

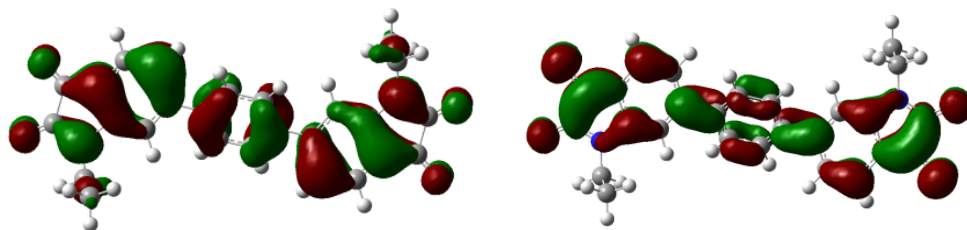
Geometries of all the neutral molecules as well as their cations and anions were fully optimized with density functional theory (DFT) of B3LYP^{32,33,34} and 6-31G(d) basis set with the Polarizable Continuum Model (PCM) using the integral equation formalism variant (IEFPCM) in tetrahydrofuran solvent (THF, $\epsilon=7.4257$) [B3LYP/6-31G(d)/THF]. The hexyl substituents on the N atoms of the isatylidene segments were replaced with ethyl to reduce calculation cost. Frequency calculations were performed to confirm the optimized geometries to be true energy minimum. On the basis of the optimized geometries at DFT-B3LYP/6-31G(d)/THF level, molecular orbital energies and electron energies were then calculated with DFT-M06L functional and 6-31G(d) basis set with IEFPCM solvent model in THF. Electronic absorption spectra were simulated based on the excited-state data calculated with time-dependent DFT (TD-DFT) method at M06L/6-31G(d)/THF level using DFT-B3LYP/6-31G(d)/THF geometries. All calculations were carried out using the Gaussian 16 program.³⁵

2) Molecular orbitals

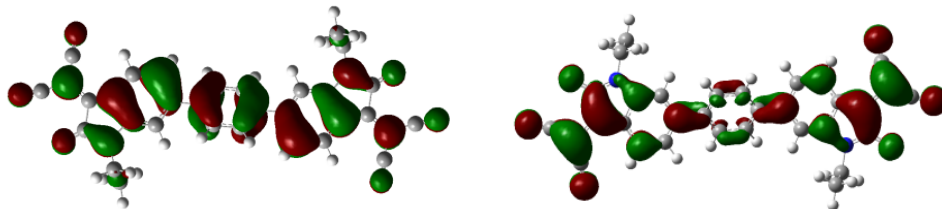
Figure 10 shows the molecular orbital maps of all the molecules. Both HOMO and LUMO are fully delocalized on the two isatylidene malononitrile terminal acceptor groups and the π -conjugated bridge donor segments. The HOMOs mainly occupy the double bonds along the long-axis direction of the molecules while the LUMOs mostly distribute on single bonds perpendicular to the long-axis direction. For bis-isatin compounds, the distribution of HOMO and LUMO decrease from center D groups to terminal A segments. On the contrary, the HOMO and LUMO of isatylidene malononitrile derivatives appear to distribute more on A than D segments.

Acronym	HOMO map	LUMO map
4Ph		
4PhCN		

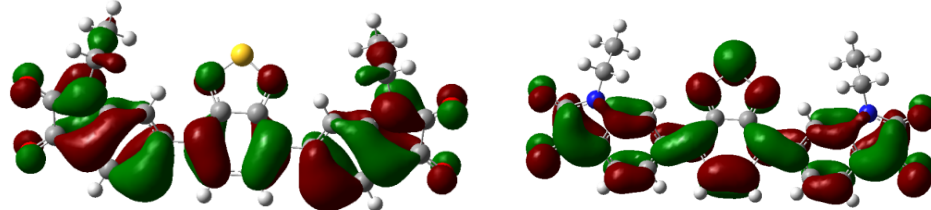
6Ph



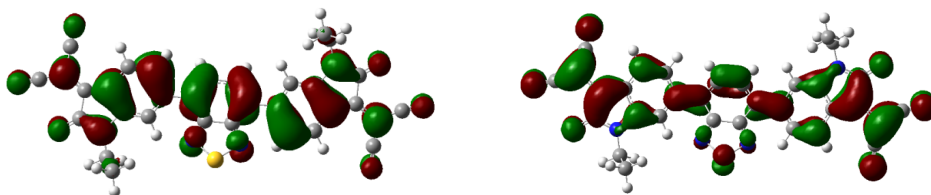
6PhCN



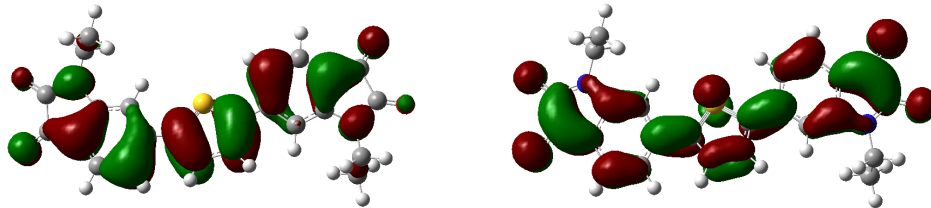
6BT



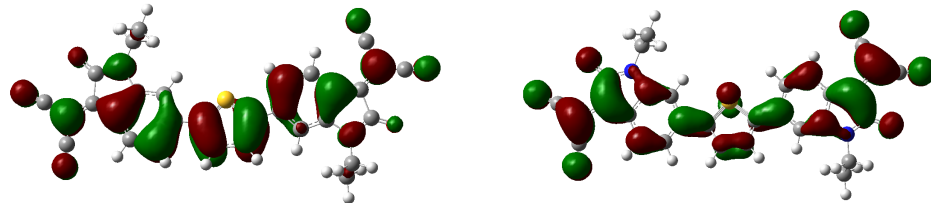
6BtCN



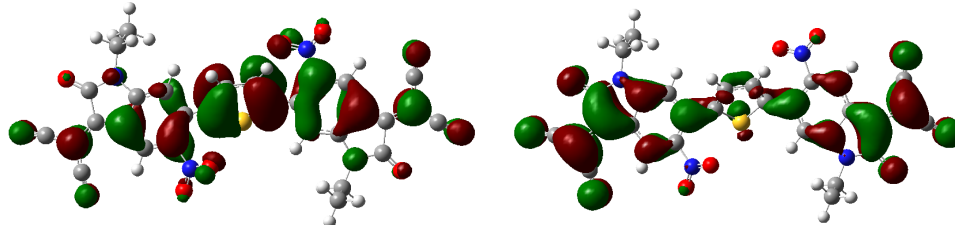
6Th



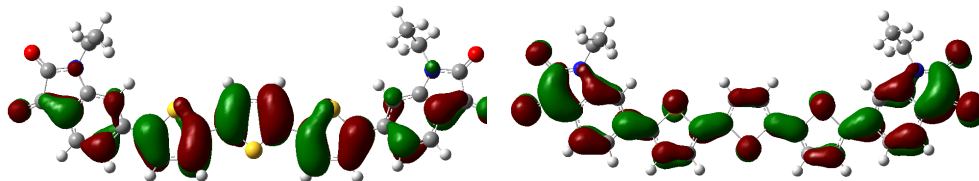
6ThCN



6ThNO₂CN



6ThThTh



6ThThThCN

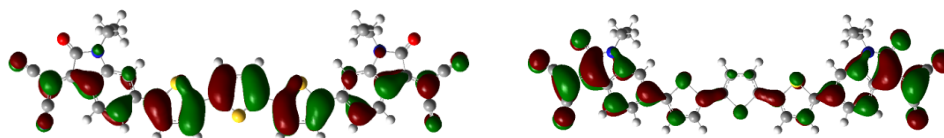
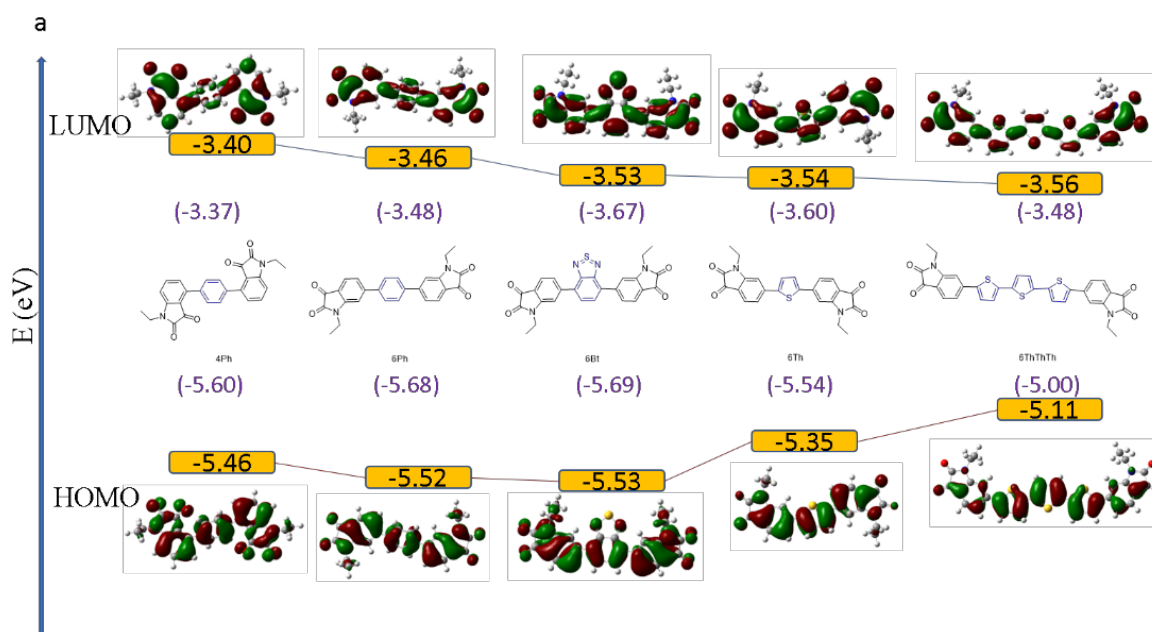


Figure 10. HOMO/LUMO maps of bis-isatin and bis-isatin CN derivatives.

The calculated HOMO and LUMO energy levels are summarized in **Table 3**. For bis-isatin compounds, the HOMO energies have the order of $6\text{Ph} \approx 6\text{BT} < 6\text{Th} < 6\text{ThThTh}$ while the LUMO energies show the trend of $6\text{BT} < 6\text{Th} < 6\text{Ph} \approx 6\text{ThThTh}$ (**Figure 11**). The resulted HOMO-LUMO gaps decrease in the order of $6\text{Ph} > 6\text{BT} > 6\text{Th} > 6\text{ThThTh}$. It is common rule that both HOMO and LUMO increase with polymer/oligomer length and the relative higher HOMO and LUMO energy of 6ThThTh than 6Th is easily understandable. The higher HOMO and LUMO energy of 6Th than 6BT indicates Th has larger electron donating ability than BT group. The higher HOMO and LUMO of 4Ph than 6Ph may be due to the larger steric hindrance between Ph and isatin groups in 4Ph than in 6Ph. Substituting one O atom of isatin with stronger electron-accepting $\text{C}(\text{CN})_2$ in dicyano derivatives decrease both the HOMO and LUMO energies largely and results in significantly smaller HOMO-LUMO gap. 6ThNO₂CN has lower HOMO and LUMO energy than 6ThCN due to the introduced electron-withdrawing NO₂ groups. However, different from the fact that strong electron-accepting $\text{C}(\text{CN})_2$ in dicyano derivatives reduces the LUMO energy more significant than the HOMO and thus induces decreased HOMO-LUMO gap, the NO₂ groups in 6ThNO₂CN reduces the HOMO energy more significantly than the LUMO energy and results in larger HOMO-LUMO gap for 6ThNO₂CN than 6ThCN. A rational lie in the fact that is the connecting C atom for NO₂ in 6ThCN has less contribution to the LUMO but has large contribution to the HOMO.



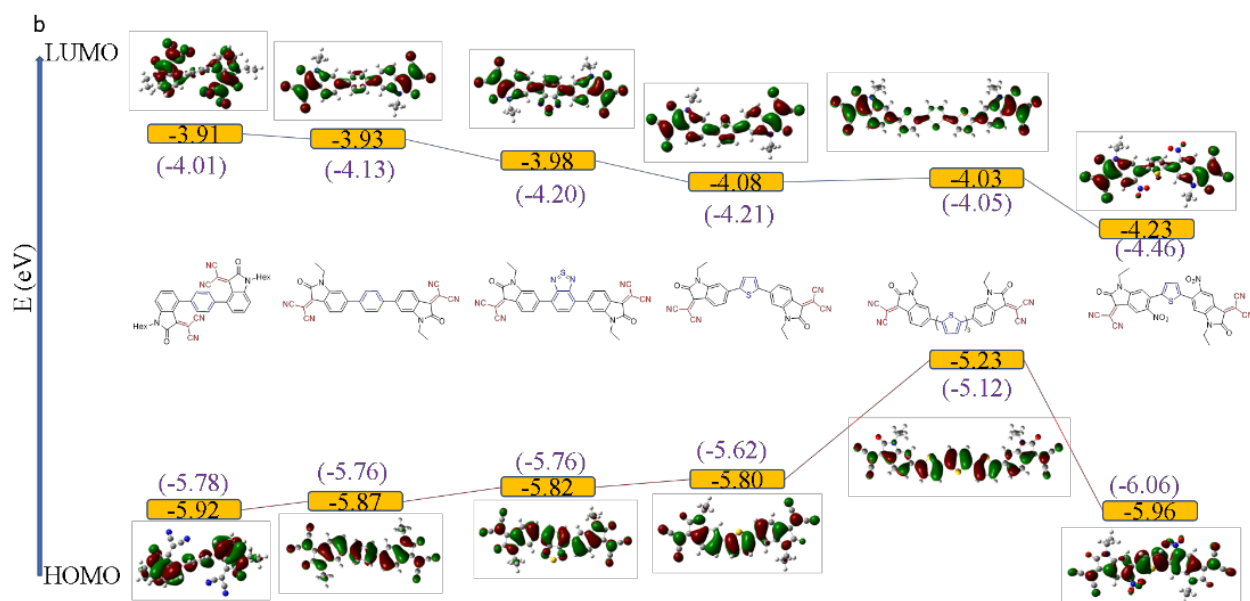


Figure 11. HOMO/LUMO energy diagram for a) bis-isatin and b) bis-isatin CNs, the values (purple) in parentheses are the HOMO and LUMO values calculated by DFT.

3) Electronic transitions

We have performed the calculation of the electronic absorption spectra and the electron transition density map of the main bands (**Figure 12**). The aforementioned changes in the orbitals' shapes and energies can be related to the differences in the electronic transitions involved in the lowest-energy and high-energy excited states of these molecules. The calculated optical gap (excitation energy of the first excited state) has the same trend with the HOMO-LUMO gaps but the optical gaps have larger values than HOMO-LUMO gaps due to orbital coupling energy. The lowest energy bands are due to electronic transitions from HOMO to LUMO and could be assigned to charge transfer transitions between the π -conjugated bridge and end-group acceptor. Charge transfer-type transitions generally have weak intensity. However, when a π -conjugated system is extended, the intensity of the lowest energy band increases due to the contribution from π - π^* transition in D bridge increase with conjugation length. For 6ThThTh, the intensity of the lowest energy band is stronger than the high energy bands. Due to the decreased optical or HOMO-LUMO gaps from 6Ph to 6ThThTh, the lowest energy bands shift significantly to red to near-infrared part of the spectrum. The high energy band is attributed to the π - π^* transition for both D and A groups.

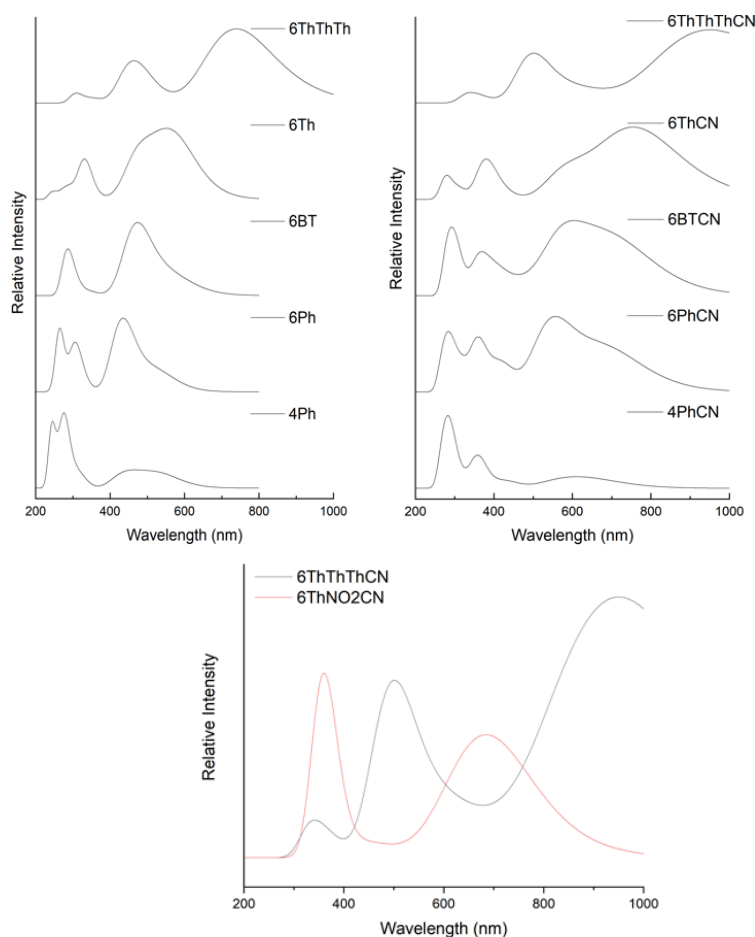


Figure 12. Simulated UV-vis spectra with half-width at half height of 2000 nm of the bis-isatin (top left); bis-isatin CNs derivatives (top right); Comparison of the simulated UV-vis spectra with half width at half height of 2000 nm between compound **16** and **22** (bottom).

In summary TD-DFT calculations were carried out to investigate the electronic effects of conjugation length and the substitution position of the end-group on the molecular orbitals and electronic absorption spectra. The calculated molecular orbital energies and gaps correspond well with the corresponding experimental data. The deviation between calculated and experimental orbital energies are less than 0.15 eV for most cases (see **Figure 13**). In addition, the calculated trends for orbital energies among different compounds are the same with the experimental ones, as shown in **Table 3**.

Table 3.

Calculated energies of the HOMO and the LUMO, HOMO-LUMO energy gap, optical gap (excitation energy of the first excited state), vertical and adiabatic ionization potential (IP) and electronic affinity (EA), and reorganization energy for hole (λ^+) and electron (λ^-) at M06L/6-31G(d) level with IEFPCM solvent model in tetrahydrofuran on the basis of the optimized geometries at B3LYP/6-31G(d) level with IEFPCM solvent model in tetrahydrofuran. All energies in eV.

Compound	$E_{g\text{-opt}}$ eV	$E_{g\text{-DFT}}$ eV	E_{LUMO} eV	$E_{\text{LUMO-DFT}}$ eV	E_{HOMO} eV	$E_{\text{HOMO-DFT}}$ eV	$E_{\text{gap electrochemical}}$ eV	$E_{\text{gap electrochemical-DFT}}$ eV
4Ph	2.34	2.30	-3.40	-3.37	-5.46	-5.60	2.06	2.23
4PhCN	1.97	1.83	-3.91	-4.01	-5.92	-5.78	2.01	1.78
6Ph	2.33	2.35	-3.46	-3.48	-5.52	-5.68	2.06	2.21
6PhCN	1.97	1.78	-3.93	-4.13	-5.87	-5.76	1.94	1.63
6Bt	2.27	2.17	-3.53	-3.67	-5.53	-5.69	2.00	2.02
6BtCN	1.90	1.72	-3.98	-4.20	-5.82	-5.76	1.84	1.55
6Th	2.24	2.17	-3.54	-3.60	-5.35	-5.54	1.81	1.94
6ThCN	1.85	1.62	-4.08	-4.21	-5.80	-5.62	1.88	1.41
6ThNO ₂ CN	1.93	1.78	-4.23	-4.46	-5.96	-6.06	1.73	1.60
6ThThTh	2.11	1.68	-3.56	-3.48	-5.11	-5.00	1.55	1.52
6ThThThCN	1.63	1.30	-4.03	-4.05	-5.23	-5.12	1.20	1.07

$E_{g\text{-opt-DFT}}$: Calculated optical gap (excitation energy of the first excited state,). $E_{\text{HOMO-DFT}}$: Calculated energies of the highest occupied orbital (HOMO), $E_{\text{LUMO-DFT}}$: Calculated energies the lowest unoccupied orbital (LUMO), $E_{\text{gap electrochemical-DFT}}$: HOMO-LUMO energy gap.

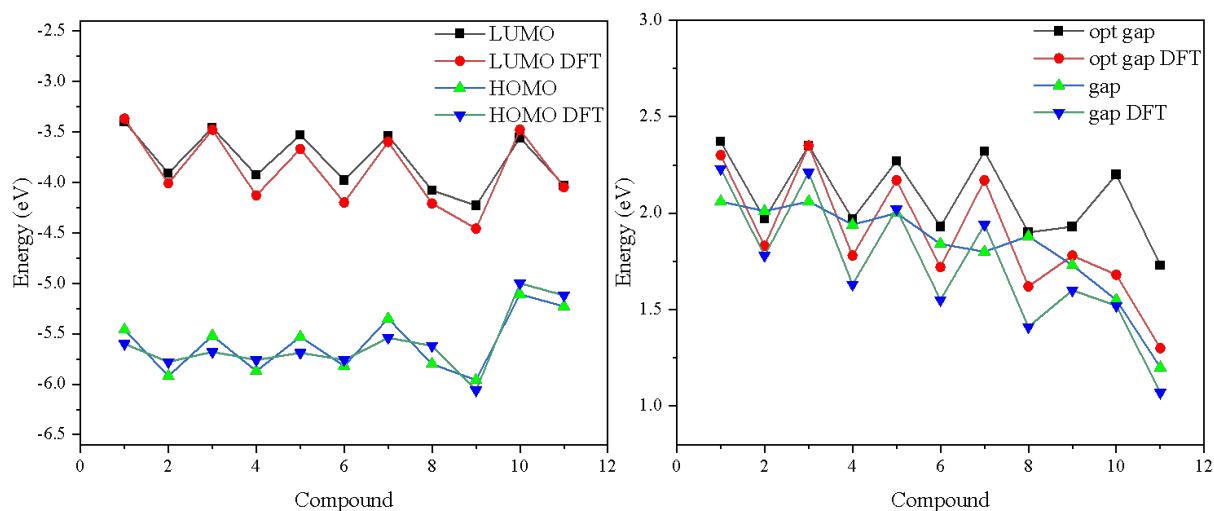
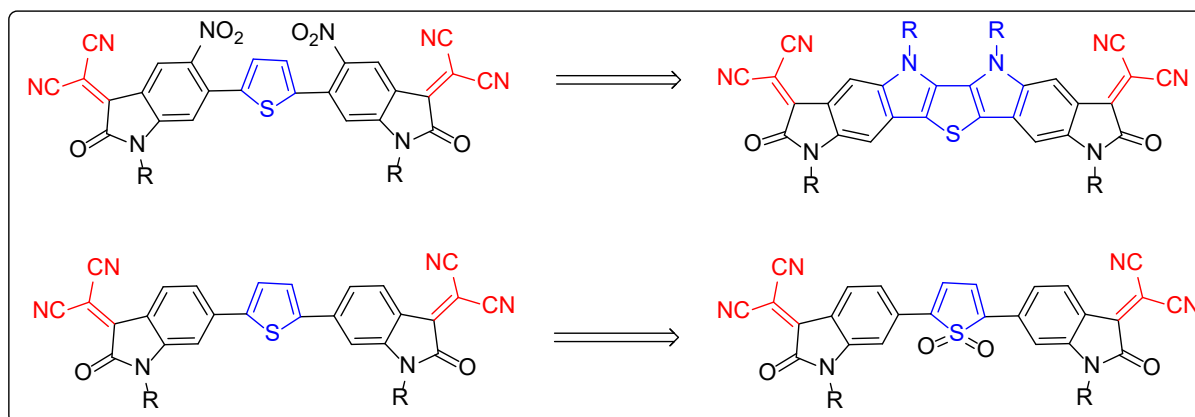


Figure 13. Variation of energy of HOMO/LUMO between calculated and measured bis-isatin and bis-isatin CNs derivatives.

3.3) Conclusion and perspective

We have designed, synthesized and characterized several A-D-A small-molecules, based on the 2-(2-oxindolin-3-ylidene) malononitrile derivatives. Appropriate chemical modifications of both π -bridge and end-group can effectively impact the optical, electrochemical, and energy levels of these molecules. When the isatin ring was replaced by the isatylidene malononitrile ring, a bathochromic shift of ca. 80-110 nm at the longest wavelength was observed, which reduced the optical band gap. The redshift induced by thiophene is more pronounced when compared to Bt or Ph, suggesting that thiophene has stronger intramolecular charge transfer properties. The LUMO energy level of the isatylidene malononitrile family obtained by electrochemical measurements is of ca. 3.95 eV, which is 0.5 eV lower than that of bi-isatin derivatives. DFT calculations show that both HOMO and LUMO are fully delocalized on the two isatylidene malononitrile terminal acceptor groups and the π -conjugated bridge

donor segments. Meanwhile, the HOMO or LUMO energy levels of the materials obtained by DFT calculations are very close to the experimental data, with many data deviation within 0.15 eV. The material 6ThThThCN with three thiophene units has a low lying LUMO energy level, near 4.0 eV, as well as a small band gap of ca. 1.20 eV. The introduction of a nitro group in bis-isatin-CNs can further significantly stabilize the LUMO energy level, which facilitate good air stability. One possible extension of this work is to develop fully-fused π -bridges, or to enhance the electron withdrawing ability by the oxidation of the sulfur of thiophene.



Experimental procedures and Characterization data

4-bromoindoline-2,3-dione (1): Procedure a) synthesis of isonitrosoacetanilide: Chloral hydrate (4.5 g, 27 mmol) and Na₂SO₄ (12 g, 84 mmol) were dissolved in water (60 ml) in a 250ml three-neck flask and warmed to 35 °C. To a warm solution of the 3-bromoaniline (4.2 g, 24 mmol) in 15 ml water, an aqueous solution of concentrated HCl (3.0 ml) was added: a white precipitate of the amine sulfate was formed, a warm solution of hydroxylamine hydrochloride (5.5g, 79 mmol) in 25ml water was ultimately added. The mixture was stirred and heated at 80-85 °C for 2 h and then allowed to cool to room temperature. The suspension was filtered to afford the intermediate isonitrosoacetanilide. The crude product was directly used in the next step without further purification. Procedure b) synthesis of 4-bromoindoline-2,3-dione. Sulfuric acid (50 ml) was heated in a 100 ml flask at 60 °C. The dry isonitrosoacetanilide was added in small portion with stirring over 30 mins so that temperature did not exceed 65 °C. The mixture was then heated to 80 °C for 15 mins, allowed to cool to room temperature. The solid was filtered and dried under vacuum to give a mixture of 4-bromoisatin and 6-bromoisatin. Dissolved the mixture in a solution of NaOH (0.72 g) in 7.2 ml water at 60 °C and then acidified with acetic acid (15 ml). The solid was filtered and dried under vacuum to give **1** as an orange solid (43% yields over two step). ¹H NMR (DMSO-d₆, 300 MHz, ppm) δ 7.46 (t, J = 8.0 Hz, 1H), 7.23 (d, J = 8.0 Hz, 1H), 6.89 (d, J = 7.8 Hz, 1H).

4-bromo-1-hexylindoline-2,3-dione (2): To an oven-dried flask, compound 1 (1.0 g, 4.42 mmol) and K₂CO₃ (0.73 g, 5.28 mmol) were dissolved in 15 ml of anhydrous dimethylformamide. The mixture was heated for 0.5h to reflux and 0.74 ml (5.27 mmol) of 1-bromohexane was added via syringe. The mixture was stirred at reflux for 24 h. After the mixture was cooled to room temperature, ethyl acetate was added to extract the product. Then the combined organic layers were concentrated under vacuum and finally purified through column chromatography to give **2** as an orange-red solid. (89% yield). ¹H NMR (CDCl₃, 300 MHz, ppm) δ 7.40 (t, J = 8.0, 1H), 7.26-7.24 (m, 1H), 6.84 (d, J = 7.9, 1H), 3.72 (t, J = 7.4, 2H), 1.74-1.61 (m, 2H), 1.45-1.25 (m, 6H), 0.90 (t, 3H). ¹³C NMR (CDCl₃, 75 MHz, ppm) δ 180.77, 156.95, 152.39, 138.78, 127.95, 120.93, 115.76, 109.41, 40.19, 31.22, 27.05, 26.39, 22.41, 13.92.

6-bromoindoline-2,3-dione (3): Procedure b) synthesis of 6-bromoindoline-2,3-dione. Sulfuric acid (50 ml) was heated in a 100 ml flask at 60 °C. The isonitrosoacetanilide was added in small portions with stirring over 30 mins so that temperature did not exceed 65 °C. The mixture was then heated to 80 °C for 15 mins, and allowed to cool to room temperature. The solid was filtered and dried under vacuum to give a mixture of 4-bromoisatin and 6-bromoisatin. Dissolved the mixture in a solution of NaOH (1.5 g) in 15 ml water at 60 °C and then acidified with HCl solution (20 mL). The solid was filtered and dried under vacuum to give **3** as an orange solid (35% yield over two steps).

6-bromo-1-hexylindoline-2,3-dione (4): To an oven-dried flask, compound 3 (2.45 g, 10.80 mmol) and K_2CO_3 (4.5 g, 32.5 mmol) were dissolved in 30 ml of anhydrous dimethylformamide. The mixture was heated for 0.5h to reflux and 1.80 ml (12.90 mmol) of 1-bromohexane was added via syringe. The mixture was stirred at reflux for 24 h. After the mixture was cooled to room temperature, ethyl acetate was added to extract the product. Then the combined organic layers were concentrated under vacuum and finally purified through column chromatography (chloroform/hexane = 1:2) to give **4** as an orange-red solid (81% yield). 1H NMR ($CDCl_3$, 300 MHz) δ 7.45 (d, 1H), 7.27 (d, 1H), 7.05 (s, 1H), 3.68 (t, 2H), 1.72-1.61 (m, 2H), 1.40-1.30 (m, 6H), 0.88 (t, 3H).

4,4'-(1,4-phenylene) bis (1-hexylindoline-2,3-dione) (5): To an oven-dried flask, the compound 2 (364 mg, 1.17 mmol), 1,4-benzenediboronic acid bis (pinacol) ester (193 mg, 0.58 mmol), $P(o\text{-tyl})_3$ (50 mg, 0.17mmol) and K_3PO_4 (747 mg, 3.52 mmol) were loaded to a flask under argon. Toluene (5 mL) and water (0.5ml) was then added to the flask. After stirring at room temperature for 0.5 h, $Pd_2(dba)_3$ (50 mg, 0.05 mmol) was added to the flask. The mixture was stirred at reflux for 20 h. The resulting mixture was extracted with ethyl acetate. The organic phase was then washed 3 times with brine and dried with Na_2SO_4 . After removal of the solvent, the crude product was purified by column chromatography (chloroform/hexane = 3:1) to afford **5** as a red solid (160 mg, 52% yield). 1H NMR ($CDCl_3$, 300 MHz) δ 7.65-7.58 (m, 3H), 7.17 (d, 1H), 6.88 (d, 1H), 3.76 (t, 2H), 1.77-1.70 (m, 2H), 1.42-1.29 (m, 6H), 0.90 (t, 3H). ^{13}C NMR ($CDCl_3$, 75 MHz) δ 182.34, 157.76, 151.89, 142.66, 137.69, 136.71, 128.87, 125.72, 113.87, 109.00, 40.32, 31.42, 27.25, 26.61, 22.53, 14.01. HRMS (ESI) calculated for $C_{34}H_{36}N_2O_4$: 536.2675; Found:536.2674.

2,2'-(1,4-phenylenebis(1-hexyl-2-oxoindoline-4-yl-3-ylidene)) dimalononitrile (6): The compound 5 (60 mg, 0.11 mmol) and malononitrile (22 mg, 0.33 mmol) were dissolved in 6 ml of anhydrous EtOH. The mixture was stirred at reflux for 12 h. The resulting mixture was extracted with ethyl acetate. The organic phase was then washed 3 times with brine and dried with Na_2SO_4 . After removal of the solvent, the crude product was purified by column chromatography (dichloromethane/hexane = 2:1) to afford **6** as a red solid. (80% yield). 1H NMR ($CDCl_3$, 300 MHz) δ 7.59-7.51 (m, 3H), 7.05 (d, 1H), 6.82 (d, 1H), 3.75 (t, 2H), 1.75-1.68 (m, 2H), 1.39-1.29 (m, 6H), 0.91 (t, 3H). ^{13}C NMR ($CDCl_3$, 75 MHz) δ 163.10, 147.22, 144.03, 140.00, 136.91, 129.77, 126.51, 116.11, 111.99, 111.04, 108.53, 85.66, 40.75, 31.35, 27.21, 26.57, 22.49, 13.99. HRMS (ESI) calculated for $C_{40}H_{36}N_6O_2$: 632.2900; Found: 632.2900.

6,6'-(1,4-phenylene) bis(1-hexylindoline-2,3-dione) (7): To an oven-dried flask, the compound 4 (210 mg, 0.64 mmol), 1,4-benzenediboronic acid bis (pinacol) ester (96 mg, 0.29 mmol), $P(o\text{-tyl})_3$ (29 mg, 0.09 mmol) and K_3PO_4 (410 mg, 1.93 mmol) were loaded to a flask under argon. Toluene (5 mL) and water (0.5 mL) was then added to the flask. After stirring at room temperature for 0.5 h, $Pd_2(dba)_3$ (29 mg, 0.03 mmol) was added to the flask. The mixture was stirred at reflux for 20 h. The resulting mixture

was extracted with dichloromethane. The organic phase was then washed with water and dried with Na₂SO₄. After removal of the solvent, the crude product was purified by column chromatography (chloroform/hexane = 3:1) to give **7** as a red solid (109 mg, 70% yield). ¹H NMR (CDCl₃, 300 MHz) δ 7.76 (s, 2H), 7.71 (d, 1H), 7.37 (d, 1H), 7.09 (s, 1H), 3.79 (t, 2H), 1.80-1.70 (m, 2H), 1.42-1.29 (m, 6H), 0.89 (t, 3H). ¹³C NMR (CDCl₃, 75 MHz) δ 182.94, 158.51, 151.75, 150.38, 140.44, 128.09, 126.02, 122.44, 116.75, 108.64, 40.33, 31.40, 27.37, 26.61, 22.53, 14.00. HRMS (ESI) calculated for C₃₄H₃₆N₂O₄: 536.2675; Found:536.2674.

2,2'-(1,4-phenylenebis(1-hexyl-2-oxoindoline-6-yl-3-ylidene)) dimalononitrile (8): The compound **7** (49 mg, 0.09 mmol) and malononitrile (18 mg, 0.27 mmol) were dissolved in 5 ml of anhydrous EtOH. The mixture was stirred at reflux for 12 h. The resulting mixture was extracted with chloroform. The organic phase was then washed 3 times with brine and dried with Na₂SO₄. After removal of the solvent, the crude product was purified by column chromatography (dichloromethane/ petroleum ether = 2:1) to give **8** as a red solid (50mg, 88% yield). ¹H NMR (CDCl₃, 300 MHz) δ 8.21 (d, 1H), 7.78 (s, 1H), 7.39 (d, 1H), 7.07 (s, 1H), 3.78 (t, 2H), 1.78-1.66 (m, 2H), 1.42-1.28 (m, 6H), 0.89 (t, 3H). ¹³C NMR (CDCl₃, 75 MHz) δ 162.74, 149.47, 148.61, 147.37, 140.27, 128.08, 127.45, 122.36, 117.71, 112.53, 108.05, 81.94, 40.58, 31.37, 27.37, 26.59, 22.50, 14.02. HRMS (ESI) calculated for C₄₀H₃₆N₆O₂: 632.2900; Found: 632.2902.

*6,6'-(benzo[*c*] [1,2,5] thiadiazole-4,7-diyl) bis (1-hexylindoline-2,3-dione) (9)*: To an oven-dried flask, the compound **4** (300 mg, 0.97 mmol), 2,1,3-benzothiadiazole-4,7-diboronic acid bis(pinacol) ester (170 mg, 0.44 mmol), P(*o*-tyl)₃ (40 mg, 0.13 mmol) and K₃PO₄ (410 mg, 1.93 mmol) were loaded to a flask under argon. Toluene (2.5 mL) and water (0.5 ml) was then added to the flask. After stirring at room temperature for 0.5 h, Pd₂(dba)₃ (40 mg, 0.04 mmol) was added to the flask. The mixture was stirred at reflux for 12 h. The resulting mixture was extracted with chloroform. The organic phase was then washed 3 times with water and dried with Na₂SO₄. After removal of the solvent, the crude product was purified by column chromatography (chloroform/hexane = 3:2) to afford **9** as a red solid. (145 mg, 55% yield). ¹H NMR (CDCl₃, 300 MHz) δ 7.95 (s, 1H), 7.78 (d, 1H), 7.64 (d, 1H), 7.62 (s, 1H), 3.82 (t, 2H), 1.84-1.74 (m, 2H), 1.44-1.28 (m, 6H), 0.89 (t, 3H). ¹³C NMR (CDCl₃, 75 MHz) δ 183.14, 158.35, 153.51, 151.23, 146.64, 133.26, 128.72, 125.62, 124.34, 117.25, 111.43, 40.41, 31.41, 27.26, 26.61, 22.53, 14.04. HRMS (ESI) calculated for C₃₄H₃₄N₄O₄S:594.2301; Found: 594.2299.

*2,2'-(benzo[*c*] [1,2,5] thiadiazole-4,7-diyl)bis(1-hexyl-2-oxoindoline-6-yl-3-ylidene)) dimalononitrile (10)*: The compound **9** (30 mg, 0.05 mmol) and malononitrile (10 mg, 0.15 mmol) were dissolved in 3.0 ml of anhydrous EtOH. The mixture was stirred at reflux for 10 h. The resulting mixture was extracted with dichloromethane. The organic phase was then washed 3 times with brine and dried with Na₂SO₄. After removal of the solvent, the crude product was purified by column chromatography

(dichloromethane/ petroleum ether = 3:1) to afford **10** as a red solid. (82% yield). ¹H NMR (CDCl₃, 300 MHz) δ 8.29 (d, 1H), 7.98 (s, 1H), 7.68 (d, 1H), 7.65 (s, 1H), 3.82 (t, 2H), 1.82-1.68 (m, 2H), 1.44-1.29 (m, 6H), 0.89 (t, 3H). ¹³C NMR (CDCl₃, 75 MHz) δ 162.61, 153.51, 148.70, 146.91, 145.80, 133.11, 128.73, 127.07, 124.19, 118.32, 112.45, 110.93, 82.46, 40.66, 31.38, 27.29, 26.59, 22.50, 14.04. HRMS (ESI) calculated for C₄₀H₃₄N₈O₂S:690.2525; Found: 690.2521.

6,6'-(thiophene-2,5-diyl) bis(1-hexylindoline-2,3-dione) (11): To an oven-dried flask, the compound **4** (90 mg, 0.29 mmol) and 2,5-bis(tributylstannyl) thiophene (88 mg, 0.13 mmol) were loaded to a flask under argon. Anhydrous dimethylformamide (2 mL) was then added to the flask. After stirring at room temperature for 20 mins, Pd(dppf)Cl₂ (15 mg, 0.02 mmol) was added to the flask. The mixture was stirred at reflux for 15 h. The resulting mixture was extracted with chloroform. The organic phase was then washed 3 times with water and dried with Na₂SO₄. After removal of the solvent, the crude product was purified by column chromatography (dichloromethane /hexane = 1:1) to afford **11** as a red solid (44 mg, 64% yield). ¹H NMR (CDCl₃, 300 MHz) δ 7.65 (d, 1H), 7.55 (s, 1H), 7.35 (d, 1H), 7.08 (s, 1H), 3.79 (t, 2H), 1.80-1.70 (m, 2H), 1.44-1.30 (m, 6H), 0.90 (t, 3H). ¹³C NMR (CDCl₃, 75 MHz) δ 182.31, 158.54, 151.82, 144.54, 142.92, 127.33, 126.30, 120.70, 116.84, 106.62, 40.30, 31.38, 27.33, 26.58, 22.54, 14.04. HRMS (ESI) calculated for C₃₂H₃₄N₂O₄S:542.2239; Found: 542.2236.

2,2'-(thiophene-2,5-diylbis(1-hexyl-2-oxoindoline-6-yl-3-ylidene)) dimalononitrile (12): The compound **11** (20 mg, 0.03 mmol) and malononitrile (8 mg, 0.11 mmol) were dissolved in 3 ml of anhydrous EtOH and 2.5 ml of DCM. 2 drops of pyridine were then added by syringe. C. The mixture was then stirred overnight at room temperature. The resulting mixture was extracted with chloroform. The organic phase was then washed 3 times with water and dried with Na₂SO₄. After removal of the solvent, the crude product was purified by column chromatography (dichloromethane/ petroleum ether = 1:2) to give **12** as a black solid (17mg, 89% yield). ¹H NMR (CDCl₃, 300 MHz) δ 8.15 (d, 1H), 7.59 (s, 1H), 7.40 (d, 1H), 7.05 (s, 1H), 3.78 (t, 2H), 1.78-1.68 (m, 2H), 1.42-1.30 (m, 6H), 0.90 (t, 3H). ¹³C NMR (CDCl₃, 75 MHz) δ 162.77, 147.88, 147.44, 144.87, 142.03, 127.60, 120.63, 117.87, 112.64, 110.81, 106.02, 81.37, 40.56, 31.34, 27.36, 26.55, 22.50, 14.04. HRMS (ESI) calculated for C₃₈H₃₄N₆O₂S:638.2464; Found: 638.2468.

1-hexyl-6-(thiophen-2-yl) indoline-2,3-dione (13): To an oven-dried flask, the compound **4** (1 g, 3.22 mmol) and 2-(tributylstannyl) thiophene (1.68 g, 4.5 mmol) and Pd(dppf)Cl₂ (71 mg, 0.09 mmol) were loaded to a flask under argon. Anhydrous dimethylformamide (5 mL) was then added to flask. The mixture was stirred at reflux for 12 h. The resulting mixture was extracted with chloroform. The organic phase was then washed 3 times with water and dried with Na₂SO₄. After removal of the solvent, the crude product was purified by column chromatography (chloroform/hexane = 1:2) to give **13** as an orange solid (0.81g, 80% yield). ¹H NMR (CDCl₃, 300 MHz) δ 7.60 (d, 1H), 7.51 (d, 1H), 7.47 (d, 1H),

7.34 (d, 1H), 7.17 (t, 1H), 7.05 (s, 1H), 3.76 (t, 2H), 1.78-1.67 (m, 2H), 1.42-1.28 (m, 6H), 0.90 (t, 3H). ¹³C NMR (CDCl₃, 75 MHz) δ 182.40, 158.74, 151.78, 144.07, 142.56, 128.73, 128.08, 126.20, 126.08, 120.67, 116.25, 106.78, 40.24, 31.37, 27.32, 26.57, 22.52, 14.01. HRMS (ESI) calculated for C₁₈H₁₉NO₂S: 313.1136; Found: 313.1132.

6-(5-bromothiophen-2-yl)-1-hexylindoline-2,3-dione (14): Under argon, to a solution of 1-hexyl-6-(thiophen-2-yl) indoline-2,3-dione (50 mg, 0.16 mmol) in THF (3 mL) was added portionwise NBS (32 mg, 0.17 mmol) at 0 °C. Catalytic amount of AcOH was added and the suspension was allowed to warm up to room temperature and stirred for 6 h. Water was then added and the solution was extracted 3 times with dichloromethane. The combined organic layer was dried over anhydrous Na₂SO₄. The solvent was then removed under reduced pressure and the crude product was further purified by column chromatography (chloroform/hexane = 1:2 to 1:1) to give **14** as an orange solid (51mg, 82% yield). ¹H NMR (CDCl₃, 300 MHz) δ 7.60 (d, 1H), 7.26-7.21 (m, 2H), 7.12 (d, 1H), 6.94 (s, 1H), 3.75 (t, 2H), 1.75-1.65 (m, 2H), 1.42-1.28 (m, 6H), 0.89 (t, 3H). ¹³C NMR (CDCl₃, 75 MHz) δ 182.32, 158.59, 151.84, 143.83, 142.98, 131.56, 126.31, 126.21, 120.29, 116.50, 115.35, 106.38, 40.28, 31.37, 27.32, 26.58, 22.53, 14.01. HRMS (ESI) calculated for C₁₈H₁₈BrNO₂S: 391.0242; Found: 391.0241.

1-(2-octyldodecyl)-6-(thiophen-2-yl) indoline-2,3-dione (13a): The 6-bromo-1-(2-octyldodecyl) indoline-2,3-dione (1.39 g, 2.75 mmol) and 2-(tributylstannyl) thiophene (147 g, 3.95 mmol), were loaded to a flask under argon. DMF (2.5 mL) was then added to the flask. The mixture was then stirred at room temperature for 0.5 h, Pd(dppf)Cl₂ (100 mg, 0.14 mmol) was added to the flask. The mixture was stirred at reflux for 12 h. The resulting mixture was extracted with chloroform. The organic phase was then washed 3 times with water and dried with Na₂SO₄. After removal of the solvent, the crude product was purified by column chromatography (chloroform/hexane = 1:3) to give **13a** as a red solid (1.15g, 82% yield). ¹H NMR (CDCl₃, 300 MHz) δ 7.61 (d, 1H), 7.50 (d, 1H), 7.46 (d, 1H), 7.35 (d, 1H), 7.17 (t, 1H), 7.06 (s, 1H), 3.64 (d, 2H), 1.93-1.83 (m, 1H), 1.32-1.20 (m, 32H), 0.88 (t, 6H). ¹³C NMR (CDCl₃, 75 MHz) δ 182.39, 159.07, 152.19, 143.96, 142.61, 128.75, 128.06, 126.16, 125.97, 120.53, 116.22, 107.06, 44.60, 36.17, 31.93, 31.90, 31.61, 29.96, 29.66, 29.59, 29.38, 29.32, 26.53, 22.71, 14.17. HRMS (ESI) calculated for C₃₂H₄₇NO₂S: 509.3328; Found: 509.3328

6-(5-bromothiophen-2-yl)-1-(2-octyldodecyl) indoline-2,3-dione (14a): Under argon, to a solution of compound 13a (330 mg, 0.64 mmol) in THF (8 mL) was added portionwise NBS (127 mg, 0.71 mmol) at 0 °C. Catalytic amount of AcOH was added and the suspension was allowed to warm up to room temperature and stirred for 6 h. Water was then added and the solution was extracted three times with dichloromethane. The combined organic layer was dried over anhydrous Na₂SO₄. The solvent was then removed under reduced pressure and the crude product was further purified by column chromatography (chloroform/hexane = 1:4 to 1:3) to give **14a** as an orange-red solid (310mg, 81% yield). ¹H NMR

(CDCl₃, 300 MHz) δ 7.60 (d, 1H), 7.26-7.21 (m, 2H), 7.12 (d, 1H), 6.94 (s, 1H), 3.63 (d, 2H), 1.93-1.82 (m, 1H), 1.44-1.20 (m, 36H), 0.87 (t, 6H). ¹³C NMR (CDCl₃, 75 MHz) δ 182.27, 158.91, 152.26, 143.87, 142.86, 131.57, 126.22, 126.09, 120.11, 116.47, 115.34, 106.66, 44.64, 36.16, 31.92, 31.89, 31.60, 29.95, 29.67, 29.64, 29.59, 29.36, 29.32, 26.51, 22.71, 22.68, 14.15. HRMS (ESI) calculated for C₃₂H₄₆BrNO₂S:587.2433; Found: 587.2431.

6,6'-([2,2':5',2''-terthiophene]-5,5''-diyl) bis(1-hexylindoline-2,3-dione) (15): To an oven-dried flask, the compound 14 (150 mg, 0.38 mmol), 2,5-bis(tributylstannyl) thiophene (105 mg, 0.15 mmol) and Pd(dppf)Cl₂ (15 mg, 0.02 mmol) were loaded to a flask under argon. DMF (5 mL) was then added to the flask. Stirring and heating was continued overnight. The resulting mixture was extracted with ethyl acetate. The organic phase was then washed 3 times with water and dried with Na₂SO₄. After removal of the solvent, the crude product was purified by column chromatography (dichloromethane /hexane = 1:1 to 2:1) to give **15** as a red solid (83 mg, 75% yield). ¹H NMR (CDCl₃, 300 MHz) δ 7.62 (d, 1H), 7.45 (d, 1H), 7.32 (d, 1H), 7.24 (d, 1H), 7.22 (s, 1H), 7.03 (s, 1H), 3.78 (d, 2H), 3.78-3.72 (m, 2H), 1.42-1.32 (m, 6H), 0.90 (t, 6H). ¹³C NMR (CDCl₃, 75 MHz) δ 182.17, 158.74, 151.79, 143.33, 141.37, 139.34, 136.37, 127.09, 126.23, 125.47, 125.26, 120.22, 116.33, 106.24, 40.25, 31.40, 27.36, 26.59, 22.55, 14.05. HRMS (ESI) calculated for C₄₀H₃₈N₂O₄S₃:706.1994; Found: 706.1986.

6,6'-([2,2':5',2''-terthiophene]-5,5''-diyl) bis(1-(2-octyldodecyl) indoline-2,3-dione) (15a): To an oven-dried flask, the compound 14a (42 mg, 0.07 mmol), 2,5-bis(tributylstannyl)thiophene (20 mg, 0.03 mmol) and Pd(dppf)Cl₂ (8 mg, 0.01 mmol) were loaded to a flask under argon. DMF (2.5 mL) was then added to the flask. Stirring and heating was continued overnight. The resulting mixture was extracted with ethyl acetate. The organic phase was then washed 3 times with water and dried with Na₂SO₄. After removal of the solvent, the crude product was purified by column chromatography (ethyl acetate/hexane = 1:15 to 6:1) to afford **15a** as a red solid (15 mg, 50% yield). ¹H NMR (CDCl₃, 300 MHz) δ 7.62 (d, 1H), 7.43 (d, 1H), 7.33 (d, 1H), 7.24 (d, 1H), 7.21 (s, 1H), 7.04 (s, 1H), 3.66 (d, 2H), 1.94-1.82 (m, 1H), 1.38-1.22 (m, 36H), 0.88 (t, 6H). ¹³C NMR (CDCl₃, 75 MHz) δ 182.17, 152.22, 141.42, 139.35, 136.39, 126.98, 126.21, 125.46, 125.29, 120.12, 116.29, 106.53, 44.60, 36.24, 31.95, 31.93, 31.62, 30.00, 29.72, 29.41, 29.37, 28.29, 26.58, 22.73, 14.18, 13.65. HRMS (ESI) calculated for C₆₈H₉₄N₂O₄S₃:1098.2376; Found: 1098.6321.

2,2'-([2,2'5',2''-terthiophene]-5,5''-diyl)bis(1-(2-octyldodecyl)-2-oxoindoline-6-yl-3-ylidene)) dimalononitrile (16a): The compound 15 (10 mg) and malononitrile (2 mg) were dissolved in 1 ml of dry EtOH and 1 ml of DCM. 1 drop of pyridine was then added by syringe. The mixture was then stirred overnight at room temperature. Ethyl acetate was added and the organic layer was washed with water 3 times. The organic phase was dried over anhydrous Na₂SO₄. After removing the solvent by rotational evaporation, the residue was purified by column chromatography (dichloromethane/petroleum ether =

1:1) to afford **16a** as a black solid (10mg, 92% yield). ¹H NMR (CDCl₃, 300 MHz) δ 8.11 (d, 1H), 7.41 (d, 1H), 7.34 (d, 1H), 7.25 (d, 1H), 7.22 (s, 1H), 6.98 (s, 1H), 3.63 (d, 2H), 1.91-1.81 (m, 1H), 1.43-1.18 (m, 36H), 0.87 (t, 6H). ¹³C NMR (CDCl₃, 75 MHz) δ 163.27, 147.86, 147.72, 142.45, 141.46, 139.84, 136.52, 127.48, 125.73, 125.51, 120.01, 117.13, 112.88, 111.08, 105.85, 80.30, 44.88, 36.43, 31.95, 31.93, 31.63, 29.98, 29.71, 29.65, 29.41, 29.36, 26.58, 22.72, 14.18. HRMS (APPI) calculated for C₇₄H₉₅N₂O₆S₃⁺: 1195.6673; Found: 1195.6653. Product **16** also uses the same preparation method. HRMS (APPI) calculated for C₄₆H₃₉N₂O₆S₃⁺: 803.2291; Found: 803.2290.

6-bromo-1-hexyl-5-nitroindoline-2,3-dione (20): To a solution of NaNO₃ (188 mg, 2.21 mmol) in concentrated H₂SO₄ (4 mL) was added dropwise a solution of 4a (685 mg, 2.21 mmol) in concentrated H₂SO₄ (3 mL) at 0 °C. After 2h, the reaction mixture was then poured into ice water (50 mL), and the precipitate was collected by filtration and washed with water three times to afford **20** as a yellow solid (680 mg, 87% yield). ¹H NMR (CDCl₃, 300 MHz) δ 8.19 (s, 1H), 7.26 (s, 1H), 3.77 (d, 2H), 1.75-1.67 (m, 2H), 1.40-1.35 (m, 6H), 0.90 (t, 3H).

6,6'-(thiophene-2,5-diyl) bis(1-hexyl-5-nitroindoline-2,3-dione) (21): The compound 20 (210 mg, 0.59 mmol), 2,5-bis(tributylstannyl) thiophene (163 mg, 0.25 mmol) and Pd(dppf)Cl₂ (21 mg, 0.03 mmol) were loaded to a flask under argon. Anhydrous dimethylformamide (2 mL) was then added to the flask. Stirring and heating was continued overnight. After the reaction, the cooled solution was extracted with ethyl acetate. The organic phase was combined and washed with brine and water, and then dried with anhydrous Na₂SO₄. The residue was purified by column chromatography (dichloromethane /hexane = 2:1) to afford **21** as a red solid (140 mg, 90% yield). ¹H NMR (CDCl₃, 300 MHz) δ 8.16 (s, 1H), 7.22 (s, 1H), 7.04 (s, 1H), 3.82 (t, 2H), 1.76-1.69 (m, 2H), 1.40-1.34 (m, 6H), 0.89 (t, 3H). ¹³C NMR (CDCl₃, 75 MHz) δ 180.82, 157.73, 152.81, 144.63, 139.81, 137.80, 129.45, 122.15, 116.44, 113.11, 40.92, 31.28, 27.30, 26.52, 22.50, 13.98. HRMS (ESI) calculated for C₃₂H₃₂N₄O₈S:632.1941; Found: 632.1935.

2,2'-(thiophene-2,5-diylbis(1-hexyl-5-nitro-2-oxoindoline-6-yl-3-ylidene)) dimalononitrile (22): The compound 21 (30 mg, 0.04 mmol) and malononitrile (10 mg, 0.14 mmol) were dissolved in 3 ml of anhydrous EtOH. This mixture in the 25 mL flask was reflux for 12 h. Ethyl acetate was added and the organic layer was washed with water 3 times. The organic phase was dried over anhydrous Na₂SO₄. The residue was purified by column chromatography (dichloromethane/ petroleum ether = 1:1) to afford **22** as a deep red solid (29 mg, 85% yield). ¹H NMR (CDCl₃, 300 MHz) δ 8.62 (s, 1H), 7.24 (s, 1H), 7.00 (s, 1H), 3.82 (t, 2H), 1.74-1.69 (m, 2H), 1.40-1.34 (m, 6H), 0.89 (t,3H). ¹³C NMR (CDCl₃, 75 MHz) δ162.22, 148.36, 146.47, 144.40, 139.97, 136.57, 129.81, 122.97, 117.57, 112.18, 111.54, 109.81, 85.73, 41.19, 31.24, 27.33, 26.49, 22.46, 13.99. HRMS (ESI) calculated for C₃₈H₃₂N₈O₆S: 728.2166; Found: 728.2164

References

- (1) Rumer, J. W.; Schroeder, B. C.; Nielsen, C. B.; Ashraf, R. S.; Beatrup, D.; Bronstein, H.; Cryer, S. J.; Donaghey, J. E.; Holliday, S.; Hurhangee, M.; James, D. I.; Lim, S.; Meager, I.; Zhang, W.; McCulloch, I. Bis-lactam-based donor polymers for organic solar cells: Evolution by design. *Thin Solid Films* **2014**, *560*, 82-85, DOI: 10.1016/j.tsf.2013.10.089.
- (2) Alsufyani, M.; Hallani, R. K.; Wang, S.; Xiao, M.; Ji, X.; Paulsen, B. D.; Xu, K.; Bristow, H.; Chen, H.; Chen, X. The effect of aromatic ring size in electron deficient semiconducting polymers for n-type organic thermoelectrics. *Journal of Materials Chemistry C* **2020**, *8* (43), 15150-15157, DOI: 10.1039/D0TC03347B.
- (3) Jeon, S. O.; Yook, K. S.; Joo, C. W.; Lee, J. Y. High-Efficiency Deep-Blue-Phosphorescent Organic Light-Emitting Diodes Using a Phosphine Oxide and a Phosphine Sulfide High-Triplet-Energy Host Material with Bipolar Charge-Transport Properties. *Advanced Materials* **2010**, *22* (16), 1872-1876, DOI: 10.1002/adma.200903321.
- (4) Kim, J. H.; Choi, M. W.; Kim, S. Y.; Jung, S.; Choi, Y. S.; Park, S. Y. Novel Organic Semiconductors Based on 1, 5-Naphthyridine-2, 6-Dione Unit for Blue-Selective Organic Phototransistor. *Advanced Optical Materials* **2020**, *8* (20), 2000695, DOI: 10.1002/adom.202000695.
- (5) Takagi, K.; Yamamoto, S. y.; Tsukamoto, K.; Hirano, Y.; Hara, M.; Nagano, S.; Ie, Y.; Takeuchi, D. Synthesis and Field-Effect Transistor Application of π -Extended Lactam-Fused Conjugated Oligomers obtained by Tandem Direct Arylation. *Chemistry—A European Journal* **2018**, *24* (53), 14137-14145, DOI: 10.1002/chem.201801399.
- (6) Gomaa, M. A. M.; Hassan, D. K. Synthesis, characterization, and antimicrobial activity of some new N-aryl-N'-(2-oxoindolin-3-ylidene)-benzohydrazonamides. *Archiv der Pharmazie* **2019**, *352* (12), 1900209, DOI: 10.1002/ardp.201900209.
- (7) Yousaf, I.; Khera, R. A.; Iqbal, J.; Gul, S.; Jabeen, S.; Ihsan, A.; Ayub, K. Isatin-derived non-fullerene acceptors for efficient organic solar cells. *Materials Science in Semiconductor Processing* **2021**, *121*, 105345, DOI: 10.1016/j.mssp.2020.105345.
- (8) Bardagot, O.; Kubik, P.; Marszalek, T.; Veyre, P.; Medjahed, A. A.; Sandroni, M.; Grévin, B.; Pouget, S.; Nunes Domschke, T.; Carella, A. Impact of Morphology on Charge Carrier Transport and Thermoelectric Properties of N-Type FBDOPV-Based Polymers. *Advanced Functional Materials* **2020**, *30* (21), 2000449, DOI: 10.1002/adfm.202000449.
- (9) Liu, Y.; Wang, H.; Wan, J. Recent Advances in Diversity Oriented Synthesis through Isatin-based Multicomponent Reactions. *Asian Journal of Organic Chemistry* **2013**, *2* (5), 374-386, DOI: 10.1002/ajoc.201200180.

- (10) Dhondge, A. P.; Chen, J. Y.; Lin, T.; Yen, F. M.; Li, K. W.; Hsieh, H. C.; Kuo, M. Y. Di-2-(2-oxindolin-3-ylidene)malononitrile Derivatives for N-Type Air-Stable Organic Field-Effect Transistors. *Org Lett* **2018**, *20* (1), 40-43, DOI: 10.1021/acs.orglett.7b03284.
- (11) Dhondge, A. P.; Tsai, P. C.; Nien, C. Y.; Xu, W. Y.; Chen, P. M.; Hsu, Y. H.; Li, K. W.; Yen, F. M.; Tseng, S. L.; Chang, Y. C.; Chen, H. J. H.; Kuo, M. Y. Angular-Shaped Naphthalene Bis(1,5-diamide-2,6-diylidene)malononitrile for High-Performance, Air-Stable N-Type Organic Field-Effect Transistors. *Org Lett* **2018**, *20* (9), 2538-2542, DOI: 10.1021/acs.orglett.8b00684.
- (12) Sumpter, W. C. The chemistry of isatin. *Chemical reviews* **1944**, *34* (3), 393-434, DOI: 10.1021/cr60109a003.
- (13) Dhondge, A. P.; Huang, Y. X.; Lin, T.; Hsu, Y. H.; Tseng, S. L.; Chang, Y. C.; Chen, H. J. H.; Kuo, M. Y. Benzodipyrrole-2,6-dione-3,7-diylidenedimalononitrile Derivatives for Air-Stable n-Type Organic Field-Effect Transistors: Critical Role of N-Alkyl Substituent on Device Performance. *J Org Chem* **2019**, *84* (21), 14061-14068, DOI: 10.1021/acs.joc.9b02207.
- (14) Yoo, D.; Luo, X.; Hasegawa, T.; Ashizawa, M.; Kawamoto, T.; Masunaga, H.; Ohta, N.; Matsumoto, H.; Mei, J.; Mori, T. n-Type Organic Field-Effect Transistors Based on Bisthienoisatin Derivatives. *ACS Applied Electronic Materials* **2019**, *1* (5), 764-771, DOI: 10.1021/acsaem.9b00105.
- (15) Zhang, G.; Zhao, Y.; Kang, B.; Park, S.; Ruan, J.; Lu, H.; Qiu, L.; Ding, Y.; Cho, K. Fused Heptacyclic-Based Acceptor–Donor–Acceptor Small Molecules: N-Substitution toward High-Performance Solution-Processable Field-Effect Transistors. *Chemistry of Materials* **2019**, *31* (6), 2027-2035, DOI: 10.1021/acs.chemmater.8b05054.
- (16) Zhao, D.; Hu, J.; Liu, Z.; Xiao, B.; Wang, X.; Zhou, E.; Zhang, Q. Isatylidene malononitrile derived acceptors for fullerene free organic solar cells. *Dyes and Pigments* **2018**, *151*, 102-109, DOI: 10.1016/j.dyepig.2017.12.054.
- (17) Zhao, D.; Hu, J.; Cao, K.; Xiao, B.; Zhou, E.; Zhang, Q. Isatin-derived non-fullerene acceptors towards high open circuit voltage solar cells. *Dyes and Pigments* **2019**, *162*, 898-904, DOI: 10.1016/j.dyepig.2018.11.027.
- (18) Pakravan, P.; Kashanian, S.; Khodaei, M. M.; Harding, F. J. Biochemical and pharmacological characterization of isatin and its derivatives: from structure to activity. *Pharmacological Reports* **2013**, *65* (2), 313-335, DOI: 10.1016/S1734-1140(13)71007-7.
- (19) Khan, F. A.; Maalik, A. Advances in pharmacology of isatin and its derivatives: A review. *Tropical Journal of Pharmaceutical Research* **2015**, *14* (10), 1937-1942, DOI: 10.4314/tjpr.v14i10.28.
- (20) Moradi, R.; Ziarani, G. M.; Lashgari, N. Recent applications of isatin in the synthesis of organic compounds. *Arkivoc* **2017**, *2017* (1), 148-201, DOI: 10.24820/ark.5550190.p009.980.
- (21) Polychronopoulos, P.; Magiatis, P.; Skaltsounis, A.-L.; Myrianthopoulos, V.; Mikros, E.; Tarricone, A.; Musacchio, A.; Roe, S. M.; Pearl, L.; Leost, M. Structural basis for the synthesis of indirubins as potent and selective inhibitors of glycogen synthase kinase-3 and cyclin-dependent kinases. *Journal of medicinal chemistry* **2004**, *47* (4), 935-946, DOI: 10.1021/jm031016d.

- (22) Chandra, A.; Yadav, N. R.; Moorthy, J. N. Facile synthesis of isatins by direct oxidation of indoles and 3-iodoindoles using NIS/IBX. *Tetrahedron* **2019**, *75* (14), 2169-2174, DOI: 10.1016/j.tet.2019.02.033.
- (23) Bura, T.; Leclerc, N.; Bechara, R.; Lévêque, P.; Heiser, T.; Ziessel, R. Triazatruxene-Diketopyrrolopyrrole Dumbbell-Shaped Molecules as Photoactive Electron Donor for High-Efficiency Solution Processed Organic Solar Cells. *Advanced Energy Materials* **2013**, *3* (9), 1118-1124, DOI: 10.1002/aenm.201300240.
- (24) Matsui, M.; Tanaka, N.; Funabiki, K.; Haishima, Y.; Manseki, K.; Jin, J.; Inoue, Y.; Higashijima, S.; Kubota, Y. Application of indoline dyes attached with strongly electron-withdrawing carboxylated indan-1,3-dione analogues linked with a hexylthiophene ring to dye-sensitized solar cells. *Tetrahedron* **2018**, *74* (27), 3498-3506, DOI: 10.1016/j.tet.2018.04.077.
- (25) Barnsley, J. E.; Shillito, G. E.; Larsen, C. B.; van der Salm, H.; Wang, L. E.; Lucas, N. T.; Gordon, K. C. Benzo [c][1, 2, 5] thiadiazole donor-acceptor dyes: A synthetic, spectroscopic, and computational study. *The Journal of Physical Chemistry A* **2016**, *120* (11), 1853-1866, DOI: 10.1021/acs.jpca.6b00447.
- (26) Chen, Y.; Geng, Y.; Tang, A.; Wang, X.; Sun, Y.; Zhou, E. Changing the pi-bridge from thiophene to thieno[3,2-b]thiophene for the D-pi-A type polymer enables high performance fullerene-free organic solar cells. *Chem Commun (Camb)* **2019**, *55* (47), 6708-6710, DOI: 10.1039/c9cc02904d.
- (27) Cordovilla, C.; Bartolomé, C.; Martínez-Ilarduya, J. s. M.; Espinet, P. The Stille reaction, 38 years later. *ACS Catalysis* **2015**, *5* (5), 3040-3053, DOI: 10.1021/acscatal.5b00448.
- (28) Oliveira, S. C. B.; Fernandes, I. P.; Silva, B. V.; Pinto, A. C.; Oliveira-Brett, A. M. Isatin nitro-derivatives redox behaviour. *Journal of Electroanalytical Chemistry* **2013**, *689*, 207-215, DOI: 10.1016/j.jelechem.2012.10.018.
- (29) Xiang, N.; Liu, Y.; Zhou, W.; Huang, H.; Guo, X.; Tan, Z.; Zhao, B.; Shen, P.; Tan, S. Synthesis and characterization of porphyrin-terthiophene and oligothiophene π -conjugated copolymers for polymer solar cells. *European Polymer Journal* **2010**, *46* (5), 1084-1092, DOI: 10.1016/j.eurpolymj.2010.01.015.
- (30) Li, Y.; Wu, Y.; Liu, P.; Birau, M.; Pan, H.; Ong, B. S. Poly (2, 5-bis (2-thienyl)-3, 6-dialkylthieno [3, 2-b] thiophene) s—High-Mobility Semiconductors for Thin-Film Transistors. *Advanced Materials* **2006**, *18* (22), 3029-3032, DOI: 10.1002/adma.200601204.
- (31) Raynor, A. M.; Gupta, A.; Plummer, C. M.; Jackson, S. L.; Bilic, A.; Patil, H.; Sonar, P.; Bhosale, S. V. Significant improvement of optoelectronic and photovoltaic properties by incorporating thiophene in a solution-processable D-A-D modular chromophore. *Molecules* **2015**, *20* (12), 21787-21801, DOI: 10.3390/molecules201219798.
- (32) Becke, A. D. Density-functional thermochemistry. III. The role of exact exchange. *The Journal of Chemical Physics* **1993**, *98* (7), 5648-5652, DOI: 10.1063/1.464913.

- (33) Lee, C.; Yang, W.; Parr, R. G. Development of the Colle-Salvetti correlation-energy formula into a functional of the electron density. *Physical Review B* **1988**, *37* (2), 785-789, DOI: 10.1103/PhysRevB.37.785.
- (34) Miehlich, B.; Savin, A.; Stoll, H.; Preuss, H. *Chem. Phys. Lett* **1989**, *157*, 200-206, DOI: 10.1016/0009-2614(89)87234-3.
- (35) Frisch, M. J.; Trucks, G. W.; Schlegel, H. B.; Scuseria, G. E.; Robb, M. A.; Cheeseman, J. R.; Scalmani, G.; Barone, V.; Petersson, G. A.; Nakatsuji, H.; Li, X.; Caricato, M.; Marenich, A. V.; Bloino, J.; Janesko, B. G.; Gomperts, R.; Mennucci, B.; Hratchian, H. P.; Ortiz, J. V.; Izmaylov, A. F.; Sonnenberg, J. L.; Williams, J.; Ding, F.; Lipparini, F.; Egidi, F.; Goings, J.; Peng, B.; Petrone, A.; Henderson, T.; Ranasinghe, D.; Zakrzewski, V. G.; Gao, J.; Rega, N.; Zheng, G.; Liang, W.; Hada, M.; Ehara, M.; Toyota, K.; Fukuda, R.; Hasegawa, J.; Ishida, M.; Nakajima, T.; Honda, Y.; Kitao, O.; Nakai, H.; Vreven, T.; Throssell, K.; Montgomery Jr., J. A.; Peralta, J. E.; Ogliaro, F.; Bearpark, M. J.; Heyd, J. J.; Brothers, E. N.; Kudin, K. N.; Staroverov, V. N.; Keith, T. A.; Kobayashi, R.; Normand, J.; Raghavachari, K.; Rendell, A. P.; Burant, J. C.; Iyengar, S. S.; Tomasi, J.; Cossi, M.; Millam, J. M.; Klene, M.; Adamo, C.; Cammi, R.; Ochterski, J. W.; Martin, R. L.; Morokuma, K.; Farkas, O.; Foresman, J. B.; Fox, D. J. *Gaussian 16 Rev. C.01*, Wallingford, CT, 2016.

Isatin as terminal group for quinoidal structures

4.1) Introduction

Quinoidal molecules have recently emerged as promising building blocks for constructing functional π -conjugated materials, due to their highly planar structure which is beneficial for efficient π - π staking and charge transport. Their π -delocalized systems enable to reduce the band gaps and to confer them an amphoteric redox behavior which makes them potential candidates as n-type, p-type and ambipolar materials.¹⁻² Among these, quinoidal small molecules having isatin as a terminal group (indophenine), have received a little attention because they exist as a mixture of all six possible geometric isomers (**Figure I-1**). The existence of isomers would affect the ability of the molecular self-assembly to form highly crystalline thin film and thus charge carrier mobility.

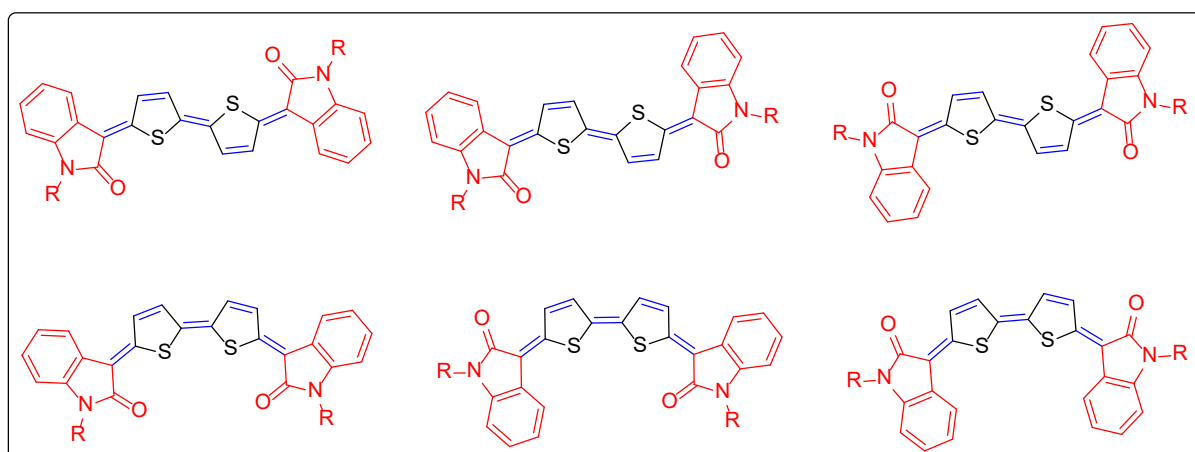


Figure I-1. Molecular structures of all six possible geometric isomers of indophenine.

Two approaches have been used to the control stereochemical issue. The first approach involves the oxidation of thiophene to form the thiophene-S, S-dioxide which in turn induces steric hindrance and leads to thiophene-S, S-dioxidized indophenine as a single pure isomer. The second approach involves the use of a noncovalent conformational locking method as the driving force for the formation of a single isomer. Deng *et al.* found that the oxidation of thiophene ring to its 1, 1-dioxidized of the quinoidal bithiophene unit in indophenine led to a dual benefit: (i) it promotes isomerization to produce a single isomeric product; (ii) it greatly reduces the energy level of LUMO/HOMO.³ 3-chloroperoxybenzoic acid (*m*CPBA), was used to oxidize the mixture of indophenine isomers producing three isomers, (E,E,E), (Z,E,E) and (Z,E,Z). The mixture of three isomers were heated in toluene under reflux to yield the pure single isomer of indophenine (Compound **I-1**, **Figure I-2**). Finally, the pure isomer was used as a co-monomer to react with 2,5-bis(trimethylstannyl)thieno[3,2-*b*] thiophene to form its corresponding polymer through a Stille coupling reaction. The obtained polymer exhibited a narrow band gap and low energy levels. The polymer exhibited unipolar electron charge transfer in organic field

effect transistors (OFETs) with an electron mobility up to $0.14 \text{ cm}^2 \text{ V}^{-1} \text{ s}^{-1}$.³ A deep insight into the effect of S, S-dioxidized thiophene on the opto-physical and electrochemical properties of indophenine derivatives was reported by Hu and coworkers.⁴ They synthesized several thiophene-S, S-dioxidized indophenine substituted at 5, 5' positions with EWG/ EDG (Compound **I-2**). Their optoelectronic, electro-chemical properties and light stability were experimentally and theoretically investigated and compared to the parent indophenine analogues. It was found that: (i) the oxidation of thiophene largely enhanced the structural stability under irradiation; (ii) the introduction of S, S-dioxidized thiophene in quinoidal system provoked significant hypsochromic shift of the absorption compared to the aromatic system; (iii) EWG were beneficial for maintaining the quinoidal state, while EDG had large effect on the electron cloud density distribution, energy levels, absorption, and light stability in both series. Geng and coworkers reported the synthesis and charge transport properties of a single-isomer of the thienoquinoidal unit, via a synthetic route involving regioselective nucleophilic addition, dihydroxylation, dehydrogenation and oxidation.⁵⁻⁶ The mixture of isomers was oxidized with *m*CPBA, followed by thermal isomerization ($120 \text{ }^\circ\text{C}$ in toluene) to give a single-isomer (Compound **I-3**). Upon substitution of peripheral hydrogen atoms with fluorine in the terminal isatin units, the resulting fluorinated indophenine exhibited lower LUMO/HOMO levels and blue-shifted of the absorption spectra.⁶ Compound **I-4** with two F atoms on the peripheral isatin units exhibited the highest electron mobility ($0.16 \text{ cm}^2 \text{ V}^{-1} \text{ s}^{-1}$), due to its two-dimensional electron transport, highly ordered thin-film, and appropriate morphology.

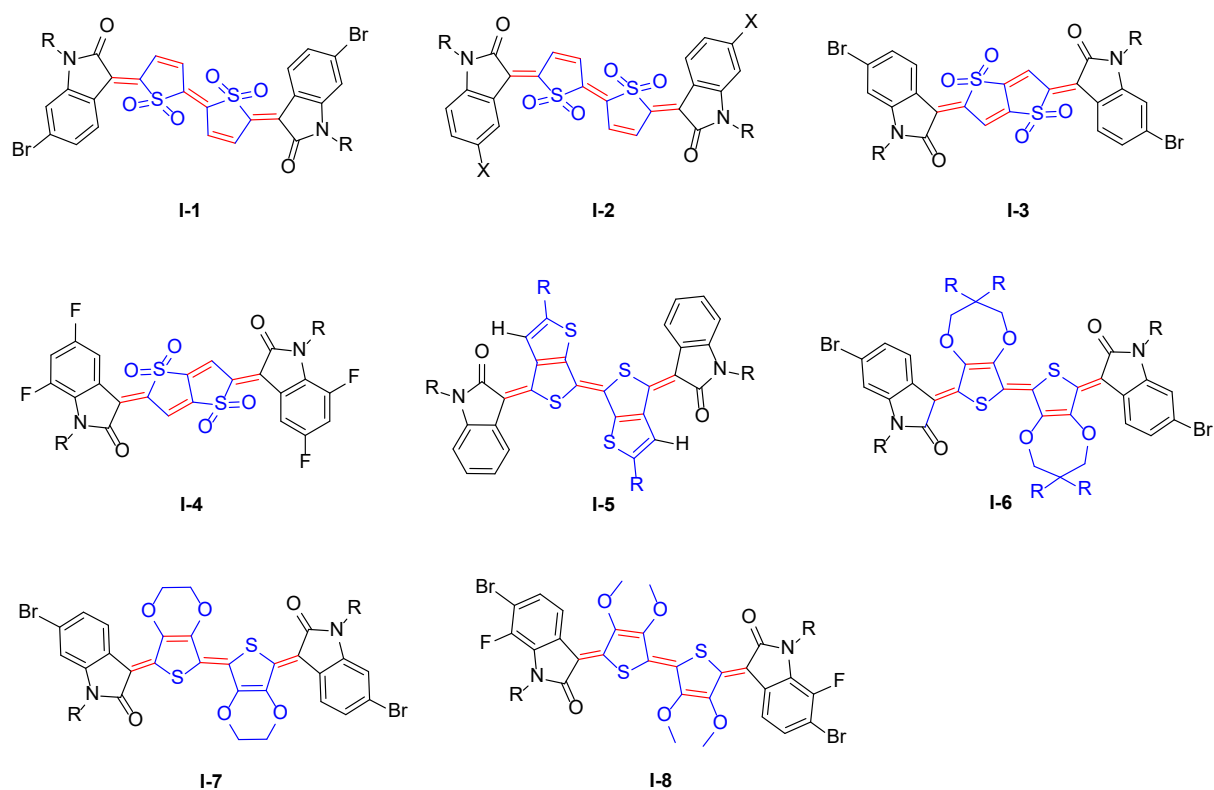


Figure I-2. Chemical structures of isomerically pure indophenine derivatives reported in the literature.

The initial synthesis of indophenine involved the condensation of thiophene with isatin in the presence of sulfuric acid. However, this reaction condition resulted in a complex mixture as reported by Cava *et al.*⁷ This limitation was elegantly overcome by Ren and coworkers who proposed mild reaction conditions using Sn^{II}-mediated reductive aromatization of diol to afford the fully quinoidal form without oxidation of the intermediate aromatic form.⁸ They designed and synthesized dithienoindophenine derivatives, DTIP-i-O (Compound **I-5**), by the introduction of thieno[3,4-*b*]thiophene (TbT) into the indophenine framework. The presence of intramolecular O...H interactions confirmed a well-defined conformation and no other isomers were generated. Using TbT as the π -bridge showed several strengths: stable E-configuration, large π -surface, and the short intermolecular S...S interactions, which were specifically favorable for hole transport. The frontier orbital energies of DTIPs were slightly increased for HOMO and dramatically increased for LUMO compared to the parent indophenine. This indicated that the aromatization tendency of the quinoidal backbone was restrained. Excellent unipolar hole mobilities up to $0.15 \text{ cm}^2 \text{ V}^{-1} \text{ s}^{-1}$ was reported for compound I-5. Further development of selective synthesis of single isomers was accomplished by Pappenfus *et al.*, who successfully obtained the production of single isomer using intramolecular interaction between sulfur of 3,4-propylenedioxythiophenes and the carbonyl oxygen of isatin, as the driving force to obtain one isomer (Compound **I-6**).⁹ By using the same approach, Hwang *et al.* adopted O...S noncovalent conformational lock and steric hindrance to manipulate syn- and anti-isomerization of a bis-3,4-ethylenedioxythiophene indophenine (bis-QEDOT, Compound **I-7**).¹⁰ As a result, single isomer of bis-QEDOT was obtained by introducing the bis-3,4-ethylenedioxy group, its geometrical structure was identified by, ¹H NMR and density functional theory calculation. More recently, replacing a H atom with a methoxy group in the thiophene ring promotes O...S conformational locking in the backbone of quinoidal indophenine.¹¹ With substitution of the methoxy group at the 3, 4-position in thiophene, only a single isomer (Z, E, Z) was observed via an indophenine standard reaction (Compound **I-8**). The existence of O...S conformational locks has been demonstrated by solving single-crystal structure. The X-ray structure of 3,4-dimethoxythiophene indophenine points to a highly planar core with a distance of only 2.69 Å between the S atom of 3,4-dimethoxythiophene and the O atom of C=O in isatin units, smaller than the sum of the van der Waals radii of these atoms, indicative of the existence of a through-space noncovalent interaction, which leads to a perfect coplanarity between the two thiophene moieties, the dihedral angle is almost 0°.

Objectives of this study

Quinoidal oligothiophene derivatives usually contain multiple *cis-trans* isomers,¹²⁻¹³ which is not favorable for structural characterization and the formation of highly crystalline film suitable for

optoelectronic applications. By introducing non-covalent intramolecular interaction,¹⁴ such as hydrogen bonding, sulfur-oxygen interaction between the π -bridge unit and flanking isatin units, one can control the conformation of resulting indophenine derivatives. In this chapter, our objective is to design and characterize of new quinoidal materials in which two isatin units are bridged by EDOT derivatives. In such structures, the π -spacer bridge not only extends the effective conjugation length of quinoidal form but also acts as conformational locking units to drive the formation of a single isomer. This family of molecules can be viewed as an isoindigo in which the middle C=C bond is replaced with π -conjugated units to extend the π -conjugated system (**Chart 1**).

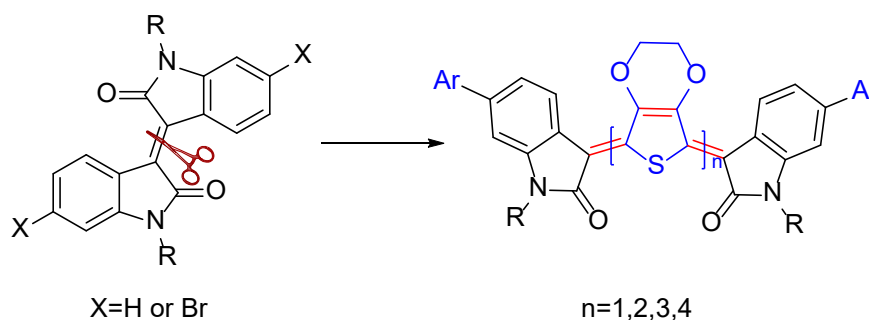


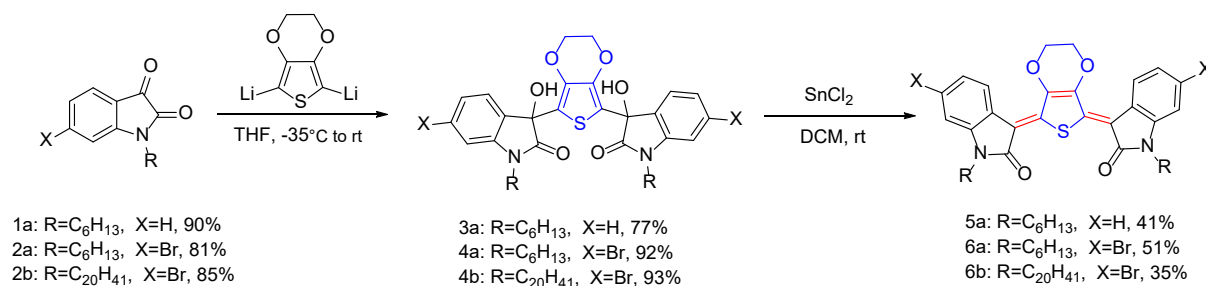
Chart 1. Cartoon representation of the approach used for the synthesis of indophenine derivatives

4.2) Results and discussion

In the following we describe the organic synthesis routes, the mechanisms of the synthesis of the molecules, their characterizations: NMR, HRMS, UV-visible, electrochemistry and the structure property relationships within these molecules. It is worth mentioning that we discuss in detail 1D and 2D NMR spectra of these new molecules, because it is very important to obtain the structural information and to assess the formation of single isomers.

4.2.1) Synthetic methodology

The synthetic routes to indophenine derivatives are illustrated in **Scheme 1-4**, detailed synthetic procedures are described in experiment part. For the solubility issue, we alkylated the isatin ring using different alkyl side-chains, linear and branched ones.¹⁵ To further derivatize the resulting indophenine molecules, we employed 6-bromo-isatin as a starting substrate. Two synthetic strategies were developed. The first one involves the nucleophilic addition of organolithium or Grignard reagents to isatin, followed by dehydration with sulfuric acid, via a delocalized carbocation intermediate, to afford the desired indophenine. An alternative way to the synthesis of indophenine dyes is the dehydration reaction of diols to generate quinoidal derivatives via reductive aromatization using SnCl_2 and subsequent oxidation with DDQ.¹⁶⁻¹⁷



Scheme 1. Synthetic route for the preparation of quinoidal structures compounds **5a**, **6a**, **6b**.

The molecular structure of EDOT, or 3,4-Ethylenedioxythiophene consists of a thiophene ring substituted at positions 3 and 4 with an ethylene glycolyl unit. This molecular is usually used as electron-donating building block for the preparation of donor-acceptor structures.¹⁸ One EDOT unit bridged with two 6-bromoisatin moieties (**6a**) was synthesized using the synthetic approach depicted in **Scheme 1**. In such reaction one equivalent of EDOT reacts with 2.2 equivalents of commercially available *n*-Butyllithium (*n*-BuLi) at -78 °C, to afford the dilithium intermediate. A slight excess of *n*-BuLi was used to completely consume the EDOT, in such a way the formation of by-products is greatly reduced. Treatment of **2a** with dilithium 2, 5-EDOT and subsequent reductive aromatization with SnCl₂ in anhydrous dichloromethane gave the desired quinoidal compound¹⁹ in yield of 41 %. ¹H, ¹³C NMR, IR, and HRMS confirm the molecular structure of the targeted compound (**6a**). The formation of the single isomer is confirmed by means of ¹H NMR spectroscopy. The three possible stereoisomers of compound **6a** are shown in **Chart 2**. The isomers with asymmetric structure (**6a-1**) will produce at least five different peaks in the aromatic region.^{7, 20} Nevertheless, in the ¹H NMR spectrum of **6a** three different proton peaks with almost identical integral ratio are observed in the aromatic region with one singlet at 4.60 ppm for ethoxy and one triplet at 3.62 ppm for N-CH₂ (H_e), **Figure 1**. This indicates that the structure of **6a** is symmetrical with respect to the EDOT moiety (isomer **6a-2** or **6a-3**). The H_a proton produces the most deshielding signal (7.93 ppm) owing to the presence of a partially negatively charged oxygen on adjacent EDOT (isomer **6a-3**). This last possibility of configuration (**6a-2**) would generate a significant steric hindrance and is hence not desirable.

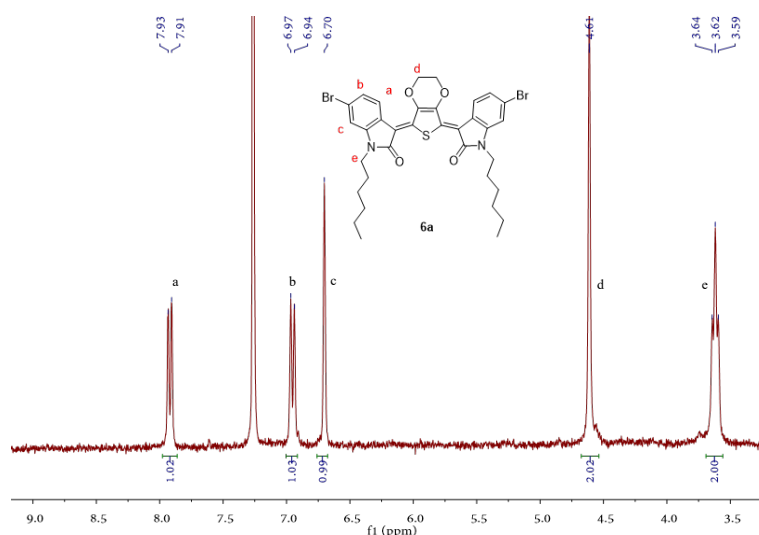


Figure 1. ^1H NMR spectrum of compound **6a**.

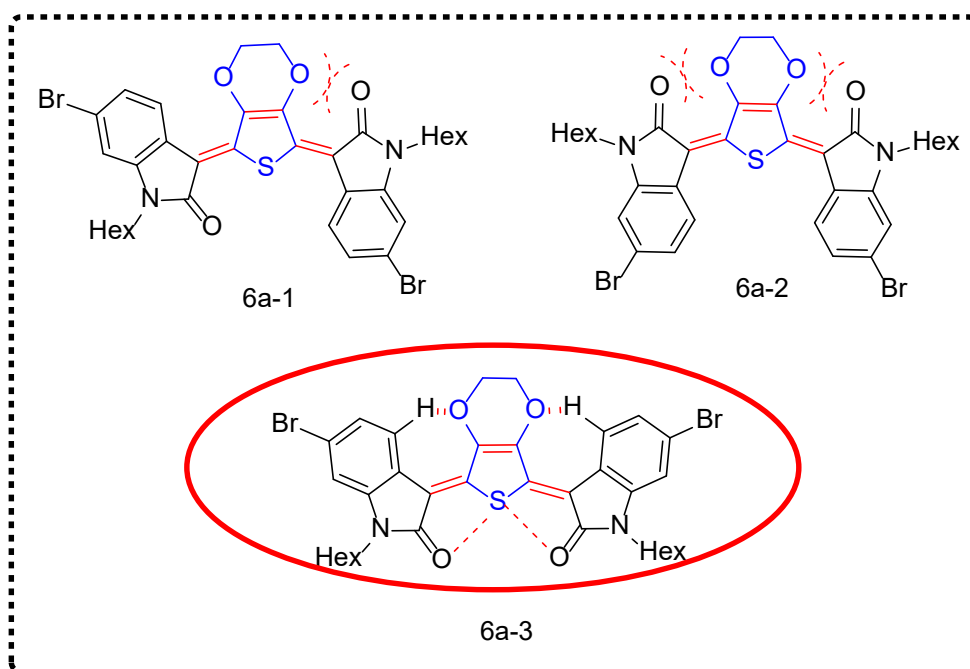


Chart 2. Molecular structures of the three possible stereoisomers of compound **6a**.

The intermediates diol (**3a** or **4a**), however, was produced as diastereomers, as shown by their ^1H NMR spectra (**Figure 2**). In particular, the splitting pattern and chemical shift of the proton of the CH_2 in aliphatic chain (N- CH_2 hexyl, H_f) can be used to confidently determine the presence and ratio of the exo and endo isomers, which is 1:1.

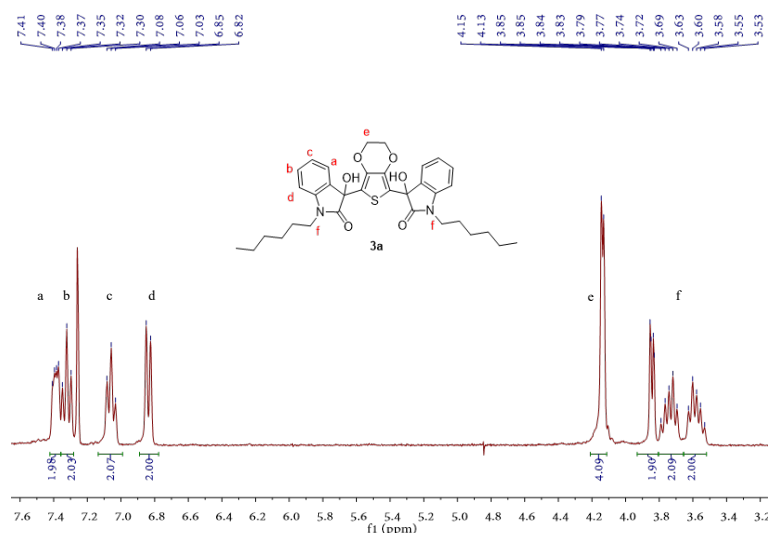
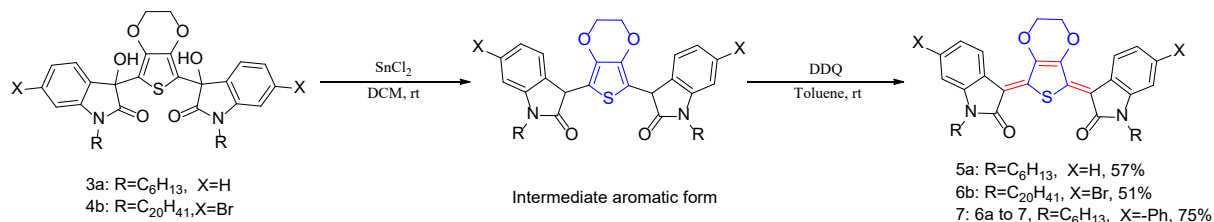


Figure 2. ¹H NMR spectrum of compound **3a**.

It should be mentioned that the Sn^{II}-mediated reductive aromatization of diols could lead to the formation of both compounds aromatic form and quinoidal form in moderate yield of 50% and 40%, respectively. Dehydrogenation of the aromatic form with 2,3-dichloro-5,6-dicyano-1,4-benzoquinone (DDQ) produced **5a** and **6b**, in respective yield of 57% and 51% (see **Scheme 2**). Further functionalization of compound **6a** was performed via Suzuki-Miyaura cross-coupling reaction and afforded the phenyl- derivative (Compound **7**).²¹⁻²²

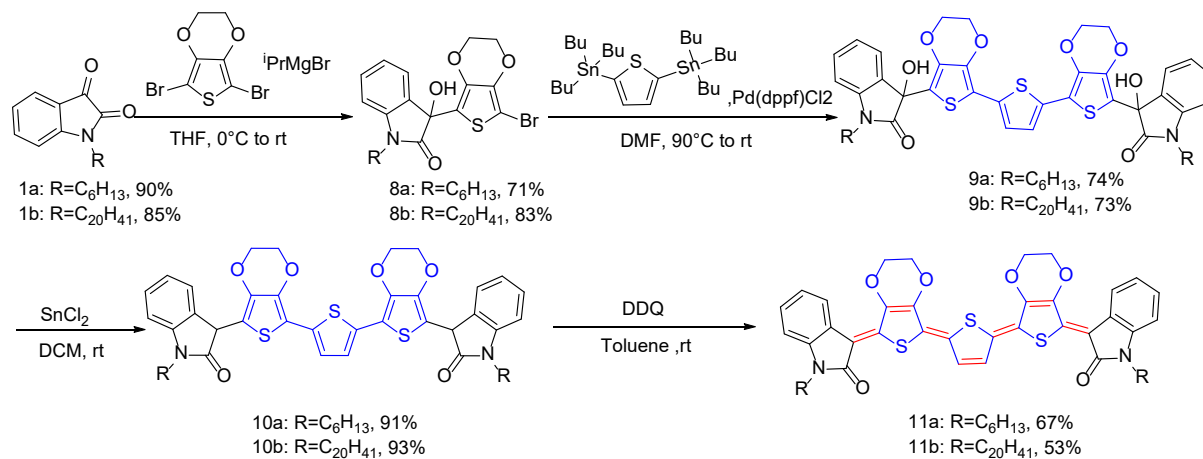


Scheme 2. Synthetic route for the preparation of quinoidal structures compounds **5a**, **6b** and **7**.

4.2.1.1) Extended bridge with an odd number of EDOT rings

The key intermediate for the synthesis of indophenine derivatives is the EDOT-alcohol derivatives (**8a** and **8b**, **Scheme 3**), which was synthesized in yield of 71% and 83% from the Grignard reagent of 2,5-dibromoEDOT, obtained by Grignard exchange of the corresponding dibromo EDOT and *i*-PrMgBr.²³ Compounds **8a** and **8b** underwent palladium-catalyzed cross-coupling reaction with dibronic aromatic to give compounds **9a** and **9b** in yield of 73%. Reductive elimination of the resulting diols using SnCl₂, under acidic conditions, followed by the oxidation with DDQ afforded the final compounds **11a** and **11b** in a good yield, as a dark blue powder. The purified fraction of **11b** was analyzed by high resolution mass spectrometry (HRMS) using two methods: atmospheric pressure chemical ionization (APCI) and photoionization (APPI). The HR-MALDI-MS spectrum of **11b** clearly

shows an intense signal at 1185.6819 for the molecular ion $[MH]^+$. The isotopic pattern closely resembles to the simulated pattern given in inside **Figure 3**.



Scheme 3. Synthetic route for the preparation of quinoidal structures compounds **11a** and **11b**.

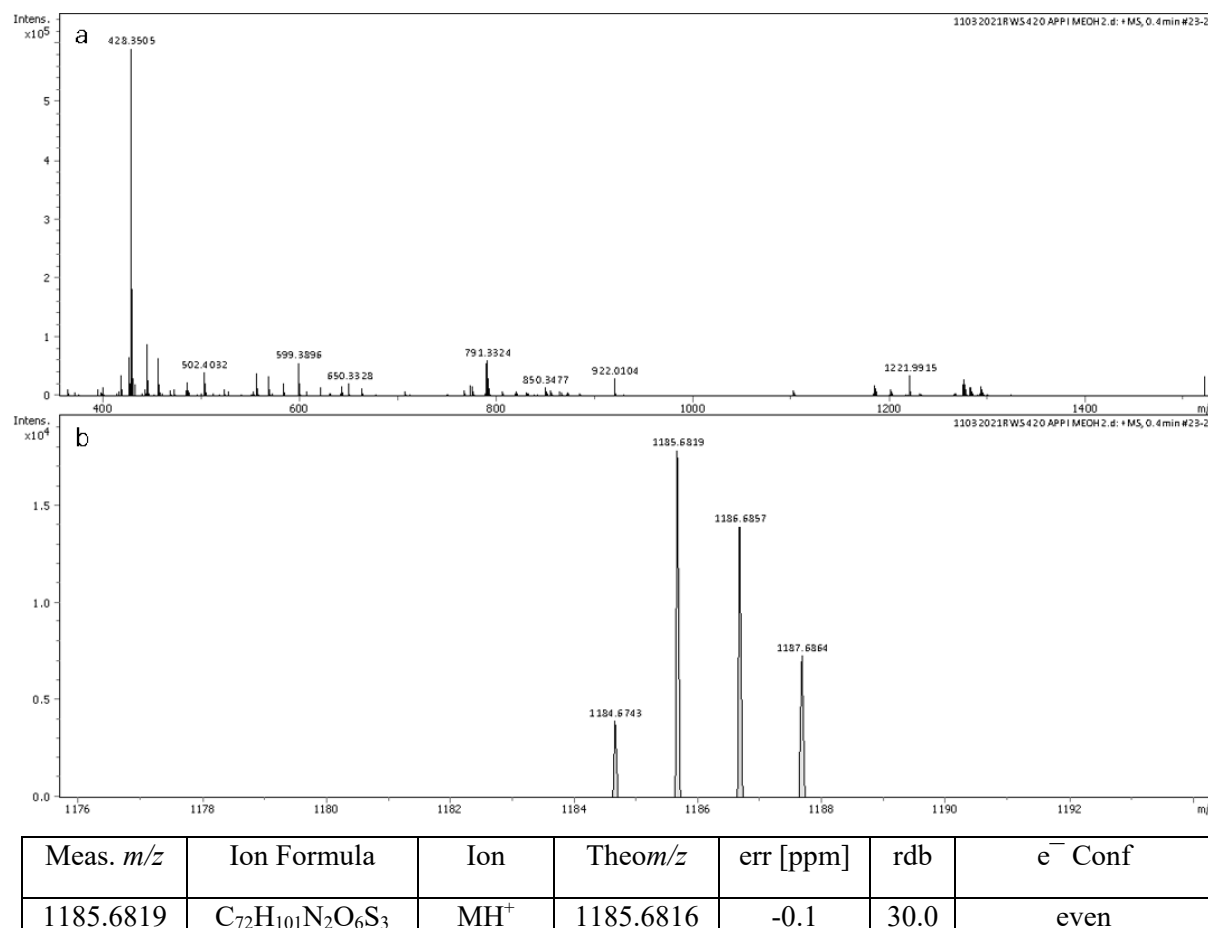


Figure 3. APPI HR-MS of compound **11b** (a) full scan and (b) zoom on isotopic pattern of m/z 1185.68 (HR-MS (APPI-P): m/z 1185.6819 $[MH]^+$; C₇₂H₁₀₁N₂O₆S₃; calcd m/z 1185.6816).

4.2.1.2) A new variant of the indophenine reaction (transition-metal-free conditions):
bridge with an even number of EDOT rings

A new variant of the indophenine reaction based on dehydration of tertiary alcohol using sulfuric acid is developed. The standard reaction for indophenine synthesis involves a one-pot procedure starting with isatin and an appropriate electron-rich 5-membered aromatic heterocycle in the presence of catalytic amount of sulfuric acid.²⁴ However, the reaction conditions lead to lower selectivity and to the formation of mixtures of isomers that were difficult to separate.²⁵ We proposed a modification of the conditions of the standard reaction to increase the yield, using tertiary alcohol as starting materials instead of isatin (**Scheme 4a-4d**). The key intermediate **12b** was prepared in 79% yield, by addition of mono-lithiated-EDOT to isatin at -35°C (**Scheme 4a**). Both *cis* and *trans* diastereomers of **12b** are produced in 1:1 ratio. As shown in **Figure 4**, the splitting pattern and chemical shift of the proton of the CH₂ in aliphatic chain (N-CH₂ branched chains, H_f) with almost identical integral ratios are observed. The single peak that appears at 6.22 ppm corresponds to H_e of EDOT. The mixture was used without further purification for the next step.

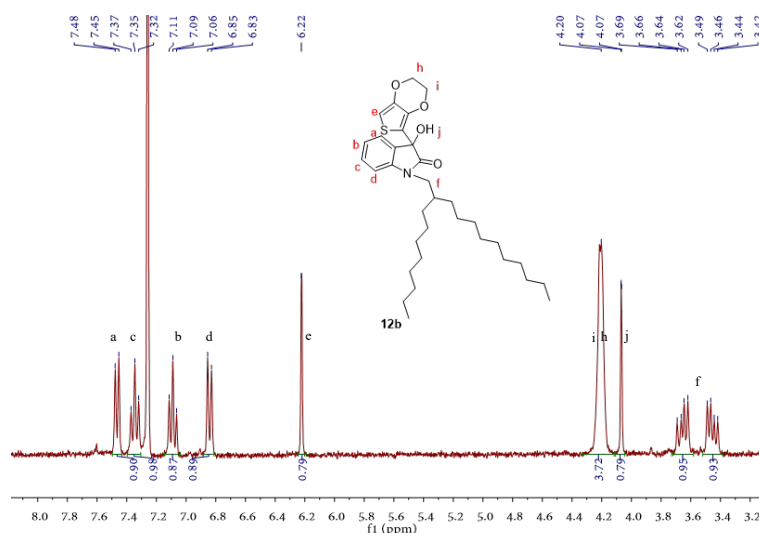
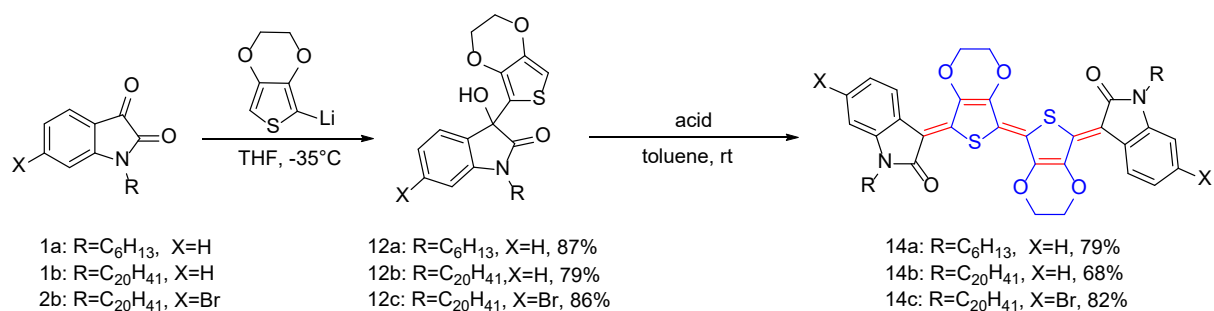
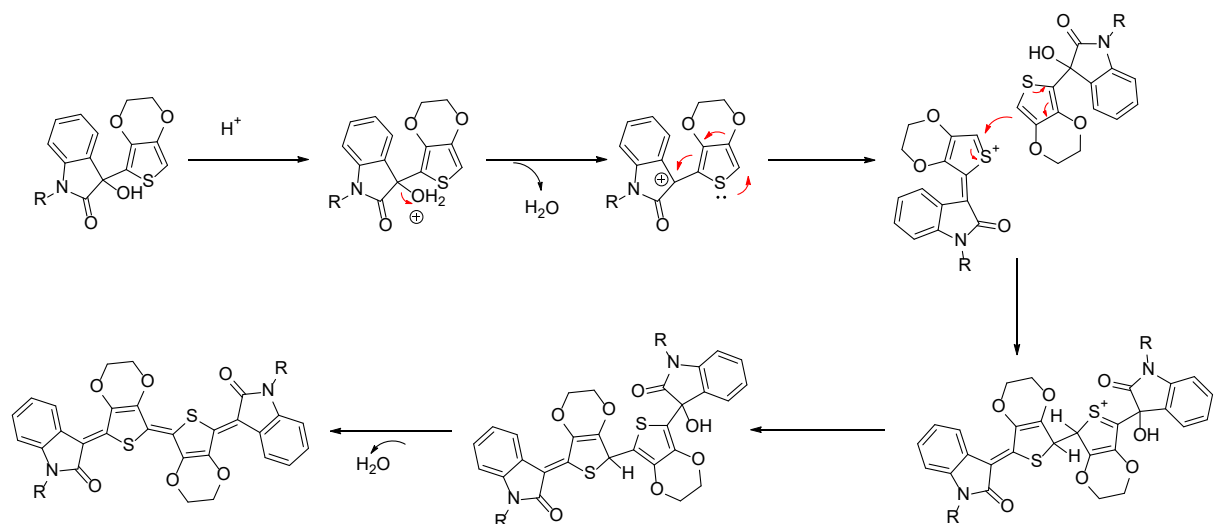


Figure 4. ¹H NMR spectrum of compound **12b**.

We hypothesized that a strong acid would lead to the formal elimination of water, via a delocalized carbocation intermediate. Nucleophilic attack occurs on the α -position of the EDOT ring of a second molecule, followed by the proton abstraction to give an alcohol intermediate (**Scheme 4b**). Two types of acids were used. The first is concentrated sulfuric acid and the second one is a *p*-toluenesulfonic acid. A catalytic amount of sulfuric acid was used to obtain dimers **14a**, with a yield of 79%. The *p*TsOH reaction also yielded to the target product with 55% yield.



Scheme 4a. Synthetic route for the preparation of quinoidal structures compounds **14a** and **14b**.



Scheme 4b. Proposed mechanism of indophenine formation from alcohol intermediate.

¹H NMR experiments showed that a single isomer of **14b**, was only formed, **Figure 5**. With the help of ¹H NMR experiments, ¹H-¹H COSY and ¹H-¹H NOESY analyses we showed a single isomer formation of **14b**. **Figure 5a** shows the ¹H NMR spectrum recorded in CDCl₃ and the proposed assignments. The ¹H NMR spectrum exhibits two doublet peaks (H_a and H_d) and two triplet peaks (H_b and H_c) for the aromatic part of isatin ring. The symmetrical peak shape belonging to the CH₂ of the EDOT part near 4.50 ppm means that the structure of the product is symmetrical. Besides, there is only one N-CH₂ peak, which also proves that the formation of one isomer.

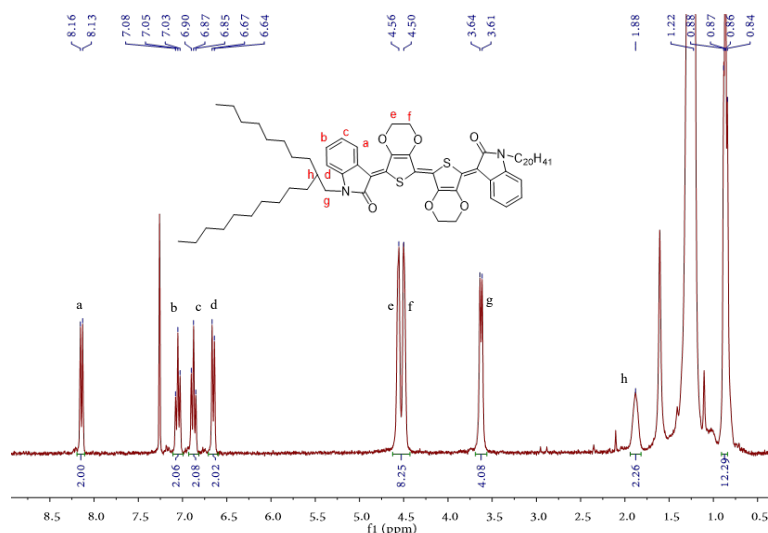


Figure 5a. ^1H NMR spectrum of compound **14b**.

The two doublet peaks at 8.15 and 6.65 ppm correspond to H_a and H_d respectively, and they are easy to distinguish (Mesomeric Effect).²⁶ The other two triplet peaks were accurately assigned using ^1H - ^1H COSY NMR. 2D ^1H - ^1H COSY analysis is a useful technique for identifying adjacent protons separated by their 2-3 bonds to correlated signals. While 2D ^1H - ^1H NOESY is useful for identifying correlation signals generated by protons even though they are not bonded and protons are usually separated from each other in space by a few angstroms.²⁷ As labeled 1, 2 3 and 4 in **Figure 5b**, three correlation peaks were identified in the aromatic region of the COSY spectrum. Each of these signals occurs because the protons are adjacent to each other. Notably the NOESY spectrum shows three additional correlation peaks, labeled 5-7, which are not found in the COSY spectrum (**Figure 5c**). Label 6-7 is easily understood because of its origin from the close spatial distance between H_d of isatin and N-alkyl chains. Label 5, on the other hand, is more interesting for its correlation between H_a originating from isatin and H_e from EDOT, since they are spatially close to each other but separated by many chemical bonds. Furthermore, NOESY experiments support that compound **14b** follows a planar conformation with a symmetric structure.

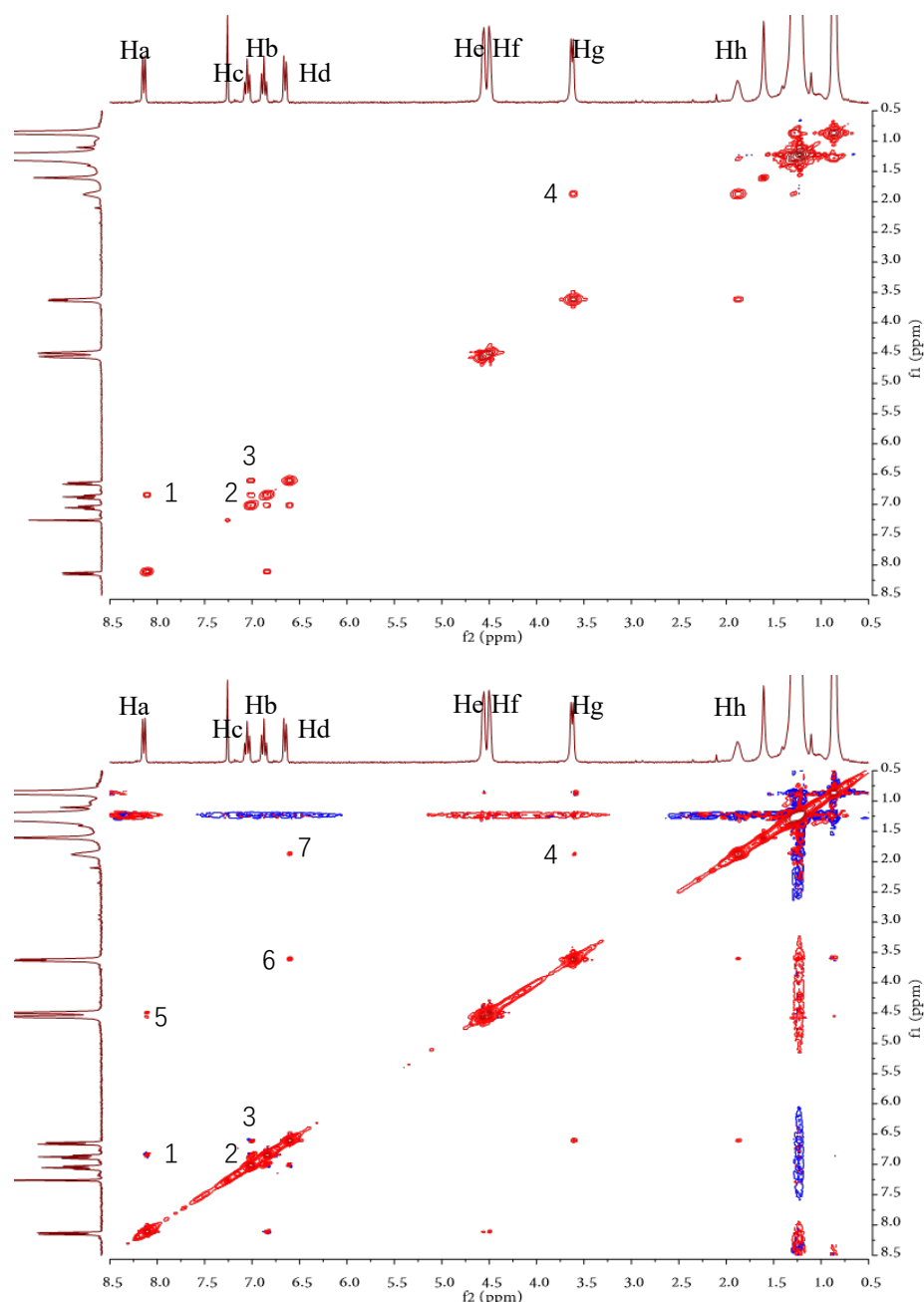


Figure 5. b) ^1H - ^1H 2D COSY; c) NOSEY spectrum of compound **14b.**

^{13}C NMR also confirms that the **14b** is isomer-free and to our best knowledge, this is the first report of ^{13}C NMR of the indophenine-EDOT derivatives. Although this indophenine derivative was early reported in 2019, no ^{13}C NMR was reported due to the solubility issue.⁸ Similar structure was published in 2020, but only incomplete and inaccurate ^{13}C NMR data were reported.⁹ An accurate assignment of ^{13}C -NMR spectra of **14b** was obtained thanks to the combination of ^{13}C NMR and DEPT 135, **Figure 5d**. In the ^{13}C NMR spectrum of **14b** (**Figure 5d**), a single peak near 170 ppm (C_1) means that there is only one product and absence of multiple isomers. The distortion less enhancement by polarization transfer (DEPT) experiment is used to determine the multiplicity of carbon atoms. DEPT 135 yields CH and CH_3 positive while CH_2 is negative. Obviously, only four positive single peaks

appeared in the DEPT 135 spectrum for the CH of isatin ring, which again confirmed the symmetry of the product.

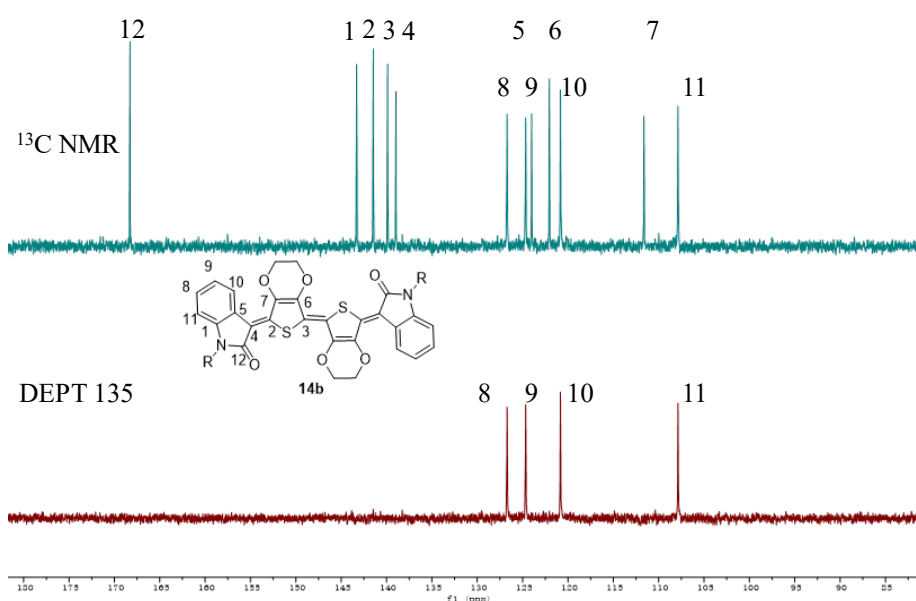
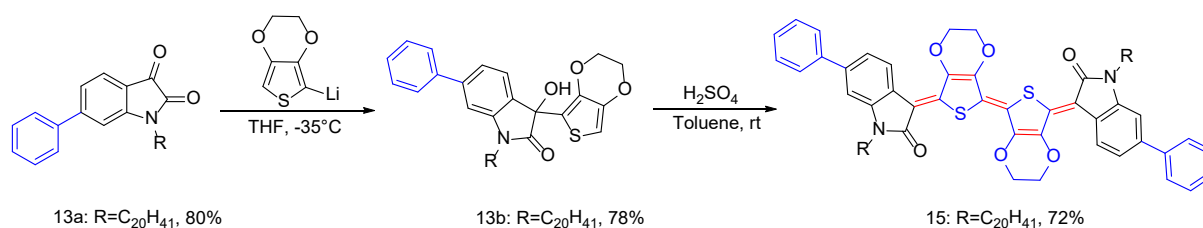


Figure 5d. ^{13}C NMR and DEPT 135 spectra of compound **14b**.

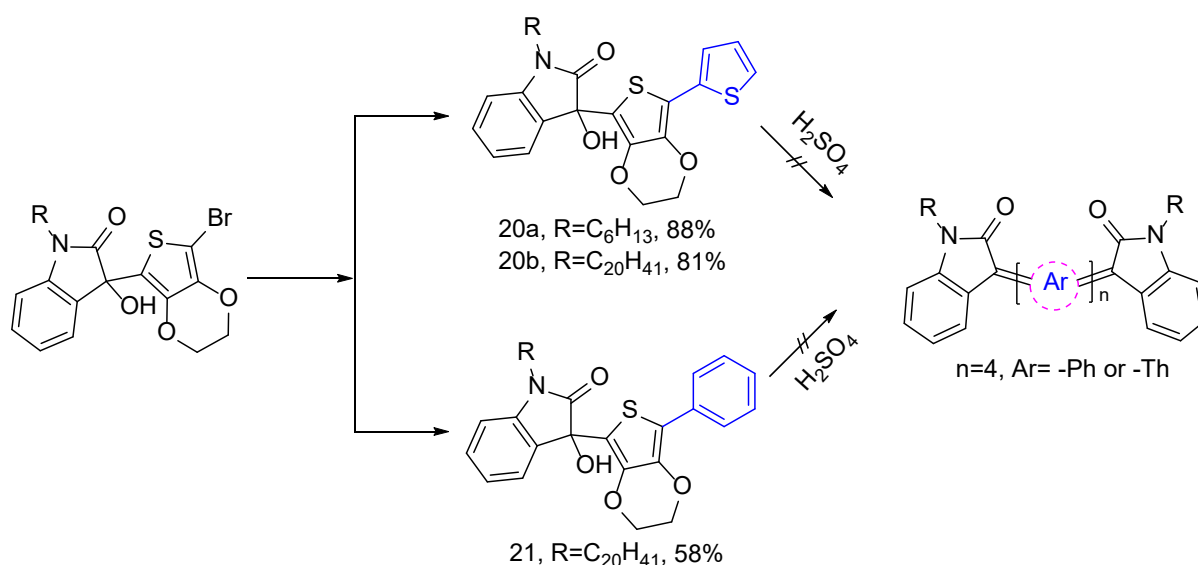
The selectivity of the reaction was further investigated. To this, we prepared the alcohol intermediate **13b** having the phenyl group on the peripheral position of the isatin. This intermediate was synthesized through a two-step reaction, firstly **2b** and phenylboronic acid are coupled via palladium catalysis, followed **13a** treated with organolithium reagent. In this molecule, there are two oxidation sites: phenyl on the isatin side¹⁷ and EDOT. Under the condition of catalytic amount of sulfuric acid, the product of the dimerization of the EDOT, product **15** was regioselectivity synthesized (**Scheme 4c**). The phenyl ring at 6-position is not attacked and oxidized by sulfuric acid. The molecular structure of **15** was confirmed by ^1H , ^{13}C NMR, IR, and HRMS. The average yield of these reactions (**14** and **15**) is 75% which is much higher than the standard reaction conditions previously reported.⁸ It is worth mentioning that this reaction has good selectivity. Specific selectivity is an advantage of this type of reaction. At the same time, this reaction condition also eliminates the by-products of one EDOT unit bridged indophenine derivative. The by-product cannot be avoided under classical reaction conditions, and the yield is about 20%.³ High yield combined with regioselectivity are the most advantages of this reaction.



Scheme 4c. Synthetic route for the preparation of quinoidal structures compound **15**.

To investigate the possible reaction mechanism and the reactivity of the aryl group in the alcohol intermediate, we carried out the reaction with **20** and **21**. These two intermediates were obtained by introducing a phenyl and a thiophene ring using a Suzuki or Stille reaction, respectively (**Scheme 4d**). Under acid-catalyzed conditions, we performed the same reaction as reported for **13b**. Unfortunately, the target product of the dimerization with four ring units, was not obtained.

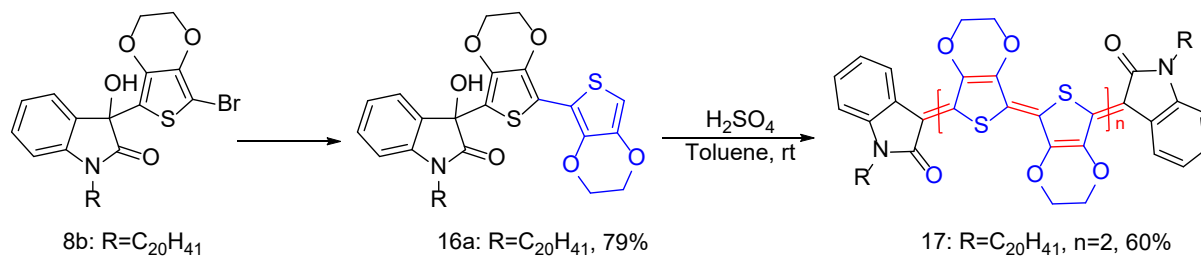
A hypothetical reaction mechanism involving carbocation species for the synthesis of indophenine derivatives thiophenes is proposed based on the reported literature and our experimental results. First, oxidative dehydration of triaryl-diol affords carbocation with the aid of sulfuric acid. The key step of this reaction involves delocalization and charge migration in the functional carbocation. Hence, for Compound **12 (a, b)** the initial step involves the formation of carbocation intermediate, with a charge highly delocalized into the adjacent EDOT ring (**Scheme 4b**). Nucleophilic attack of alcohol gives intermediate, which subsequently undergoes further elimination of H₂O to afford the final indophenine. In reactions of compounds **20** and **21**, indophenine were not formed. While the cation is formed upon the addition of the acid, it does not delocalize to the most remote position across both rings (EDOT/phenyl or EDOT/thiophene) to generate the intermediate which can be involved through nucleophilic attack to give final product (**Scheme 4d**).



Scheme 4d. Synthetic route of attempted synthesis of indophenine

Encouraged by these results, the scope of the new variant of the indophenine reaction with regard to bis-EDOT was then examined to synthesis indophenine having four EDOTs as a π -bridge, (**Scheme 4e**). Stille coupling reaction of **8b** with 2-tributylstannyl-3,4-ethylenedioxythiophene affords the intermediate **16a**, which has two EDOT units. Its structure was characterized by ¹H NMR, and **Figure 6a** shows the obtained spectrum. There are a total of five peaks in the aromatic's region. Among them,

H_a-H_d corresponds to the four CH of isatin ring. The singlet at 6.22 ppm corresponds to H_k of the EDOT. The chemical shift appears at the same ppm as that of the singlet of H_e in compound **12a**. A clear ¹³C NMR spectrum was also obtained to establish the structure of **16a**. **16a** is soluble in toluene and its solution is red. After the addition of a catalytic amount of sulfuric acid, a large number of solid precipitates and the solution becomes dark blue. **Figure 6b** shows the ¹H NMR spectrum of purified fraction of **17** recorded in CDCl₃ and the proposed assignments. HRMS provides a molecular ion peak with an m/z value of 1383.6825. **Figure 7** shows the observed HRMS spectrum and its theoretical isotropic distribution pattern for C₈₀H₁₀₇N₂O₁₀S₄ [MH]⁺.



Scheme 4e. Synthetic route for the preparation of quinoidal structures compound **17**.

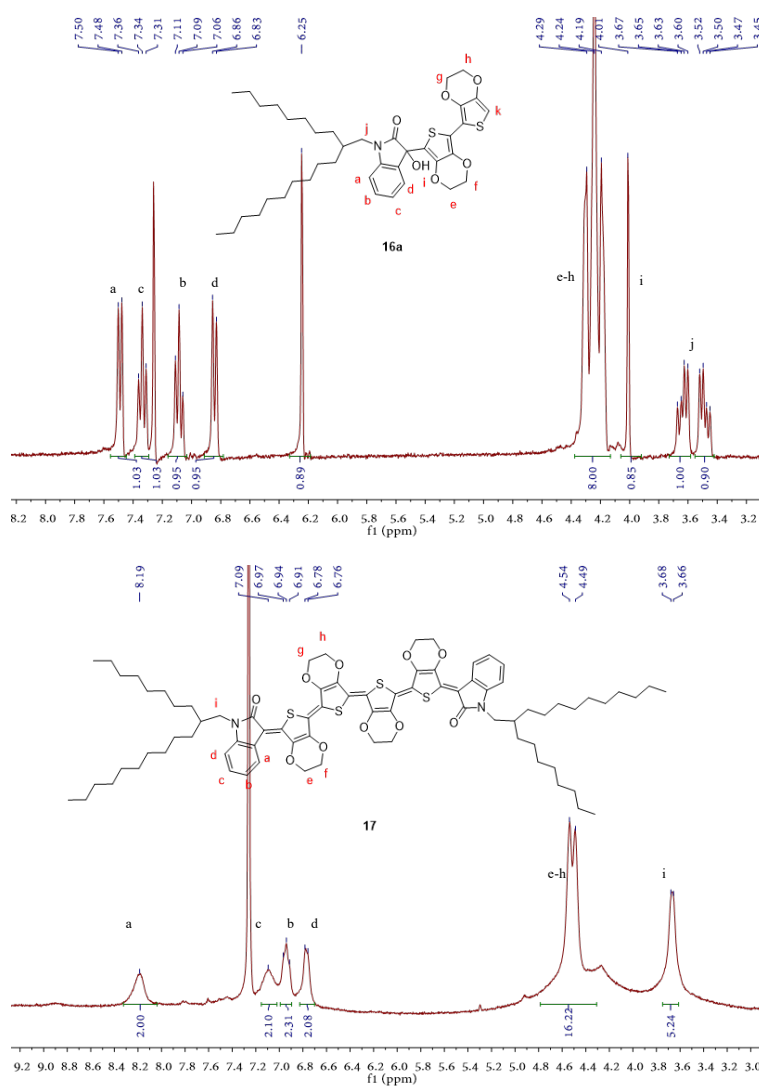
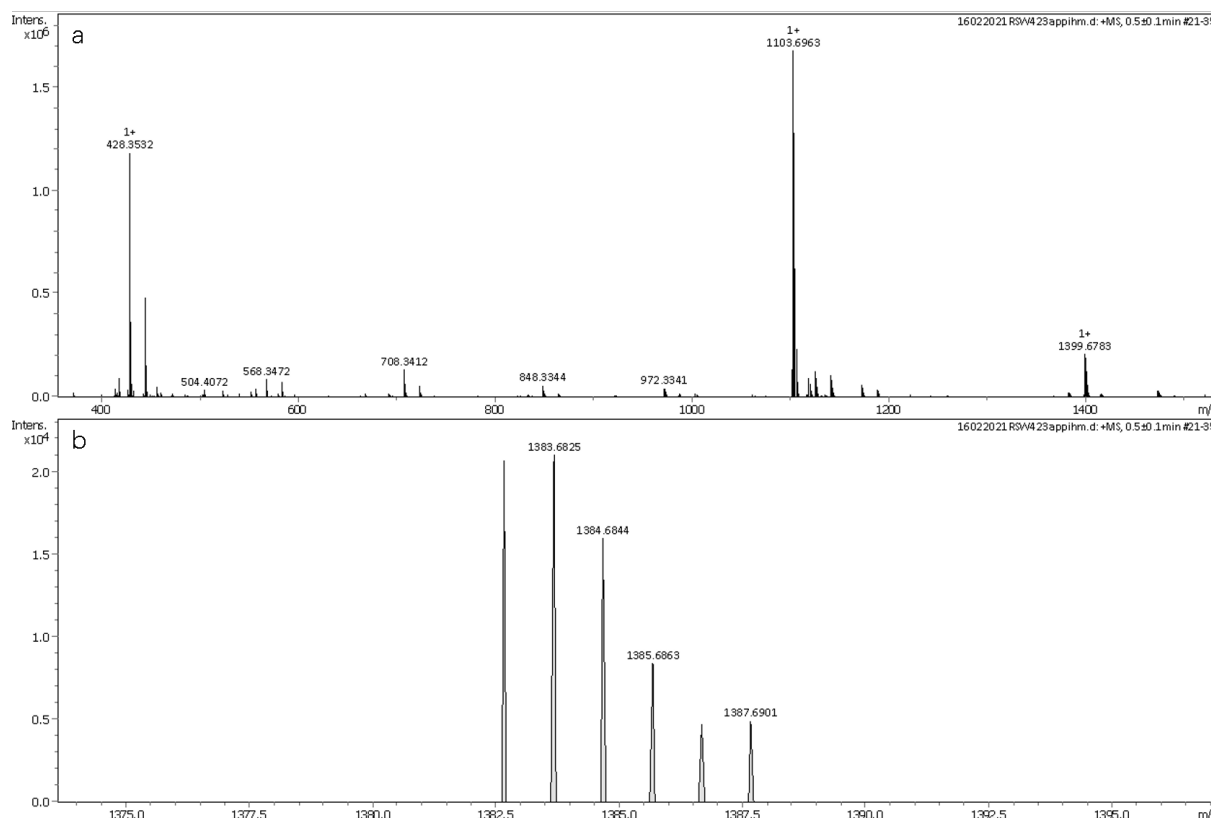


Figure 6. a) ^1H NMR spectrum of compound **16a**; b) and **17**.



Meas. m/z	Ion Formula	Ion	Theo m/z	err [ppm]	rdb	e^- Conf
1383.6825	$\text{C}_{80}\text{H}_{107}\text{N}_2\text{O}_{10}\text{S}_4$	MH^+	1383.6803	-1.6	37.0	even

Figure 7. APPI HR-MS of compound **17** (a) full scan and (b) zoom on isotopic pattern of m/z 1383.67 (HR-MS (APPI-P): m/z 1383.6825 [MH^+]; $\text{C}_{80}\text{H}_{107}\text{N}_2\text{O}_{10}\text{S}_4$; calcd m/z 1383.6803).

4.2.1.3) Conformational locks via intramolecular O...S or Br...S interactions

In organic semiconductors non-covalent interactions play an important role as noncovalent conformational lock, which can improve backbone planarity, molecular stacking and charge carrier transport. Building blocks with O...S noncovalent interactions have been widely used as conformational locks to construct organic semiconductors.²⁸ There are many examples of EDOT-based materials. For instance, crystal structure of the bis(EDOT) reveals strong intramolecular noncovalent interactions.²⁹ Structural analysis (**Figure 8**) shows that the distances between oxygen and sulfur (2.92 Å) are significantly shorter than the sum of the van der Waals radii of the two atoms (3.25 Å), and locks the π -conjugated structure into a fully planar *anti* conformation with a torsion angle of 6.9°. Another building block that shows intramolecular O...S conformational locks is dicarboxylic-bithiophene based isomers which are excellent examples of the intrinsic factors governing conformational locks (**Figure 8**). The

crystal structure indicates that this molecule is planar, featuring a small torsional angle of 2.7° and a sulfur–oxygen distance of only 2.668 \AA .

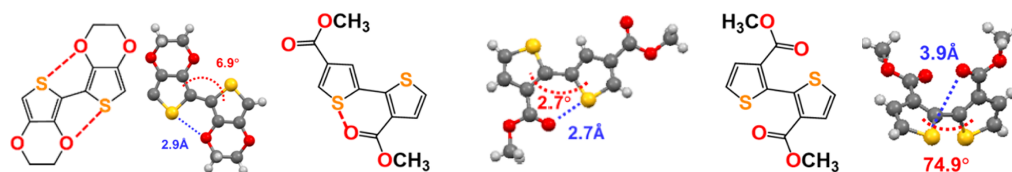


Figure 8. Chemical structures and single-crystal structures of some bithiophene derivatives showing conformational locking. Adapted from ref.²⁹

Intramolecular Br...S interactions are observed in other π -conjugated molecules (**Figure 9**). For example, bithiophene derivatives show that the presence of bromine at the 3-position of the thiophene ring results in a noncovalent intramolecular Br...S interaction in addition to the noncovalent O...S interactions in these compounds³⁰. As shown in **Figure 9**, its X-ray structure reveals a good planarity of the π -conjugated system with the two thiophene heterocycles in an anti-conformation. The dihedral angle between thienyl rings is less than 1° . The observed distances of sulfur from oxygen or bromine are 2.834 and 3.220 \AA , respectively. The distances are considerably shorter than the sum of the van der Waals radii of sulfur and oxygen (3.25 \AA) or sulfur and bromine (3.80 \AA), thus indicating that both S...O and S...Br intramolecular interactions contribute to the conformational locks.

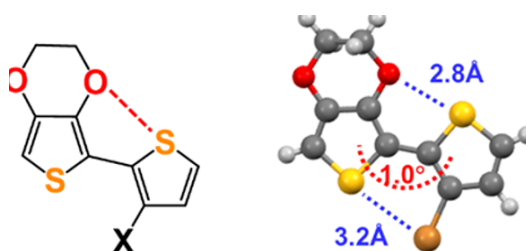
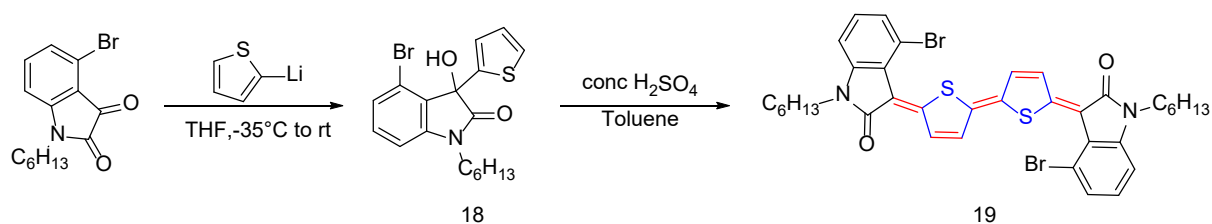
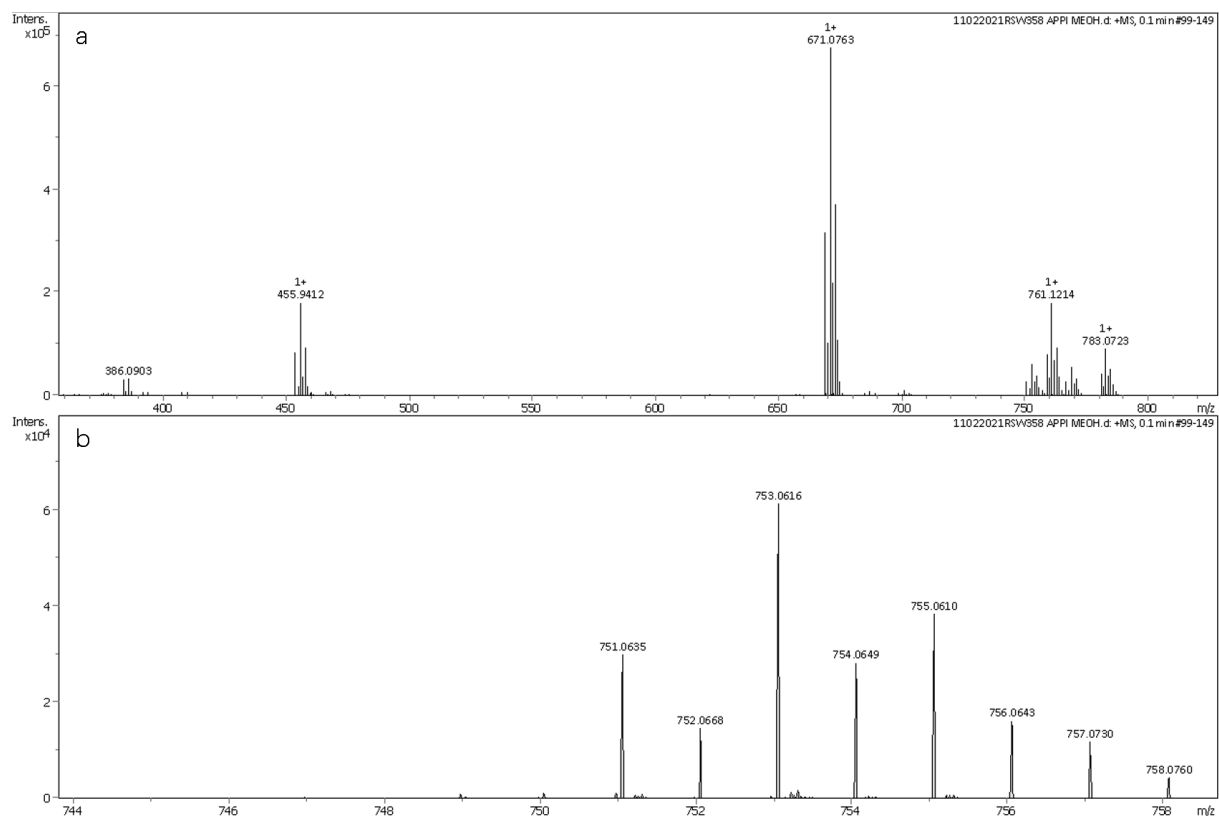


Figure 9. Chemical structures and single-crystal structures of bithiophene derivative showing conformational locking via Br...S. Adapted from ref.³⁰

In this part we report the design, synthesis and mass spectroscopy characterization of novel indophenine derivatives **19** based on 4-bromoisatin comprising S...Br conformational locks. Indophenine having 4-bromoisatin as terminal group was obtained under similar acid catalysis conditions (**Scheme 5**).



Scheme 5. Synthetic route of quinoidal structure compound **19**.



Meas. m/z	Ion Formula	Ion	Theor m/z	err [ppm]	rdb	e^- Conf
751.0635	$C_{36}H_{37}Br_2N_2O_2S_2$	MH^+	761.0657	3.1	27.0	even

Figure 10. APPI HR-MS of compound **19** (a) full scan and (b) zoom on isotopic pattern of m/z 751.06 (HR-MS (APPI-P): m/z 751.0635 $[MH]^+$; $C_{36}H_{37}Br_2N_2O_2S_2$; calcd m/z 751.0657).

The purified fraction of **19** was subjected to investigation by means of mass spectroscopy. The mass spectrum obtained presents an ion at m/z 751.0635, with an expected isotopic pattern due to the presence of two bromide atoms, corresponding to the protonated molecule (**Figure 10**). However, the single-stage mass spectrometry cannot provide us information on the presence of isomers due to their identical elemental composition. By contrast the ion mobility mass spectrometry (IMMS) is a powerful technique to discriminate and identify the regioisomeric ions. This technique allows for the temporal separation of ions based on their mobility in a cell filled with a buffer gas (N_2) under the influence of an electric field. The drift time of the ions across the mobility cell is directly proportional to their collisional cross section (CCS) which reflects the three-dimensional shape of the ions in the gas phase. The indophenine **19** was diluted in acetonitrile and subsequently ionized and transferred to the gas phase of the mass spectrometer by an electrospray ionization ion source (ESI). When indophenine **19** is subjected to ion mobility experiments, only one monomodal distribution (i.e., one ion family) is observed for the mass-to-charge ratio (**Figure 11**) corresponding to the charged molecular ion $[M]^+$.

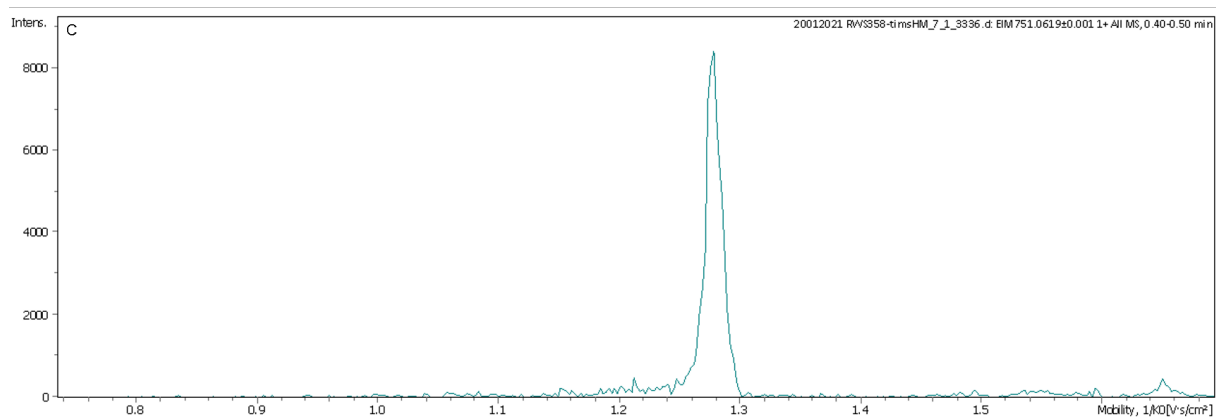
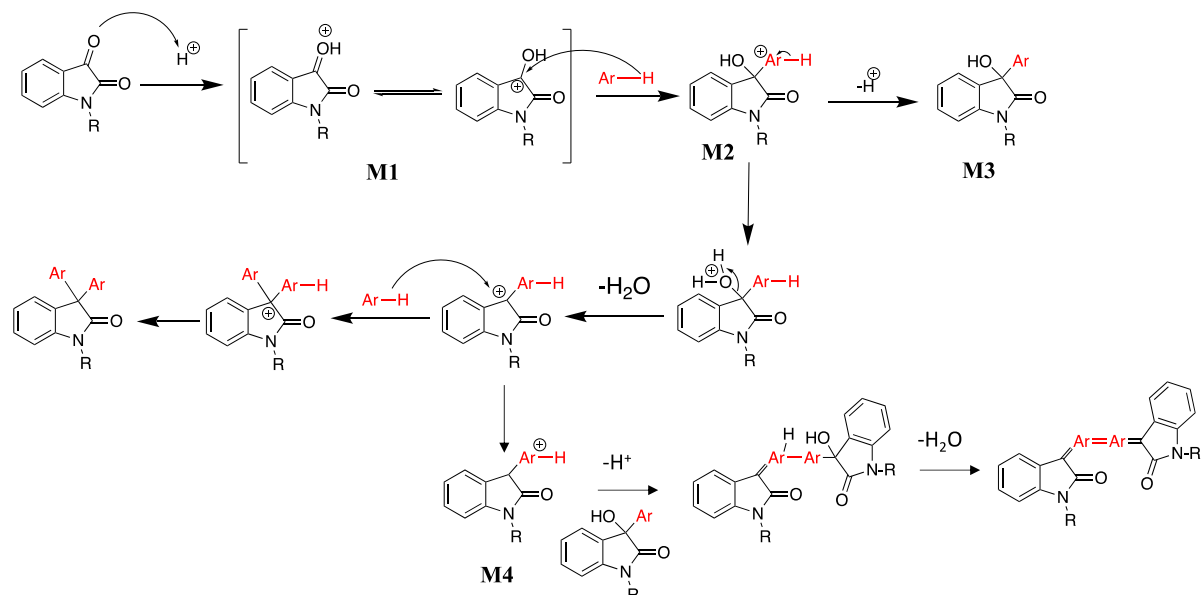


Figure 11. Mobilogram of single isomer of compound **19**.

4.2.1.4) Discussion of the mechanism

The proposed mechanism for the formation of indophenine **14** is shown in Scheme 6, originally discovered by Adolf von Baeyer in the 19th century.³¹ This reaction is based on the activation of carbonyl group by superelectrophilic chemistry. This chemistry involves a condensation reaction at the isatin ketone group developed by Zolotukhin.³² In this transformation, the isatin monomer react in strong or superacidic media to provide the reactive carboxonium ion electrophiles or superelectrophiles. The rate-determining step is the addition of the hydrocarbon to form the first σ bond with the superelectrophile. Theoretical studies on isatin with aromatic hydrocarbons were also performed. In this specific case the formation of diprotonated species increased reactivity by facilitating the σ bond formation. The role of the acid strength and the presence of the substituents (electronic and steric effects) play a crucial role in the second σ bond formation. Olah and co-workers reported libraries of 3,3-diaryloxindole products, in high yields by reaction of isatin derivatives with aromatics in triflic acid. The reaction shows a significant dependence on acid strength which suggests the formation of diprotonated, superelectrophilic intermediates. Reaction of isatin, benzene, and acid systems of varying strength (composed of $\text{CF}_3\text{SO}_3\text{H}$ and $\text{CF}_3\text{CO}_2\text{H}$) showed that the acid strength must be more acidic than $\text{H}_0 = -11.5$ for complete conversion to product³³. Klumpp and coworkers investigated the reactivity of the carbocation intermediates and the chemistry of tricationic superelectrophiles³⁴. A series of triaryl methanols were ionized in Brønsted superacids and the corresponding tricationic intermediates were formed. The trications are found to participate in two types of reactions, both are characteristic of highly charged organic cations. One set of reactions occurs through charge migration. A second set of reactions occurs through deprotonation of an unusually acidic site on the tricationic species. The key step of this chemistry involves delocalization and charge migration in the functional cation. Hence, these cationic superelectrophiles react with arene nucleophiles at a remote site. Without a nucleophilic reactant, cyclizations occur to provide novel N-heterocyclic products. The functionalized heterocycles are produced in good to excellent yields. Based on the literature reports, the mechanism of indophenine

formation is depicted on **Scheme 6**. The initial step involves the formation of activated isatin (**M1**) followed by its reaction with EDOT to generate intermediate **M2** which can evolve through two different pathways, elimination of proton and formation of alcohol or protonation, to give intermediate **M3**. The elimination of H₂O gives carbocation intermediate **M4**, with a charge highly delocalized into the adjacent EDOT ring. Nucleophilic attack of alcohol gives an intermediate, which subsequently undergoes further elimination of H₂O to afford the final products, indophenine.³⁵



Scheme 6. Reaction mechanism for the indophenine reaction discovered by Adolf von Baeyer and its variant.

4.2.2) UV-visible absorption spectroscopy

We briefly investigated the photophysical properties of these indophenine molecules. The photophysical properties of indophenines derivatives were characterized using UV/Vis spectroscopy in dilute DCM solutions at room temperature, as shown in **Figure 12a-12f**. All compounds show one main peak and two small shoulders. The shoulder is assigned to the vibrator structure, which is usually observed in quinoline oligomers.³⁶ The optical band gap (E_g^{opt}) estimated from the absorption onset is 1.96 eV for the Compound **5a** and 1.85eV for Compound **7**. The compound **7** shows a spectrum with a λ_{max} of 575 nm, which is red-shifted by 100 nm compared with that of Compound **5a** (**Figure 12a**). Introducing a bromine atom at the 6,6'-position has a small red-shift effecting on the maximum of the absorption peak and reduced the optical band gap to 1.93 eV, (**Figure 12b**). Substituting a phenyl ring at 6,6'-position, produces a red shift of ca. 25nm of the maximum of the absorption peak (**Figure 12c**). A bathochromic shift of the main absorption peak is observed, from 473 nm for **5a** to 633 nm for **14b** upon extending the π -conjugation length of the quinoidal core (**Figure 12d**).

The color of the solution in DCM has also changed, while a solution of **5a** is wine-red and deep blue for **14b**. The spectra of **14a** and **14b** (Figure 12e), which have the same central core bis-EDOT, are almost identical, indicating that the alkyl side-chains had little effect on the electronic structures of the molecules. Introducing phenyl group on the terminal isatin ring gave rise to a bathochromic shift of ca. 30 nm (Figure 12f). This shows that increasing the conjugate length in small molecules is an effective method to control the absorption peak wavelength.

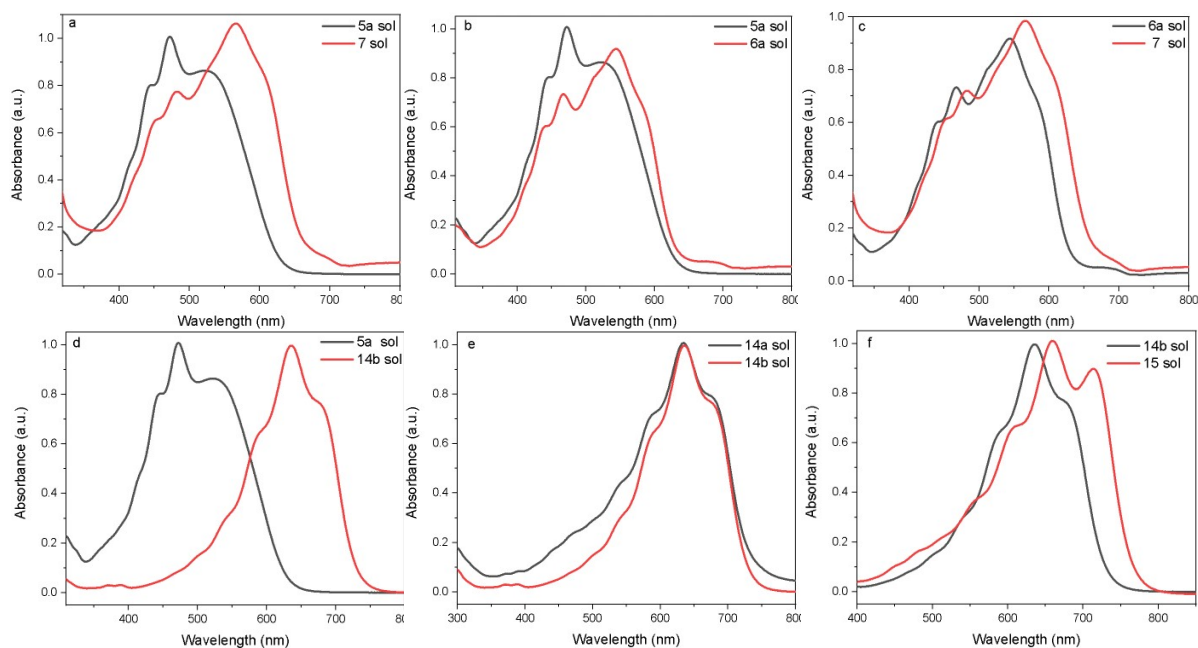


Figure 12. UV-vis absorption spectra of: a). **5a** and **7**. b). **5a** and **6a**. c) **6a** and **7**. d) **5a** and **14b**. e) **14a** and **14b**. d) **14b** and **15**.

The compounds containing three or four EDOT units as bridges resulted in strong near-infrared absorption due to further extended π -conjugation lengths with band gaps of 1.36 and 1.18 eV, respectively. As shown in Figure 13. The main absorption peaks of Compound **11** at 740 nm and Compound **17** at 820 nm, while losing the fine peak-splitting features.

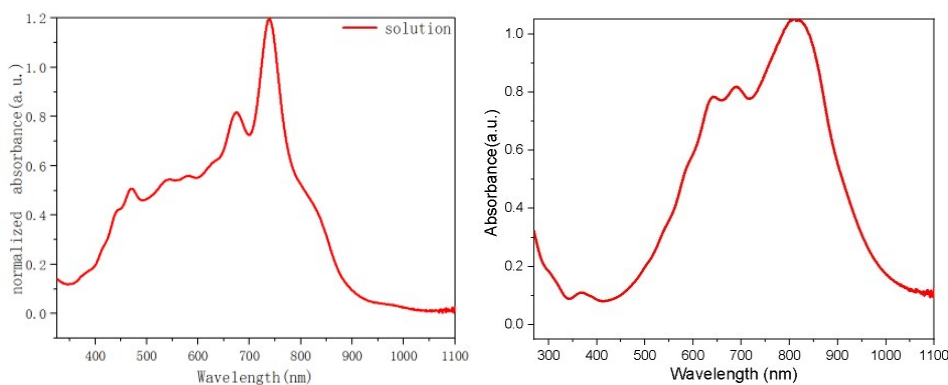


Figure 13. UV-vis absorption spectra of compound **11** (left) and **17**(right).

4.2.3) Electrochemical studies

The electrochemical properties of compound **5a** and **14b** were investigated by solution cyclic voltammetry (CV, **Figure 14a**) and square-wave voltammetry (SWV) methods, **Figure 14b-14e**. All indophenine derivatives showed an amphoteric behavior, which is typical of quinoidal molecules. They undergo reversible electron oxidation to cation and reduction to anion, indicating that the cation/anion species are well-stabilized by the quinoidal skeleton. All the compounds showed low-lying LUMO levels of less than -3.7 eV (**Table 1**), and are comparable to those of the dicyanomethylene-substituted quinoids. The compounds 14a and 14b exhibited identical HOMO/LUMO energy levels, suggesting that the influence of the alkyl chains on the HOMO/LUMO energy level is negligible. As the π -conjugation length of the central core increased, the LUMO levels slightly increase from -1.36 V (-3.77 eV) for mono-EDOT (**Figure 14b**), to -1.40 V (-3.73 eV) for Bis-EDOT, whereas the HOMO levels significantly increased from 0.61 V (-5.73 eV) for Mono-EDOT to 0.26 V (-5.28 eV) for Bis-EDOT (**Figure 14d**). Compared with the HOMO level, the LUMO level is less influenced by the central core, indicating that the band-gap reduction is mainly caused by the increase of HOMO level as the π -conjugated system extends. The HOMO/LUMO energy levels could also be modulated by introducing various substituents on the terminal isatin block. Incorporating phenyl group increased the HOMO levels to 0.26 V (-5.38 eV) for Compound **7** and -5.12 eV for Compound **14**.

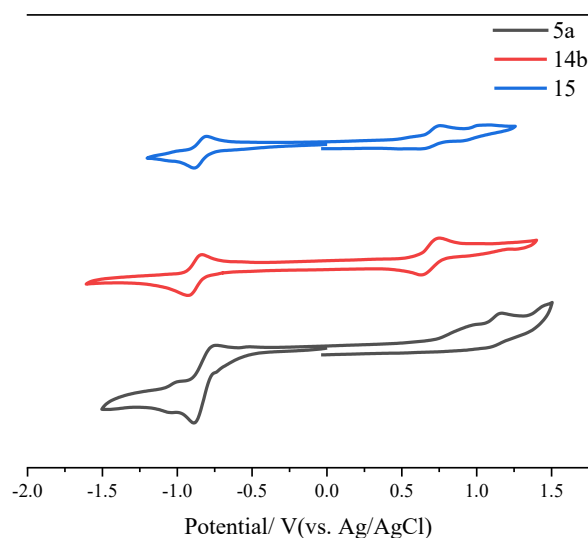


Figure 14. a) Cyclic Voltammetry of three quinoidal compounds in dichloromethane:
black: compound **5a**; red: compound **14b**; blue: compound **15**.

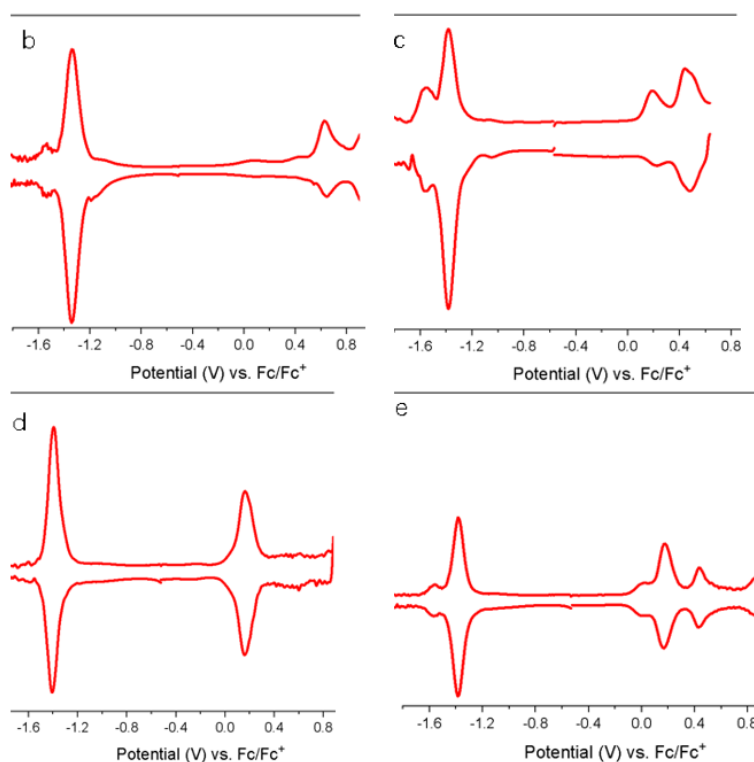


Figure 14. **b)** Square-wave Voltammetry of compound **5a** in dichloromethane with a scanning rate of 5 mv/s, step 10 mv, amplitude 20 mv, frequency 0.5 Hz. **c)** Square-wave Voltammetry of compound **7** in dichloromethane with a scanning rate of 5 mv/s, step 10 mv, amplitude 20 mv, frequency 0.5 Hz. **d)** Square-wave Voltammetry of compound **14b** in dichloromethane with a scanning rate of 5 mv/s, step 10 mv, amplitude 20 mv, frequency 0.5 Hz. **e)** Square-wave Voltammetry of compound **15** in dichloromethane with a scanning rate of 5 mv/s, step 10 mv, amplitude 20 mv, frequency 0.5 Hz.

Compounds	λ_{\max} nm	λ_{onset} nm	$E_{g \text{ opt}}$ eV	E_{LUMO} eV	E_{HOMO} eV	$E_{g \text{ electrochemical}}$ eV
5a	473	630	1.96	-3.44	-5.40	1.96
7	575	670	1.85	-3.45	-5.05	1.60
14b	633	760	1.63	-3.40	-4.95	1.55
15	661	800	1.55	-3.42	-4.79	1.37

Table 1.

Electrochemical Energy levels are estimated from equations from: $E_{\text{HOMO}} = -(E_{\text{ox}} + 4.80)$ eV. $E_{\text{LUMO}} = -(E_{\text{red}} + 4.80)$, where E_{ox} and E_{red} were determined from oxidation and reduction peaks of SWV respectively. Electrochemical band gap: $E_{\text{HOMO}} - E_{\text{LUMO}}$.

At last, the HOMO/LUMO energy information was calculated and shown in **Figure 15**.

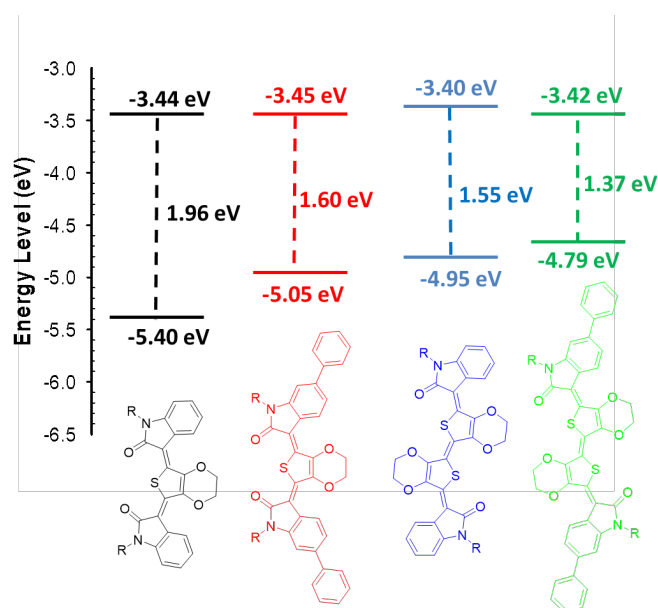


Figure 15. Calculated HOMO/LUMO energy diagram from square-wave voltammetry of compound **5a**, **7**, **14b**, and **15**.

4.3) Conclusion

In summary, a novel family of quinoidal indophenine materials made by connecting two isatin end-group by a π -bridge core has been synthesized via different strategies and fully characterized. In these quinoidal systems, bis-isatin end group- $[n]$ thienoEDOT ($n = 1-4$), the EDOT moieties in the π -bridge act as conformational locking units due to carbonyl-sulfur interaction between the EDOT unit and flanking isatin units, thus providing a driving force to the formation of one isomer. The design of molecules with extended π -conjugated system with EDOT 1-mer to 4-mer led to establish a clear relationship between properties-molecular structure. An in-depth experimental insight has been gained by making use of different complementary techniques such as UV/Vis absorption spectroscopy, electrochemical studies and advanced mass spectrometry methods. It was found that extending the π -conjugated system of molecules resulted in a reduction of the band gap and a shift of the HOMO energy level. In particular, the longest molecule 4-EDOTs showed a band gap of 1.18 eV. Ion mobility mass spectrometry was exploited for the first time to study organic semiconductors comprising intramolecular conformational locks. An accurate 2D NOESY NMR investigations revealed without any doubt a single isomer formation confirming the role of conformational locks allowed by intramolecular O...S interactions.

Experimental procedures and Characterization data

1-hexylindoline-2,3-dione (1a): To an oven-dried flask, isatin (0.64 g, 4.35 mmol) and K₂CO₃ (0.72 g, 5.22 mmol) were dissolved in 25 ml of anhydrous dimethylformamide. The mixture was heated to reflux for 30 mins followed by the dropwise addition of 0.75 ml (5.22 mmol) of 1-bromohexane. The stirring and heating were continued overnight. Ethyl acetate was added and the organic layer was washed with water three times. The organic phase was dried over MgSO₄. After removing the solvent by rotary evaporation, the residue was chromatographed on flash silica (chloroform/hexane = 1:3) to get **1a** as an orange-red solid (0.90g, 90% yields). ¹H NMR (CDCl₃, 300 MHz) δ 7.61-7.55 (m, 2H), 7.11 (t, 1H), 6.89 (d, 1H), 3.71 (t, 2H), 1.75-1.66 (m, 2H), 1.44-1.22 (m, 8H), 0.88 (t, 3H).

1-(2-octylododecyl) indoline-2,3-dione (1b): To an oven-dried flask, isatin (2.0 g, 13.60 mmol) and K₂CO₃ (2.26 g, 16.32 mmol) were dissolved in 30 ml of anhydrous dimethylformamide. The mixture was heated for 30 mins to reflux and 5.90 g (16.32 mmol) of 9-(bromomethyl)nonadecane was added via syringe. Then improve the heating temperature to 85 °C for 5h. Ethyl acetate was added and the organic layer was washed with water three times. The organic phase was dried over anhydrous MgSO₄. Concentrating the resulting mixture and transferred it onto a silica gel column (chloroform/hexane = 1:3) to get **1b** as an orange-red oil (4.93g, 85% yield). ¹H NMR (CDCl₃, 300 MHz) δ 7.53-7.60 (m, 2H), 7.10 (t, 1H), 6.86 (d, 1H), 3.59 (d, 2H), 1.91-1.78 (m, 1H), 1.32-1.20 (m, 32H), 0.88 (t, 6H). ¹³C NMR (CDCl₃, 75 MHz,) δ 183.62, 158.45, 151.45, 138.29, 125.34, 123.55, 117.54, 110.40, 44.70, 36.00, 31.91, 31.86, 31.46, 29.94, 29.62, 29.57, 29.52, 29.34, 29.28, 26.37, 22.69, 22.67, 14.14.

6-bromo-1-hexylindoline-2,3-dione (2a): To an oven-dried flask, 6-bromoisatin (2.45 g, 10.9 mmol) and K₂CO₃ (4.5 g, 32.5 mmol) were dissolved in 15 ml of anhydrous dimethylformamide. 1.83 ml (2.16 g, 13.07 mmol) of 1-bromohexane was added via syringe. Stirring at room temperature was continued overnight. Concentrating the resulting mixture under reduced pressure to get the yellow oily substances and washed with water two times. The residue was purified by column chromatography (chloroform/hexane = 1:4) to get **2a** as a red solid (2.72g, 81% yield). ¹H NMR (CDCl₃, 300 MHz) δ 7.45 (d, 1H), 7.27 (d, 1H), 7.05 (s, 1H), 3.68 (t, 2H), 1.72-1.61 (m, 2H), 1.40-1.30 (m, 6H), 0.88 (t, 3H).

6-bromo-1-(2-octylododecyl) indoline-2,3-dione (2b): The oven dry flask, 6-bromoisatin (1.39 g, 6.18 mmol) and K₂CO₃ (1.70 g, 12.36 mmol, 2eq) were dissolved in 30 ml of anhydrous dimethylformamide. The mixture was heated for 30 mins to reflux and followed 2.68 g (7.41 mmol, 1.2eq) of 9-(bromomethyl)nonadecane was added drop by drop via syringe. The stirring and heating were continued overnight. Ethyl acetate was added and the organic layer was washed with water two times. The organic phase was dried over MgSO₄. After removing the solvent by rotary evaporation, the residue was

chromatographed on silica gel (chloroform/hexane = 1:5) to get **2b** as a red oil (2.65g, 85% yield). ¹H NMR (CDCl₃, 300 MHz) δ 7.46 (d, 1H), 7.27 (d, 1H), 7.02 (s, 1H), 3.58 (d, 2H), 1.89-1.76 (m, 1H), 1.40-1.18 (m, 32H), 0.88 (t, 6H). ¹³C NMR (CDCl₃, 75 MHz,) δ 182.34, 158.30, 152.27, 133.50, 126.78, 126.34, 116.23, 114.00, 44.88, 35.93, 31.92, 31.87, 31.37, 29.95, 29.64, 29.59, 29.54, 29.36, 29.30, 26.28, 22.71, 22.68, 14.15.

3,3'-(2,3-dihydrothieno[3,4-b][1,4]dioxine-5,7-diyl)bis(1-hexyl-3-hydroxyindolin-2-one) (**3a**): To a solution of EDOT (0.196 g, 0.147 ml, 1.38 mmol) in anhydrous THF (15 mL) at - 78 °C, *n*-BuLi (1.87 mL, 3.00 mmol) was added dropwise, and the mixture was stirred at this temperature under argon for 1 h. Then the solution of compound 1a (0.67 g, 2.90 mmol) in 5 ml of anhydrous THF was added dropwise, and the mixture was stirred at - 30 °C for 1 h and then slowly warm to room temperature overnight. Water was added to the flask to quench the reaction, and the product was extracted with DCM. Then the organic layers were combined and dried with MgSO₄. The solvent was removed under reduced pressure to give **3a** as a dark brown solid (0.60 g, 77% yield). ¹H NMR (CDCl₃, 300 MHz) δ 7.43-7.35 (m, 2H), 7.32 (t, 2H), 7.06 (t, 2H) 6.84 (d, 2H), 4.18 (s, 4H), 3.85-3.82 (m, 2H), 3.79-3.72 (m, 2H), 3.64-3.57 (m, 2H), 1.73-1.61 (m, 4H), 1.42-1.23 (m, 12H), 0.86 (t, 6H). ¹³C NMR (CDCl₃, 75 MHz) δ 175.41, 143.02, 138.94, 130.28, 129.22, 125.52, 123.03, 114.89, 108.75, 75.09, 64.48, 40.31, 31.50, 27.16, 26.50, 22.55, 14.07. IR (ν, cm⁻¹) 3330(-OH), 2929, 2858, 1711 (C=O), 1612, 1507, 1488, 1466, 1360 (C-N-C), 1140 (O-C-C-O), 1080 (C-O-C), 752, 690.

3,3'-(2,3-dihydrothieno[3,4-b][1,4]dioxine-5,7-diyl)bis(6-bromo-1-hexyl-3-hydroxyindolin-2-one) (**4a**): To a solution of EDOT (0.197 g, 0.147 ml, 1.38 mmol) in anhydrous THF (20 mL) at - 78 °C, *n*-BuLi (1.88 mL, 3.00 mmol) was added dropwise, and the mixture was stirred at this temperature under argon for 1 h. Then the solution of compound 2a (0.90 g, 2.90 mmol) in 6 ml of anhydrous THF was added dropwise, and the mixture was stirred at - 30 °C for 1 h and then slowly warm to room temperature overnight. Water was added to the flask to quench the reaction, and the product was extracted with ethyl acetate. The organic phase was combined and washed with brine and water two times, and then dried with anhydrous Na₂SO₄. The solvent was removed under reduced pressure to give **4a** as a black solid (0.97 g, 92% yield). **4a** was used for next step without further purification.

3,3'-(2,3-dihydrothieno[3,4-b][1,4]dioxine-5,7-diyl)bis(6-bromo-3-hydroxy-1-(2-octyldodecyl) indolin-2-one) (**4b**): To a solution of EDOT (0.12 g, 0.85 mmol) in anhydrous THF (20 mL) at - 78 °C, *n*-BuLi (1.16 mL, 1.86 mmol) was added dropwise, and the mixture was stirred at this temperature under a nitrogen atmosphere for 1 h. Then the solution of compound 2b (0.94 g, 1.86 mmol) in 7 ml of anhydrous THF was added dropwise, and the mixture was stirred at - 30 °C for 1 h and then slowly warm to room temperature overnight. The mixture was poured into water, the solution was extracted with ethyl acetate. The organic phase was combined and washed with brine and water two times, and then dried with

MgSO₄. The solvent was removed under reduced pressure to give **4b** as a dark brown solid (0.92 g, 93% yield). **4b** was used for next step without further purification.

(3Z,3'Z)-3,3'-(2,3-dihydrothieno[3,4-*b*][1,4]dioxine-5,7-diylidene)bis(1-hexylindolin-2-one) (**5a**): The compound **3a** (110 mg, 0.18 mmol) was dissolved in anhydrous degassed dichloromethane (3 ml), and then SnCl₂ (172 mg, 0.91 mmol, 5eq) was added. The mixture was stirred from ice to room temperature overnight. The crude product was dissolved in dichloromethane, washed with water (20 ml) and dried over MgSO₄, and then concentrated under reduced pressure. The obtained dark red oil was chromatographed on silica gel (chloroform/hexane = 3:1) to afford **5a** as a red solid (42 mg, 41% yield). The aromatic form of the intermediate was further oxidised by DDQ to give the same product **5a** in 57% yield. ¹H NMR (CDCl₃, 300 MHz) δ 8.23 (d, 2H), 7.22 (t, 2H), 6.96 (t, 2H) 6.81 (d, 2H), 4.58 (s, 4H), 3.77 (t, 4H), 1.73-1.62 (m, 4H), 1.42-1.22 (m, 12H), 0.88 (t, 6H). Sufficiently concentrated solutions for ¹³C NMR could not be prepared, thus a ¹³C NMR spectrum was not obtained. IR (ν, cm⁻¹) 2955, 2918, 2849, 1734 (C=O), 1683, 1607, 1586 (-C=C-), 1507, 1466, 1376 (C-N-C), 1178 (O-C-C-O), 1077 (C-O-C), 775, 742.

(3Z,3'Z)-3,3'-(2,3-dihydrothieno[3,4-*b*][1,4]dioxine-5,7-diylidene)bis(6-bromo-1-hexylindolin-2-one) (**6a**): The compound **4a** (394 mg, 0.52 mmol) was dissolved in anhydrous degassed dichloromethane (5 ml), SnCl₂ (492 mg, 2.59 mmol, 5eq) was subsequently added. The mixture was stirred from ice to room temperature overnight. The crude product was dissolved in dichloromethane and was washed with water (20 mL) and dried over Na₂SO₄, concentrated under reduced pressure. The obtained dark red oil was precipitated with cosolvent (methanol / dichloromethane = 4:1) and then filtered to yield a dark red solid. Finally washing with methanol to afford **6a** as a wine-red solid (195 mg, 51% yield). ¹H NMR (CDCl₃, 300 MHz) δ 8.01(d, 2H), 7.03 (d, 2H), 6.84 (s, 2H), 4.60 (s, 4H), 3.69 (t, 4H), 1.73-1.62 (m, 4H), 1.42-1.22 (m, 12H), 0.88 (t, 6H). ¹³C NMR (CDCl₃, 75 MHz) δ 167.53, 143.10, 142.59, 140.76, 126.57, 123.73, 122.18, 120.29, 115.84, 110.84, 64.53, 40.01, 31.52, 27.65, 26.66, 22.58, 14.10. Mass calculated for C₃₄H₃₆Br₂N₂O₄S:726.0763. Found: 726.0757.

(3Z,3'Z)-3,3'-(2,3-dihydrothieno[3,4-*b*][1,4]dioxine-5,7-diylidene)bis(6-bromo-1-(2-octyldodecyl)indolin-2-one) (**6b**): The aromatic form intermediate (55 mg, 0.07 mmol) of SnCl₂ reaction was dissolved in anhydrous degassed toluene (5 ml), and then was further oxidized by DDQ (32 mg, 0.14 mmol, 3eq) at room temperature. The resulting mixture was extracted with DCM. The organic phase was then washed 3 times with brine and dried with Na₂SO₄. After removal of the solvent, the crude product was purified by by washing with methanol to obtain **6b** as a wine-red solid (27 mg, 51% yield). ¹H NMR (CDCl₃, 300 MHz) δ 7.95 (d, 2H), 6.97 (d, 2H), 6.71 (s, 2H), 4.61 (s, 4H), 3.52 (d, 4H), 1.90-1.72 (m, 2H), 1.32-1.12 (m, 64H), 0.86 (t, 12H). ¹³C NMR (CDCl₃, 75 MHz) δ 167.84, 143.50, 142.58, 140.78, 126.47, 123.60, 122.07, 120.22, 115.67, 111.10, 64.53, 44.50, 36.17, 31.94, 31.90, 31.66, 29.99,

29.72, 29.65, 29.59, 29.37, 29.31, 26.57, 22.70, 14.14.

(3*Z*,3'*Z*)-3,3'-(2,3-dihydrothieno[3,4-*b*][1,4]dioxine-5,7-diylidene)bis(1-hexyl-6-phenylindolin-2-one) (**7**): The compound **6a** (55 mg, 0.075 mmol), phenylboronic acid (36 mg, 0.30 mmol), P(*o*-tyl)₃ (4 mg, 0.01 mmol), Pd₂(dba)₃ (7 mg, 0.01 mmol) and K₃PO₄ (80 mg, 0.377 mmol) were loaded to a flask under argon. Toluene (6 mL) and 0.05 ml of water was then added to the flask. The reactant mixture was stirred at reflux for 12 h. The solution was cooled down to room temperature, and the solvent evaporated to dryness. The crude product was dissolved in ethyl acetate and was washed with water (10 mL) and dried over Na₂SO₄ and concentrated under reduced pressure. The residue was chromatographed on silica gel (chloroform/hexane = 1:5 to 1:1) to get **7** as a dark red solid (41 mg, 75% yield). ¹H NMR (CDCl₃, 300 MHz) δ 8.24 (d, 2H), 7.59-7.52 (m, 4H), 7.47-7.34 (m, 6H), 7.17 (d, 2H), 6.82 (s, 2H), 4.65 (s, 4H), 3.75 (t, 4H), 1.73-1.62 (m, 4H), 1.42-1.22 (m, 12H), 0.88 (t, 6H). ¹³C NMR (CDCl₃, 75 MHz) δ 167.99, 142.69, 142.58, 140.66, 140.50, 140.17, 128.77, 127.51, 126.82, 125.96, 120.92, 119.54, 116.31, 105.89, 64.54, 39.87, 31.56, 27.75, 26.71, 22.58, 14.10. Mass calculated for C₄₆H₄₆N₂O₄S₃:722.3178. Found: 722.3170. IR (ν, cm⁻¹) 2924, 2849, 1682 (C=O), 1611, 1585 (-C=C-), 1564, 1434, 1380 (C-N-C), 1177 (O-C-C-O), 1083 (C-O-C), 752, 733.

5,7-dibromo-2,3-dihydrothieno[3,4-*b*][1,4]dioxine: N-Bromosuccinimide (11.22 g, 63.0 mmol) was added to a solution of 3,4-ethylenedioxythiophene (4.26 g, 30.0 mmol) in THF:AcOH (120 mL, 1:1 v/v), and the reaction mixture was stirred at room temperature for 2 h. The resulting black solution was poured into water (700 mL). The precipitate was collected, washed with water (100 mL) and dried under vacuum to give a gray-green solid (8.32 g, 92% yield). ¹H NMR (300 MHz, CDCl₃) δ 4.27 (s, 4H).

3-(7-bromo-2,3-dihydrothieno[3,4-*b*][1,4]dioxin-5-yl)-1-hexyl-3-hydroxyindolin-2-one (**8a**): 5,7-dibromo-2,3-dihydrothieno[3,4-*b*][1,4]dioxine (194 mg, 0.65 mmol) was added in anhydrous THF (7 mL) and argon for 15 mins. 1 M of THF solution of *i* PrMgCl (0.7 mL, 0.7 mmol, 1.1 equivalents) was added. The reaction was carried out at room temperature for 2 h. The reaction mixture was then cooled down to 0 °C and a solution of compound **1a** (150 mg, 0.65 mmol) in 3 ml of THF was added. The mixture was stirred at room temperature overnight. After removing the solvent under reduced pressure, ethyl acetate was added and the organic layer was wash 3 times with water. The organic phase was dried over anhydrous MgSO₄. After removing the solvent by rotary evaporation, the residue was chromatographed on silica gel (Ethyl acetate / Hexane = 1:4) to get **8a** as a purple-red solid (209 mg, 71% yield). ¹H NMR (CDCl₃, 300 MHz) δ 7.43 (d, 1H), 7.35 (t, 1H), 7.06 (t, 1H), 6.86 (d, 1H), 4.27-4.13 (m, 4H), 3.79-3.69 (m, 1H), 3.64-3.54 (m, 1H), 1.74-1.63 (m, 2H), 1.41-1.22 (m, 6H), 0.87 (t, 3H). ¹³C NMR (CDCl₃, 75 MHz) δ 175.21, 143.06, 140.09, 138.53, 130.52, 128.90, 125.44, 123.11, 116.02, 108.88, 86.60, 75.22, 64.82, 64.65, 40.35, 31.49, 27.17, 26.49, 22.55, 14.03. Mass calculated for

C₂₀H₂₂BrNO₄S: 451.0453. Found: 451.0447. IR (ν, cm⁻¹) 3324 (-OH), 2929, 2986, 1699 (C=O), 1505 (-C=C-), 1467, 1386 (C-N-C), 1198 (O-C-C-O), 1177, 1095 (C-O-C), 756.

3-(7-bromo-2,3-dihydrothieno[3,4-b][1,4]dioxin-5-yl)-3-hydroxy-1-(2-octyldodecyl)indolin-2-one (8b): 5,7-dibromo-2,3-dihydrothieno[3,4-b][1,4]dioxine (2.31 g, 7.71 mmol) was added in anhydrous THF (20 mL) and argon for 15mins. 1 M of THF solution of *i* PrMgCl (7.75 mL, 7.75 mmol, 1.1 equivalents) was added. The reaction was carried out at room temperature for 2 h. The reaction mixture was then cooled down to 0 °C and a solution of compound 1b (3.00 g, 7.01 mmol) in 5 ml of THF was added. The mixture was stirred at room temperature overnight. Ethyl acetate was added and the organic layer was wash with water 3 times. The organic phase was dried over anhydrous MgSO₄. After removing the solvent by rotary evaporation, the residue was chromatographed on silica gel (ethyl acetate / Hexane = 1:5) to get **8b** as a yellow solid (3.76 g, 83% yield). ¹H NMR (CDCl₃, 300 MHz) δ 7.45 (d, 1H), 7.35 (t, 1H), 7.09 (t, 1H), 6.84 (d, 1H), 4.27-4.13 (m, 4H), 4.04 (s, 1H), 3.69-3.62 (m, 1H), 3.49-3.41 (m, 1H), 1.90-1.80(m, 1H), 1.42-1.08 (m, 32H), 0.87 (t,6H). ¹³C NMR (CDCl₃, 75 MHz,) δ 175.65, 143.51, 140.09, 138.84, 130.51, 128.83, 125.47, 123.04, 115.84, 109.08, 86.67, 75.25, 64.81, 64.71, 44.72, 36.10, 31.93, 31.89, 31.49, 31.32, 30.05, 30.02, 29.69, 29.66, 29.63, 29.57, 29.37, 29.32, 26.52, 26.33, 22.70, 14.15. IR (ν, cm⁻¹) 3365 (-OH), 2922, 2852, 1706 (C=O), 1511 (-C=C-), 1427, 1368 (C-N-C), 1125 (O-C-C-O), 1077 (C-O-C), 754.

3,3'-(thiophene-2,5-diylbis(2,3-dihydrothieno[3,4-b][1,4]dioxine-7,5-diyl))bis(1-hexyl-3-hydroxyindolin-2-one) (9a): The compound 8a (269 mg, 0.59 mmol), 2,5-bis (tributylstannyl) thiophene (180 mg, 0.27 mmol) and Pd(dppf)Cl₂ (43 mg, 0.05 mmol) were loaded to a flask under argon. DMF (2.5 mL) was then added to the flask. Stirring and heating was continued overnight. The solution was cooled down to room temperature, and the solvent evaporated to dryness. The crude product was dissolved in ethyl acetate and was washed with water (10 mL) and dried over Na₂SO₄ and concentrated under reduced pressure. The purification was carried out by chromatography on flash silica as static phase (dichloromethane / Hexane = 2:1) to get **9a** as a dark red solid (165 mg, 74% yield). ¹H NMR (CDCl₃, 300 MHz) δ 7.47 (d, 2H), 7.34 (t, 2H), 7.08 (t, 2H), 6.99 (s, 2H), 6.86 (d, 2H), 4.33-4.16 (m, 8H), 4.13-4.10 (m, 2H), 3.82-3.72 (m, 2H), 3.63-3.52 (m, 2H), 1.75-1.57 (m, 4H), 1.44-1.19 (m, 12H), 0.87 (t, 6H). ¹³C NMR (CDCl₃, 75 MHz) δ 175.51, 143.04, 139.23, 137.30, 132.86, 130.34, 129.39, 125.51, 123.08, 122.96, 112.98, 111.42, 108.81, 75.20, 64.78, 64.69, 40.33, 31.51, 27.19, 26.51, 22.56, 14.05. Mass calculated for C₄₄H₄₆N₂O₈S₃: 826.2416. Found: 826.2419. IR (ν, cm⁻¹) 3340 (-OH), 2926, 2855, 1708 (C=O), 1665, 1535 (-C=C-), 1465, 1360 (C-N-C), 1139 (O-C-C-O), 1082 (C-O-C), 752.

3,3'-(thiophene-2,5-diylbis(2,3-dihydrothieno[3,4-b][1,4]dioxine-7,5-diyl))bis(3-hydroxy-1-(2-octyldodecyl)indolin-2-one) (9b): The compound 8b (400 mg, 0.61 mmol), 2,5-bis (tributylstannyl)thiophene (186 mg, 0.28 mmol) and Pd(dppf)Cl₂ (10 mg, 0.01 mmol) were loaded to a

flask under argon. DMF (3 mL) was then added to the flask. Stirring and heating was continued overnight. The solution was cooled down to room temperature, and the solvent evaporated to dryness. The crude product was dissolved in ethyl acetate and was washed with water (10 mL) and dried over Na₂SO₄ and concentrated under reduced pressure. The purification was carried out by chromatography on flash silica as static phase (dichloromethane / Hexane = 1:1) to get **9b** as a light green solid (0.25 g, 73% yield). ¹H NMR (CDCl₃, 300 MHz) δ 7.48 (d, 2H), 7.36 (t, 2H), 7.10 (t, 2H), 6.98 (s, 2H), 6.85 (d, 2H), 4.33-4.22 (m, 8H), 4.11(s, 2H), 3.69-3.62 (m, 2H), 3.49-3.42 (m, 2H), 1.99-1.80 (m, 2H), 1.33-1.09 (m, 64H), 0.87 (t, 12H). ¹³C NMR (CDCl₃, 75 MHz) δ 175.87, 143.60, 139.75, 137.31, 132.85, 130.37, 129.17, 125.61, 122.95, 112.62, 111.59, 108.97, 75.32, 64.77, 44.72, 36.12, 31.91, 31.87, 31.55, 31.40, 30.04, 30.01, 29.69, 29.64, 29.60, 29.55, 29.34, 29.30, 26.54, 26.37, 22.67, 14.11. IR (ν, cm⁻¹) 3357 (-OH), 2955, 2921, 2851, 1716 (C=O), 1653, 1506 (-C=C-), 1488, 1361 (C-N-C), 1169 (O-C-C-O), 1081 (C-O-C), 745.

3,3'-(thiophene-2,5-diylbis(2,3-dihydrothieno[3,4-b][1,4]dioxine-7,5-diyl))bis(1-hexylindolin-2-one) (**10a**): The compound 9a (10 mg, 0.01 mmol) was dissolved in anhydrous degassed dichloromethane (2 ml), and then SnCl₂ (11 mg, 0.06 mmol, 5eq) was added. The mixture was stirred at room temperature overnight. The crude product was dissolved in DCM and was washed with water (10 mL) and dried over MgSO₄ and concentrated under reduced pressure to afford **10a** as a dark red solid (9 mg, 91% yield). ¹H NMR (CDCl₃, 300 MHz) δ 7.35-7.26 (m, 4H), 7.04 (t, 2H), 6.96 (s, 2H), 6.87 (d, 2H), 4.89 (s, 2H), 4.41-4.22 (m, 8H), 3.81-3.65 (m, 4H), 1.75-1.58 (m, 4H), 1.40-1.21 (m, 12H), 0.89 (t, 6H). ¹³C NMR (CDCl₃, 75 MHz) δ 174.52, 143.67, 140.38, 137.13, 132.86, 128.61, 128.09, 125.09, 122.62, 122.50, 110.86, 108.72, 108.47, 65.04, 64.75, 43.85, 40.33, 31.53, 27.31, 26.55, 22.57, 14.07. IR (ν, cm⁻¹) 2964, 2922, 1713 (C=O), 1515 (-C=C-), 1360 (C-N-C), 1178 (O-C-C-O), 1076 (C-O-C).

3,3'-(thiophene-2,5-diylbis(2,3-dihydrothieno[3,4-b][1,4]dioxine-7,5-diyl))bis(1-(2-octyld-odecyl)indolin-2-one) (**10b**): The compound 9b (50mg, 0.04 mmol) was dissolved in anhydrous degassed dichloromethane (5 ml), and then SnCl₂ (38 mg, 0.2 mmol, 5eq) was added. The mixture was stirred at room temperature overnight. The crude product was dissolved in DCM and was washed with water (10 mL) and dried over Na₂SO₄ and concentrated under reduced pressure to afforded **10b** as a dark red solid (45mg, 93% yield). ¹H NMR (CDCl₃, 300 MHz) δ 7.35-7.27 (m, 2H), 7.04 (t, 1H), 6.91 (s, 1H), 6.86 (d, 1H), 4.92 (s, 1H), 4.41-4.28 (m, 4H), 3.68-3.52 (m, 2H), 1.95-1.83 (m, 1H), 1.40-1.09 (m, 32H), 0.87 (t, 6H). ¹³C NMR (CDCl₃, 75 MHz) δ 174.85, 144.02, 140.42, 137.06, 132.87, 128.59, 128.00, 125.06, 122.46, 110.89, 108.77, 108.72, 65.04, 64.79, 44.73, 43.77, 36.03, 31.96, 31.93, 31.58, 31.44, 30.09, 30.06, 29.75, 29.72, 29.68, 29.63, 29.40, 29.36, 26.60, 26.54, 22.74, 14.20.

(3Z,3'Z)-3,3'-((7E,7'E)-thiophene-2,5-diylidenebis(2,3-dihydrothieno[3,4-b][1,4]dioxine-7,5(7H)-diylidene))bis(1-hexylindolin-2-one) (**11a**): The compound 10a (15 mg, 0.019 mmol) was dissolved in

anhydrous degassed toluene (3 ml), and then DDQ (16 mg, 0.056 mmol, 3eq) was added. The mixture was stirred at room temperature overnight. The mixture was wash with AcOH and then extracted with dichloromethane. The organic phase was combined and washed with brine and water, and then dried with anhydrous Na₂SO₄ to afford **11a** as a deep blue solid (10 mg, 67% yield).

(3Z,3'Z)-3,3'-((7E,7'E)-thiophene-2,5-diylidenebis(2,3-dihydrothieno[3,4-b][1,4]dioxine-7,5(7H)-diylidene))bis(1-(2-octyldodecyl)indolin-2-one) (**11b**): Compound 10b (10mg, 0.008 mmol) was dissolved and stirred in anhydrous degassed toluene (2 ml), and then DDQ (6 mg, 0.025 mmol, 3eq) was added. The mixture was wash with AcOH and then extracted with dichloromethane. The organic phase was combined and washed with brine and water, and then dried with anhydrous MgSO₄ to afford **11b** as a deep blue solid (5 mg, 53% yield). HRMS (ESI) calculated for C₇₂H₁₀₁N₂O₆S₃: 1185.6816. Found:1188.6819.

3-(2,3-dihydrothieno[3,4-b][1,4]dioxin-5-yl)-1-hexyl-3-hydroxyindolin-2-one (**12a**): To a solution of EDOT (0.30 g, 0.147 ml, 2.11 mmol) in anhydrous THF (20 mL) at - 78 °C., *n*-BuLi (1.45 mL, 2.32 mmol) was added dropwise, and the mixture was stirred at this temperature under a nitrogen atmosphere for 1 h. Then the solution of compound 1a (0.50 g, 2.10 mmol) in 5 ml of anhydrous THF was added dropwise, and the mixture was stirred at - 30 °C for 1 h and then slowly warm to room temperature overnight. The mixture was poured into water, the solution was extracted with ethyl acetate. The organic phase was combined and washed with water two times, and then dried with anhydrous Na₂SO₄. The solvent was removed at a reduced pressure to give **12a** as a yellow solid (0.70 g, 87% yield). ¹H NMR (CDCl₃, 300 MHz) δ 7.43 (d, 1H), 7.33 (t, 2H), 7.06 (t, 1H), 6.85 (d, 1H), 6.22 (s, 1H), 4.15 (s, 4H), 3.81-3.73 (m, 1H), 3.61-3.53 (m, 1H), 1.71-1.62 (m, 2H), 1.40-1.23 (m, 6H), 0.88 (t, 3H). ¹³C NMR (CDCl₃, 75 MHz) δ 175.66, 143.04, 141.69, 139.05, 130.15, 129.61, 125.43, 122.94, 116.03, 108.70, 98.47, 75.24, 64.67, 64.35, 40.25, 31.48, 27.15, 26.47, 22.52, 14.01. Mass calculated for C₂₀H₂₃NO₄S: 373.1348. Found: 373.1340. IR (ν, cm⁻¹) 3366(-OH), 2959, 2930, 1705 (C=O), 1498 (-C=C-), 1466, 1368 (C-N-C), 1162 (O-C-C-O), 1092 (C-O-C), 755, 626.

3-(2,3-dihydrothieno[3,4-b][1,4]dioxin-5-yl)-3-hydroxy-1-(2-octyldodecyl)indolin-2-one (**12b**): To a solution of EDOT (0.66 g, 4.64 mmol) in anhydrous THF (10 mL) at - 78 °C, *n*-BuLi (1.74 mL, 2.78 mmol) was added dropwise, and the mixture was stirred at - 30 °C under a nitrogen atmosphere for 1 h. Then the solution of compound 1b (0.94 g, 2.20 mmol) in 5 ml of anhydrous THF was added dropwise, and the mixture was stirred at -30 °C for 1 h and then slowly warm to room temperature overnight. The mixture was poured into water, the solution was extracted with ethyl acetate. The organic phase was combined and washed with water for two times, and then dried with anhydrous Na₂SO₄. After removing the solvent by rotary evaporation, the residue was chromatographed on silica gel (chloroform/hexane =

1:1) to give **12b** as an orange oil (0.99 g, 79 % yield). ¹H NMR (CDCl₃, 300 MHz) δ 7.47 (d, 1H), 7.35 (t, 1H), 7.09 (t, 1H), 6.84 (d, 1H), 6.22 (s, 1H), 4.27-4.15 (m, 4H), 4.07 (s, 1H), 3.69-3.66 (m, 1H), 3.49-3.42 (m, 1H), 1.95-1.81 (m, 1H), 1.40-1.10 (m, 32H), 0.87 (t, 6H). ¹³C NMR (CDCl₃, 75 MHz) δ 176.12, 143.50, 141.69, 139.20, 130.09, 129.70, 125.43, 122.87, 116.00, 108.87, 98.48, 75.19, 64.72, 64.35, 44.62, 36.08, 31.95, 31.91, 30.04, 29.69, 29.66, 29.63, 29.58, 29.38, 29.34, 22.72, 22.70, 14.16. Mass calculated for C₃₄H₅₁NO₄S: 569.3539. Found: 569.3530.

6-bromo-3-(2,3-dihydrothieno[3,4-b][1,4]dioxin-5-yl)-3-hydroxy-1-icosylindolin-2-one (12c): To a solution of EDOT (0.71 g, 5.04 mmol) in anhydrous THF (20 mL) at -78 °C, *n*-BuLi (1.31 mL, 3.27 mmol) was added dropwise, and the mixture was stirred at -30 °C under a nitrogen atmosphere for 1 h. Then the solution of compound 2b (1.27 g, 2.52 mmol) in 6 mL of anhydrous THF was added dropwise, and the mixture was stirred at -30 °C for 1 h and then slowly warm to room temperature overnight. The mixture was poured into water, the solution was extracted with ethyl acetate. The organic phase was combined and washed with water for two times, and then dried with anhydrous Na₂SO₄. After removing the solvent by rotary evaporation, the residue was chromatographed on silica gel (chloroform/hexane = 1:2) to give **12c** as an orange-green oil (1.40 g, 86 % yield). ¹H NMR (CDCl₃, 300 MHz) δ 7.30 (d, J = 7.9 Hz, 1H), 7.20 (d, J = 8.1 Hz, 1H), 6.96 (s, 1H), 6.23 (s, 1H), 4.17 (s, 5H), 3.63 (dd, J = 14.1, 7.8 Hz, 1H), 3.40 (dd, J = 14.1, 7.0 Hz, 1H), 1.86 (d, J = 8.5 Hz, 1H), 1.27 (m, 32H), 0.87 (t, J = 6.8 Hz, 6H). ¹³C NMR (CDCl₃, 75 MHz) δ 175.89, 144.91, 141.77, 139.41, 128.35, 126.79, 125.76, 123.97, 115.08, 112.40, 98.80, 74.86, 64.80, 64.36, 44.74, 35.95, 31.93, 31.90, 31.33, 31.14, 30.02, 29.68, 29.65, 29.62, 29.58, 29.56, 29.37, 29.34, 26.37, 26.16, 22.72, 22.70, 14.16.

1-(2-octyldodecyl)-6-phenylindoline-2,3-dione (13a): The compound 2b (1.02 g, 2.01 mmol), phenylboronic acid (0.49 g, 4.02 mmol, 2eq), P(*o*-tyl)₃ (90 mg, 0.3 mmol), K₃PO₄ (1.28 g, 6.04 mmol, 3eq) and Pd₂(dba)₃ (180 mg) were loaded to a flask under argon. Toluene (10 mL) and 0.5 mL of water was then added to the flask. Stirring and heating was continued overnight. The solution was cooled down to room temperature, and the solvent evaporated to dryness. The crude product was dissolved in chloroform and was washed with water (15 mL) and dried over MgSO₄ and concentrated under reduced pressure. The residue was chromatographed on silica gel (chloroform/hexane = 1:5 to 1:3) to give **13a** as a light red solid (810 mg, 80% yield). ¹H NMR (CDCl₃, 300 MHz) δ 7.67 (d, 1H), 7.57-7.63 (m, 2H), 7.55-7.42 (m, 3H), 7.32 (d, 1H), 7.04 (s, 1H), 3.65 (d, 2H), 1.99-1.82 (m, 1H), 1.49-1.13 (m, 32H), 0.87 (t, 6H). ¹³C NMR (CDCl₃, 75 MHz) δ 183.04, 158.99, 152.08, 151.56, 139.60, 129.32, 129.19, 127.23, 125.83, 122.44, 116.35, 109.03, 44.67, 36.09, 31.91, 31.87, 31.52, 29.97, 29.63, 29.35, 29.31, 26.43, 22.69, 14.15.

3-(2,3-dihydrothieno[3,4-b][1,4]dioxin-5-yl)-3-hydroxy-1-(2-octyldodecyl)-6-phenylindolin-2-one (13b): To a solution of EDOT (0.17 g, 1.19 mmol) in anhydrous THF (10 mL) at -78 °C, *n*-BuLi (0.44

mL, 0.70 mmol) was added dropwise, and the mixture was stirred at -40 °C under a nitrogen atmosphere for 1 h. Then the solution of compound 17 (0.30 g, 0.59 mmol) in 3 mL of anhydrous THF was added dropwise, and the mixture was stirred at -30 °C for 1 h and then slowly warmed to room temperature overnight. The mixture was poured into water, the solution was extracted with ethyl acetate. The organic phase was combined and washed with water two times, and then dried with anhydrous Na₂SO₄. After removing the solvent by rotary evaporation, the residue was chromatographed on silica gel (chloroform/hexane = 1:3) to get **13b** as a red oil (0.30 g, 78% yield). ¹H NMR (CDCl₃, 300 MHz) δ 7.60-7.57 (m, 2H), 7.54-7.38 (m, 4H), 7.31 (d, 1H), 7.03 (s, 1H), 6.24 (s, 1H), 4.23-4.20 (m, 4H), 4.10 (s, 1H), 3.74-3.64 (m, 1H), 3.55-3.47 (m, 1H), 1.97-1.84 (m, 1H), 1.40-1.05 (m, 32H), 0.87 (t, 6H). ¹³C NMR (CDCl₃, 75 MHz) δ 176.26, 144.16, 143.73, 141.81, 140.84, 139.58, 128.90, 128.25, 127.85, 127.20, 125.76, 121.95, 115.60, 107.89, 98.69, 75.25, 64.83, 64.41, 44.65, 36.09, 31.94, 31.91, 30.06, 29.67, 29.38, 29.35, 22.71, 14.17.

(3Z,3'Z)-3,3'-((E)-2,2',3,3'-tetrahydro-7H,7'H-[5,5'-bithieno[3,4-b][1,4]dioxinylidene]-7,7'-diylidene) bis(1-hexylindolin-2-one) (14a): Compound 12a (60 mg, 0.16 mmol) was dissolved and stirred in toluene (3 mL) at room temperature, to which was slowly added concentrated sulfuric acid (0.15 mL). After the mixture was stirred for 3 h at room temperature, the reaction was quenched by pouring into water (1 mL), extracted by DCM (3×10 mL) and dried by Na₂SO₄. The solvent was removed under vacuum and the residue was purified by washing with acetone to afford **14a** as a blue solid (45 mg, 79% yield). ¹H NMR (CDCl₃, 300 MHz) δ 8.18 (d, 2H), 7.12 (t, 2H), 6.92 (t, 2H), 6.76 (d, 2H), 4.57-4.44 (m, 8H), 3.76 (t, 4H), 1.75-1.64 (m, 4H), 1.42-1.22 (m, 12H), 0.87 (t, 6H). Solutions of sufficient concentration needed for ¹³C NMR could not be prepared, thus a ¹³C NMR spectrum was not obtained. Mass calculated for C₄₀H₄₂N₂O₆S₂: 710.2484. Found: 710.2479.

(3Z,3'Z)-3,3'-((E)-2,2',3,3'-tetrahydro-7H,7'H-[5,5'-bithieno[3,4-b][1,4]dioxinylidene]-7,7'-diylidene) bis(1-(2-octyldecyl)indolin-2-one) (14b): Compound 12b (160 mg, 0.28 mmol) was dissolved and stirred in toluene (6 mL) at room temperature, to which was slowly added concentrated sulfuric acid (0.15 mL). After the mixture was stirred for 2 h at room temperature, the reaction was quenched by pouring into water (20 mL), extracted by DCM (3×10 mL) and dried by Na₂SO₄. The solvent was removed under vacuum and the residue was purified by washing with methanol and then acetone, the residue was chromatographed on silica gel (chloroform/hexane = 1:2) to get **14b** as a blue-purple solid (105 mg, 68% yield). ¹H NMR (CDCl₃, 300 MHz) δ 8.21 (d, 2H), 7.14 (t, 2H), 6.94 (t, 2H), 6.77 (d, 2H), 4.55-4.48 (m, 8H), 3.66 (d, 4H), 1.95-1.78 (m, 2H), 1.40-1.10 (m, 64H), 0.87 (t, 12H). ¹³C NMR (CDCl₃, 75 MHz) δ 168.26, 143.28, 141.45, 139.88, 138.94, 126.66, 124.65, 123.99, 122.04, 120.78, 111.61, 107.83, 65.14, 64.67, 44.64, 36.44, 31.94, 31.90, 31.74, 30.03, 29.71, 29.65, 29.59, 29.53, 29.37, 29.30, 26.72, 22.71, 22.69, 14.16. HRMS (ESI) calculated for C₆₈H₉₈N₂O₆S₂: 1102.6866; Found: 1102.6865. IR (ν, cm⁻¹) 2921, 2852, 1644 (C=O), 1507 (-C=C-), 1466, 1384 (C-N-C), 1347, 1175,

1111 (O-C-C-O), 1063 (C-O-C), 844, 606.

(3Z,3'Z)-3,3'-((*E*)-2,2',3,3'-tetrahydro-7*H*,7'*H*-[5,5'-bithieno[3,4-*b*][1,4]dioxinylidene]-7,7'-diylidene)bis(6-bromo-1-(2-octyldodecyl)indolin-2-one) (**14c**): Compound 12c (100 mg, 0.15 mmol) was dissolved and stirred in toluene (6 mL) at room temperature, to which was slowly added concentrated sulfuric acid (0.15 mL). After the mixture was stirred for 2 h at room temperature, the reaction was quenched by pouring into water (30 mL), extracted by DCM and dried by MgSO₄. The solvent was removed under vacuum and the residue was purified by washing with methanol and then acetone, the residue was chromatographed on silica gel (chloroform/hexane = 1:2) to get **14c** as a blue-purple solid (79 mg, 82 % yield). ¹H NMR (CDCl₃, 300 MHz) δ 7.86 (d, 2H), 6.93 (d, *J* = 8.6 Hz, 2H), 6.65 (s, 2H), 4.55 (d, *J* = 18.3 Hz, 8H), 3.53 (d, *J* = 7.1 Hz, 4H), 1.80 (s, 2H), 1.23 (s, 64H), 0.86 (t, *J* = 6.6 Hz, 12H). Sufficiently concentrated solutions for ¹³C NMR could not be prepared, thus a ¹³C NMR spectrum was not obtained.

(3Z,3'Z)-3,3'-((*E*)-2,2',3,3'-tetrahydro-7*H*,7'*H*-[5,5'-bithieno[3,4-*b*][1,4]dioxinylidene]-7,7'-diylidene)bis(1-(2-octyldodecyl)-6-phenylindolin-2-one) (**15**): Compound 13b (30 mg, 0.04 mmol) was dissolved and stirred in toluene (3 mL) at room temperature, to which was slowly added concentrated sulfuric acid (0.1 mL). After the mixture was stirred for 2 h at room temperature, the reaction was quenched by pouring into water (15 mL), extracted by DCM (3×10 mL) and dried by Na₂SO₄. The solvent was removed under vacuum and the residue was purified by washing with methanol and then acetone, the residue was chromatographed on silica gel (chloroform) to afford **15** as a blue-purple solid (21 mg, 72% yield). ¹H NMR (CDCl₃, 300 MHz) δ 8.19 (d, 2H), 7.54-7.50 (m, 4H), 7.39-7.32 (m, 6H), 7.18 (d, 2H), 6.77 (s, 2H), 4.61-4.54 (m, 8H), 3.63 (d, 4H), 1.93-1.82 (m, 2H), 1.40-1.05 (m, 64H), 0.86 (t, 12H). ¹³C NMR (CDCl₃, 75 MHz) δ 168.40, 143.13, 141.80, 140.74, 140.01, 138.68, 138.44, 128.68, 127.11, 126.56, 124.84, 123.98, 121.30, 119.15, 111.27, 106.06, 65.13, 64.64, 44.50, 39.75, 39.48, 36.38, 32.54, 31.88, 29.99, 29.62, 29.31, 26.80, 26.54, 22.66, 14.11. HRMS (ESI) calculated for C₈₀H₁₀₆N₂O₆S₂: 1254.7492; Found: 1254.7499. IR (ν, cm⁻¹) 2921, 2852, 2363, 1653 (C=O), 1513 (-C=C-), 1476, 1328 (C-N-C), 1328, 1173, 1125 (O-C-C-O), 1067 (C-O-C), 852, 774, 756, 697, 606.

*3-hydroxy-1-(2-octyldodecyl)-3-(2,2',3,3'-tetrahydro-[5,5'-bithieno[3,4-*b*][1,4]dioxin]-7-yl)indolin-2-one* (**16a**): The compound 8b (250 mg, 0.38 mmol), 2-tributylstannyl-3,4-ethylenedioxythiophene (332 mg, 0.77 mmol) and Pd(dppf)Cl₂ (28 mg, 0.04 mmol) were loaded to a flask under argon. Toluene (5 mL) was then added to the flask. Stirring and heating was continued overnight. The solution was cooled down to room temperature, and the solvent evaporated to dryness. The crude product was dissolved in ethyl acetate and was washed with water (10 mL) and dried over Na₂SO₄ and concentrated under reduced pressure. The purification was carried out by flash-chromatography on silica as static phase (ethyl acetate / hexane = 1:4) to afford **16a** as a red-yellow oil (216 mg, 79% yield). ¹H NMR (CDCl₃, 300

MHz) δ 7.47 (d, 1H), 7.31 (t, 1H), 7.06 (t, 1H), 6.83 (d, 1H), 6.22 (s, 1H), 4.27-4.20 (m, 8H), 3.99 (s, 1H), 3.68-3.60 (m, 1H), 3.50-3.42 (m, 1H), 1.89-1.79 (m, 1H), 1.36-1.14 (m, 32H), 0.87 (t, 6H). ^{13}C NMR (CDCl_3 , 75 MHz) δ 175.99, 143.65, 141.12, 138.94, 137.05, 136.99, 130.18, 129.36, 125.62, 122.95, 113.12, 109.53, 109.27, 108.94, 97.88, 75.33, 64.95, 64.75, 64.55, 44.74, 36.13, 31.90, 31.87, 31.50, 31.38, 30.01, 29.65, 29.62, 29.34, 29.30, 26.51, 26.37, 22.67, 14.10. IR (ν , cm^{-1}) 3351 (-OH), 2922, 2853, 1713 (C=O), 1469, 1436, 1359 (C-N-C), 1125 (O-C-C-O), 1093 (C-O-C), 1065, 903, 753, 705.

(3Z,3'Z)-3,3'-((5*E*,5''*E*,5'''*E*)-2,2',2'',2''',3,3',3'',3'''-octahydro-7*H*,7'''*H*-[5,5':7',5'':7'',5'''-quaterthieno [3,4-*b*][1,4]dioxine]-7,7'''-diylidene)bis(1-(2-octyldodecyl)indolin-2-one) (**17**): Compound 16a (60 mg, 0.08 mmol) was dissolved and stirred in toluene (3 mL) at room temperature, to which was slowly added concentrated sulfuric acid (0.15 mL). After the mixture was stirred for 2 h at room temperature, the reaction was quenched by pouring into water (10 mL), extracted by DCM (3 \times 10 mL) and dried by Na_2SO_4 . The solvent was removed under vacuum and the residue was purified by washing with methanol and then acetone to afford **17** as a blue-purple solid (35 mg, 60 % yield). ^1H NMR (CDCl_3 , 300 MHz) δ 8.19 (m, 1H), 7.09 (m, 1H), 6.94 (t, 1H), 6.77 (d, 1H), 4.58-4.45 (m, 8H), 3.67 (m, 2H), 1.95-1.78 (m, 1H), 1.40-1.10 (m, 32H), 0.87 (t, 6H). HRMS (ESI) calculated for $\text{C}_{80}\text{H}_{107}\text{N}_2\text{O}_{10}\text{S}_4$:1382.6730; Found: 1382.6724

4-bromo-1-hexyl-3-hydroxy-3-(thiophen-2-yl)indolin-2-one (**18**): To a solution of thiophene (0.39 g, 4.63 mmol) in anhydrous THF (10 mL) at $-78\text{ }^\circ\text{C}$, *n*-BuLi (1.11 mL, 2.78 mmol) was added dropwise, and the mixture was stirred at $-30\text{ }^\circ\text{C}$ under a nitrogen atmosphere for 1 h. Then the solution of 4-bromo-1-hexylindoline-2,3-dione (0.72 g, 2.31 mmol) in 5 mL of anhydrous THF was added dropwise, and the mixture was stirred at $-30\text{ }^\circ\text{C}$ for 1 h and then slowly warm to room temperature overnight. The mixture was poured into water, the solution was extracted with ethyl acetate. The organic phase was combined and washed with water for two times, and then dried with anhydrous Na_2SO_4 . After removing the solvent by rotary evaporation, the residue was chromatographed on silica gel (chloroform/hexane = 1:2) to give **18** as a brown oil (0.74 g, 82 % yield). ^1H NMR (CDCl_3 , 300 MHz) δ 7.31 (d, $J = 4.9\text{ Hz}$, 1H), 7.30 – 7.19 (m, 2H), 6.99 – 6.90 (m, 2H), 6.86 (dt, $J = 6.8, 1.5\text{ Hz}$, 1H), 3.73 (dt, $J = 14.5, 7.5\text{ Hz}$, 1H), 3.59 (d, $J = 11.0\text{ Hz}$, 2H), 1.75 – 1.61 (m, 2H), 1.26 (q, $J = 4.7\text{ Hz}$, 6H), 0.90 – 0.80 (m, 3H). ^{13}C NMR (CDCl_3 , 75 MHz) δ 174.22, 144.84, 141.68, 131.66, 129.17, 126.99, 126.95, 126.61, 125.43, 120.20, 108.04, 40.47, 31.35, 27.04, 26.35, 22.47, 13.97.

*1-hexyl-3-hydroxy-3-(7-(thiophen-2-yl)-2,3-dihydrothieno[3,4-*b*][1,4]dioxin-5-yl)indolin-2-one* (**20a**): The compound 8a (115 mg, 0.25 mmol), 2-(tributylstannyl) thiophene (188 mg, 0.50 mmol) and $\text{Pd}(\text{dppf})\text{Cl}_2$ (43 mg, 0.05 mmol) were loaded to a flask under argon. DMF (2.5 mL) was then added to the flask. Stirring and heating was continued overnight. The solution was cooled down to room

temperature, and the solvent evaporated to dryness. The crude product was dissolved in ethyl acetate and was washed with water (10 mL) and dried over Na₂SO₄ and concentrated under reduced pressure. The purification was carried out by flash-chromatography on silica as static phase (dichloromethane /hexane = 1:3 to 3:1) to give **20a** as a dark red solid (102 mg, 88% yield). ¹H NMR (CDCl₃, 300 MHz) δ 7.48 (d, 1H), 7.36 (t, 1H), 7.20-7.06 (m, 3H), 6.97 (s, 1H), 6.87 (d, 1H), 4.33-4.20 (m, 4H), 4.08 (s, 1H) 3.82-3.53 (m, 2H), 1.75-1.57 (m, 2H), 1.44-1.19 (m, 6H), 0.87 (t, 3H).

3-hydroxy-1-(2-octyldodecyl)-3-(7-(thiophen-2-yl)-2,3-dihydrothieno[3,4-b][1,4]dioxin-5-yl)indolin-2-one (20b): The compound 8b (210 mg, 0.32 mmol), 2-(tributylstannyl) thiophene (230 mg, 0.61 mmol) and Pd(dppf)Cl₂ (23 mg, 0.03 mmol) were loaded into a flask under argon. Toluene (4 mL) was then added to the flask. Stirring and heating was continued overnight. The solution was cooled down to room temperature, and the solvent evaporated to dryness. The crude product was dissolved in ethyl acetate and was washed with water (10 mL) and dried over MgSO₄ and concentrated under reduced pressure. The purification was carried out by flash-chromatography on silica as static phase (ethyl acetate / hexane = 1:5) to get **20b** as a yellow oil (170 mg, 81% yield). ¹H NMR (CDCl₃, 300 MHz) δ 7.49 (d, 1H), 7.36 (t, 1H), 7.17 (d, 1H), 7.13-7.02 (m, 2H), 6.95 (t, 1H), 6.85 (d, 1H), 4.32-4.26 (m, 4H), 4.18 (s, 1H), 3.71-3.63 (m, 1H), 3.49-3.41 (m, 1H), 1.97-1.79 (m, 1H), 1.36-1.10 (m, 32H), 0.87 (t, 6H). ¹³C NMR (CDCl₃, 75 MHz,) δ 175.92, 143.55, 139.67, 137.34, 134.24, 130.40, 129.21, 127.04, 125.58, 123.93, 123.01, 122.98, 112.71, 111.37, 109.02, 75.29, 64.78, 64.74, 44.69, 36.11, 31.93, 31.89, 31.52, 31.35, 30.08, 30.04, 29.68, 29.64, 29.59, 29.37, 29.34, 26.56, 26.38, 22.72, 22.70, 14.16.

Reference

- (1) Huang, J.; Yu, G. Recent progress in quinoidal semiconducting polymers: structural evolution and insight. *Materials Chemistry Frontiers* **2021**, *5* (1), 76-96, DOI: 10.1039/d0qm00509f.
- (2) Zhang, C.; Zhu, X. n-Type quinoidal oligothiophene-based semiconductors for thin-film transistors and thermoelectrics. *Advanced Functional Materials* **2020**, *30* (31), 2000765, DOI: 10.1002/adfm.202000765.
- (3) Deng, Y.; Sun, B.; He, Y.; Quinn, J.; Guo, C.; Li, Y. Thiophene-S, S-dioxidized Indophenine: A Quinoid-Type Building Block with High Electron Affinity for Constructing n-Type Polymer Semiconductors with Narrow Band Gaps. *Angewandte Chemie International Edition* **2016**, *55* (10), 3459-3462, DOI: 10.1002/anie.201508781.
- (4) Hu, Q.; Jiang, H.; Cui, Z. H.; Chen, W. G. An insight into the effect of S,S-dioxidized thiophene on the opto-physical/electro-chemical properties and light stability for indophenine derivatives. *Dyes and Pigments* **2020**, *173*, DOI: 10.1016/j.dyepig.2019.107891.
- (5) Guo, K.; Wu, B.; Jiang, Y.; Wang, Z.; Liang, Z.; Li, Y.; Deng, Y.; Geng, Y. Synthesis of an isomerically pure thienoquinoid for unipolar n-type conjugated polymers: effect of backbone curvature on charge transport performance. *Journal of Materials Chemistry C* **2019**, *7* (33), 10352-10359, DOI: 10.1039/c9tc03556g.
- (6) Gao, R.; Wu, B.; Liang, Z.; Zhao, X.; Deng, Y.; Tian, H.; Geng, Y. Electronic properties modulation of tetraoxidothiopheno[3,2-b]thiophene-based quinoidal compounds by terminal fluorination. *Materials Chemistry Frontiers* **2020**, *4* (3), 891-898, DOI: 10.1039/c9qm00690g.
- (7) Tormos, G. V.; Belmore, K. A.; Cava, M. P. The indophenine reaction revisited. Properties of a soluble dialkyl derivative. *Journal of the American Chemical Society* **1993**, *115* (24), 11512-11515, DOI: 10.1021/ja00077a057.
- (8) Ren, L.; Fan, H.; Huang, D.; Yuan, D.; Di, C.-a.; Zhu, X. Dithienoindophenines: p-Type Semiconductors Designed by Quinoid Stabilization for Solar-Cell Applications. *Chemistry – A European Journal* **2016**, *22* (48), 17136-17140, DOI: 10.1002/chem.201603112.
- (9) Pappenfus, T. M.; Helmin, A. J.; Wilcox, W. D.; Severson, S. M.; Janzen, D. E. ProDOT-Assisted Isomerically Pure Indophenines. *The Journal of Organic Chemistry* **2019**, *84* (17), 11253-11257, DOI: 10.1021/acs.joc.9b01525.
- (10) Hwang, K.; Lee, M.-H.; Kim, J.; Kim, Y.-J.; Kim, Y.; Hwang, H.; Kim, I.-B.; Kim, D.-Y. 3,4-Ethylenedioxythiophene-Based Isomer-Free Quinoidal Building Block and Conjugated Polymers for Organic Field-Effect Transistors. *Macromolecules* **2020**, *53* (6), 1977-1987, DOI: 10.1021/acs.macromol.9b02237.
- (11) Sun, Y.; Zhang, Y.; Ran, Y.; Shi, L.; Zhang, Q.; Chen, J.; Li, Q.; Guo, Y.; Liu, Y. Methoxylation of quinoidal bithiophene as a single regioisomer building block for narrow-bandgap conjugated

polymers and high-performance organic field-effect transistors. *Journal of Materials Chemistry C* **2020**, DOI: 10.1039/D0TC02199G.

(12) Casado, J.; Ponce Ortiz, R.; Lopez Navarrete, J. T. Quinoidal oligothiophenes: new properties behind an unconventional electronic structure. *Chem Soc Rev* **2012**, *41* (17), 5672-86, DOI: 10.1039/c2cs35079c.

(13) Xiong, Y.; Tao, J.; Wang, R.; Qiao, X.; Yang, X.; Wang, D.; Wu, H.; Li, H. A Furan-Thiophene-Based Quinoidal Compound: A New Class of Solution-Processable High-Performance n-Type Organic Semiconductor. *Adv Mater* **2016**, *28* (28), 5949-53, DOI: 10.1002/adma.201600120.

(14) Bartell, L. On the effects of intramolecular van der Waals forces. *The Journal of Chemical Physics* **1960**, *32* (3), 827-831, DOI: 10.1063/1.1730804.

(15) Kaur, K.; Utreja, D.; Dhillon, N. K.; Pathak, R. K.; Singh, K. N-alkyl isatin derivatives: Synthesis, nematocidal evaluation and protein target identifications for their mode of action. *Pesticide Biochemistry and Physiology* **2021**, *171*, 104736, DOI: 10.1016/j.pestbp.2020.104736.

(16) Mazaki, Y.; Murata, S.; Kobayashi, K. Thermal and photochemical formation of quinonoid derivatives of condensed polythiophenes and their spectral properties. *Tetrahedron letters* **1991**, *32* (34), 4367-4370, DOI: 10.1016/S0040-4039(00)92172-5.

(17) Wang, J.; Xu, X.; Phan, H.; Heng, T. S.; Gopalakrishna, T. Y.; Li, G.; Ding, J.; Wu, J. Stable Oxindolyl-Based Analogues of Chichibabin's and Muller's Hydrocarbons. *Angew Chem Int Ed Engl* **2017**, *56* (45), 14154-14158, DOI: 10.1002/anie.201708612.

(18) Jiang, P.; Ming, S.; Jia, Q.-Q.; Liu, Y.; Lu, H.; Li, M.; Xu, X.; Li, H.-B.; Bo, Z. The influence of the π -bridging unit of fused-ring acceptors on the performance of organic solar cells. *Journal of Materials Chemistry A* **2018**, *6* (43), 21335-21340, DOI: 10.1039/c8ta08410f.

(19) Jousselein-Oba, T.; Mamada, M.; Okazawa, A.; Marrot, J.; Ishida, T.; Adachi, C.; Yassar, A.; Frigoli, M. Modulating the ground state, stability and charge transport in OFETs of biradicaloid hexahydro-diindenopyrene derivatives and a proposed method to estimate the biradical character. *Chemical Science* **2020**, *11* (44), 12194-12205, DOI: 10.1039/D0SC04583G.

(20) Kim, Y.; Hwang, H.; Kim, N. K.; Hwang, K.; Park, J. J.; Shin, G. I.; Kim, D. Y. π -Conjugated Polymers Incorporating a Novel Planar Quinoid Building Block with Extended Delocalization and High Charge Carrier Mobility. *Adv Mater* **2018**, *30* (22), 1706557, DOI: 10.1002/adma.201706557.

(21) Wang, D.; Ying, W.; Zhang, X.; Hu, Y.; Wu, W.; Hua, J. Near-infrared absorbing isoindigo sensitizers: Synthesis and performance for dye-sensitized solar cells. *Dyes and Pigments* **2015**, *112*, 327-334, DOI: 10.1016/j.dyepig.2014.07.017.

(22) Han, J.; Chen, Y.; Chen, W.; Yu, C.; Song, X.; Li, F.; Wang, Y. High Performance Small-Molecule Cathode Interlayer Materials with D-A-D Conjugated Central Skeletons and Side Flexible Alcohol/Water-Soluble Groups for Polymer Solar Cells. *ACS Appl Mater Interfaces* **2016**, *8* (48), 32823-32832, DOI: 10.1021/acsami.6b10900.

- (23) Marrocchi, A.; Lanari, D.; Facchetti, A.; Vaccaro, L. Poly(3-hexylthiophene): synthetic methodologies and properties in bulk heterojunction solar cells. *Energy & Environmental Science* **2012**, *5* (9), DOI: 10.1039/c2ee22129b.
- (24) Baeyer, A. Untersuchungen über die gruppe des indigblaus. *Berichte der deutschen chemischen Gesellschaft* **1879**, *12* (2), 1309-1319, DOI: 10.1002/cber.18790120221.
- (25) Hwang, H.; Khim, D.; Yun, J. M.; Jung, E.; Jang, S. Y.; Jang, Y. H.; Noh, Y. Y.; Kim, D. Y. Quinoidal molecules as a new class of ambipolar semiconductor originating from amphoteric redox behavior. *Advanced Functional Materials* **2015**, *25* (7), 1146-1156, DOI: 10.1002/adfm.201402758.
- (26) Murrell, J. The electronic spectrum of aromatic molecules VI: The mesomeric effect. *Proceedings of the Physical Society. Section A* **1955**, *68* (11), 969, DOI: 10.1088/0370-1298/68/11/303.
- (27) Willker, W.; Leibfritz, D. Determination of heteronuclear long-range H, X coupling constants from gradient-selected HMBC spectra. *Magnetic resonance in chemistry* **1995**, *33* (8), 632-638, DOI: 10.1002/mrc.1260330804.
- (28) Huang, H.; Yang, L.; Facchetti, A.; Marks, T. J. Organic and Polymeric Semiconductors Enhanced by Noncovalent Conformational Locks. *Chemical Reviews* **2017**, *117* (15), 10291-10318, DOI: 10.1021/acs.chemrev.7b00084.
- (29) Leriche, P.; Turbiez, M.; Monroche, V.; Frère, P.; Blanchard, P.; Skabara, P. J.; Roncali, J. Strong π -electron donors based on a self-rigidified 2, 2'-bi (3, 4-ethylenedioxy) thiophene-tetrathiafulvalene hybrid π -conjugated system. *Tetrahedron letters* **2003**, *44* (4), 649-652, DOI: 10.1016/S0040-4039(02)02702-8.
- (30) Hergué, N.; Leriche, P.; Blanchard, P.; Allain, M.; Gallego-Planas, N.; Frère, P.; Roncali, J. Evidence for the contribution of sulfur-bromine intramolecular interactions to the self-rigidification of thiophene-based π -conjugated systems. *New Journal of Chemistry* **2008**, *32* (6), 932-936, DOI: 10.1039/B802313A.
- (31) Baeyer, A. Ueber die Einwirkung des Fünffachchlorphosphors auf Isatin und auf verwandte Substanzen. *Berichte der deutschen chemischen Gesellschaft* **1879**, *12* (1), 456-461, DOI: 10.1002/cber.187901201130.
- (32) Romero-Hernández, J. E.; Cruz-Rosado, A.; Zolotukhin, M. G.; Vivaldo-Lima, E. Modeling of Superacid Catalyzed Step-Growth Polymerization of Isatin and Biphenyl or Terphenyl Monomers. *Macromolecular Theory and Simulations* **2017**, *26* (5), 1700031, DOI: 10.1002/mats.201700031.
- (33) Klumpp, D. A.; Yeung, K. Y.; Prakash, G. K. S.; Olah, G. A. Preparation of 3,3-Diaryloxindoles by Superacid-Induced Condensations of Isatins and Aromatics with a Combinatorial Approach. *The Journal of Organic Chemistry* **1998**, *63* (13), 4481-4484, DOI: 10.1021/jo980588g.
- (34) Naredla, R. R.; Zheng, C.; Nilsson Lill, S. O.; Klumpp, D. A. Charge Delocalization and Enhanced Acidity in Tricationic Superelectrophiles. *Journal of the American Chemical Society* **2011**, *133* (33), 13169-13175, DOI: 10.1021/ja2046364.

(35) Joule, J. A. Thiophenes from Viktor Meyer to Poly(Thiophene) Some Reactions and Synthesis. *Phosphorus, Sulfur, and Silicon and the Related Elements* **2013**, *188* (4), 287-316, DOI: 10.1080/10426507.2012.736892.

(36) Pappenfus, T. M.; Raff, J. D.; Hukkanen, E. J.; Burney, J. R.; Casado, J.; Drew, S. M.; Miller, L. L.; Mann, K. R. Dinitro and quinodimethane derivatives of terthiophene that can be both oxidized and reduced. Crystal structures, spectra, and a method for analyzing quinoid contributions to structure. *The Journal of organic chemistry* **2002**, *67* (17), 6015-6024, DOI: 10.1021/jo025572b.

Exploration of the utility of block conjugated copolymers as a bio-interface for sensing

5.1) Introduction

The convergence of materials science, electronics, and biology, namely bioelectronic interfaces (BEIs), leads novel and precise communication with biological systems; they can be manipulated to couple the flows of electrons and ions in dual directions.¹ Biological systems vary from standard electronics by their mechanisms of signal generation and transmission. In conventional electronics devices the free charge carriers are electrons. In biological systems the electric current is carried mostly by ionic fluxes.² These two modes of conduction are, in principle, very different, which requires a specific interface in which signals can be transduced. The unique electrical, mechanical and biocompatibility properties of BEIs qualify them as promising candidates for neural interfaces,³⁻⁴ simulation,⁵ and electrically triggered-response toward the release and pumping of small molecules.⁶ **Figure 1** illustrates examples of applications of BEIS in electrical sensing, recording and stimulation.

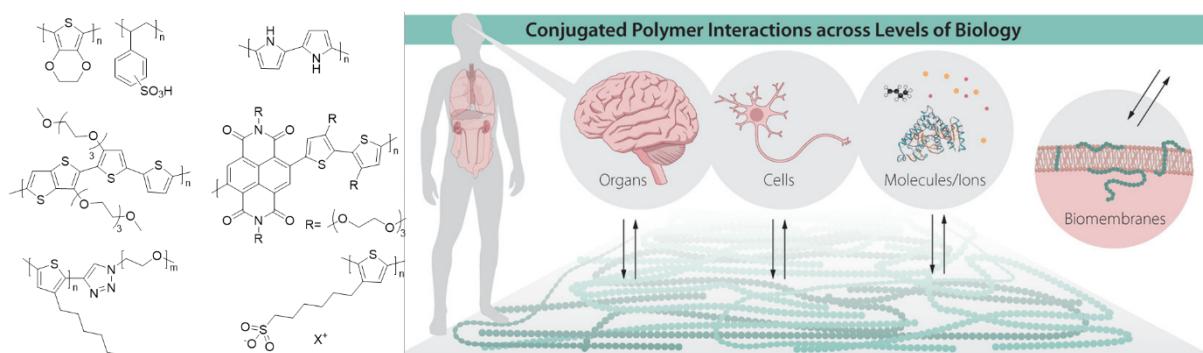


Figure 1. Examples of applications of BEIs in biomedicine and polymers with ionic conductivity for bioelectronic applications, PEDOT:PSS, polypyrrole, polythiophene derivatives, poly(3-hexylthiophene)-*b*-poly(ethylene oxide) and anionic polythiophene. Adapted from ref.⁷

Inorganic materials are widely used to interface conventional electronic devices with biological materials, ranging from proteins to whole organs.⁸ However, the major drawbacks of inorganic semiconductors are their mechanical rigidity,⁹ nature of charge transport (non-ionic conductivity),¹⁰ biofouling, and non-biocompatibility.¹¹

5.1.1) π -Conjugated polymers as bioelectronic material.

Semiconducting polymers have the virtue of being mechanically flexible¹² and biocompatible.⁷ They are chemically tunable, solution-processable, they have easily modifiable surface structure,¹³⁻¹⁴ and possess mixed ionic and electronic charge transport.¹⁵⁻¹⁶ The most used conjugated polymers (CPs) for bioelectronics are polypyrrole, polyaniline, and functionalized polythiophene derivatives. Poly(3,4-ethylenedioxythiophene) polystyrene sulfonate (PEDOT:PSS) and its derivatives have recently emerged

as the dominant materials. Because of their good ion and electron mobility, their excellent coating ability for metal electrodes that reduces interface capacitance and enhance tissue integration. In recent years, a considerable amount of literature has emerged on the use of tuned CPs for bioelectronic applications.^{15, 17} The motivation behind many of these studies is (i) to improve the biotic/non-biotic interface with living cells and (ii) to functionalize with biomolecules (e.g. nucleotides or proteins) for sensing. To improve the biotic/non-biotic interface, different methods have been used to functionalize the CPs. A facile approach is to physically entrap biomolecules and proteins on top of the CPs where they will adsorb to the surface. However, biomolecules may desorb or denature from the surface, resulting in unwanted changes in device performance.¹⁸ Covalent functionalization is the most used route to tune the CPs.

5.1.2) Mixed ionic-electronic semiconducting polymers.

Polymer-based mixed ionic–electronic conductors (MIECs) recently emerged as new materials in many applications¹⁹ such as energy storage e.g., batteries²⁰ and supercapacitors,²¹ transconductance in bioelectronics⁷ and organic electrochemical transistors.²² Polymeric mixed ionic–electronic conductors typically comprise semiconducting polymers that solvate and transport ionic species. They contain two principal components, one for electronic conduction and the other for ionic conduction. Different strategies have been used to design and fabricate MIECs. A variety of copolymer architectures of CPs has been published, including: PEDOT:PSS;²³ blend of ionic liquid and conjugated polymers,²⁴ incorporating of oligo(ethylene glycol) side-chains on π -conjugated polymers;²⁵ *rod-coil* with ion conducting and electronic conducting blocks, e.g., poly(3-hexylthiophene).

5.1.3) Transducing, bioelectronic devices, impedimetric sensors.

The primary goal of bioelectronic interfaces is to achieve an efficient ionic-to-electronic transduction, i.e., to create devices, such as implants, drug delivery systems, artificial skin, and sensors for *in vivo* or *in vitro* environments, that translate biological signals (often ionic in nature) to high-fidelity electronic signals and *vice versa*.

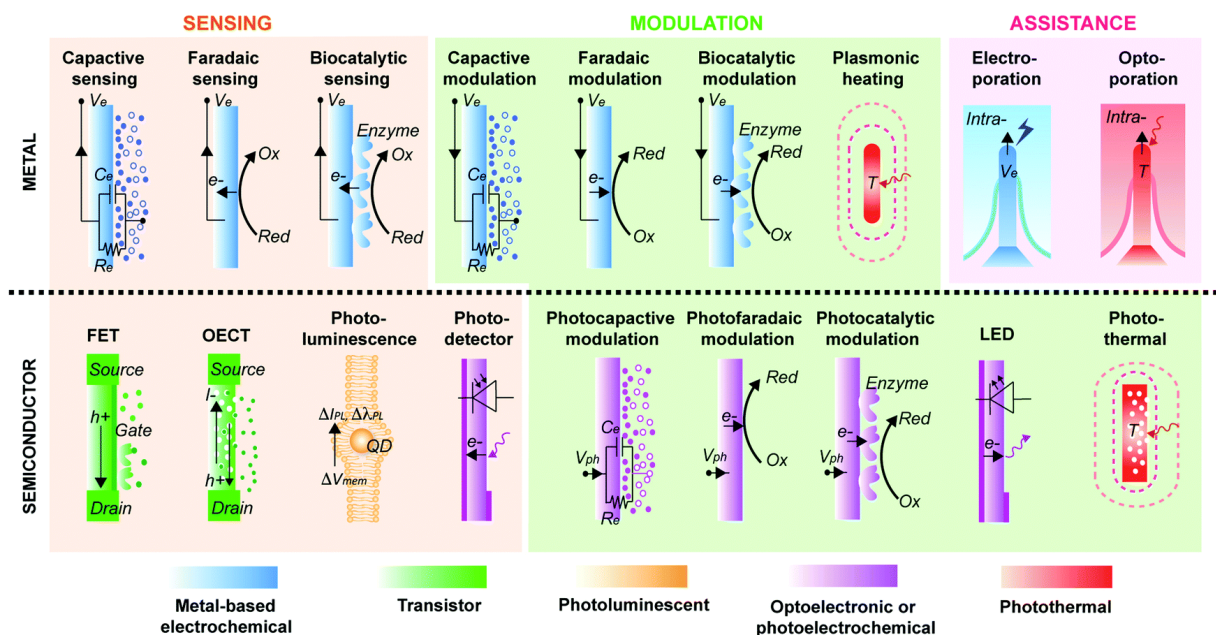


Figure 2. Schematic overview of bioelectronic interfaces. Top: Metal-based electrodes for recording or injecting capacitive, faradaic, and biocatalytic currents. Bottom: Semiconductor-electrodes for recording of bioelectric signals using field-effect transistors (FETs) and organic electrochemical transistors (OECTs). Adapted from Ref.²

However, the novel functionalities of the biointerface of such devices should also be evaluated. Electrochemical impedance spectroscopy (EIS) is a method of choice for characterizing the electrical behavior of BEIs in which the overall system behavior, Faradaic (impedimetric) and non-Faradaic (capacitive), is determined by a number of strongly coupled processes, (**Figure 2**). There are many reviews summarizing the basis of the EIS technique as well as its implementation as impedimetric biosensors using functional BEIs as highly sensitive transducer platforms.²⁶

Objectives of this study

The objective of this chapter is to synthesize and characterize novel copolymers for fabrication of bio-interface. This bio-interface is formed by self-assembly of P3HT-*b*-P3TEGT into core-shell nanoparticles, which was further decorated with mannose, leading to an easy-to-use water dispersible nanoparticle material for biosensing, as shown in **Figure 3**. In this system, the hydrophilic sub-block P3TEGT promotes antifouling and prevents non-specific interactions while improving the ionic and electronic transport properties, thus enhancing the electrochemical-sensing capability in aqueous solution. This bio-interface was used to capture and sense bacterial pathogens such as *E. coli*. This work was a collaborative effort between PICM and ICMMO, for which my contribution was focused on the synthesis and characterization of monomers and copolymers.

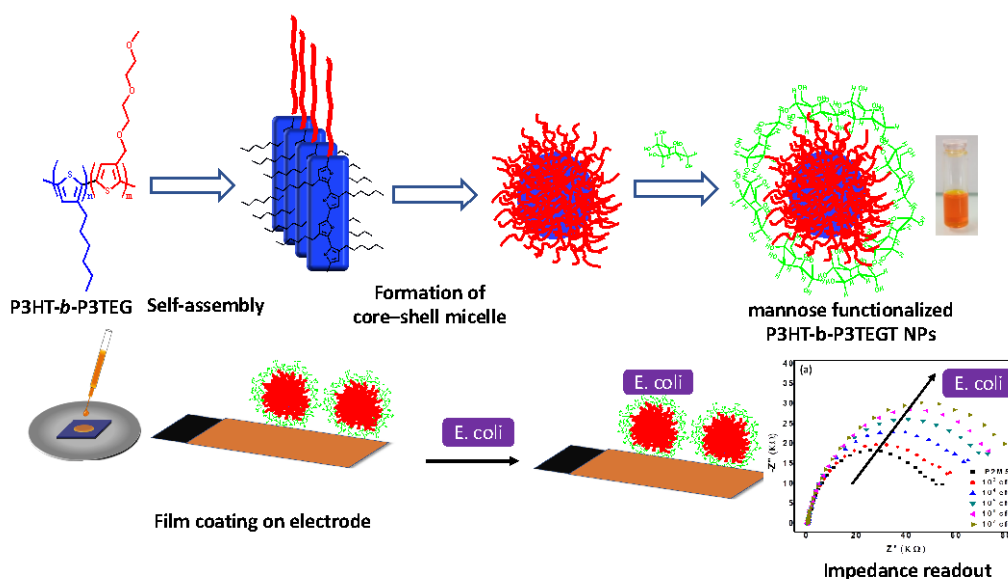


Figure 3. Cartoon representation of self-assembly P3HT-*b*-P3TEGT, mannose functionalized π -conjugated polymer nanoparticles and label-free impedimetric sensor for *E. coli* detection. Top, chemical structure of P3HT-*b*-P3TEGT, aggregation of the P3HT sub-block via-interaction in methanol, formation of core-shell micelles through the precipitation of P3HT-sub-block and good solubility of P3TEGT-sub-block in methanol, and mannose decorated P3HT-*b*-P3TEGT nanoparticles (NPs) through hydrophilic non-covalent interactions between hydrophilic TEGT segments on the outer surface of the NPs and hydroxyl group of the mannose. Bottom, mannose-P3HT-*b*-P3TEGT film coated on the electrode surface, *E. coli* attachment via Pili-mannose binding and label-free impedimetric *E. coli* detection.

5.2) Results and discussion

5.2.1) Synthesis and characterization of copolymers.

Scheme 1 was a general synthetic method for the synthesis of these A-*b*-B diblock copolymers. The synthesis started with the preparation of 3-*n*-hexylthiophene. The bromination was then carried out with NBS to give 2,5-dibromo-3-hexylthiophene monomer **M1**. In the same way the bromination with NBS was used to access to 2,5 dibromo-3-methyl-thiophene, compound **5**, from 3-methylthiophene. Compound **6** was obtained by the reaction of compound **5** with NBS in carbon tetrachloride with the addition of benzoyl peroxide (BPO) serving as a catalyst. This step was followed by Williamson ether synthesis to afford the monomer **M2**. 2-Bromo-5-chloro-magnesium-3-hexylthiophene, **8**, was obtained by the treatment of monomer **M1** with 1.1 equivalent of isopropylmagnesium chloride. It should be remarked that the magnesium-bromine exchange reaction proceeded with moderate regioselectivity,

resulting in the distribution of regiochemical isomers in the ratio of 72:28 and 54:46, respectively. These values were estimated from the integral area ratio of the peak in the ^1H NMR spectrum, **Figure 4**. All these synthetic procedures are described in detail in experiment part.

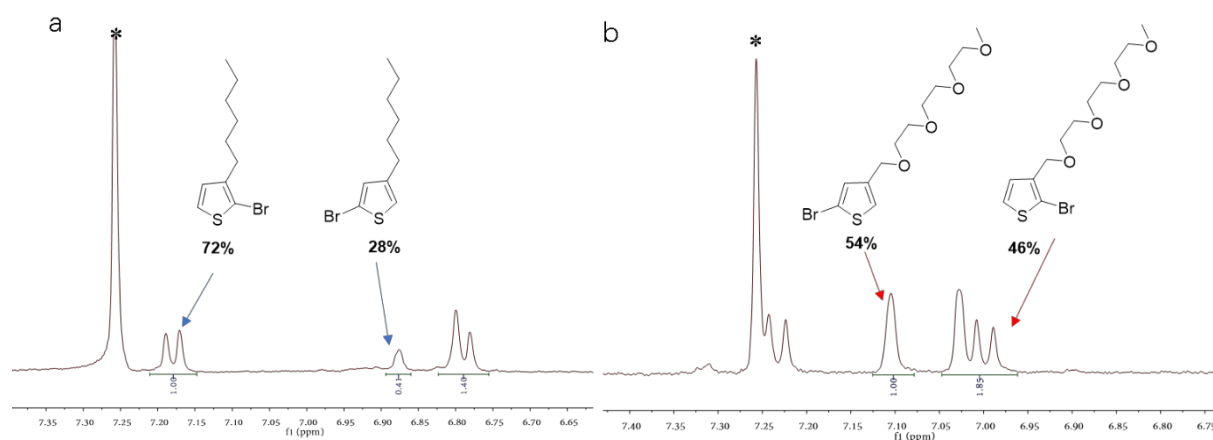
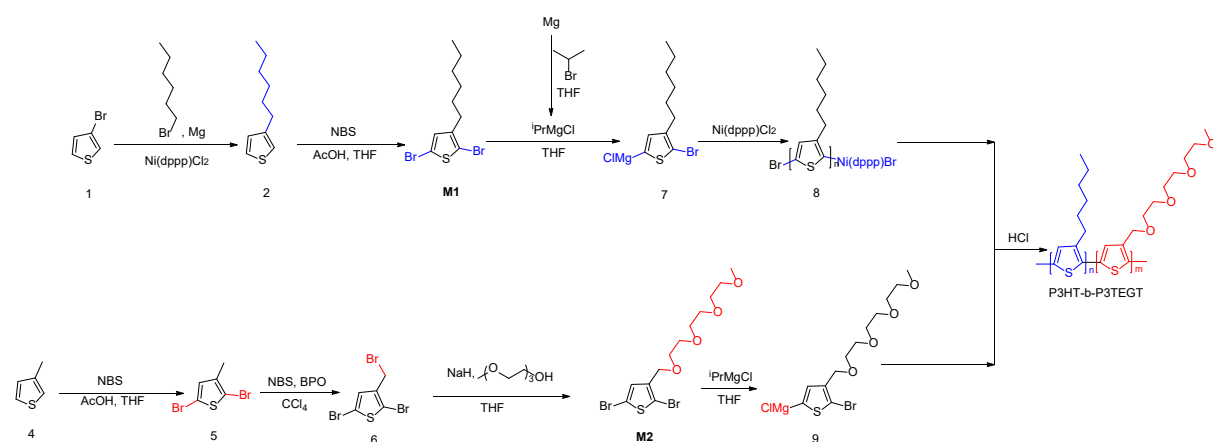


Figure 4. ^1H NMR spectra of (a) Mixture isomers of compound **7**, (b) Mixture isomers of compound **9** (*: solvent peak).

5.2.1.1) Synthesis of P3HT-*b*-P3TEGT block copolymers

P3HT block was prepared by Grignard metathesis polymerization in the presence of a Nickel catalyst to obtain the macroinitiator P3HT with a living chain-end. The macroinitiator sub-block P3HT was added to the chain-extended reaction solution of the triethylene glycol (TEG) substituted thiophene monomer (Compound **9**) for the formation of a diblock structure. The obtained diblock copolymer P3HT-*b*-P3TEGT was purified by sequential Soxhlet extraction with methanol and hexane, and the chloroform's fraction was then collected.



Scheme 1. Synthesis route to the P3HT-*b*-P3TEGT diblock polymer

The macromolecular structure of chloroform-soluble fraction was confirmed by ^1H -NMR spectroscopy, and the peaks were assigned to confirm the diblock nature of the copolymer (See **Figure 5a**). It is noticeable that for all protons in the P3HT-*b*-P3TEGT, only two sets of signals (red and blue)

are observed in the spectra. This is because of the highly symmetrical structure of P3HT-*b*-P3TEGT in whereby the protons at specific positions in each thiophene unit are in a chemically identical environment. The block copolymer in the aromatic region shows two singlets at 7.26 and 6.98 ppm corresponding to the aromatic proton of the thiophene ring of the P3HT sub-block (assigned as Ha) and the P3TEGT sub-block (assigned as Hb), respectively. The signals at 2.80 and 4.66 ppm are assigned to the protons of the α -methylene units in the α -position of the thiophene ring of the P3HT sub-block (Hf) and the oxyethylene protons of the TEGT segment (Hc), respectively. The peaks at 2.60 and 2.80 ppm corresponding to the α -CH₂ groups (assigned Hf) from hexyl chains have been used to determine the molecular weight distribution and regioregularity of P3HT. These peaks are assigned to the α -CH₂ groups on the terminal tail of 3-hexylthiophene units and the to all the α -CH₂ groups in the internal hexyl chains from the polymer, respectively.

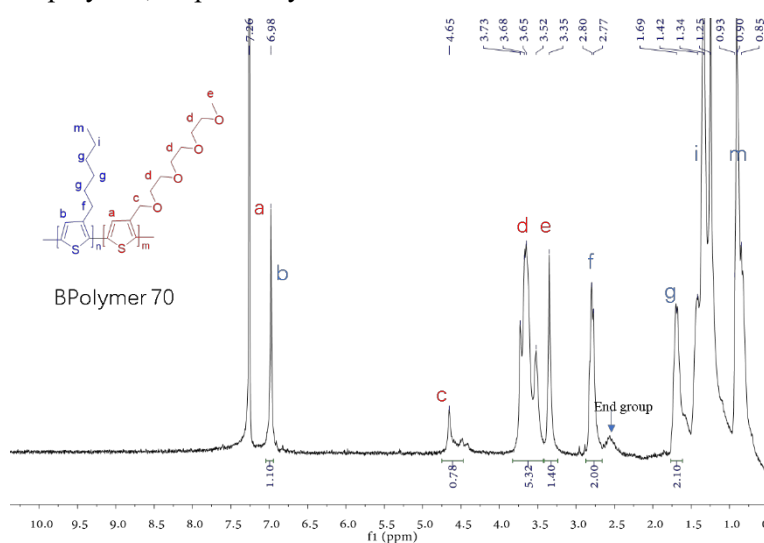


Figure 5a. ¹H-NMR spectrum of P3HT-*b*-P3TEGT (**BPolymer 70**) and its peak assignment

The degree of polymerization (*n*) of P3HT block was estimated to be ca. 18-20 by NMR analysis, which is close to the estimated molecular weight of the copolymer as determined using gel permeation chromatography (GPC), *M_n* = 15 Kg/mol. The block distribution was estimated by ¹H NMR integration, and the ratio of the two fragments derived from the comparison of Hc and Hb was 28:72 and a similar ratio of 32:68 was obtained by comparing He and Hf. The results demonstrate that P3HT-*b*-P3TEGT consists of 70 mol% of 3-hexyl-thiophene and 30 mol% of thiophene unit substituted with oxyethylene groups (**BPolymer 70**). This ratio is very comparable to the feed ratio of the monomers used in the copolymerization process. By varying the feeding ratio of the monomer, we also obtained a range of other ratios of the diblock polymer (**BPolymer 80** and **BPolymer 30**). As shown in the **Figure 5b** below, the percentage of the P3HT fraction here was found to be 80% by comparing Hc to Hb.

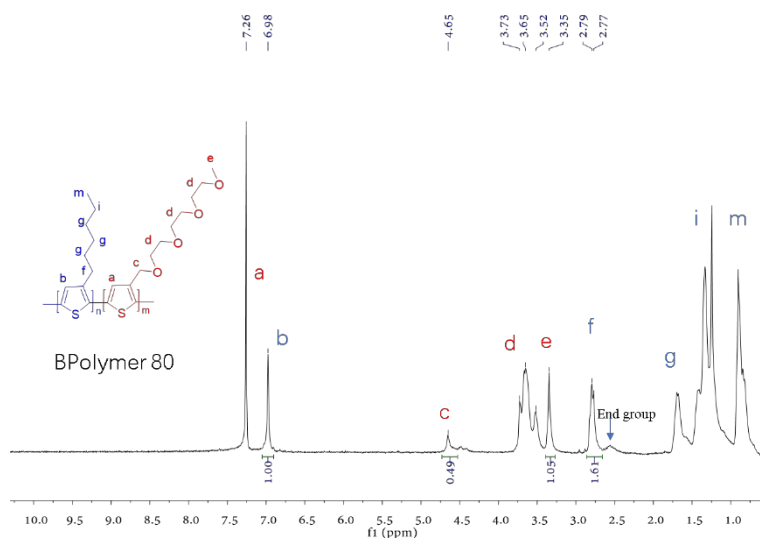
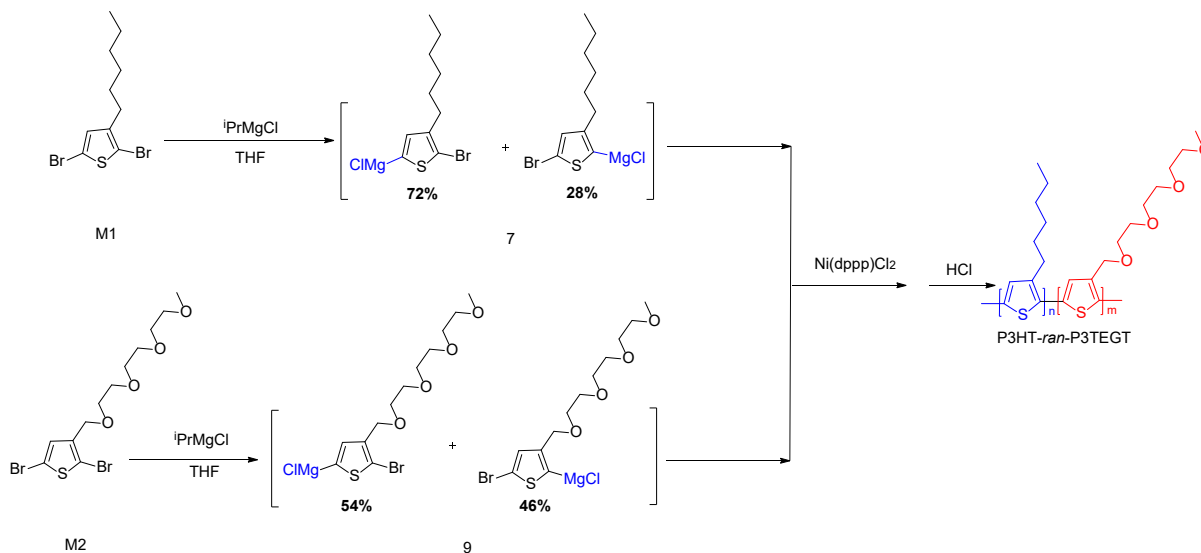


Figure 5b. ¹H-NMR spectrum of P3HT-*b*-P3TEGT (**BPolymer 80**) and its peak assignment.

5.2.1.2) Synthesis of P3HT-*ran*-P3TEGT random polymers

The random copolymer, P3HT-*ran*-P3TEGT has been prepared as illustrated in **Scheme 2**. In separated flasks the Grignard monomers **7** and **9** were prepared from **M1** and **M2**, respectively. The bromination of the Grignard monomers was followed by NMR test until complete conversion of the starting materials. Then the Grignard monomers were transferred into flask containing 1% mol of the Ni(dppp)Cl₂ as a catalyst, and the copolymerization conducted overnight at room temperature. The copolymer was purified following the same procedure as described previously.



Scheme 2. Synthesis route of P3HT-*ran*-P3TEG random polymer

In the aromatic region, the random copolymer shows a broad peak corresponding to at least four singlets arising from the four possible triads (**Figure 6**). This confirms the statistical distribution of

the monomers in the chain. In contrast, the block copolymer shows two singlets in the aromatic region corresponding to each sub-block.

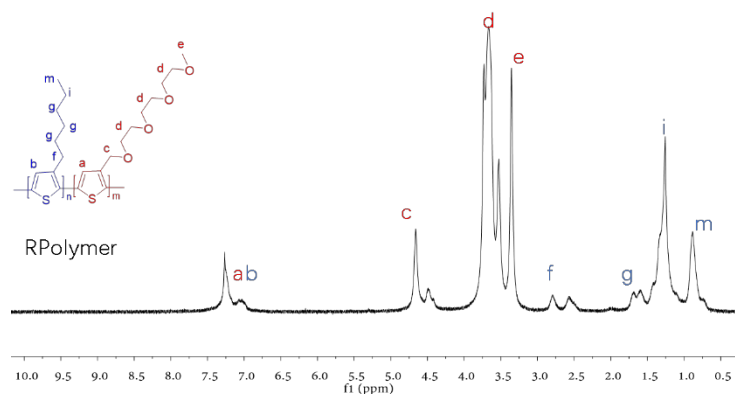


Figure 6. ¹H-NMR spectrum of P3HT-*ran*-P3TEGT and its peak assignment

5.2.2) Gel permeation chromatography characterization

Gel permeation chromatography (GPC) was performed to assess the average molecular weight and dispersity of the copolymers, the results are shown in **Table 1**.

Table 1.

Polymer ^a	Mn ^b	Mw ^c	<i>D</i> ^d
BPolymer 80	6996	10587	1.51
BPolymer 70	15605	25092	1.60
BPolymer 30	7605	9263	1.21
RPolymer	9436	11077	1.17

^aTHF was used as an eluent; Polystyrene for the calibration;

^bMn: weight average molecular weight;

^cMw: number average molecular weight; ^d*D*: dispersity: $D_w = M_w/M_n$

5.2.3) Self-assembly of P3HT-*b*-P3TEGT

The first indication of successful self-assembly and micelle formation by P3HT-*b*-P3TEGT came from the ¹H and ¹H-¹H NOESY NMR analysis. The NMR spectrum in **Figure 7** showed that various changes were observed after the addition of a small amount of MeOD (10%) to the chloroform solution of the block copolymer P3HT-*b*-P3TEGT: i) gradual broadening of the aromatic and aliphatic proton signals; ii) decrease of the intensity of the deshielded narrow aromatic peaks; iii) appearance of new peaks. The modification was pronounced for high amount of MeOD added. At higher concentration of methanol-*d*₄ (30%), top spectrum in **Figure 7**, the hyperfine structure disappeared completely and the line width of the signals broadened. The changes of line-shape, chemical shift, and line width and the appearance of the new resonance signal are observed. These modifications in NMR spectra reflect the

π - π aggregation and micellization induced by the methanol. The broad ^1H line width was a result of restricted molecular mobility of P3HT sub-block chains which stick together and form aggregates.

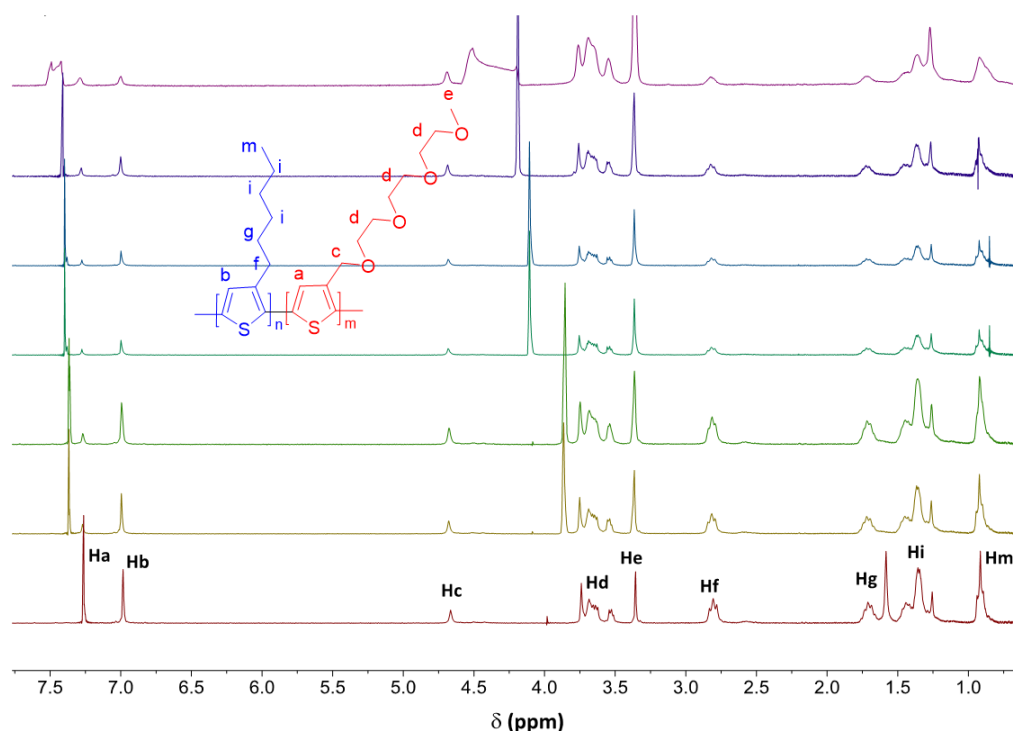


Figure 7. ^1H NMR of P3HT-*b*-P3TEGT (5 mg/ml CDCl_3) with successive addition of methanol- d_4 from bottom to up: 0, 0.1 ml, 0.15 ml, 0.2 ml, 0.25 ml, 0.3 ml, 0.4 ml.

To better understanding the self-assembly behavior of P3HT-*b*-P3TEGT, 2D NOESY NMR experiments were performed. This technique allows the correlation of proton-proton interaction at relatively close distances through space. The short distance between proton of alkyl groups and the proton of thiophene rings is sufficient to produce the NOE transfer. Consequently, 2D NOESY experiments could provide information regarding the self-assembly of copolymer and the chemical core/shell structure of nanomicelle. The NOESY spectra of P3HT-*b*-P3TEGT were recorded with the addition of methanol- d_4 in CDCl_3 (**Figure 8a**). The spectrum of the P3HT-*b*-P3TEGT in CDCl_3 with 5% of methanol- d_4 showed that there were at least as many as six cross-peaks existing between the thiophene ring and hexyl group. The α -methylene protons (labeled H_f) had a strong interaction with the aromatic proton of thiophene ring in P3HT block (labeled H_a) and also with β -methylene protons (labelled H_g) in hexyl chain (**Figure 8a**). In addition, the spectra demonstrated that both the β -methylene protons and the methylene protons in the hexyl chain (labelled H_i) interacted intensely with the terminal methyl of hexyl chain (labelled H_m). However, no NOE effects were detected among all oxymethylene protons of the TEG segments, and only the oxymethylene proton neighboring thiophene ring (labelled H_c) interacted with the aromatic proton of thiophene in the P3TEGT block (labelled H_b). NOE is a type of dipole-dipole interaction through space, which is sensitive to nuclei that are close together by bonding

structures as well as the nuclei that are close together by (~ 0.5 nm).²⁷ The lack of the oxyethylene protons interactions was attributed to large space between the chains.

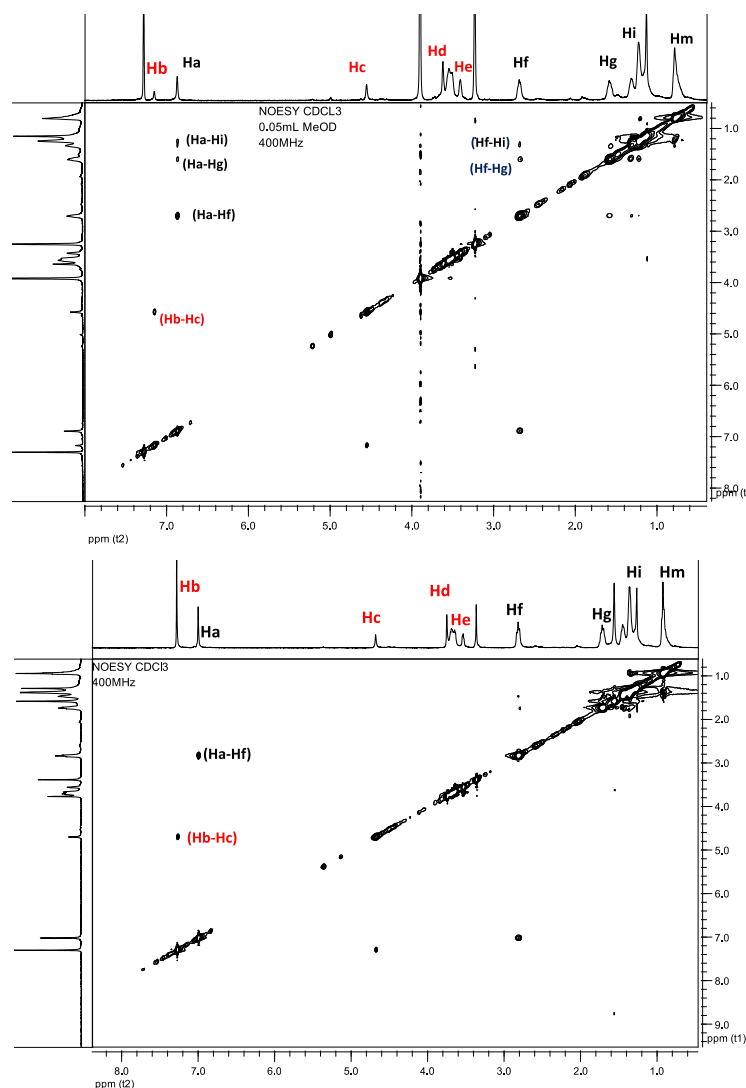


Figure 8. ¹H-¹H NOESY NMR spectra of (a) P3HT-*b*-P3TEGT in CDCl₃ with 5% of methanol-d₄, (b) without methanol-d₄.

As a matter of fact, it has been evidenced that the P3HT-*b*-P3TEGT self-assembly on lamellar structure and stacks with chain packing situations in the P3HT and P3TEGT phases, where d-spacing of 0.52 nm was assigned to the average inter-distance of the oxyethylene side groups between the P3TEGT sub-block chains, while the other d-spacing of 0.46 nm was assigned to the average inter-distance of the *n*-hexyl side-chains between the P3HT sub-block chains.²⁸ Accordingly, the NOE was less sensitive to proton-proton interaction of the TEGT side groups. These six cross-peaks supported that the P3HT sub-block were self-assembling into a lamellar organization, reinforced by π - π stacking interactions. In this way, the hexyl chains of P3HT sub-block were interdigitated between flanked highly ordered π -stacked aggregates (face-to-face) surrounded by domains of the hydrophilic P3HT blocks, core-shell nanomicelles. For the purpose of comparison, we have performed an analysis of the NOESY

NMR spectrum of P3HT-*b*-P3TEGT in CDCl₃ without the addition of the methanol-d₄. ¹H-¹H NOESY NMR spectrum of P3HT-*b*-P3TEGT in CDCl₃ shows only two major cross-peaks (H_a-H_f, H_b-H_c, **Figure 8b**). The α -methylene protons at 2.6 ppm strongly interact with the aromatic proton of thiophene ring in P3HT sub-block and oxymethylene protons next to thiophene ring interact with the aromatic proton of thiophene in the P3TEGT sub-block. This result is in agreement with previous work which reported that the alkyl chains are interdigitated, with the methylene groups next to the ring interact with the aromatic rings of an adjacent stack.²⁹ Thus, all NMR results clearly support the self-assembly of P3HT-*b*-P3TEGT into polymer core-shell nanomicelles with a bilayer architecture formed by a hydrophobic P3HT sub-block interior and surrounded by a hydrophilic exterior PEGT sub-block. These observations are well supported by previous literature reports.³⁰

5.2.4) UV-visible absorption spectroscopy

The successful self-assembly of P3HT-*b*-P3TEGT was verified by the recording of the solution absorption spectra of P3HT-*b*-P3TEGT together with P3HT after continuously increasing the amount of the methanol-d₄ (**Figure 9**). In the case of P3HT (**Figure 9A**), the polymer chains were well solubilized, with an absorption band near 435 nm observed in tetrahydrofuran. The maximum absorption peak shifted to 515 nm at 30% methanol and there were additional absorption peaks at 555 and 610 nm. The new bands were attributed to the formation of aggregations in solution due to the π - π stacking of the P3HT chains. With further increase in the methanol ratio, the low-energy band broaden and decreased gradually until it disappeared in 100% methanol, which was due to the precipitation of the copolymer aggregates. In the case of the copolymer P3HT-*b*-P3TEGT (**Figure 9B**), some different behaviors were observed. Firstly, the main peak of around 425 nm observed in THF indicated that the two blocks of P3HT-*b*-P3TEGT were fully dissolved. At a methanol ratio of 30%, additional absorption peaks at 555, and 610 nm appear due to the improved π - π stacking of the P3HT sub-block which is the same behavior as P3HT homopolymer. Nevertheless, these low-energy peaks increased gradually when methanol ratio was further increased, as in contrast to the P3HT homopolymer, stable micelles with a hydrophilic shell were formed. Hence, this result proved that methanol, as a poor solvent, induced the aggregation of P3HT and as selective solvent for P3TEGT induced the formation of stable nanomicelles of the block copolymer P3HT-*b*-P3TEGT with a core of P3HT block and a shell of P3TEGT block.

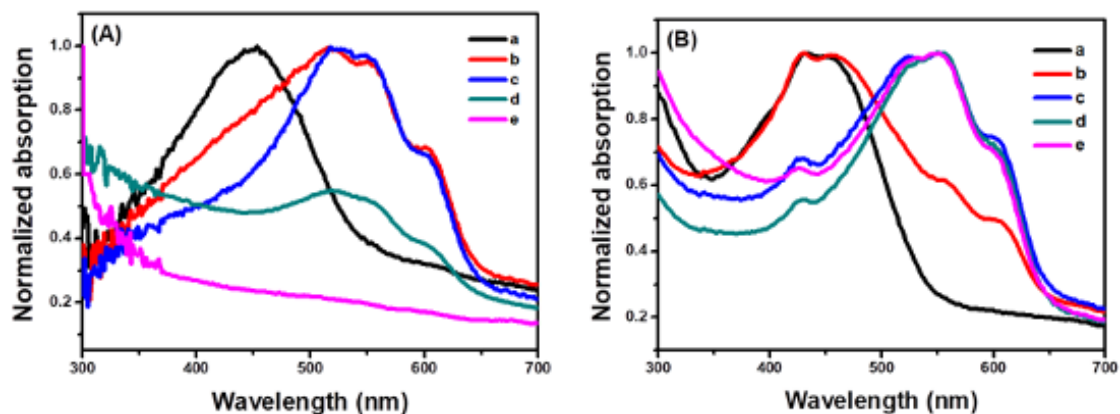


Figure 9. UV-vis absorption spectra of: (A) P3HT, (B) P3HT-*b*-P3TEGT in tetrahydrofuran solutions with different methanol ratios a) 0%, b) 30%, c) 50%, d) 70%, e) 100%

5.2.5) Fabrication of biosensing surface, bacteria attachment and impedance sensing

To demonstrate the utility of these materials in the development of highly efficient sensors, impedimetric sensors for the detection of bacteria were fabricated and the performance of the sensors was evaluated. During the past decade, carbohydrates have been increasingly considered as alternative bioreceptors as they are involved in key recognition events.³¹ Carbohydrates are more resistant to denaturation than nucleic acids and antibodies. Their small size also provides a higher carbohydrate density per unit surface area, which enhances the binding affinity. In particular, mannose is a typical carbohydrate molecule with good targeting ability to *E. coli* pili owing to its binding with the Fim H lectin proteins. P3HT-*b*-P3TEGT was blended with mannose in different weight ratios in methanol to determine the optimal sensing capability. Three weight ratios of P3HT-*b*-P3TEGT to mannose (1:5, 2:5, and 3:5) were prepared and studied by FTIR and angle contact. This was followed by incubation with *E. Coli* and measuring detection of *E. coli* by EIS.

Optical microscope images of glass substrate modified film after incubation with (1.0×10^7 CFU/mL) *E. coli*. P3HT film (**Figure 10**) shows image with bacteria attachment corresponding to the non-specific interaction of the surface with bacteria. While P3HT-*b*-P3TEGT film (**Figure 10b**) shows any bacterial cell attachment. This result is related to the antifouling surface provided by the association of water within TEG side-chains leading to the exclusion of biomolecules from the surface. In the case of the film of P3HT-*b*-P3TEGT coated with mannose (**Figure 10c**), the image shows attachment of bacterial cells on the surface. This is due to Fim H lectin in bacteria surface able to bind mannose conjugated/P3HT-*b*-P3TEGT film.

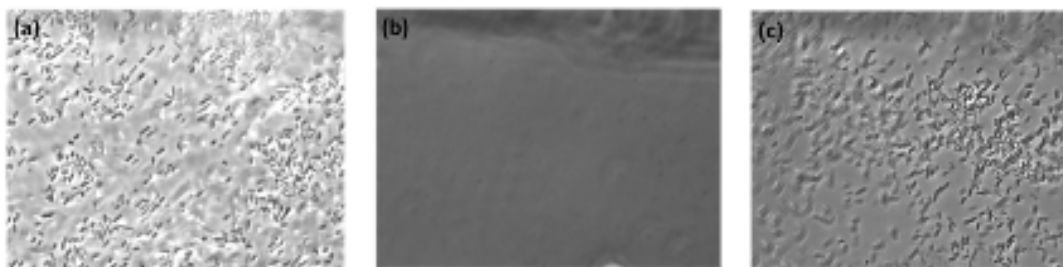


Figure 10. Optical microscope images of glass substrate modified (a) P3HT, (b)P3HT-*b*-P3TEGT, (c) mannose functionalized P3HT-*b*-P3TEGT/mannose

Scanning electron microscopy (SEM) was used to evaluate the antifouling properties of the P3HT-*b*-P3TEG films and to confirm bacterial attachment to the mannose-modified P3HT-*b*-P3TEG films. As shown in **Figure 11a**, when a P3HT-*b*-P3TEG film was incubated with a solution of *E. coli* (1.0×10^7 CFU/mL), no attached bacteria were observed on the film surface. Nevertheless, after exposing the substrate surface mannose/P3HT-*b*-P3TEG film to (1.0×10^7 CFU/mL) of the *E. coli* solution, the SEM image clearly reveal *E. coli* cells attached to the surface of the film (**Figure 11b**). This implies that mannose-decorated P3HT-*b*-P3TEG provides an ideal bio-surface for selective immobilization of *E. coli* bacteria due to mannose–lectin binding interaction.

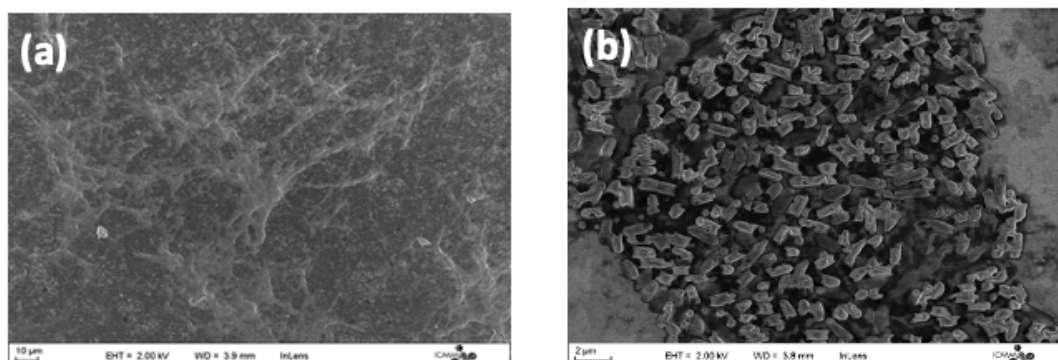


Figure 11. SEM images after incubation with *E. Coli* (1.0×10^7 CFU/mL), a) P3HT-*b*-P3TEGT film, b) mannose/P3HT-*b*-P3TEGT film.

The detection of *E. coli* by combining P3HT-*b*-P3TEGT/mannose modified glassy carbon electrode was characterized by electrochemical impedance spectroscopy (**Figure 12**). As shown in the figure, the electrode showed linear variation from 10^3 CFU/mL to 10^7 CFU/mL.

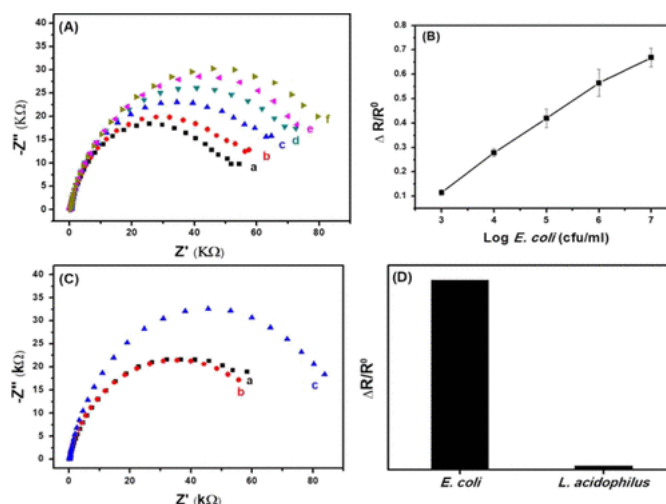


Figure 12. (A) Nyquist diagrams of a P3HT-*b*-P3TEGT/mannose-modified GCE obtained with increasing concentrations of *E. coli* in PBS: (a) Biosensors in PBS free of bacteria, (b) 10³cfu/mL, (c) 10⁴ cfu/mL, (d) 10⁵ cfu/mL, (e) 10⁶ cfu/mL, (f)10⁷ cfu/mL; (B) calibration curve; (C) Nyquist plot for selectivity test of P3HT-*b*-P3TEGT/mannose-modified GCE; (c) *E. coli* detection compared to (b) *L. acidophilus* and (a) free of bacteria; (D) histogram of average variation between the two bacteria.

5.3) Conclusion and perspectives

In this chapter we have synthesized P3HT-P3TEGT copolymers through Grignard metathesis polymerization. These copolymers were characterized by ¹H-NMR, 2D NOESY NMR, ¹³C-NMR, GPC UV-visible absorption spectroscopy. In the methanol solution, the diblock copolymer was found to self-assemble into core shell nanoparticles with P3HT as the core and P3TEGT hydrophilic segments as the corona. The blend of P3HT-*b*-P3TEGT was used to fabricate a biosensor for the detection of Gram-negative bacteria *E. coli* by electrochemical impedance spectroscopy. The benefits for the use of amphiphilic P3HT-*b*-P3TEGT come from several main aspects: (i) the P3HT sub-block is responsible for π - π stacking, which drives the self-assembly behavior and mediates micelle formation; (ii) the hydrophilic P3TEGT sub-block promotes the antifouling property and prevents non-specific interaction of other types of bacterial cells, (iii) enhancing ionic transport and the electroactivity in aqueous solution; (iv) the redox activity of the π -conjugated backbone is exploited as electrochemical transducer using the EIS.

The possible extension of this work is to develop new boronic acid-functionalized π -conjugated block copolymer (**Figure 13**). In fact, a weakness of our approach is that the bioreceptor is not covalently attached to the copolymer, which may lead to the stability issue. Boronic acid derivatives show high ability to covalently bind with great affinity to 1,2- or 1,3-diols commonly found on carbohydrates of various surface cells and biological membranes of viruses, and bacteria.

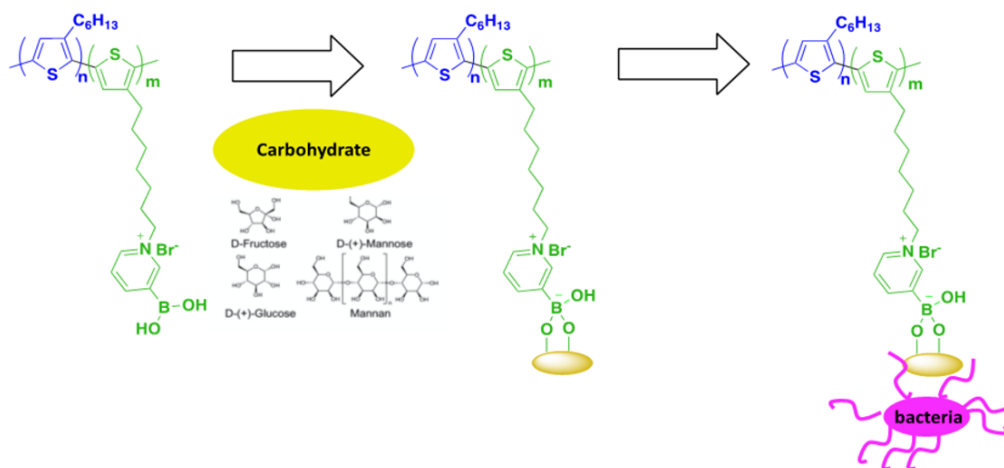
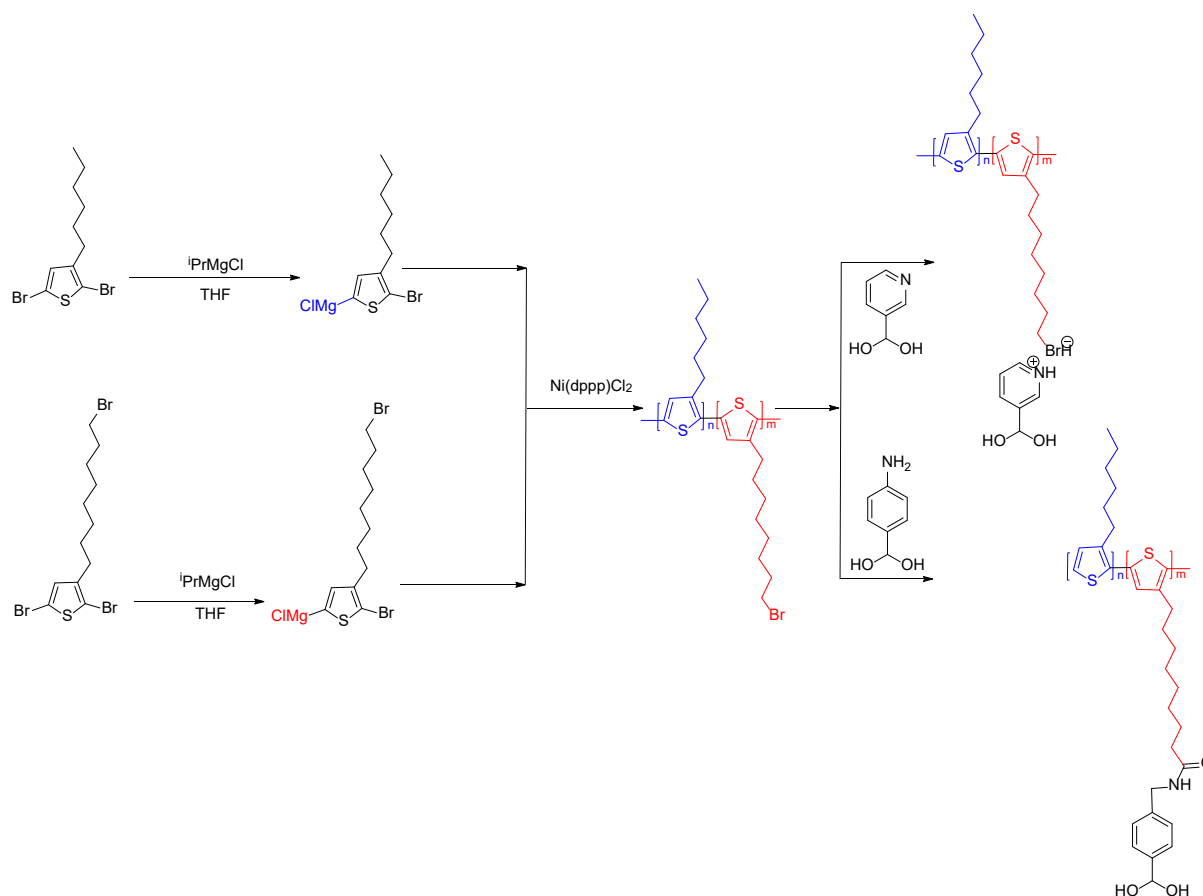


Figure 13. Possible extension of this work

We propose to develop a class of boronic acid-functionalized π -conjugated polymers, following the protocol developed (**Scheme 3**). An alternative method will consist to prepare block copolymers carboxylic acid reactive function end-capped side chain, then transform the carboxylic acid to the amide.



Scheme 3. Synthesis route of boronic acid functionalized conjugated polymers.

Experimental procedures and Characterization data

3-hexylthiophene (2): Magnesium (0.75 g, 30 mmol, 1.5eq) was introduced into a flask with dry diethyl ether (16 mL) and heated for 5 min to make the magnesium active. A solution of 1-bromohexane (4.12 g, 25 mmol, 1.25eq) was added dropwise via syringe. The resulting mixture was stirred under argon for 2 h and then transferred to a dropping funnel of a second flask containing 3-bromothiophene (1) (3.26 g, 1.87 mL, 20 mmol, 1eq) and Ni(dppp)Cl₂ (0.05 g) in dry Et₂O. After cooling with an ice bath, the Grignard reagent was added slowly dropwise over 0.5 h, and the resulting adduct was allowed to warm gradually to room temperature and then stirred under argon overnight. Ethyl acetate was added and the organic layer was washed with water 3 times. The organic phase was dried over anhydrous Na₂SO₄. After removing the solvent by rotary evaporation, the crude product was distilled under reduced pressure to afford **2** as a colorless oil (2.07 g, 62% yield). ¹H NMR (CDCl₃, 300 MHz) δ 7.24 (m, 1H), 6.95-6.92 (m, 2H), 2.64 (t, 2H), 1.66-1.60 (m, 2H), 1.36-1.25 (m, 6H), 0.91 (t, 3H). ¹³C NMR (CDCl₃, 75 MHz) δ 143.27, 128.29, 125.03, 119.75, 31.71, 30.55, 30.31, 29.04, 22.64, 14.12.

2,5-dibromo-3-hexylthiophene (M1): NBS (1.95 g, 10.95 mmol, 2.1eq) was added to a stirred solution of 3-hexylthiophene (2) (850 mg, 5.05 mmol, 1eq) in acetic acid (10 mL) and THF (10 mL). The mixture was stirred at rt overnight. Ethyl acetate was added and the organic layer was washed with water 3 times. The organic phase was dried over anhydrous Na₂SO₄. After removing the solvent by rotary evaporation, the residue was dissolved in hexanes and the byproduct (succinimide) was filtered by celite. The crude product was distilled under reduced pressure to afford **M1** as a colorless oil (1.37 g, 83% yield). ¹H NMR (CDCl₃, 300 MHz) δ 6.78 (s, 1H), 2.50 (t, 2H), 1.56-1.50 (m, 2H), 1.34-1.27 (m, 6H), 0.91 (t, 3H). ¹³C NMR (CDCl₃, 75 MHz) δ 142.99, 130.95, 110.28, 107.91, 31.58, 29.56, 29.49, 28.79, 22.58, 14.09.

2,5-dibromo-3-methylthiophene (4): NBS (20.0 g, 112.4 mmol, 2.1eq) was added to a stirred solution of 3-hexylthiophene (2) (5.08 g, 51.7 mmol, 1eq) in acetic acid (10 mL) and THF (30 mL). The mixture was stirred at rt overnight. Ethyl acetate was added and the organic layer was washed with water 3 times. The organic phase was dried over anhydrous Na₂SO₄. After removing the solvent by rotary evaporation, the residue was dissolved in hexanes and the byproduct (succinimide) was filtered through celite. The crude product was distilled under reduced pressure to afford **4** as a colorless oil (11.78 g, 89% yield). ¹H NMR (CDCl₃, 300 MHz) δ 6.77 (s, 1H), 2.15 (s, 3H). ¹³C NMR (CDCl₃, 75 MHz) δ 138.06, 131.87, 110.13, 108.37, 15.18.

2,5-dibromo-3-(bromomethyl) thiophen (6): benzoyl peroxide (0.002 g, 0.01 mmol) and compound 4 (11.78 g, 46 mmol, 1eq) were added to 5 mL of CCl₄. After heating to reflux, a mixture of NBS (9.8 g, 55 mmol, 1.2eq) and benzoyl peroxide (0.11 g, 0.45 mmol) were slowly added. After refluxing for 1h, the solution was cooled and distilled in vacuo. Ethyl acetate was added and the organic layer was washed

with water 3 times. The organic phase was dried over anhydrous Na₂SO₄. After removing the solvent by rotary evaporation, the residue was dissolved in hexanes and the byproduct (succinimide) was filtered through celite. The crude product was distilled under reduced pressure to afford **6** as a colorless oil (11.78 g, 89% yield). ¹H NMR (CDCl₃, 300 MHz) δ 7.00 (s, 1H), 4.36 (s, 2H).

1-(2,5-dibromothiophen-3-yl)-2,5,8,11-tetraoxadodecane (M2): Triethyleneglycol monomethyl ether (4.71 g, 28 mmol, 1.5 eq) was dropped to a stirred solution of NaH (0.87 g, 36 mmol, 1.9eq) in THF (60 mL) at room temperature with a stream of argon. The reaction mixture was stirred for 1 h, and then a solution of compound **6** (6.4 g, 19 mmol) was added to the mixture. The reaction was continued for overnight and quenched by the addition of water and then the reactant was extracted. Ethyl acetate was added and the organic layer was washed with water 3 times. The organic phase was dried over anhydrous Na₂SO₄. After removing the solvent by rotary evaporation, the residue was chromatographed on silica gel (ethyl acetate/ hexane = 1: 3) to afford **M2** as an orange-red oil (5.5 g, 69% yield). ¹H NMR (CDCl₃, 300 MHz) δ 7.00 (s, 1H), 4.43 (s, 2H), 3.67-3.61 (m, 12H), 3.38-3.36 (m, 3H). ¹³C NMR (CDCl₃, 75 MHz) δ 139.30, 130.90, 111.22, 109.92, 71.94, 70.67, 70.63, 70.57, 70.52, 69.62, 66.93, 59.06.

Compound **7** (mixture of isomers): M1 (0.39 g, 1.2 mmol) and THF (10 mL) were added to a dried three-neck flask under argon, and the mixture was stirred at 0 °C for 10 min. To the mixture was added ¹PrMgCl (2.0M solution in THF) via a syringe, and the mixture was stirred for 30 min from 0 °C to room temperature. Similar experimental procedures were also used to prepare compound **9**: M2 (1.50 g, 3.60 mmol).

Block copolymer: A suspension of Ni(dppp)Cl₂ (7.5 mg, 0.012 mmol, 1%) in dry THF (2.0 mL) was added to the mixture (Compound **7**) via a syringe. The polymerization continued for 15 min at room temperature, and then a solution of compound **9** in dry THF (5 mL) was added to the mixture. The polymerization of the second monomer was continued for 4 h at room temperature and quenched by addition of HCl solution. Then, the polymer solution was poured into a mixture solution of methanol (200 mL) and water (50 mL), and the residue was filtered and purified via a sequential Soxhlet washing with methanol and hexane. The chloroform's fraction was then collected. Chloroform was removed by evaporation under reduced pressure, and the polymer was dried overnight under reduced pressure to afford P3HT-*b*-P3TEGT as a purple solid (0.145 g, 28% yield).

Random copolymer: A suspension of Ni(dppp)Cl₂ (15 mg, 0.025 mmol, 1.5%) in dry THF (3.0 mL) was added to the mixture of compound **7** (0.15 g of M1) and compound **9** (0.58 g of M2) via a syringe. The polymerization continued for 4h at room temperature, and then quenched by addition of HCl solution. Then, the polymer solution was poured into a mixture solution of methanol (200 mL) and water (50 mL), and the residue was filtered and purified via a sequential Soxhlet washing with methanol and hexane.

The chloroform's fraction was then collected. Chloroform was removed by evaporation under reduced pressure, and the polymer was dried overnight under reduced pressure to afford P3HT-*r*-P3TEGT as a purple solid (0.12 g, 28% yield).

Reference

- (1) Schiavone, G.; Fallegger, F.; Kang, X.; Barra, B.; Vachicouras, N.; Roussinova, E.; Furfaro, I.; Jiguet, S.; Seáñez, I.; Borgognon, S. Soft, implantable bioelectronic interfaces for translational research. *Advanced Materials* **2020**, *32* (17), 1906512, DOI: 10.1002/adma.201906512.
- (2) Fang, Y.; Meng, L.; Prominski, A.; Schaumann, E. N.; Seebald, M.; Tian, B. Recent advances in bioelectronics chemistry. *Chemical Society Reviews* **2020**, *49* (22), 7978-8035, DOI: 10.1039/D0CS00333F.
- (3) Yang, S. Y.; Kim, B. N.; Zakhidov, A. A.; Taylor, P. G.; Lee, J. K.; Ober, C. K.; Lindau, M.; Malliaras, G. G. Detection of transmitter release from single living cells using conducting polymer microelectrodes. *Advanced Materials* **2011**, *23* (24), H184-H188, DOI: 10.1002/adma.201100035.
- (4) Ferro, M. D.; Melosh, N. A. Electronic and ionic materials for neurointerfaces. *Advanced Functional Materials* **2018**, *28* (12), 1704335, DOI: 10.1002/adfm.201704335.
- (5) Lu, C.-H.; Hsiao, Y.-S.; Kuo, C.-W.; Chen, P. Electrically tunable organic bioelectronics for spatial and temporal manipulation of neuron-like pheochromocytoma (PC-12) cells. *Biochimica et Biophysica Acta (BBA)-General Subjects* **2013**, *1830* (9), 4321-4328, DOI: 10.1016/j.bbagen.2012.08.028.
- (6) Hsiao, Y. S.; Kuo, C. W.; Chen, P. Multifunctional graphene–PEDOT microelectrodes for on-chip manipulation of human mesenchymal stem cells. *Advanced Functional Materials* **2013**, *23* (37), 4649-4656, DOI: 10.1002/adfm.201203631.
- (7) Zeglio, E.; Rutz, A. L.; Winkler, T. E.; Malliaras, G. G.; Herland, A. Conjugated polymers for assessing and controlling biological functions. *Advanced Materials* **2019**, *31* (22), 1806712, DOI: 10.1002/adma.201806712.
- (8) Jiang, Y.; Tian, B. Inorganic semiconductor biointerfaces. *Nature Reviews Materials* **2018**, *3* (12), 473-490, DOI: 10.1038/s41578-018-0062-3.
- (9) Someya, T.; Bao, Z.; Malliaras, G. G. The rise of plastic bioelectronics. *Nature* **2016**, *540* (7633), 379-385, DOI: 10.1038/nature21004.
- (10) Snyder, P. J.; Reddy, P.; Kirste, R.; Collazo, R.; Ivanisevic, A. Bulk and Surface Electronic Properties of Inorganic Materials: Tools to Guide Cellular Behavior. *Small Methods* **2018**, *2* (9), 1800016, DOI: 10.1002/smtd.201800016.
- (11) Wang, L.; Chen, D.; Jiang, K.; Shen, G. New insights and perspectives into biological materials for flexible electronics. *Chemical Society Reviews* **2017**, *46* (22), 6764-6815, DOI: 10.1039/C7CS00278E.
- (12) Gao, D.; Parida, K.; Lee, P. S. Emerging Soft Conductors for Bioelectronic Interfaces. *Advanced Functional Materials* **2020**, *30* (29), 1907184, DOI: 10.1002/adfm.201907184.
- (13) Wang, N.; Yang, A.; Fu, Y.; Li, Y.; Yan, F. Functionalized organic thin film transistors for biosensing. *Accounts of chemical research* **2019**, *52* (2), 277-287, DOI: 10.1021/acs.accounts.8b00448.

- (14) Inal, S.; Rivnay, J.; Suiiu, A.-O.; Malliaras, G. G.; McCulloch, I. Conjugated polymers in bioelectronics. *Accounts of chemical research* **2018**, *51* (6), 1368-1376, DOI: 10.1021/acs.accounts.7b00624.
- (15) Jia, M.; Rolandi, M. Soft and Ion-Conducting Materials in Bioelectronics: From Conducting Polymers to Hydrogels. *Advanced healthcare materials* **2020**, *9* (5), 1901372, DOI: 10.1002/adhm.201901372.
- (16) Berggren, M.; Crispin, X.; Fabiano, S.; Jonsson, M. P.; Simon, D. T.; Stavriniidou, E.; Tybrandt, K.; Zozoulenko, I. Organic Electrochemical Devices: Ion Electron–Coupled Functionality in Materials and Devices Based on Conjugated Polymers (Adv. Mater. 22/2019). *Advanced Materials* **2019**, *31* (22), 1970160, DOI: 10.1002/adma.201970160.
- (17) Fidanovski, K.; Mawad, D. Conjugated polymers in bioelectronics: addressing the interface challenge. *Advanced healthcare materials* **2019**, *8* (10), 1900053, DOI: 10.1002/adhm.201900053.
- (18) Strakosas, X.; Wei, B.; Martin, D. C.; Owens, R. M. Biofunctionalization of polydioxithiophene derivatives for biomedical applications. *Journal of Materials Chemistry B* **2016**, *4* (29), 4952-4968, DOI: 10.1039/C6TB00852F
- (19) Paulsen, B. D.; Tybrandt, K.; Stavriniidou, E.; Rivnay, J. Organic mixed ionic–electronic conductors. *Nature materials* **2020**, *19* (1), 13-26, DOI: 10.1038/s41563-019-0435-z.
- (20) Reeja-Jayan, B.; Kovacic, P.; Yang, R.; Sojoudi, H.; Ugur, A.; Kim, D. H.; Petruczok, C. D.; Wang, X.; Liu, A.; Gleason, K. K. A route towards sustainability through engineered polymeric interfaces. *Advanced Materials Interfaces* **2014**, *1* (4), 1400117, DOI: 10.1002/admi.201400117.
- (21) Malti, A.; Edberg, J.; Granberg, H.; Khan, Z. U.; Andreasen, J. W.; Liu, X.; Zhao, D.; Zhang, H.; Yao, Y.; Brill, J. W. An organic mixed ion–electron conductor for power electronics. *Advanced science* **2016**, *3* (2), 1500305, DOI: 10.1002/advs.201500305.
- (22) Savva, A.; Hallani, R.; Cendra, C.; Surgailis, J.; Hidalgo, T. C.; Wustoni, S.; Sheelamantula, R.; Chen, X.; Kirkus, M.; Giovannitti, A. Balancing Ionic and Electronic Conduction for High-Performance Organic Electrochemical Transistors. *Advanced Functional Materials* **2020**, *30* (11), 1907657, DOI: 10.1002/adfm.201907657.
- (23) Rivnay, J.; Inal, S.; Collins, B. A.; Sessolo, M.; Stavriniidou, E.; Strakosas, X.; Tassone, C.; Delongchamp, D. M.; Malliaras, G. G. Structural control of mixed ionic and electronic transport in conducting polymers. *Nature communications* **2016**, *7* (1), 1-9, DOI: 10.1038/ncomms11287.
- (24) Sreeram, A.; Krishnan, S.; DeLuca, S. J.; Abidnejad, A.; Turk, M. C.; Roy, D.; Honarvarfard, E.; Goulet, P. J. Simultaneous electronic and ionic conduction in ionic liquid imbedded polyacetylene-like conjugated polymer films. *RSC advances* **2015**, *5* (107), 88425-88435, DOI: 10.1039/C5RA14360H.
- (25) Meng, B.; Liu, J.; Wang, L. Oligo (ethylene glycol) as side chains of conjugated polymers for optoelectronic applications. *Polymer Chemistry* **2020**, *11* (7), 1261-1270, DOI: 10.1039/C9PY01469A.
- (26) Bertok, T.; Lorencova, L.; Chocholova, E.; Jane, E.; Vikartovska, A.; Kasak, P.; Tkac, J. Electrochemical impedance spectroscopy based biosensors: Mechanistic principles, analytical examples

and challenges towards commercialization for assays of protein cancer biomarkers. **2019**, DOI: 10.1002/celec.201800848.

(27) Tu, G.; Li, H.; Forster, M.; Heiderhoff, R.; Balk, L. J.; Sigel, R.; Scherf, U. Amphiphilic conjugated block copolymers: synthesis and solvent-selective photoluminescence quenching. *Small* **2007**, *3* (6), 1001-1006, DOI: 10.1002/sml.200600351.

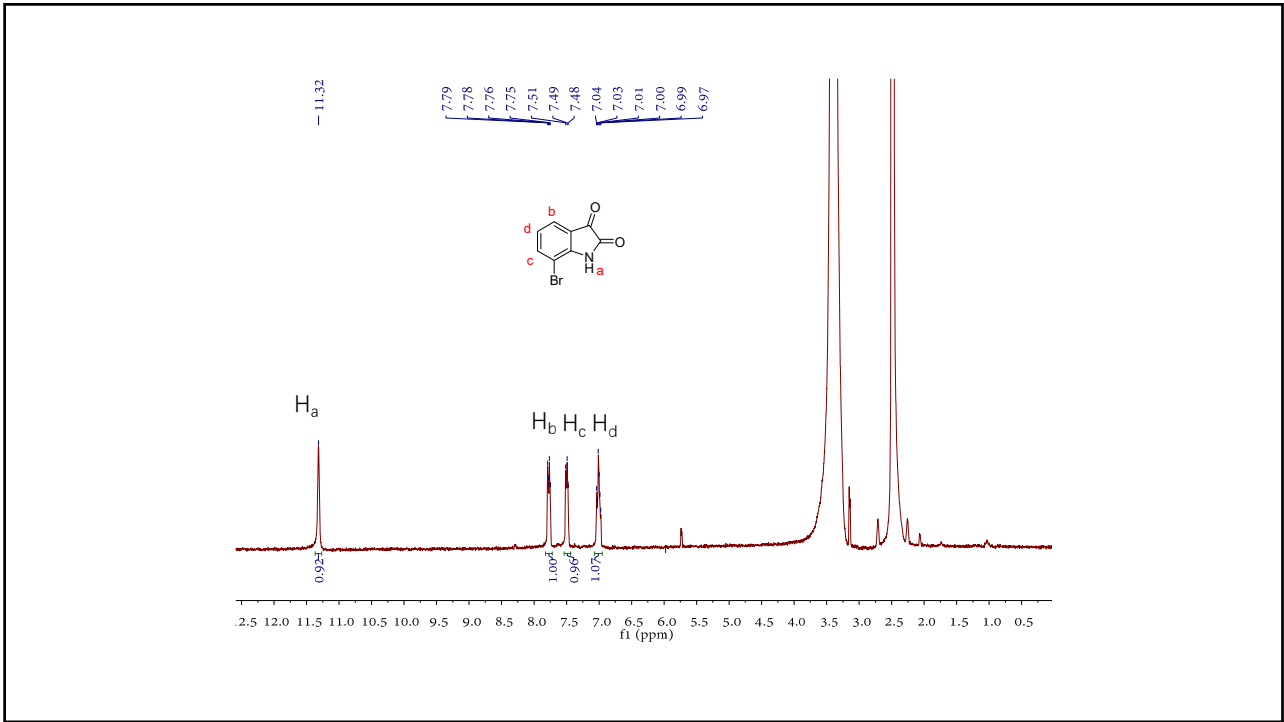
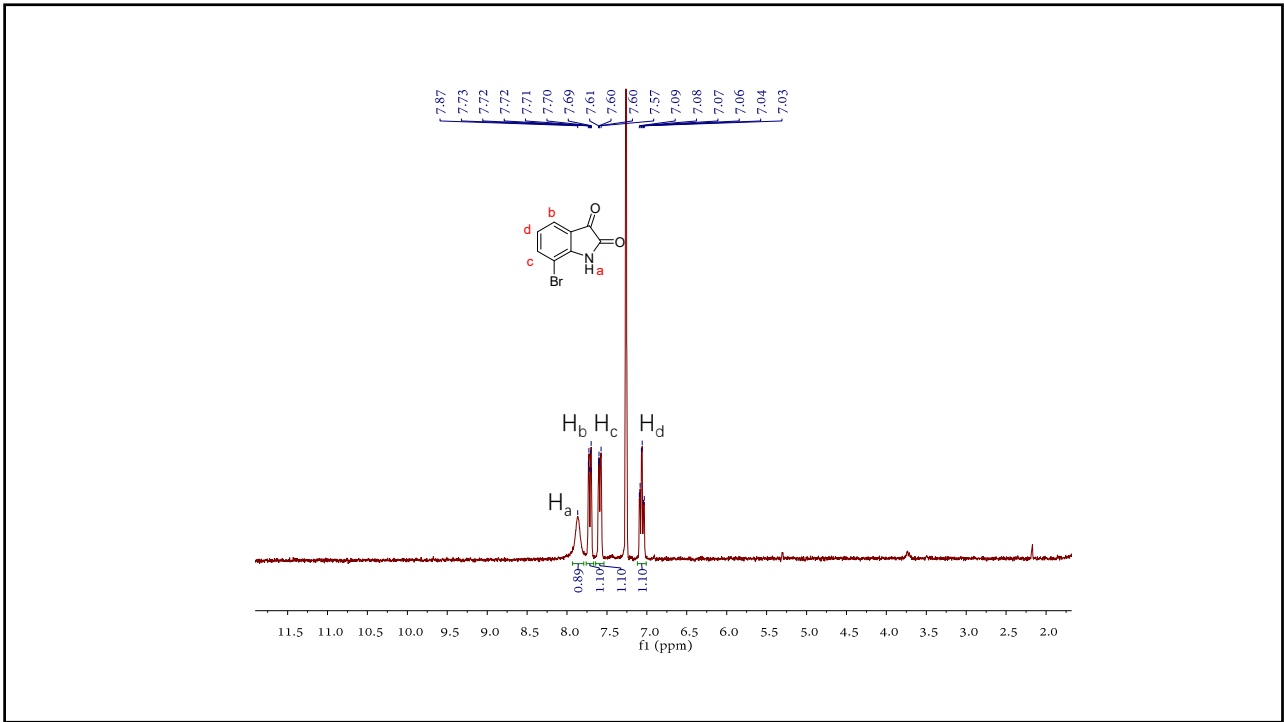
(28) Jiao, H.-F.; Wang, X.; Yao, K.; Chen, P.; Jia, Z.; Peng, Z.; Li, F. Self-assembly of all-conjugated block copolymer nanoparticles with tailoring size and fluorescence for live cell imaging. *Journal of Materials Chemistry B* **2016**, *4* (48), 7882-7887, DOI: 10.1039/C6TB02211A.

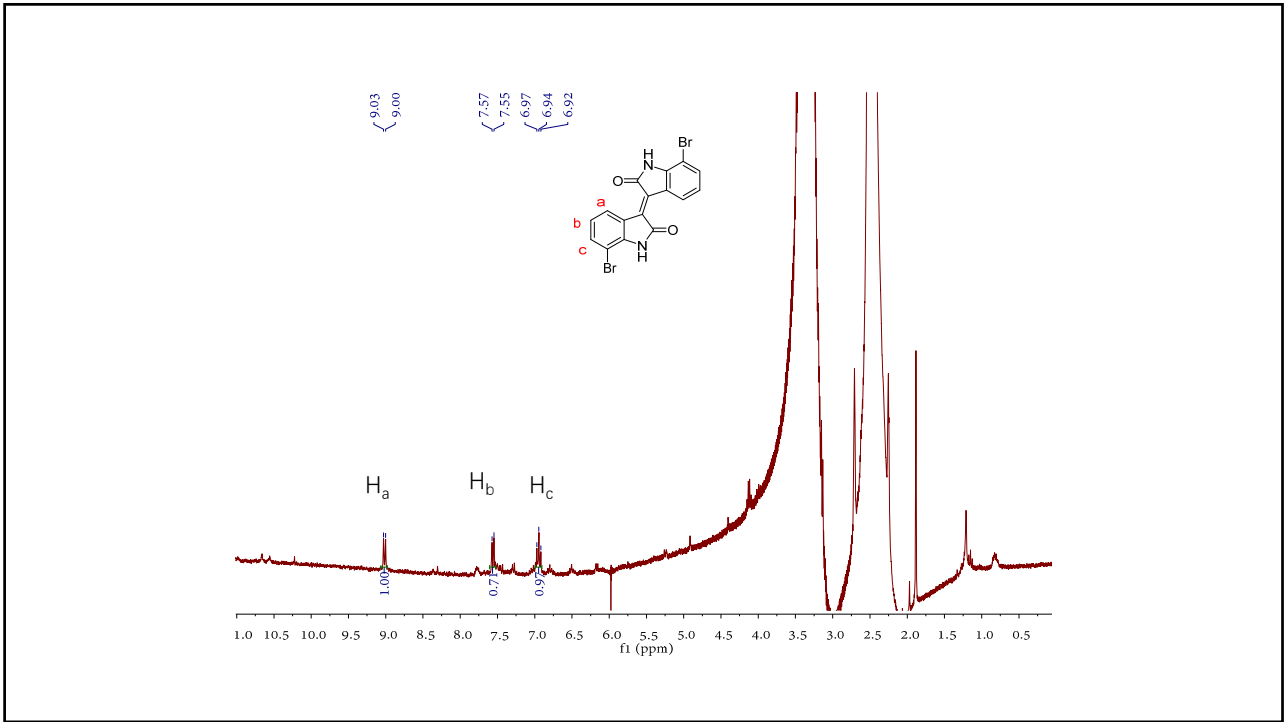
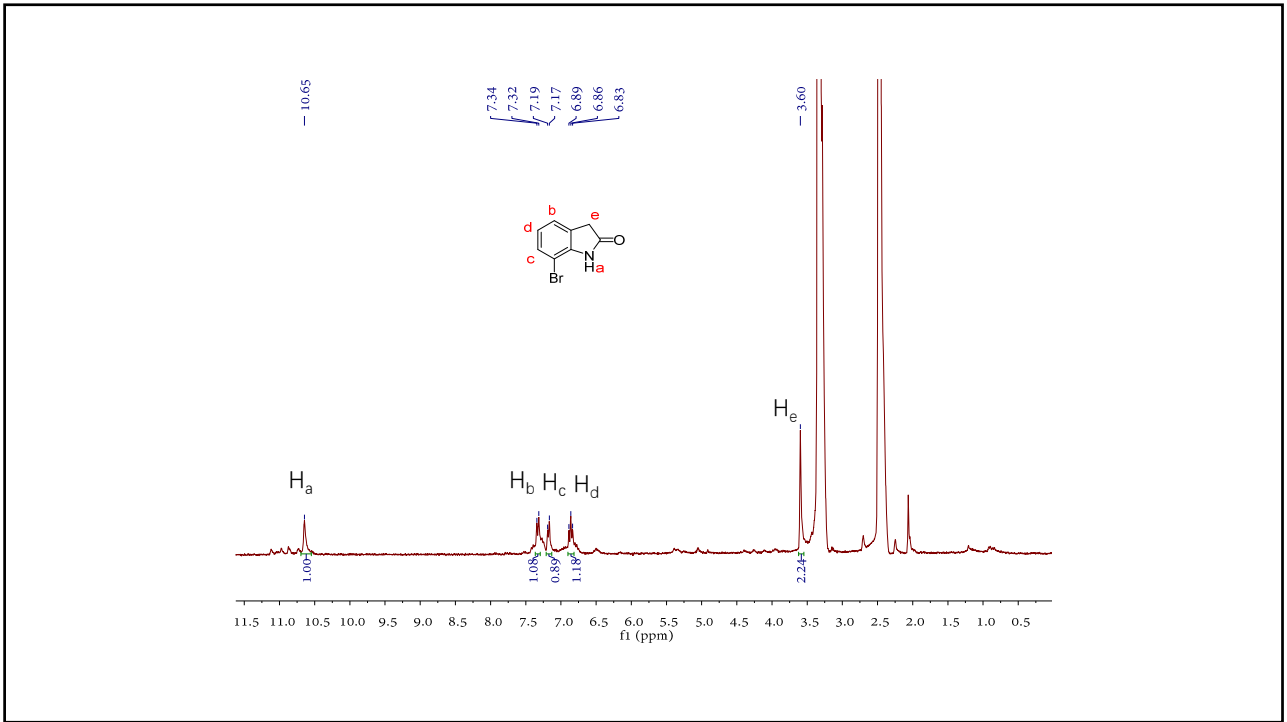
(29) Yu, Z.; Yan, H.; Lu, K.; Zhang, Y.; Wei, Z. Self-assembly of two-dimensional nanostructures of linear regioregular poly (3-hexylthiophene). *Rsc Advances* **2012**, *2* (1), 338-343, DOI: 10.1039/C1RA00833A.

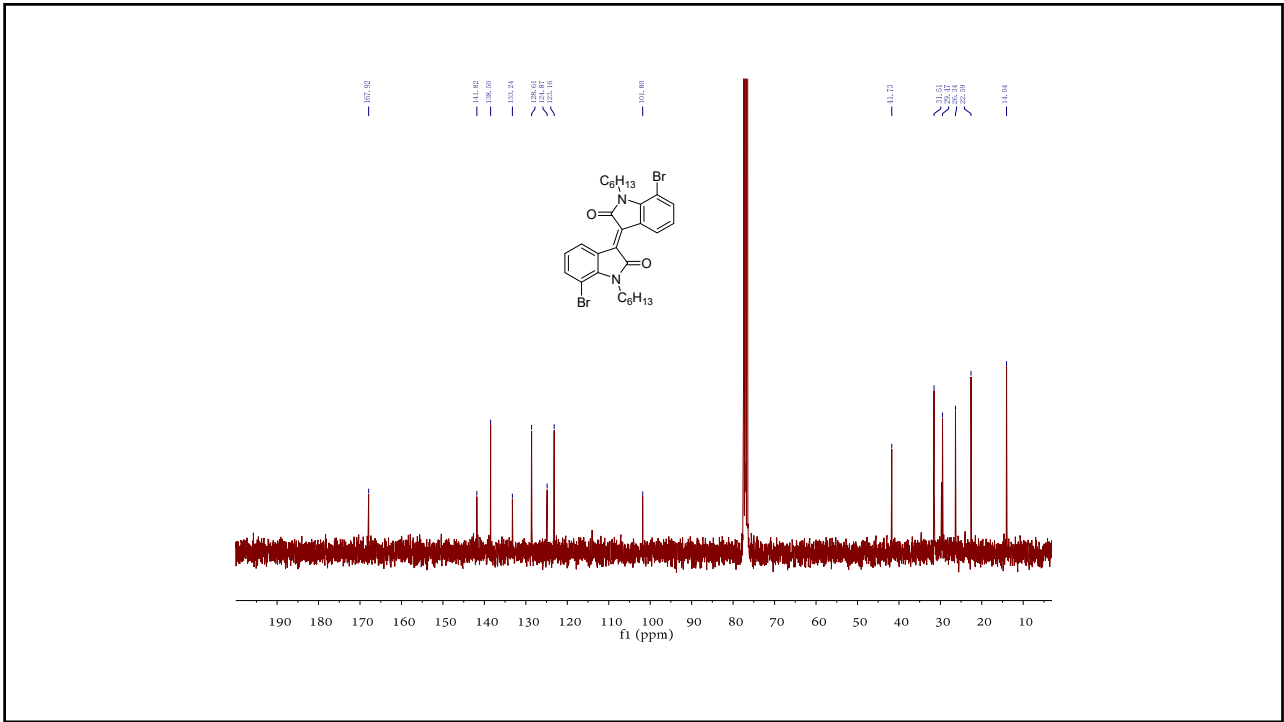
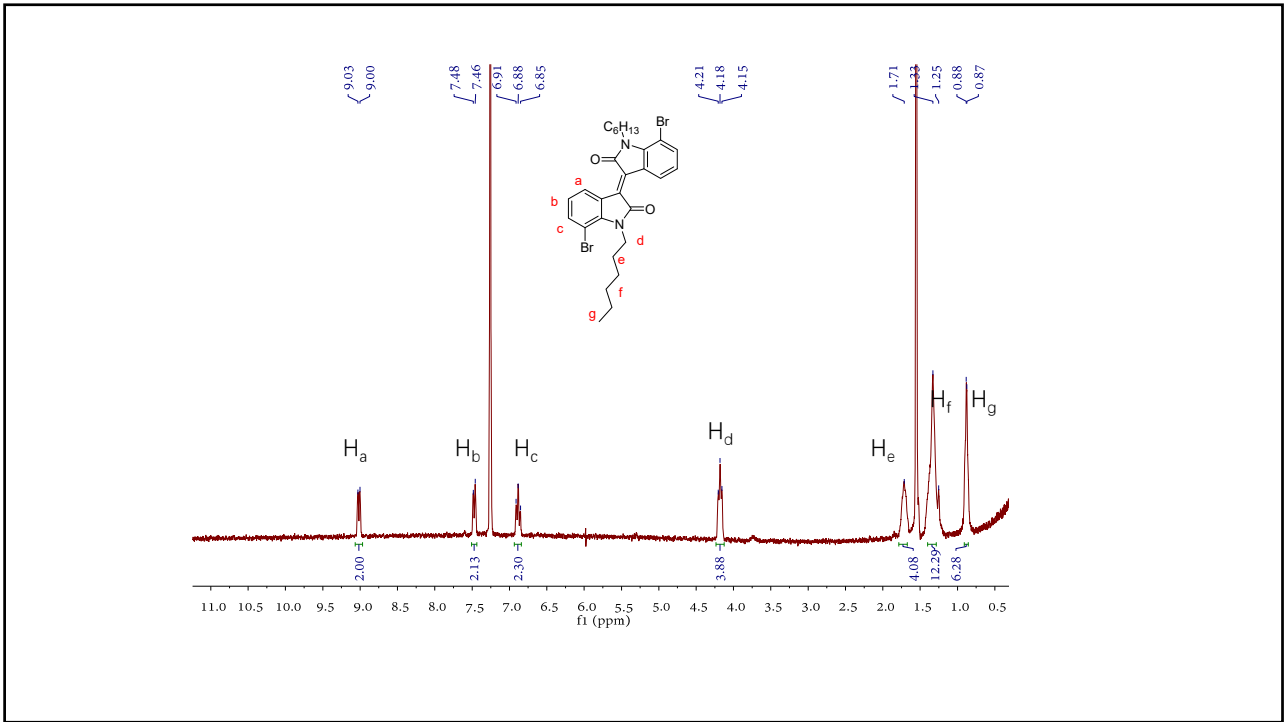
(30) Zhou, B.; Hu, X.; Zhu, J.; Wang, Z.; Wang, X.; Wang, M. Release properties of tannic acid from hydrogen bond driven antioxidative cellulose nanofibrous films. *International journal of biological macromolecules* **2016**, *91*, 68-74, DOI: 10.1016/j.ijbiomac.2016.05.084.

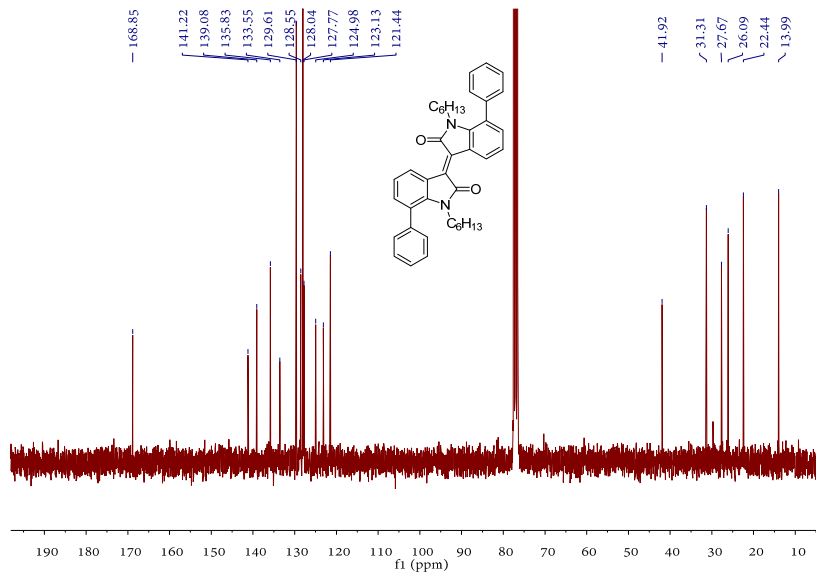
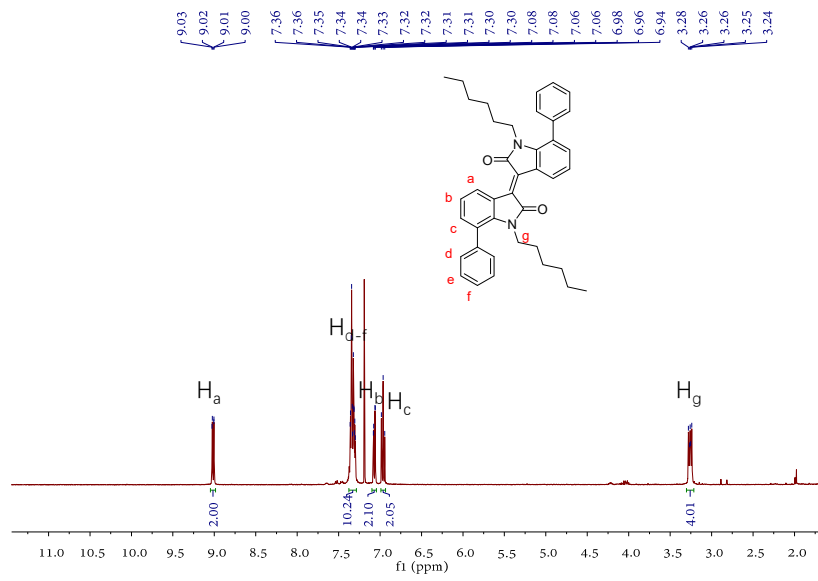
(31) Templier, V.; Roux, A.; Roupioz, Y.; Livache, T. Ligands for label-free detection of whole bacteria on biosensors: A review. *TrAC Trends in Analytical Chemistry* **2016**, *79*, 71-79, DOI: 10.1016/j.trac.2015.10.015.

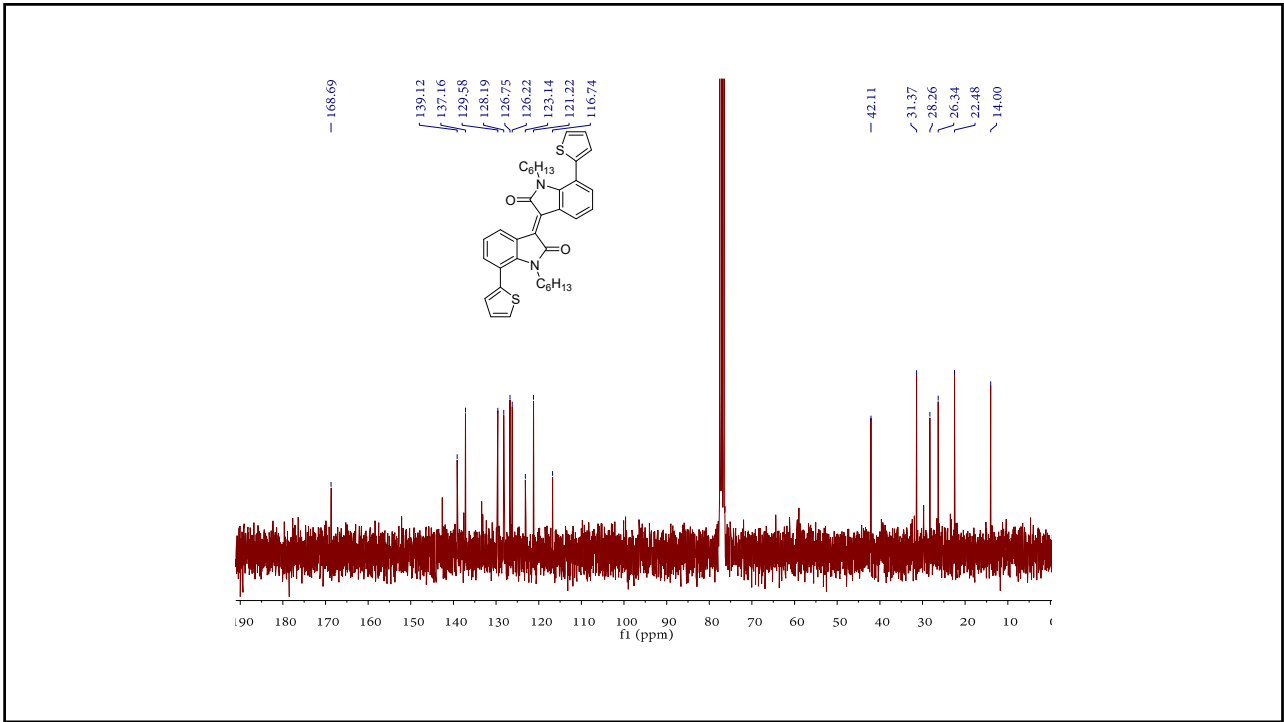
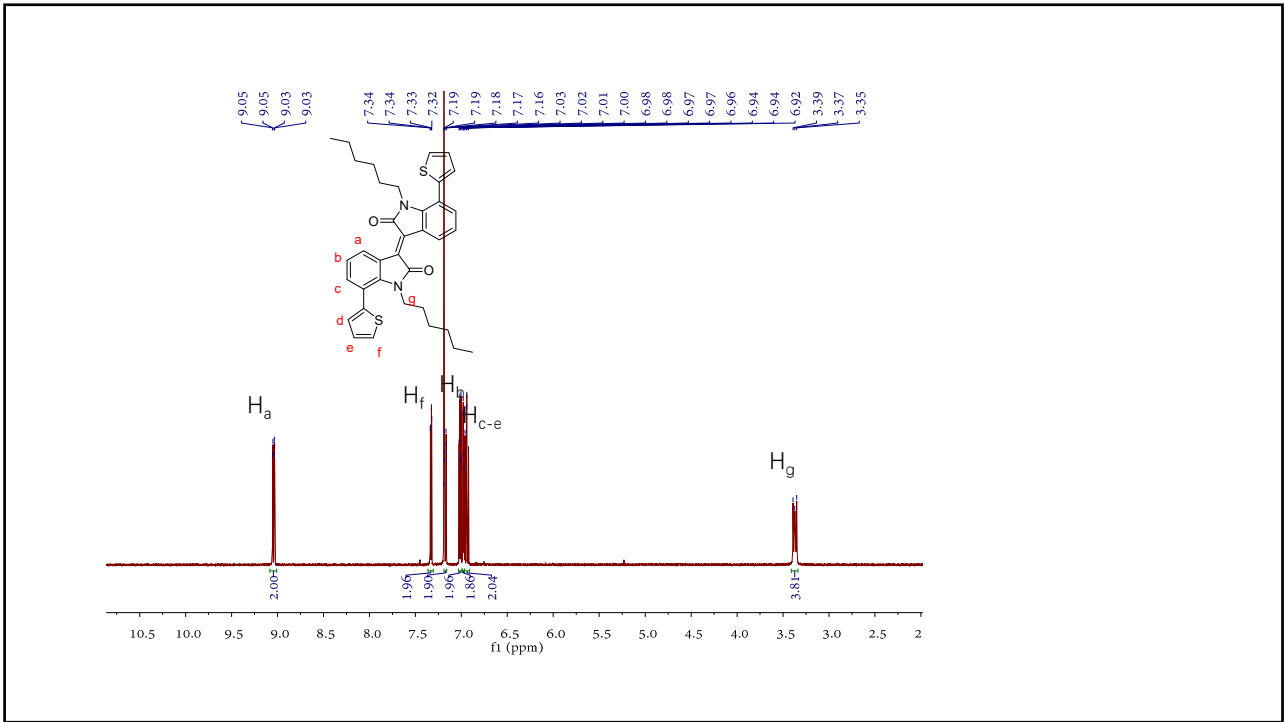
Chapter 2

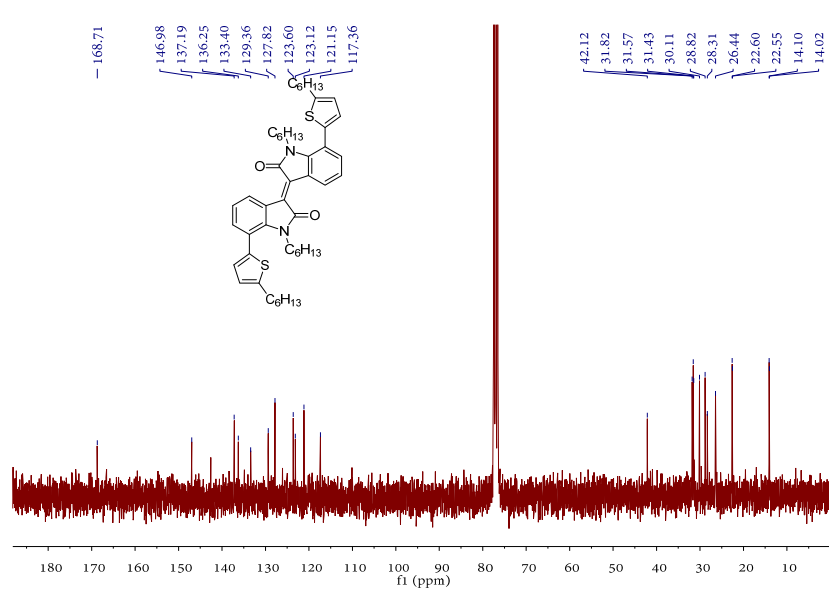
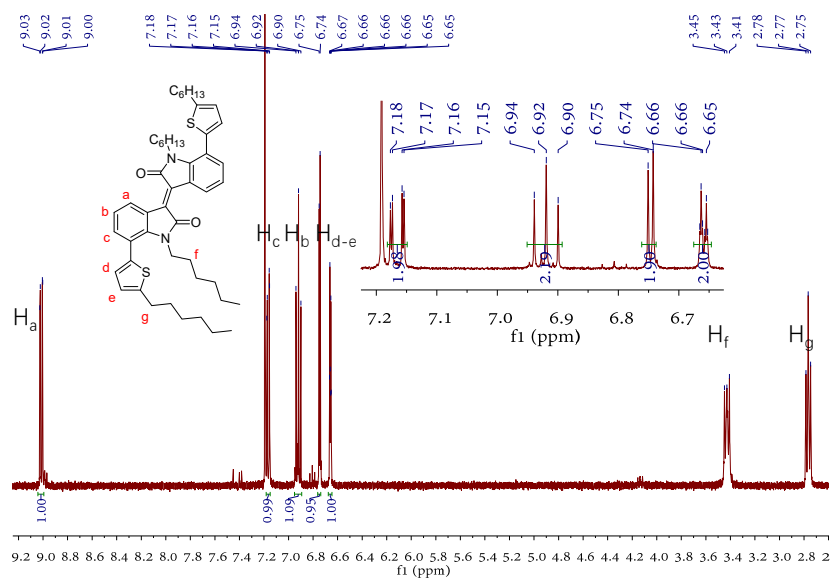


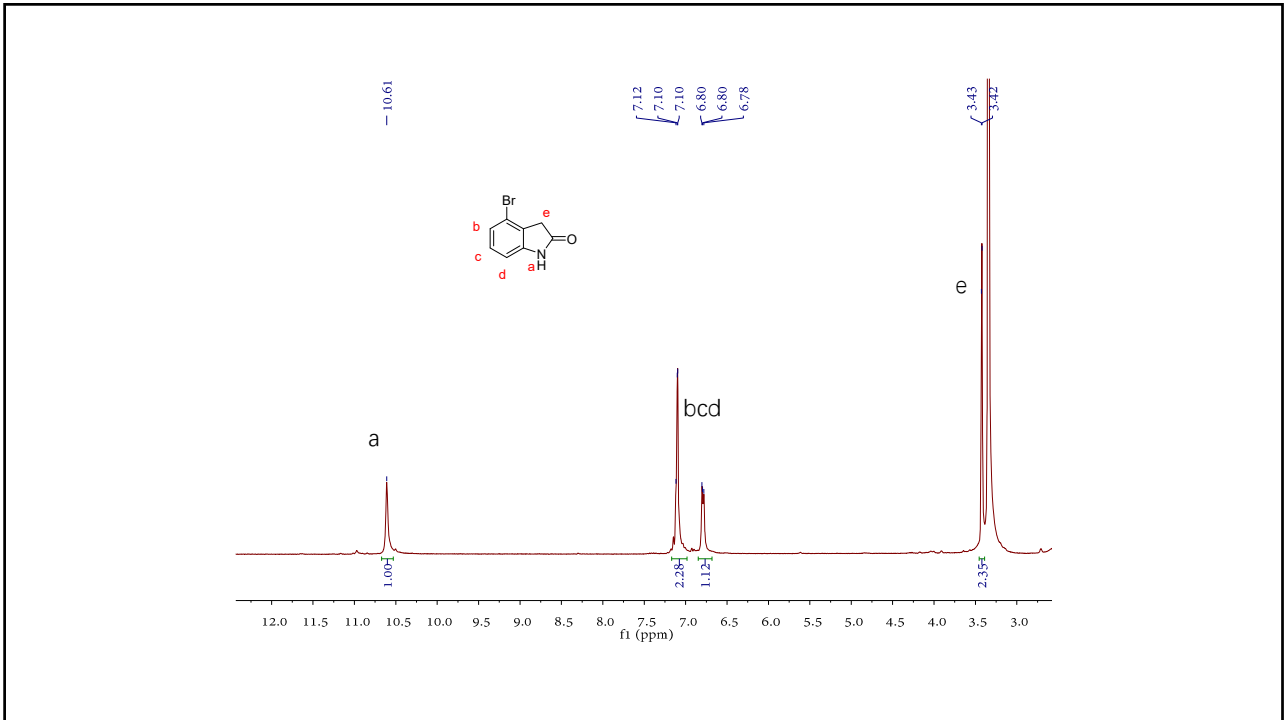
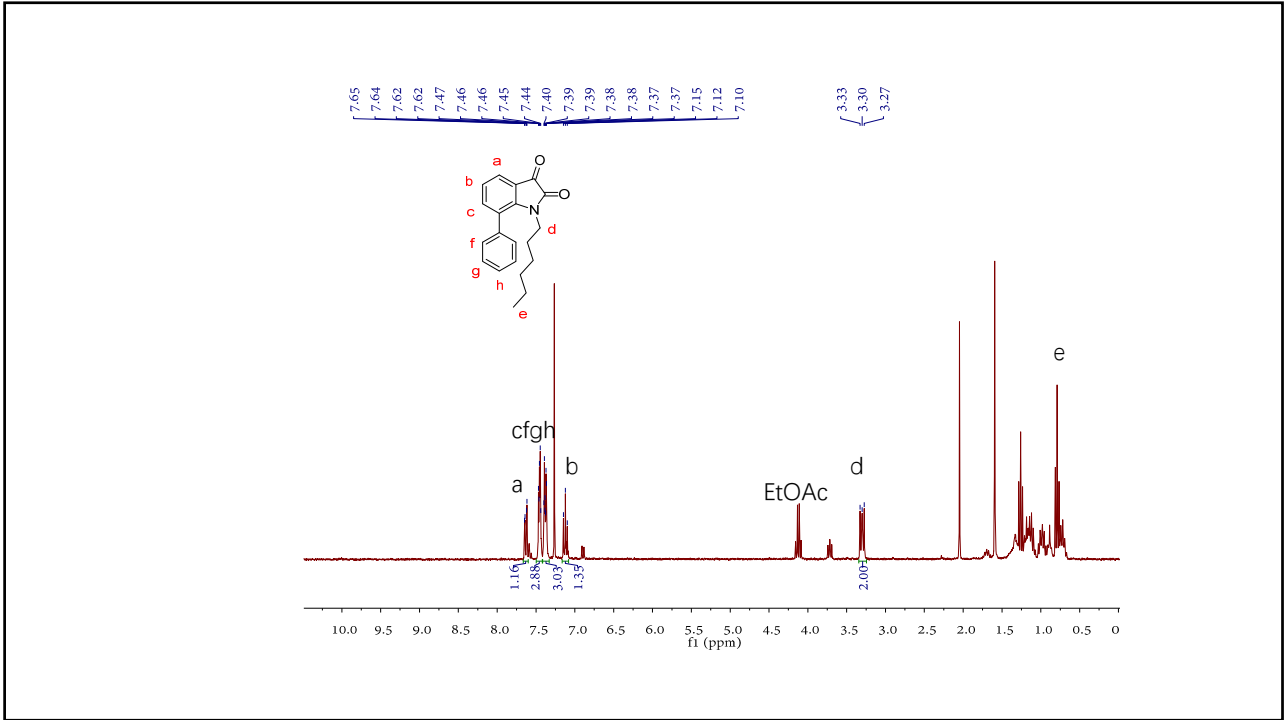


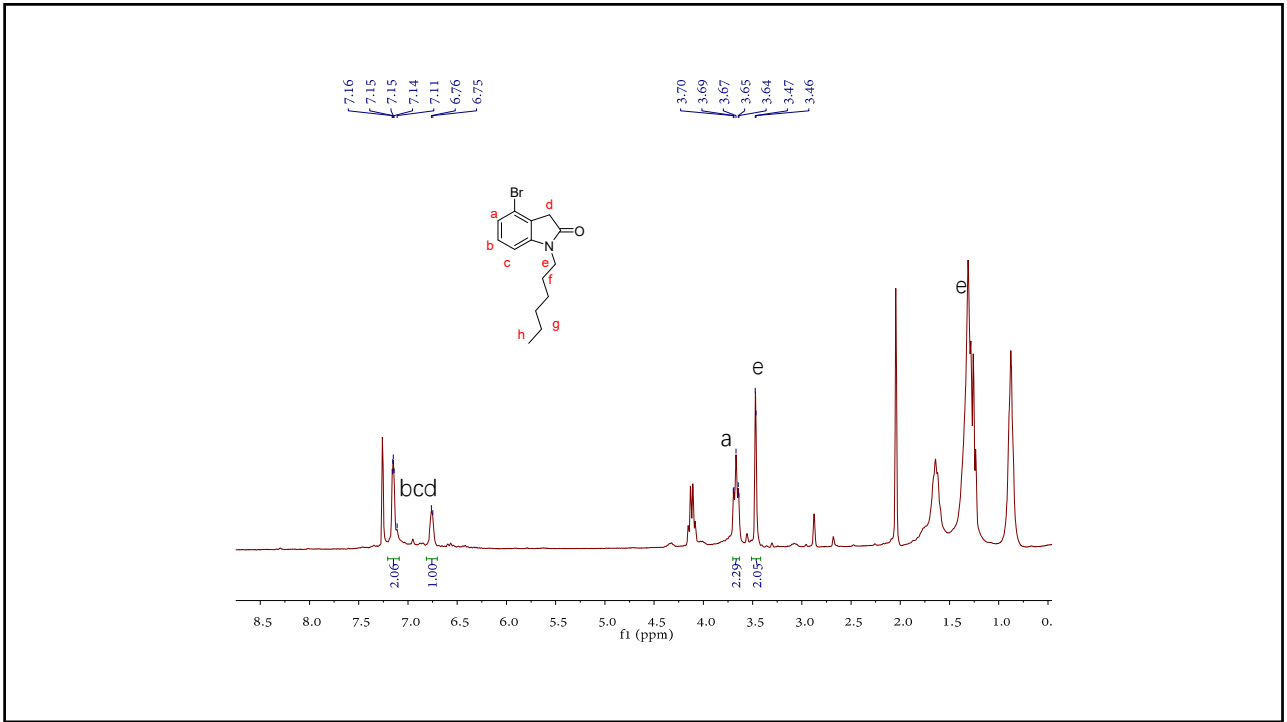
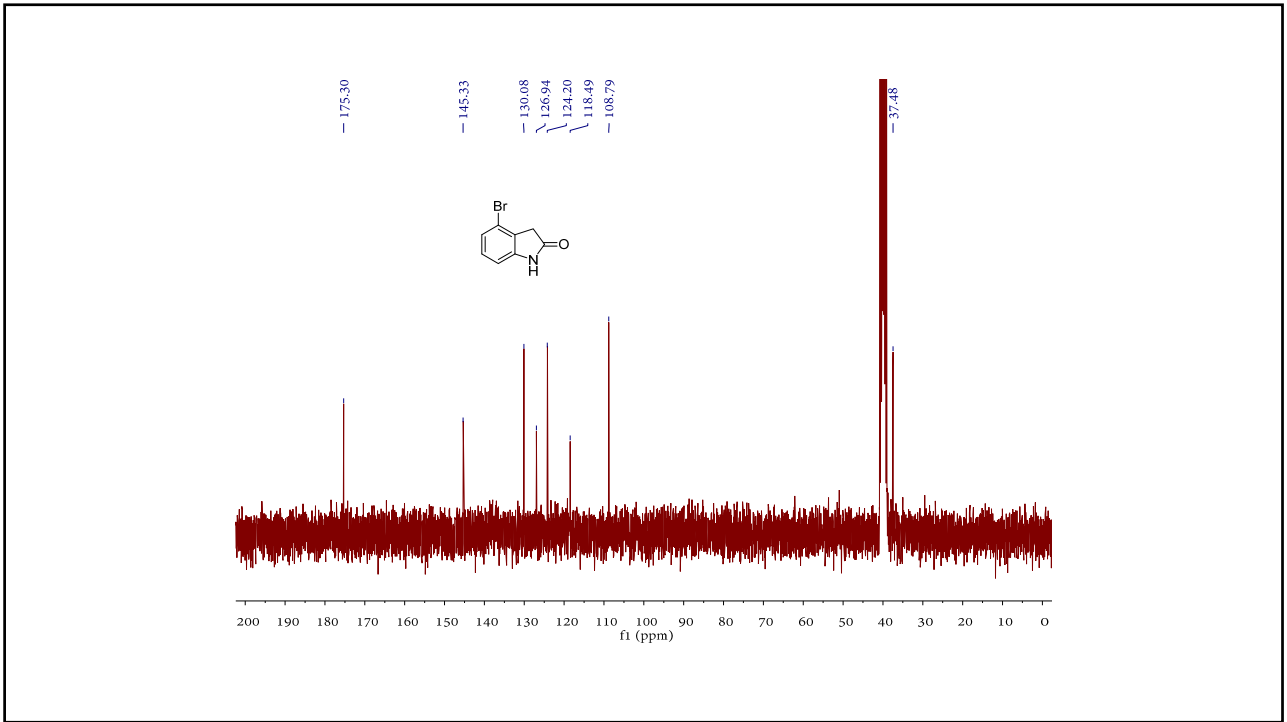


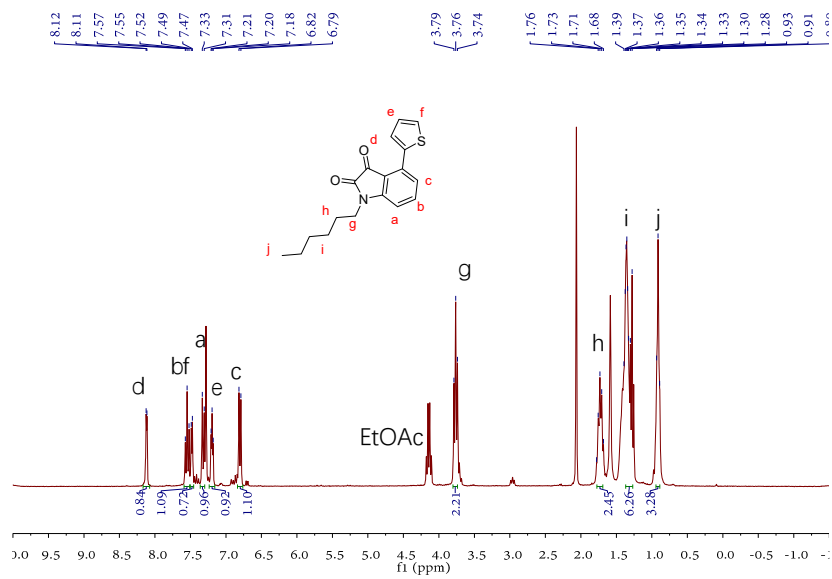
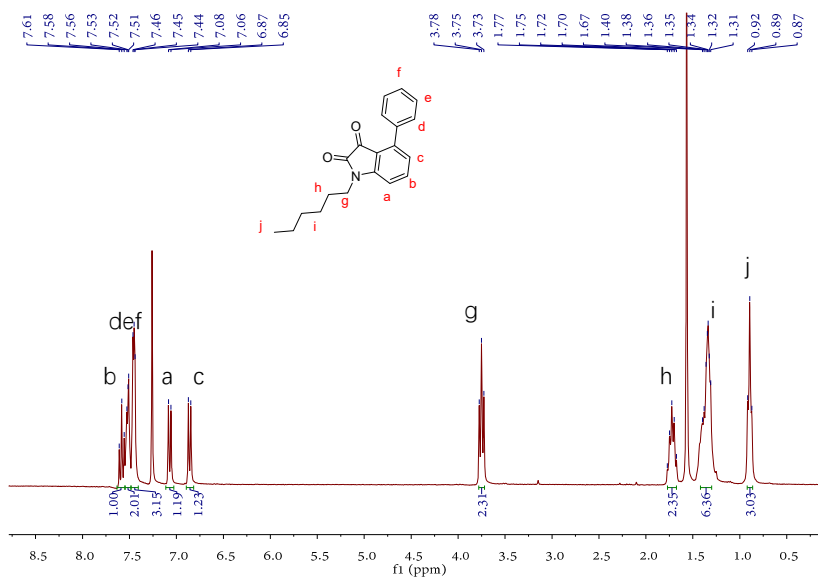


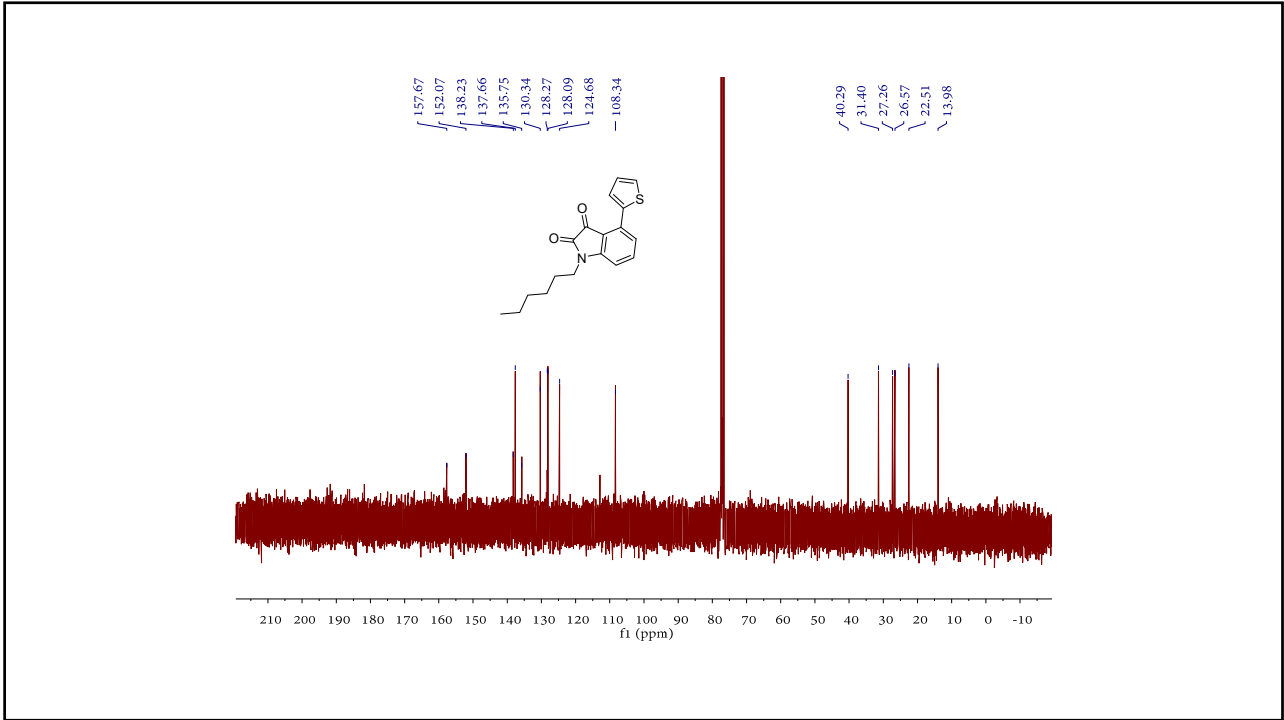




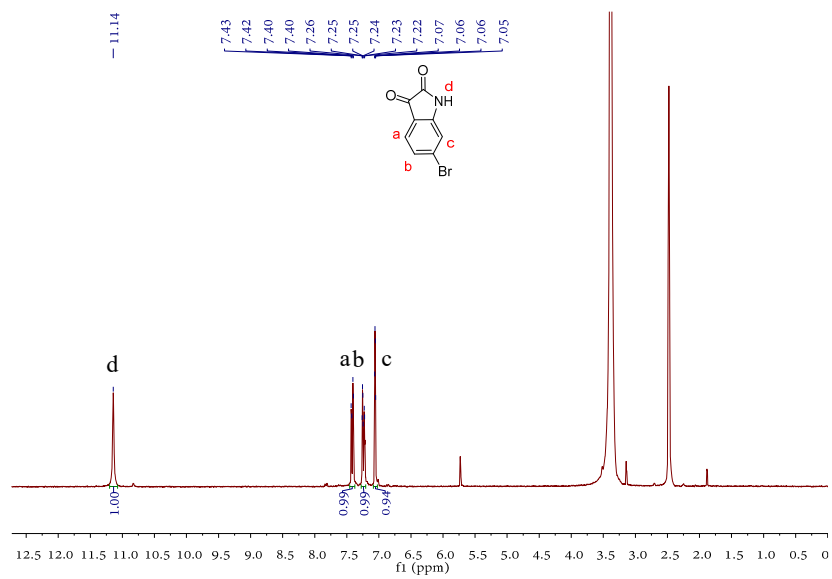
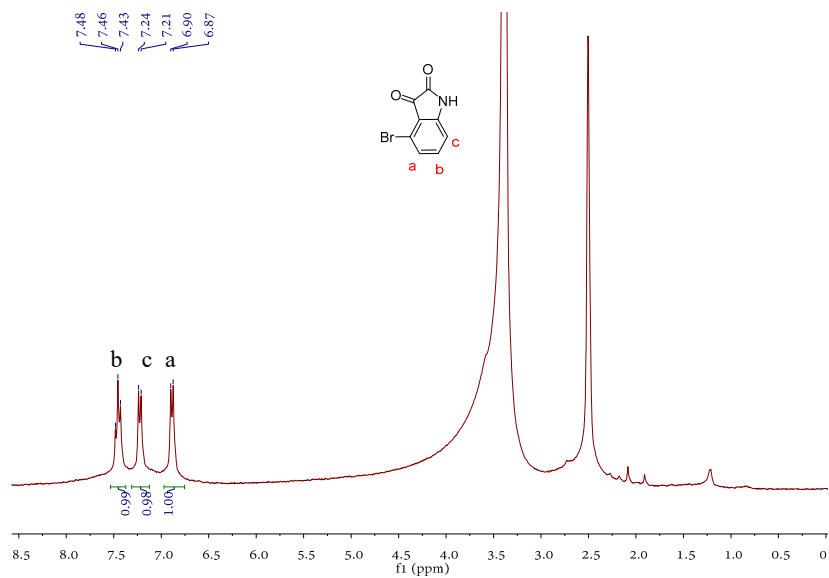


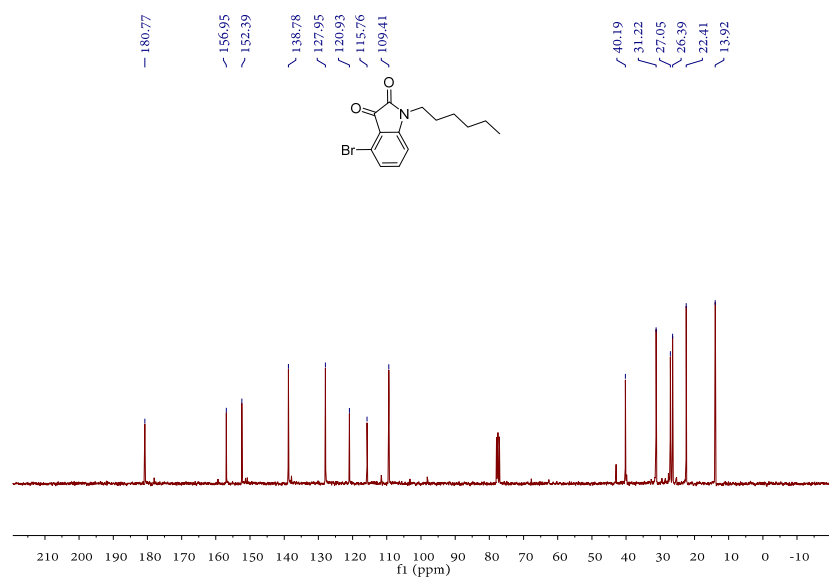
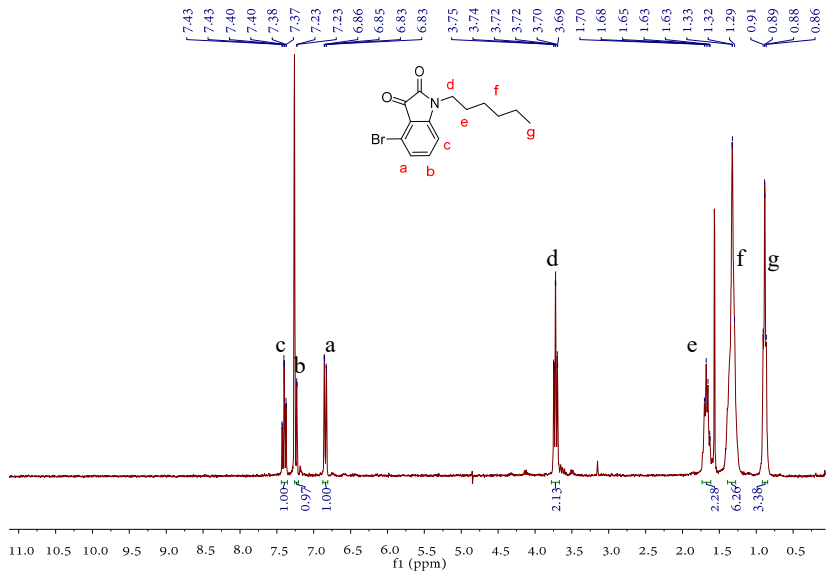


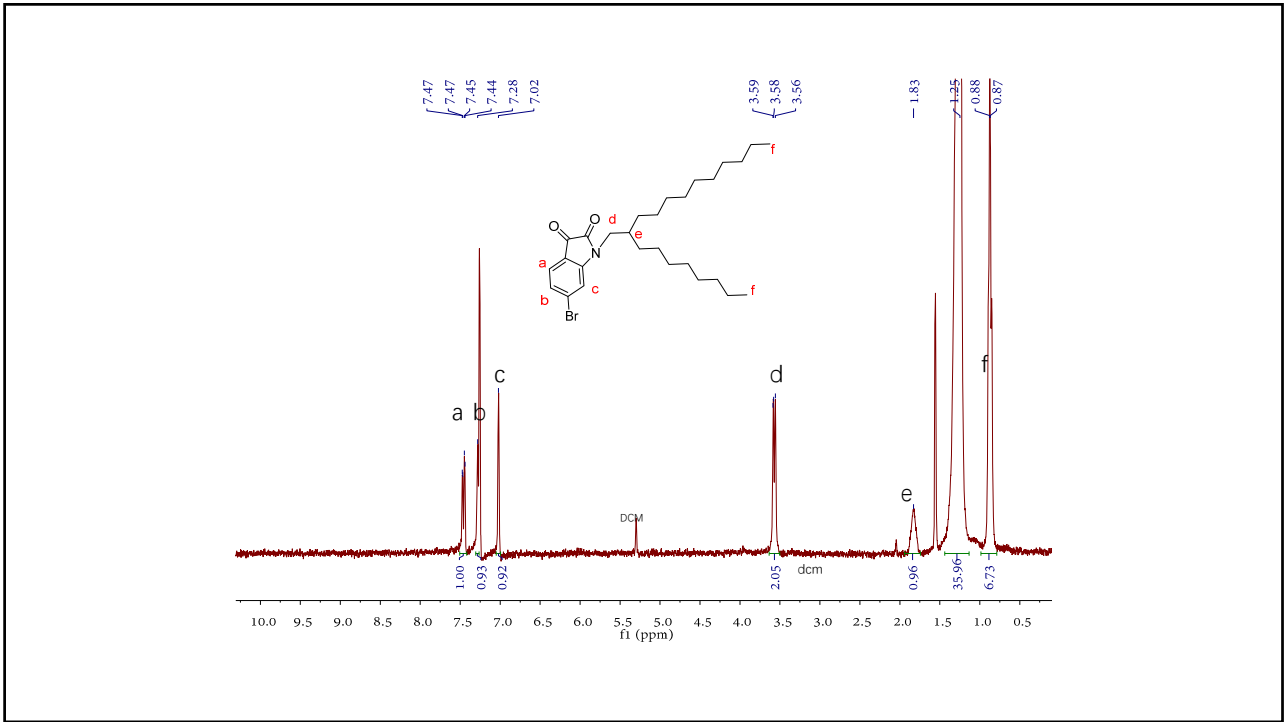
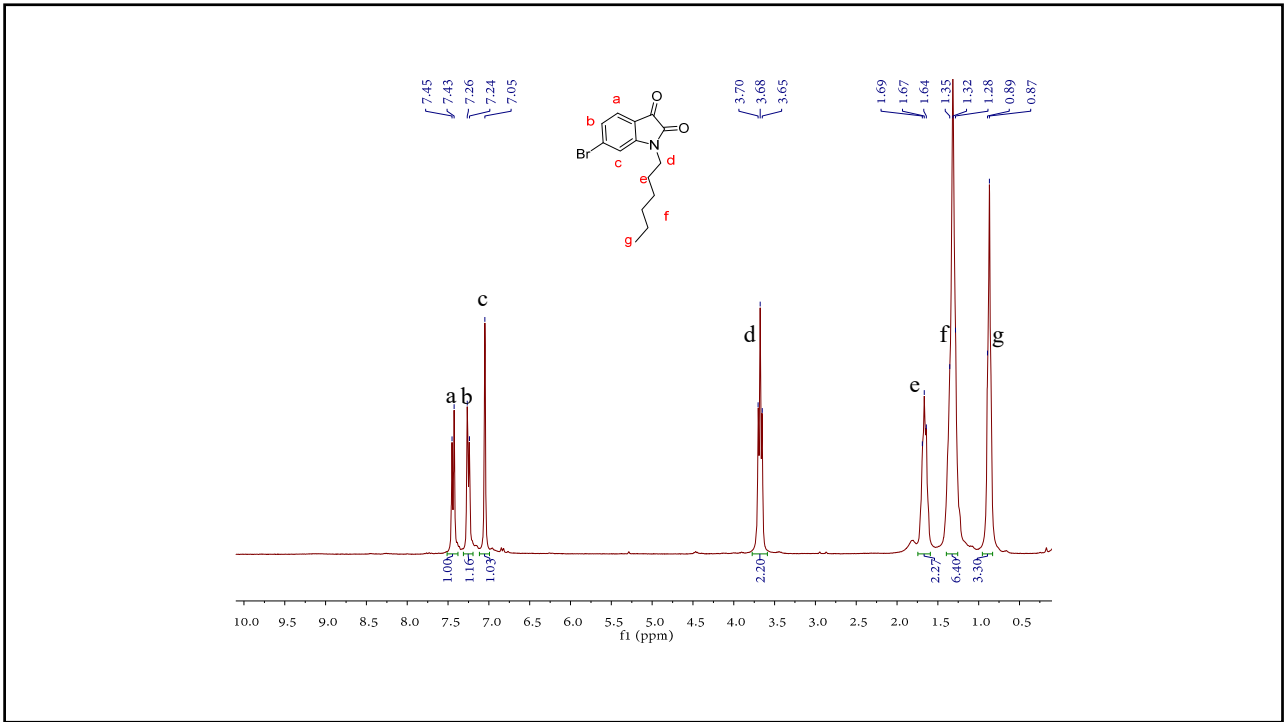


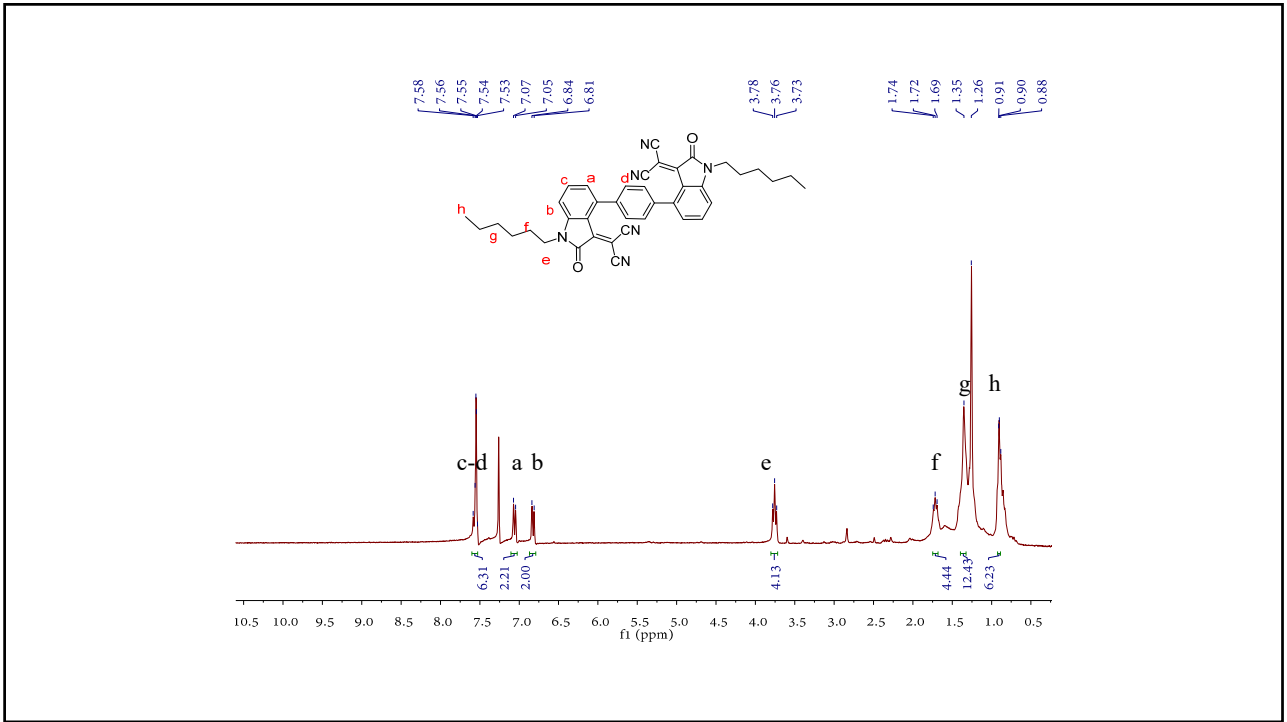
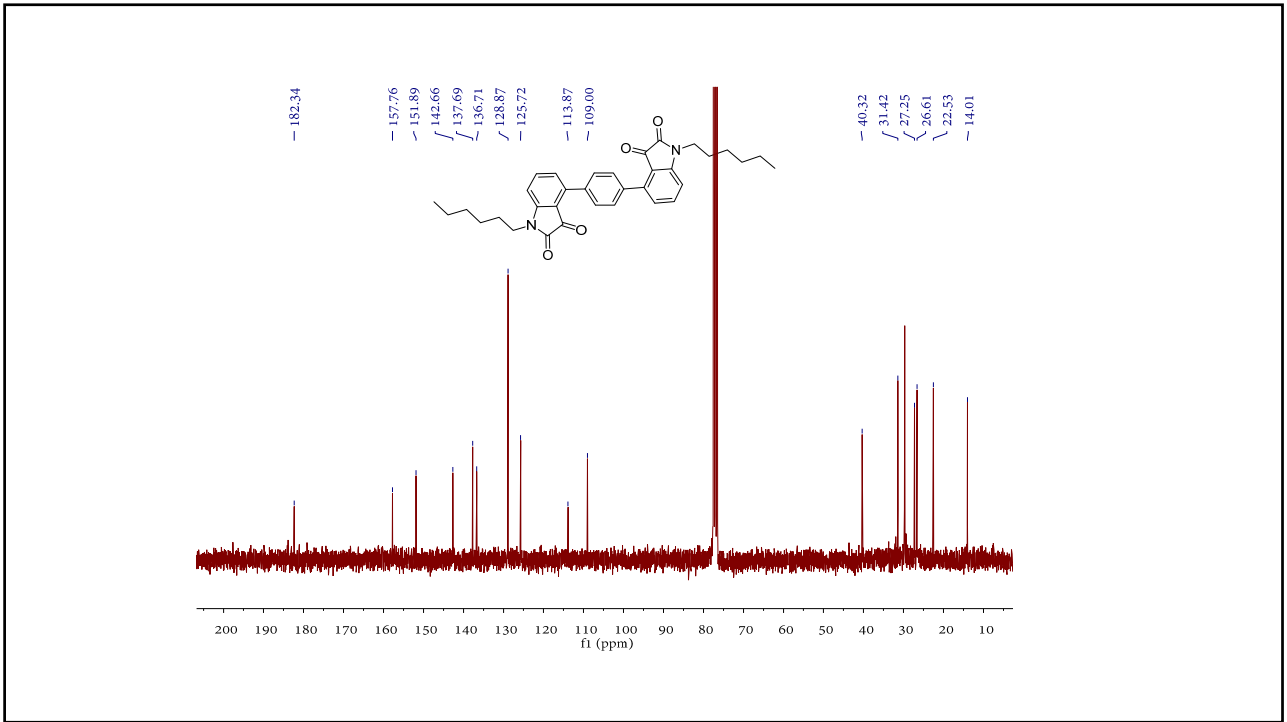


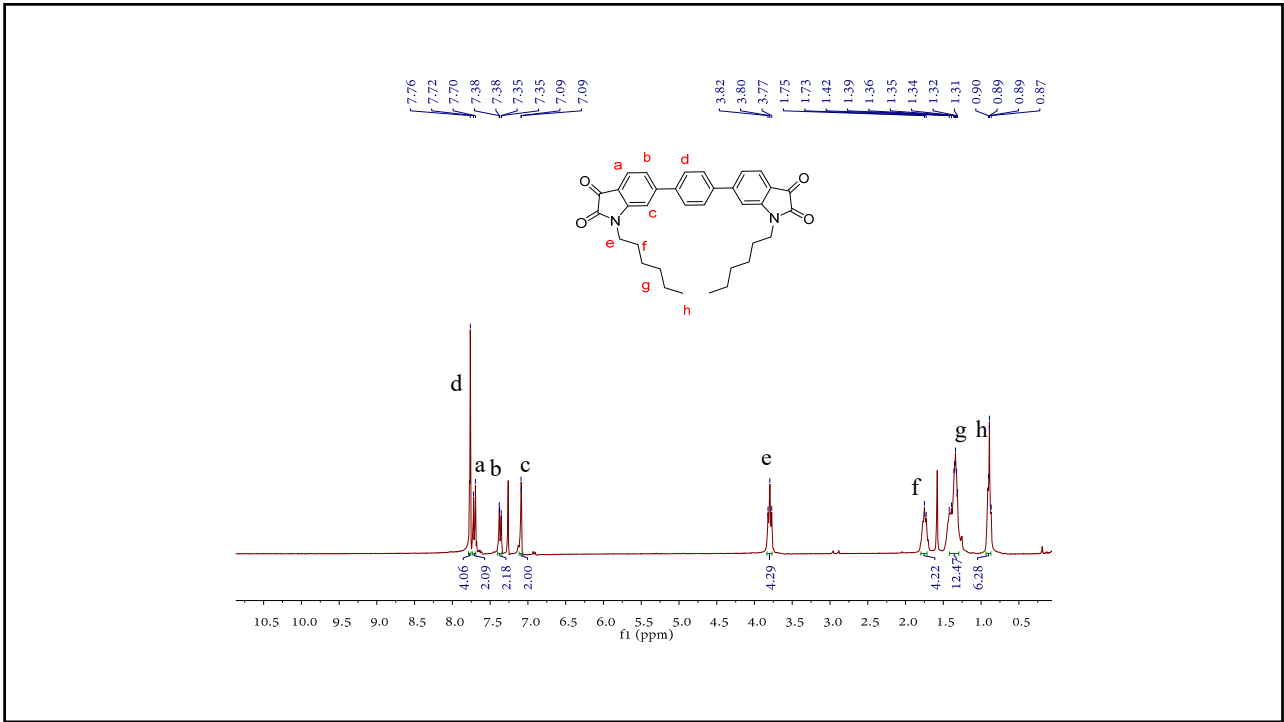
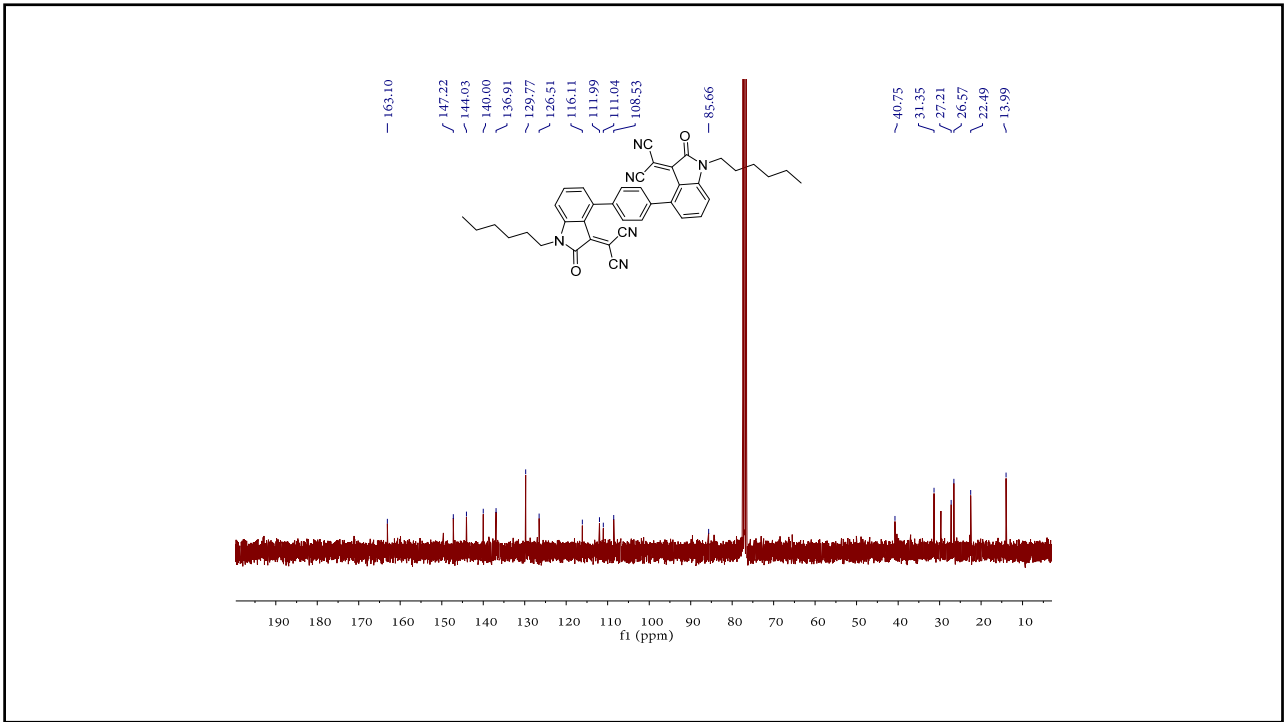
Chapter 3

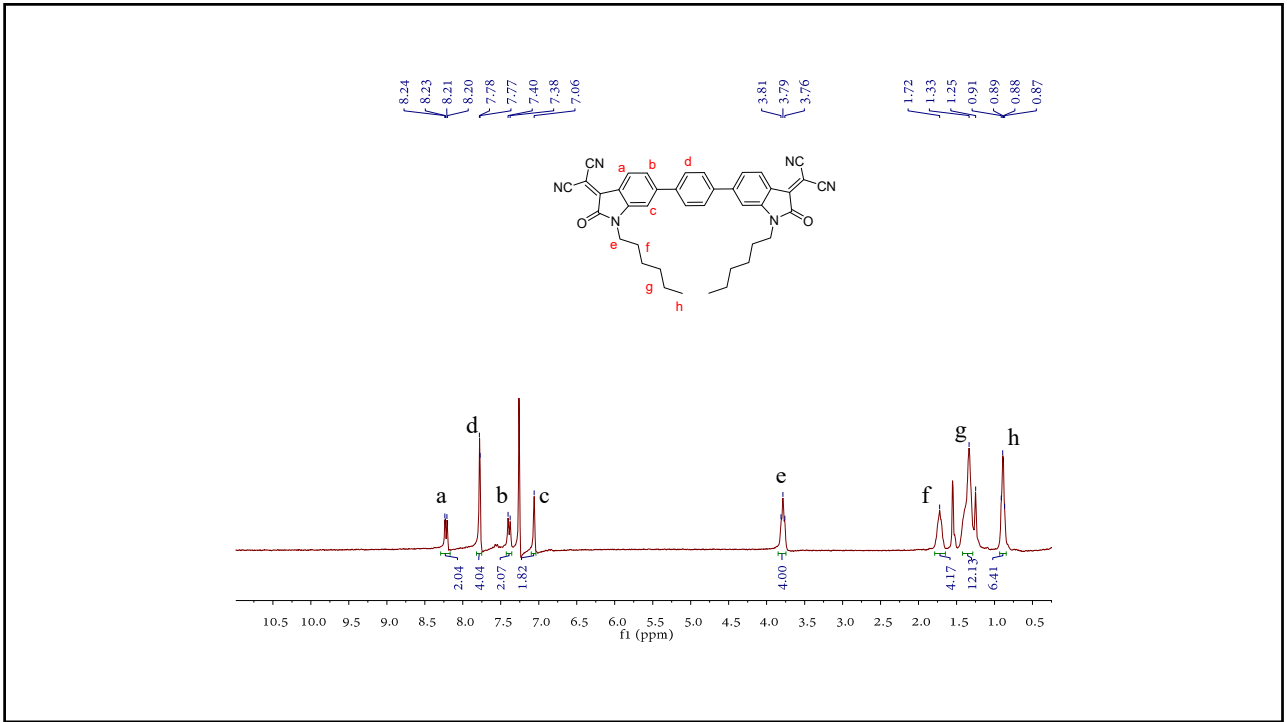
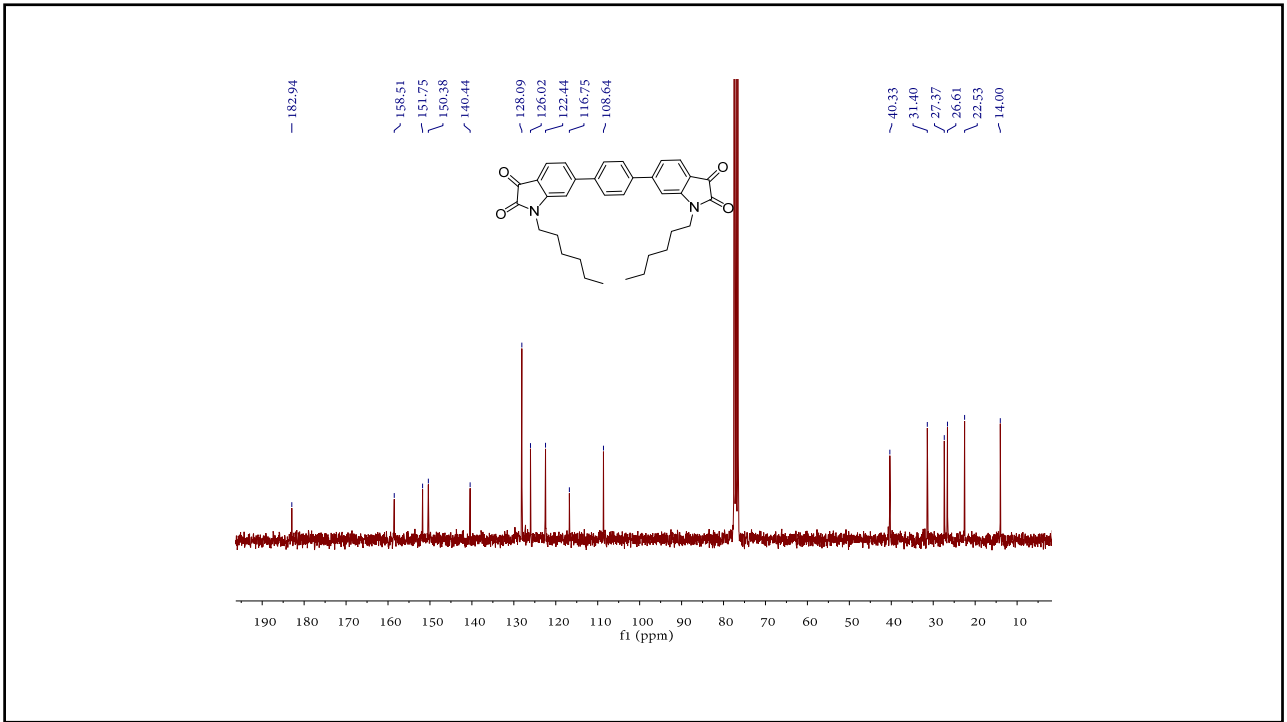


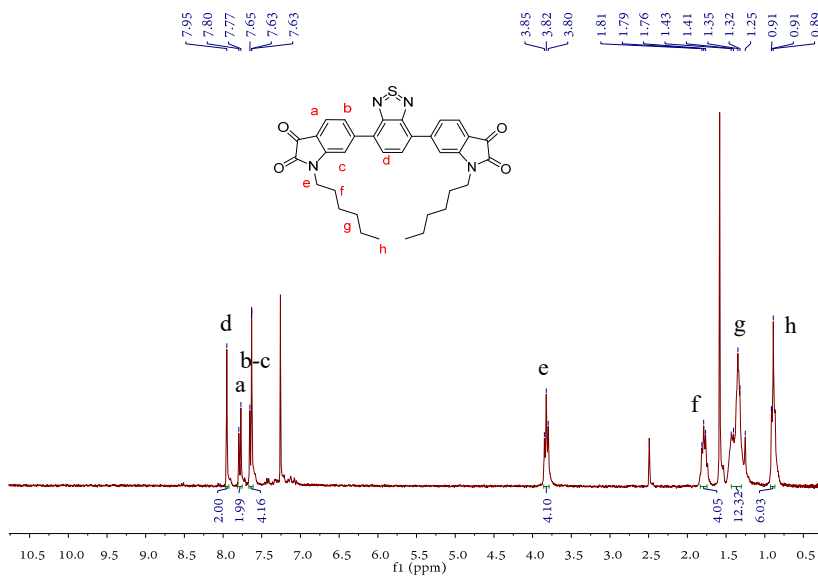
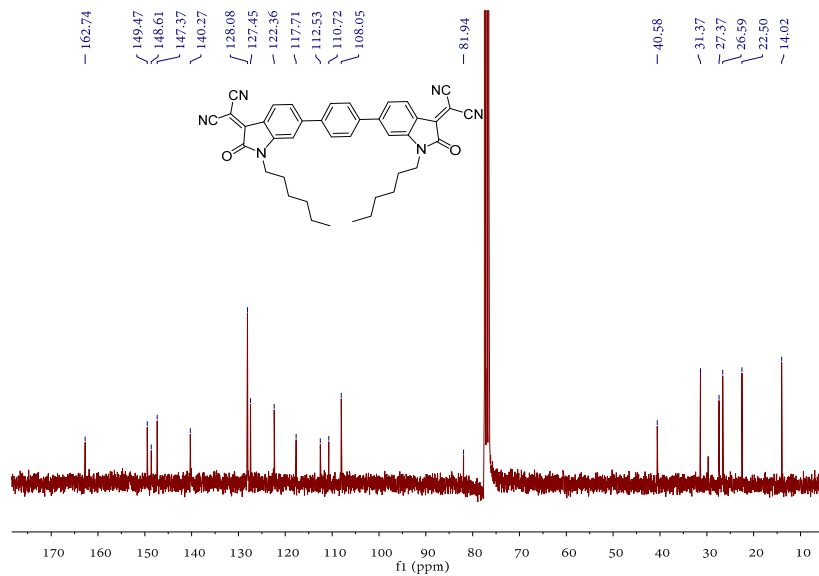


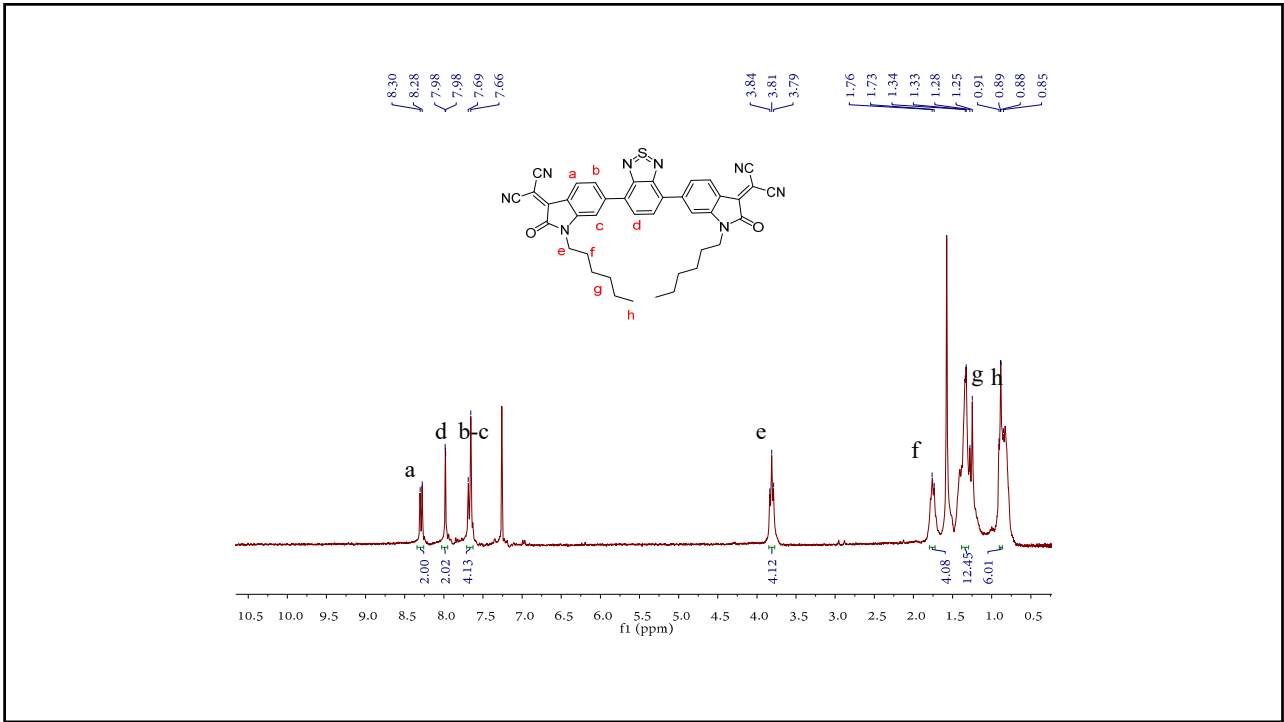
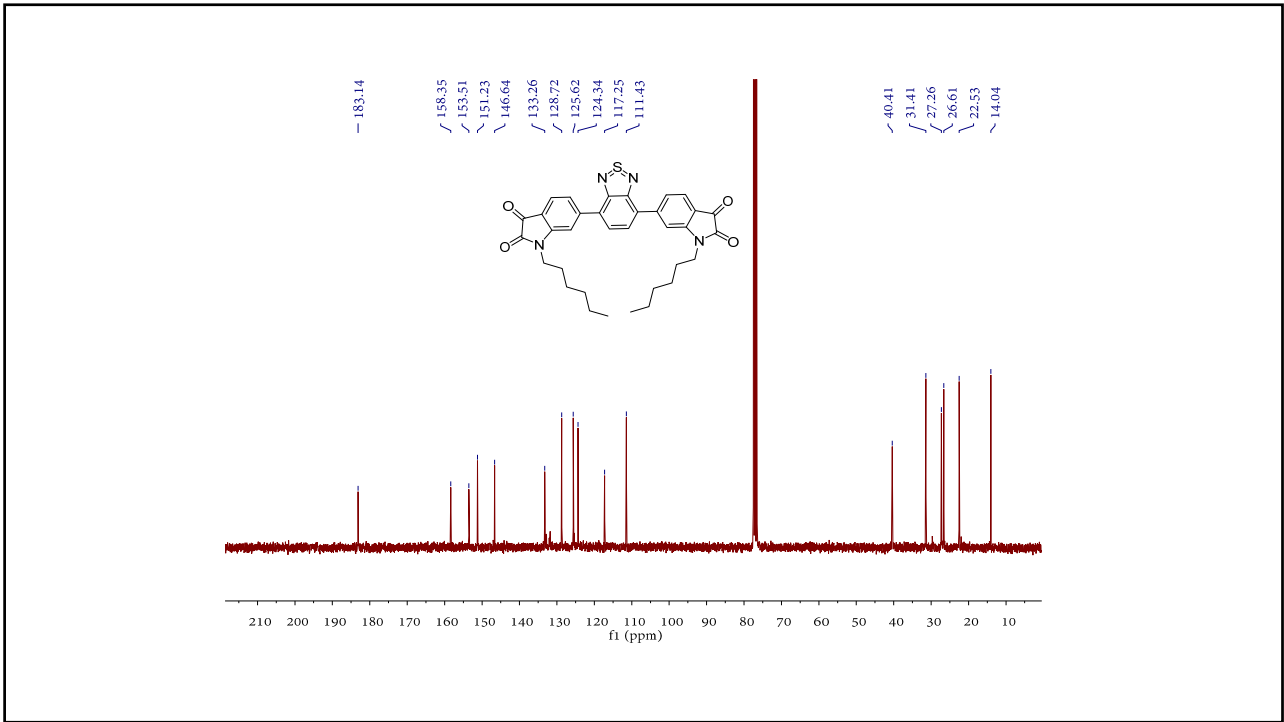


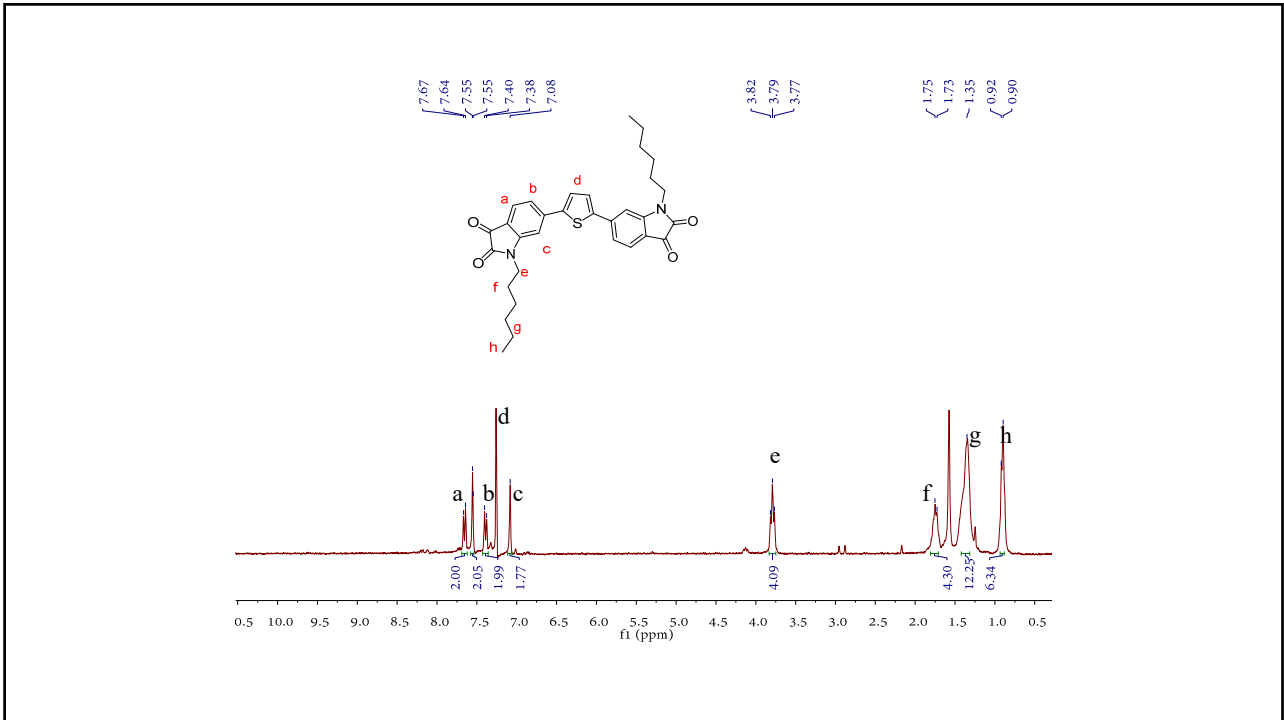
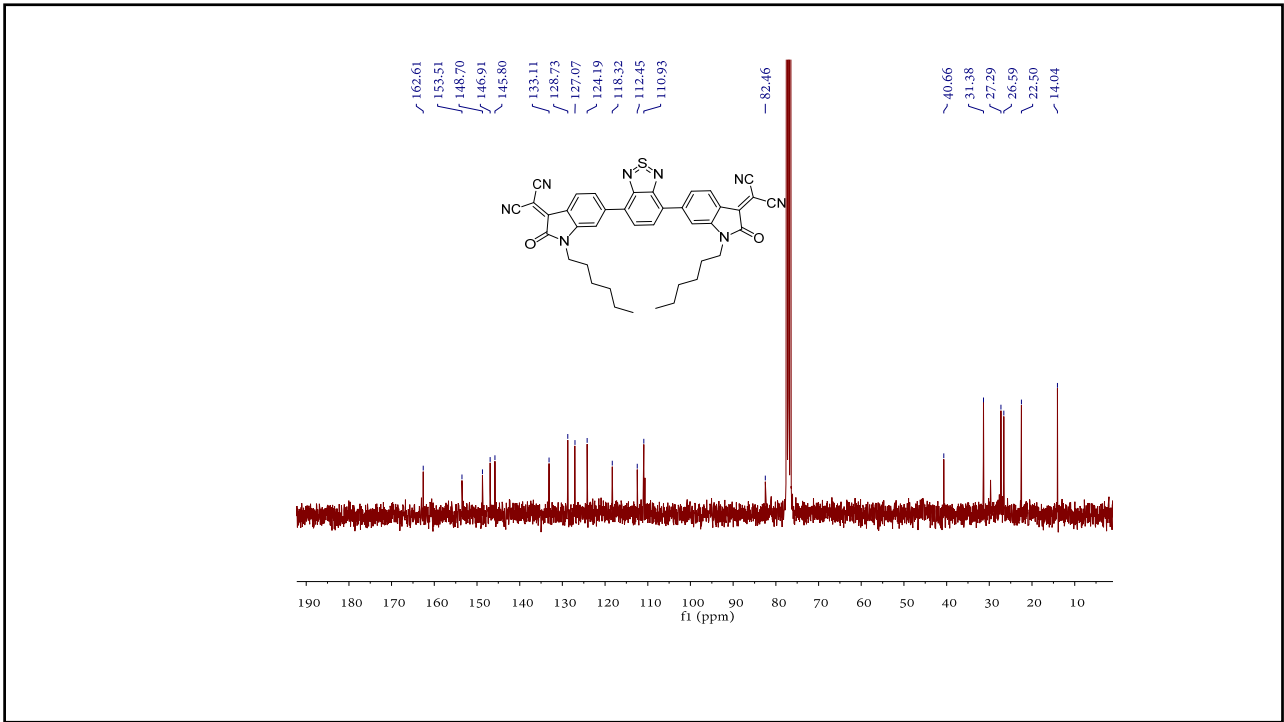


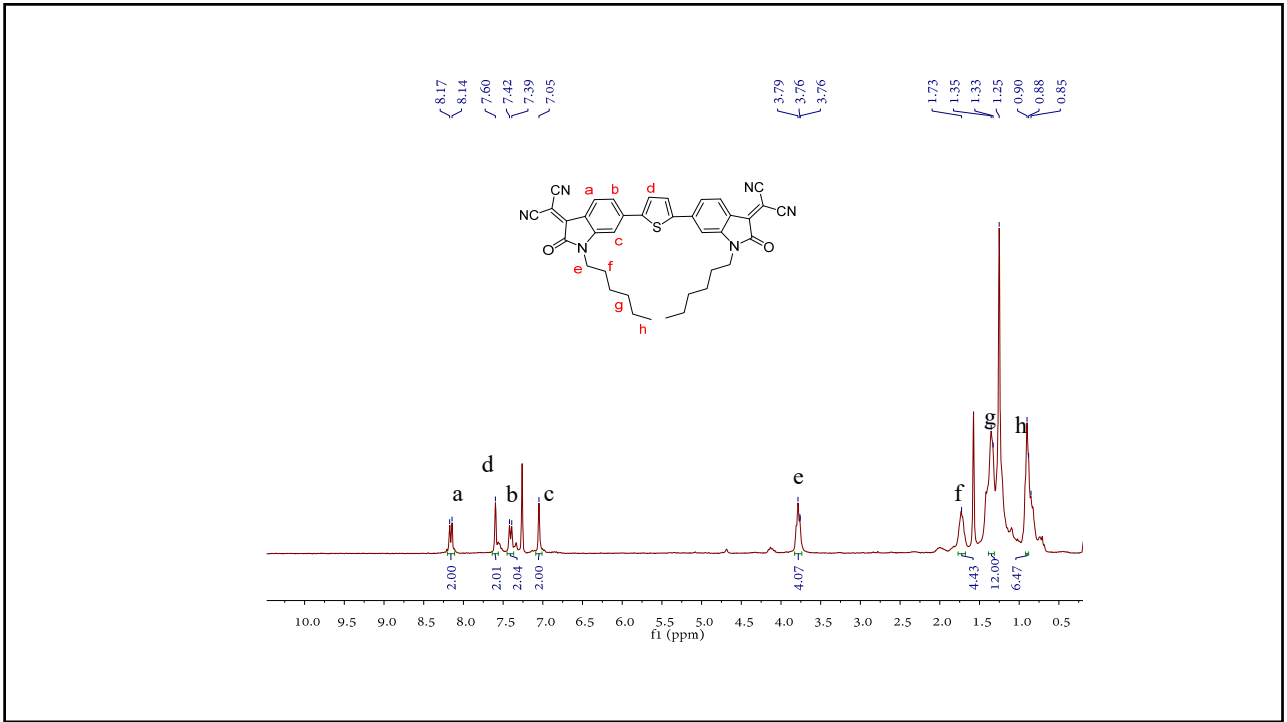
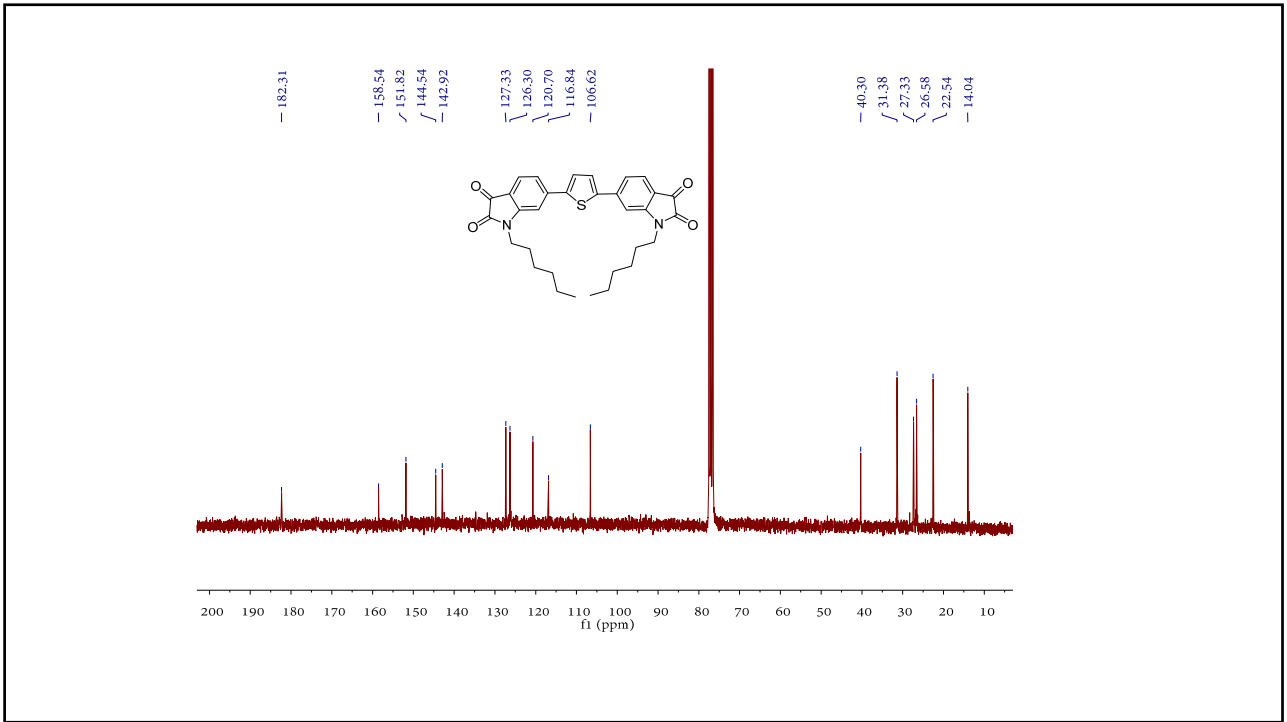


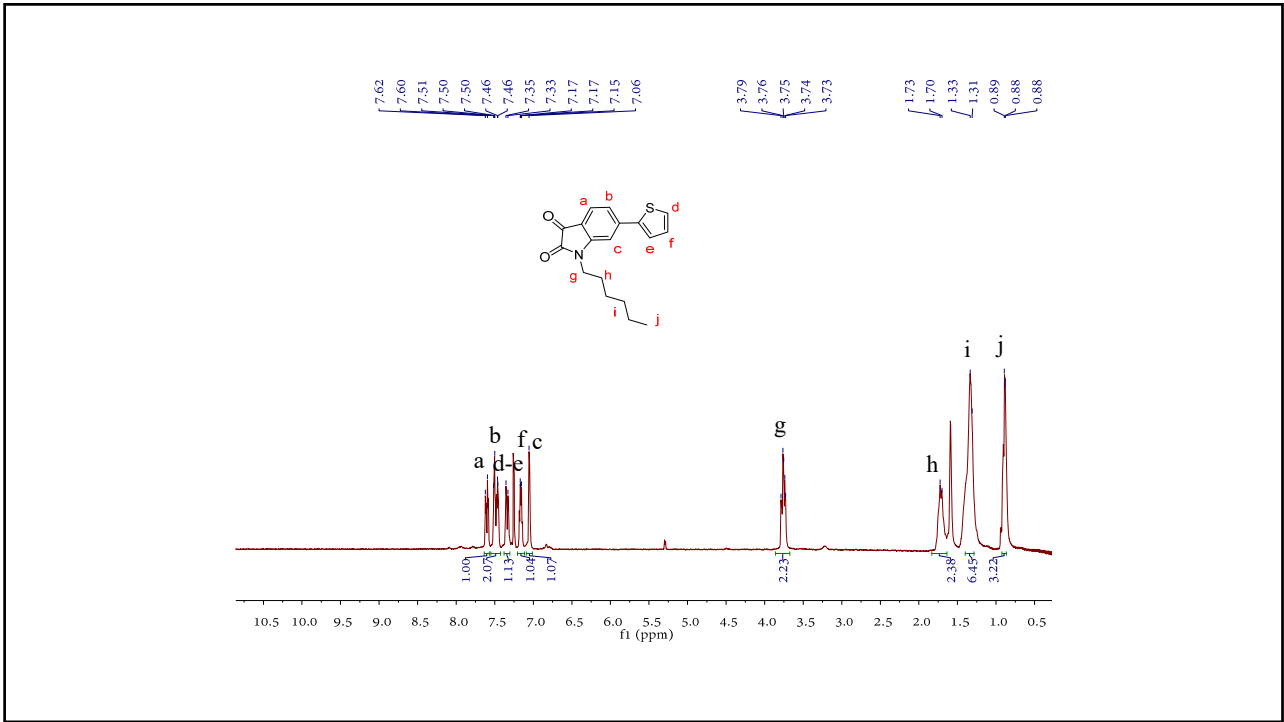
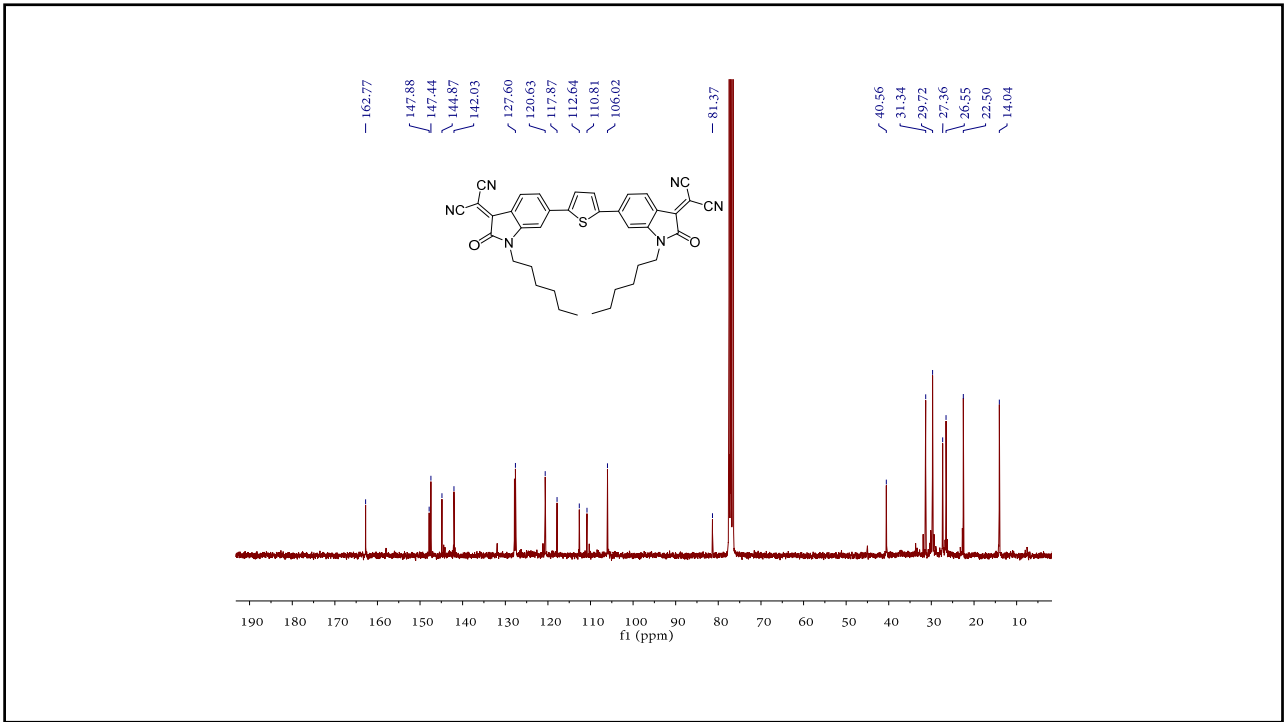


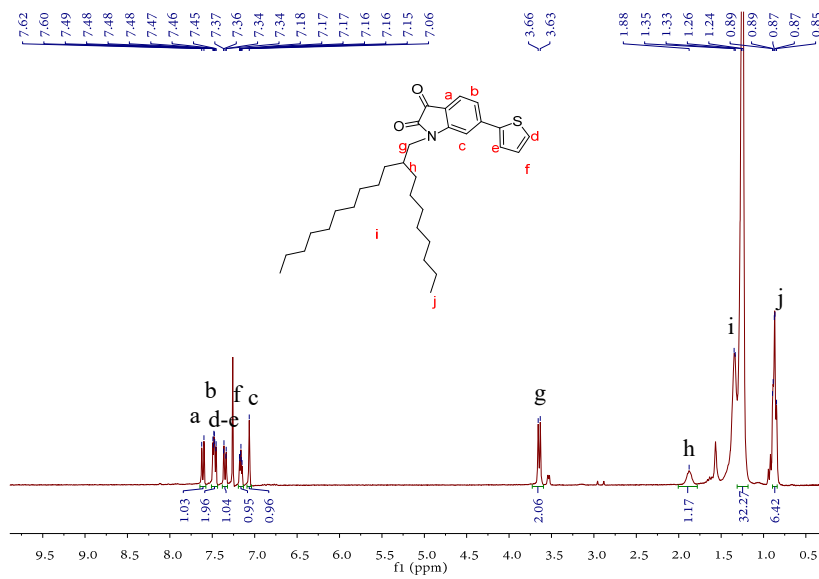
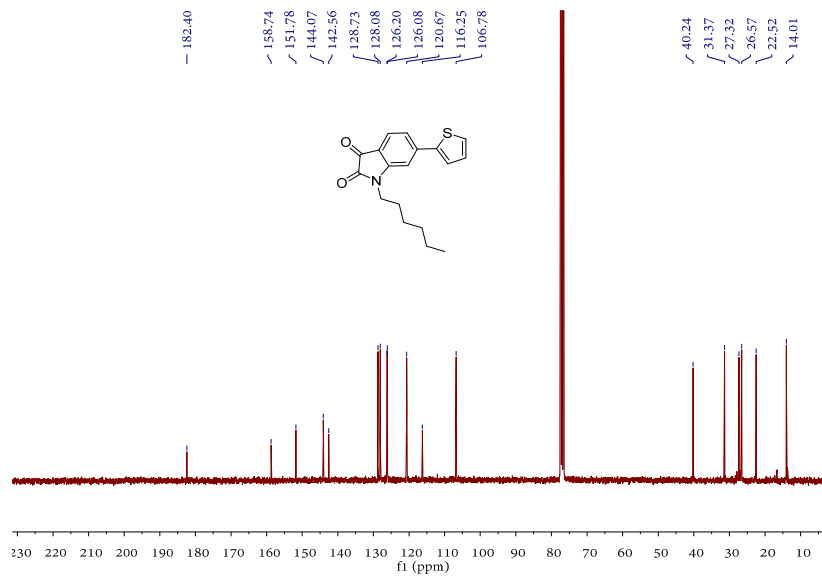


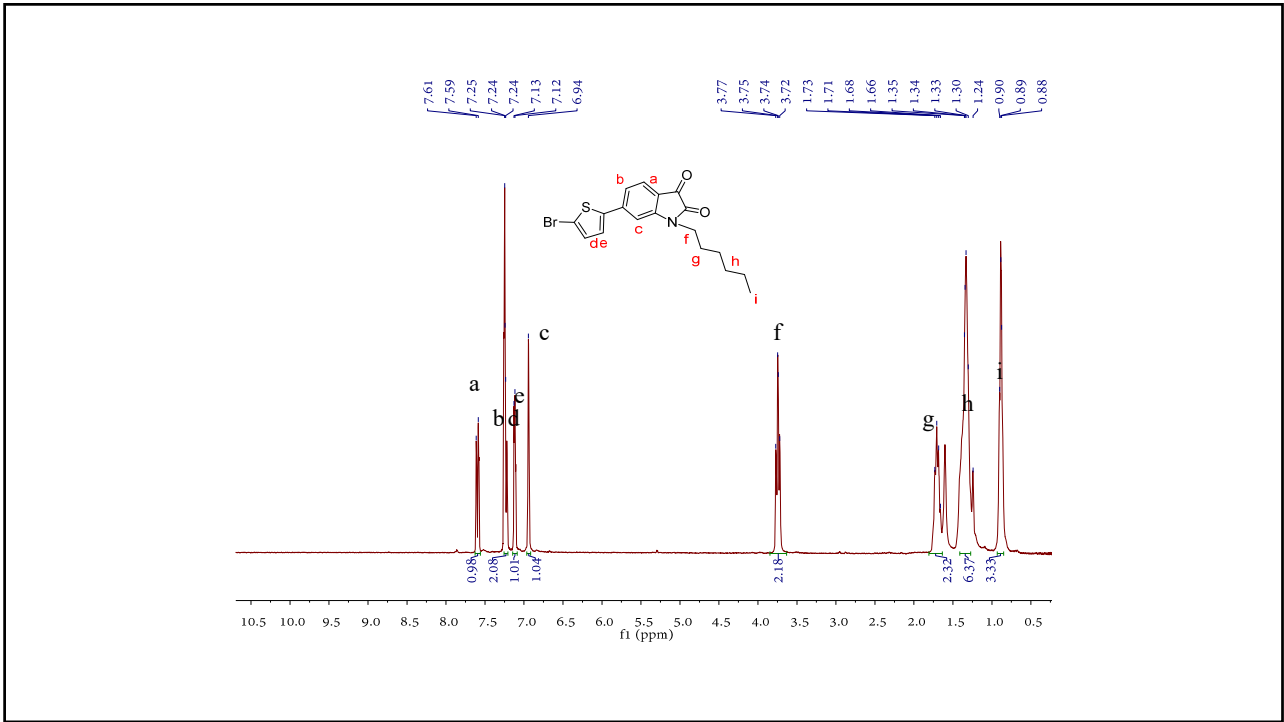
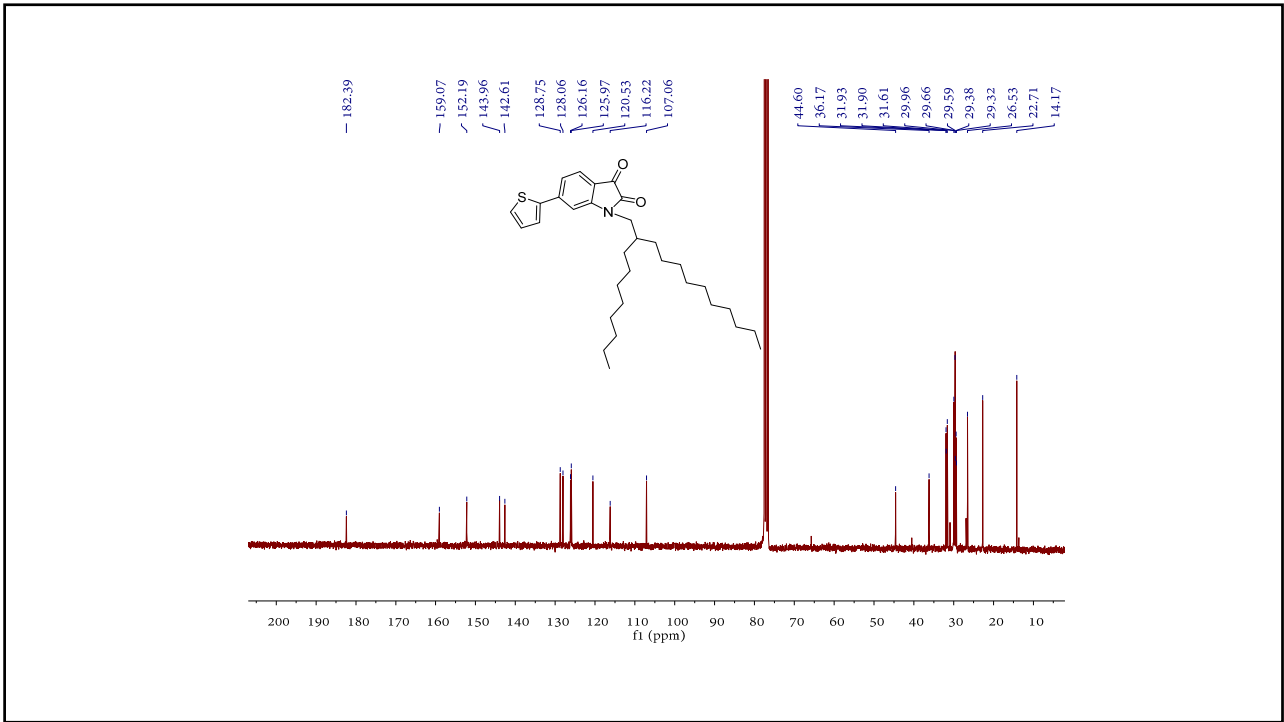


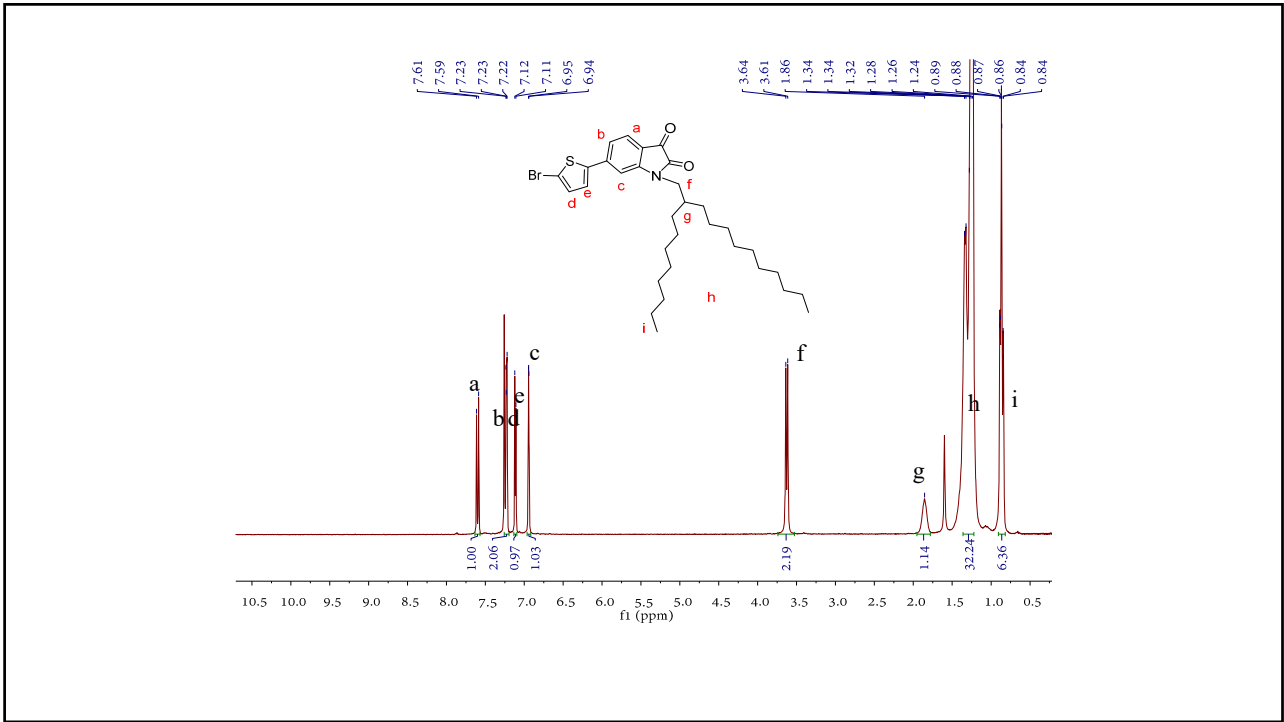
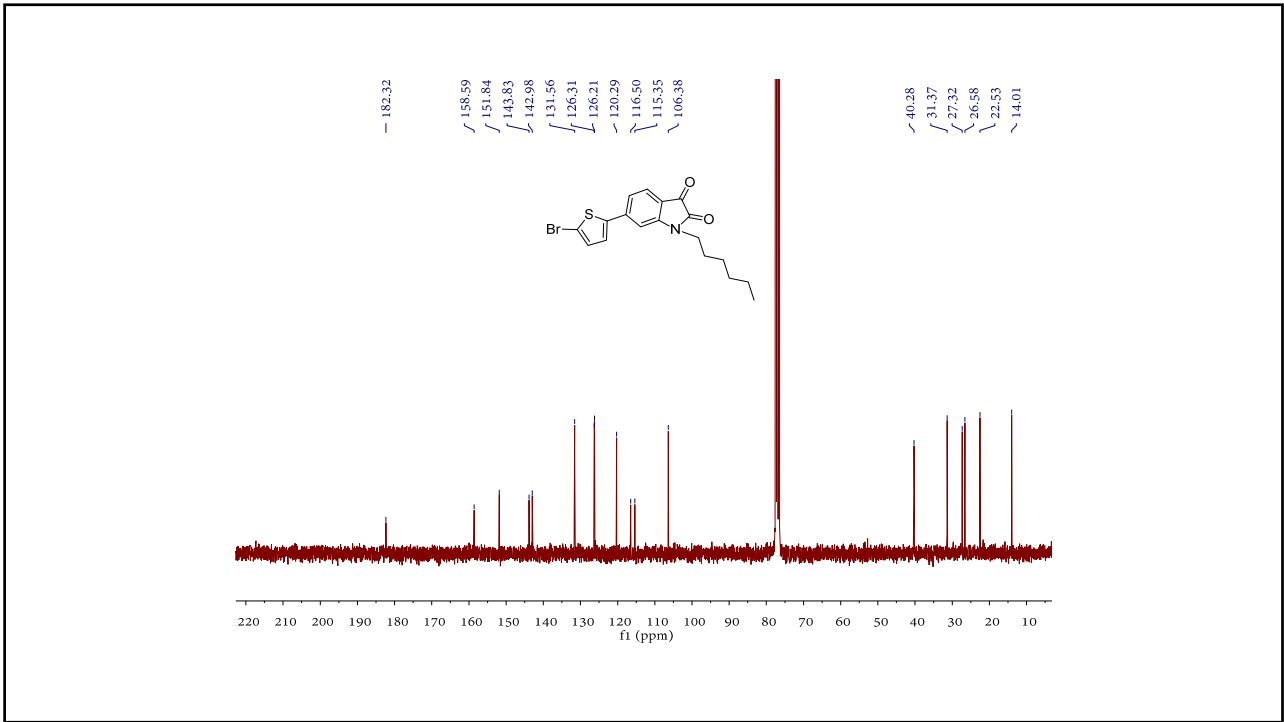


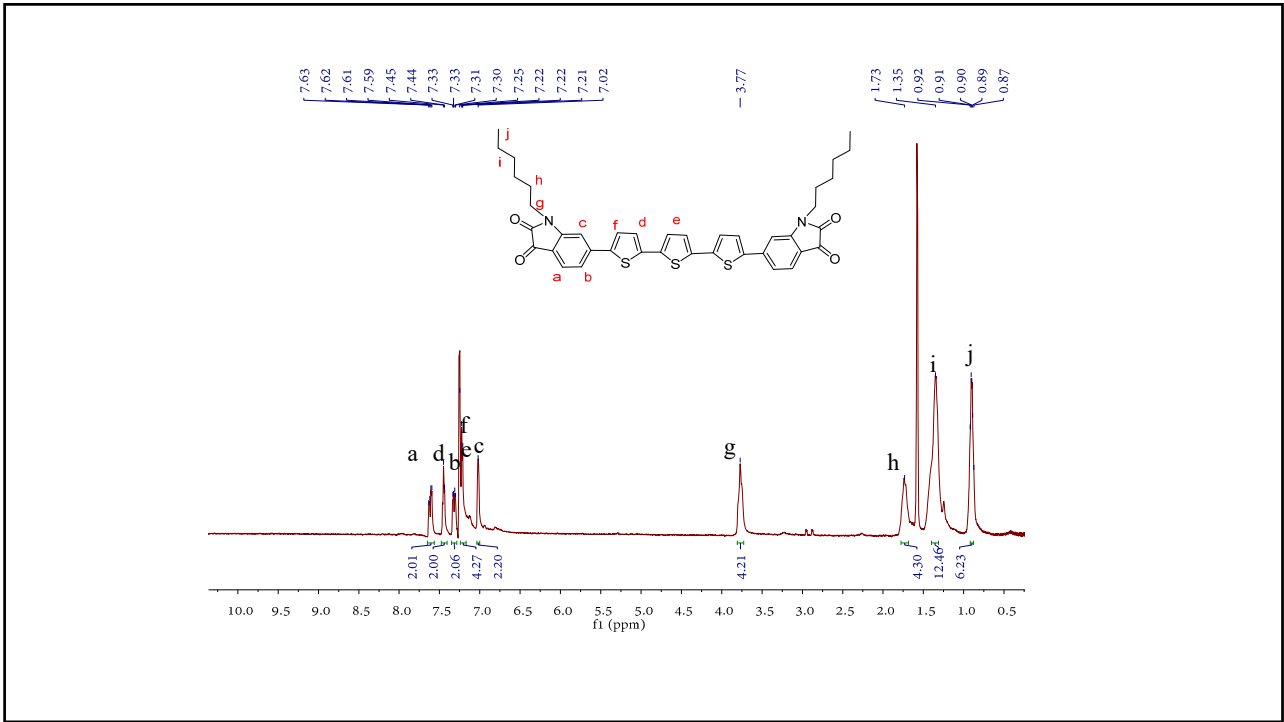
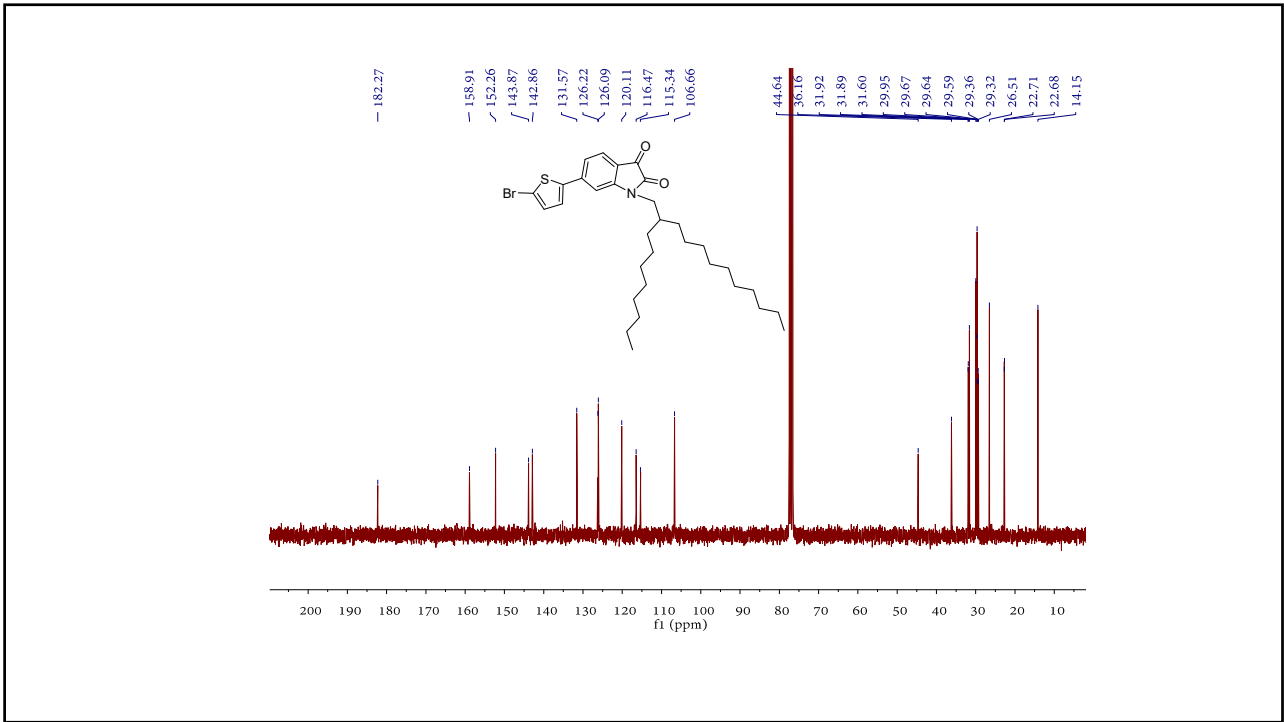


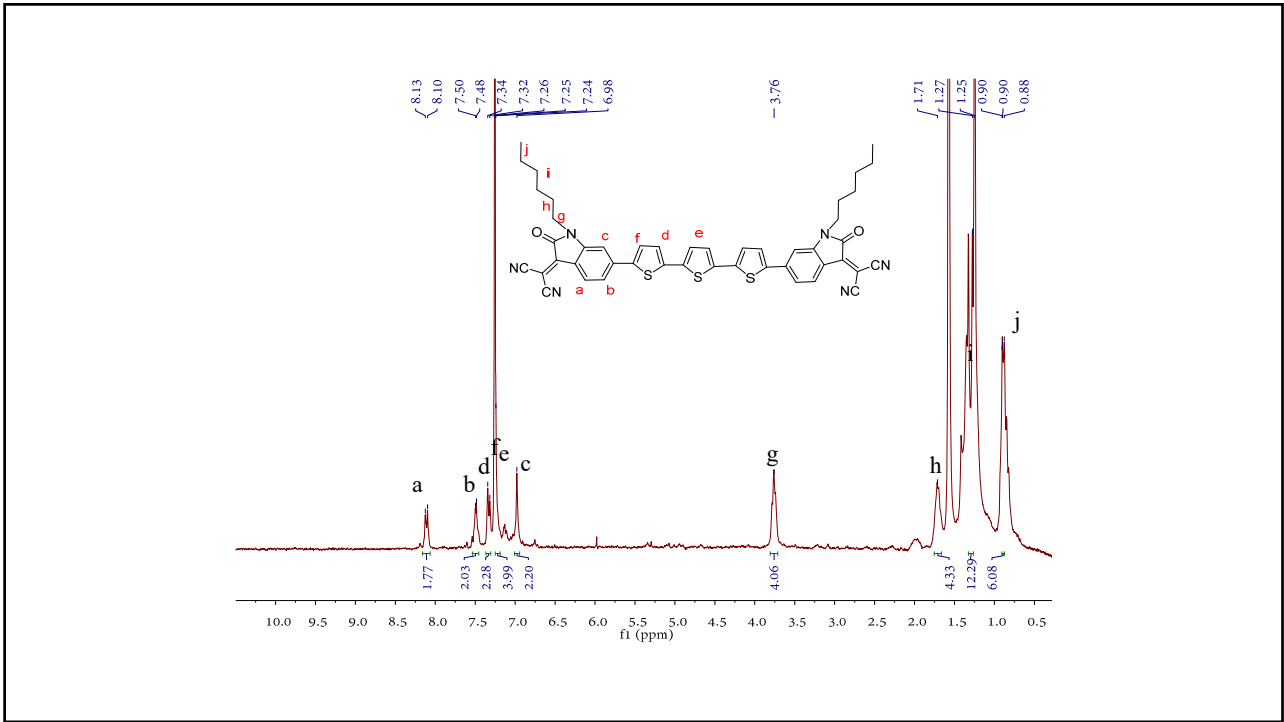
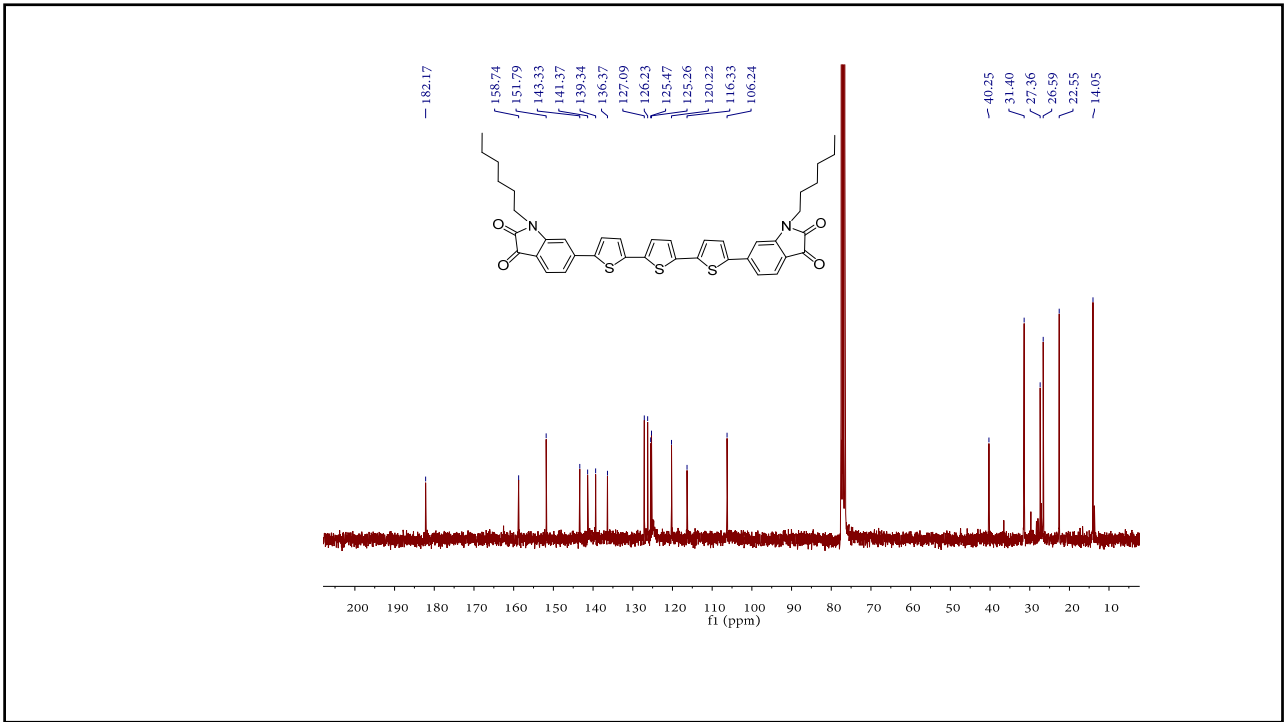


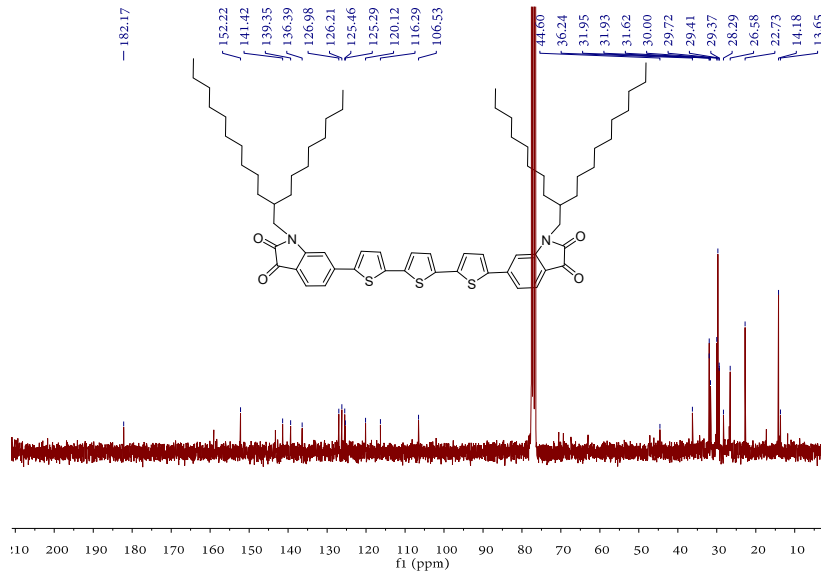
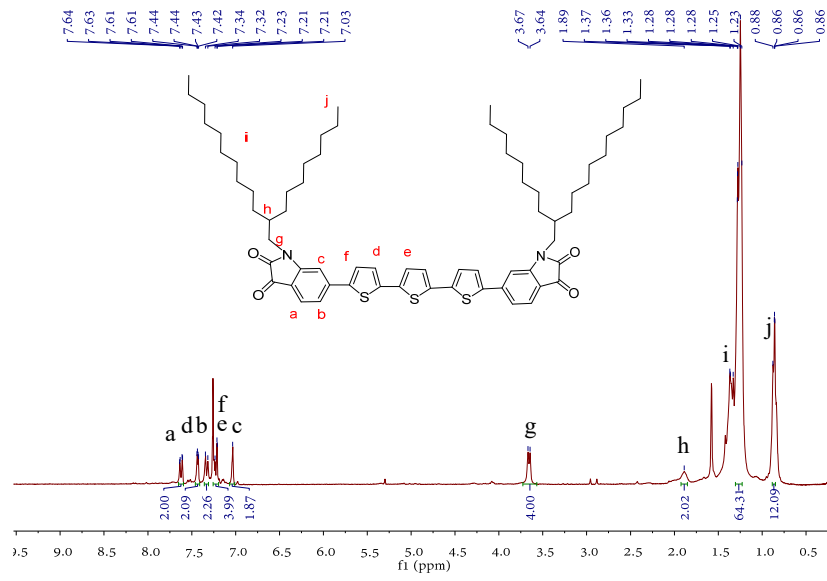


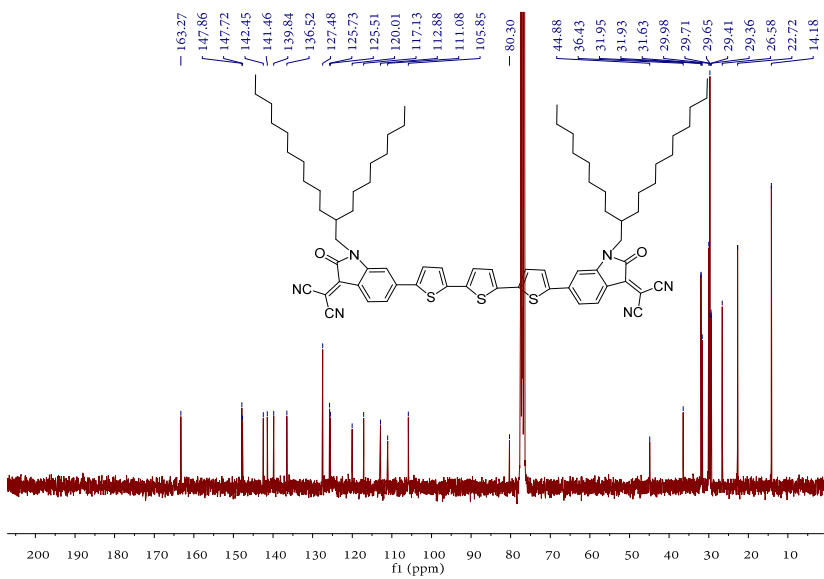
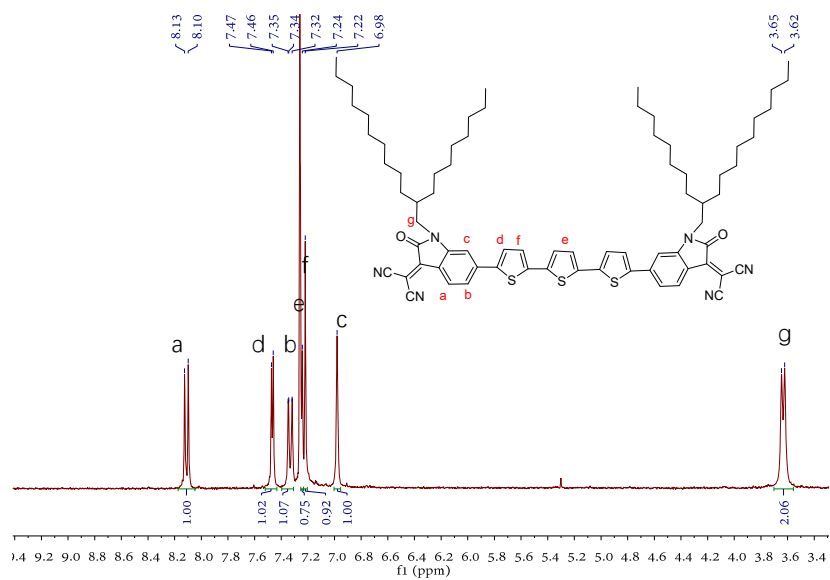


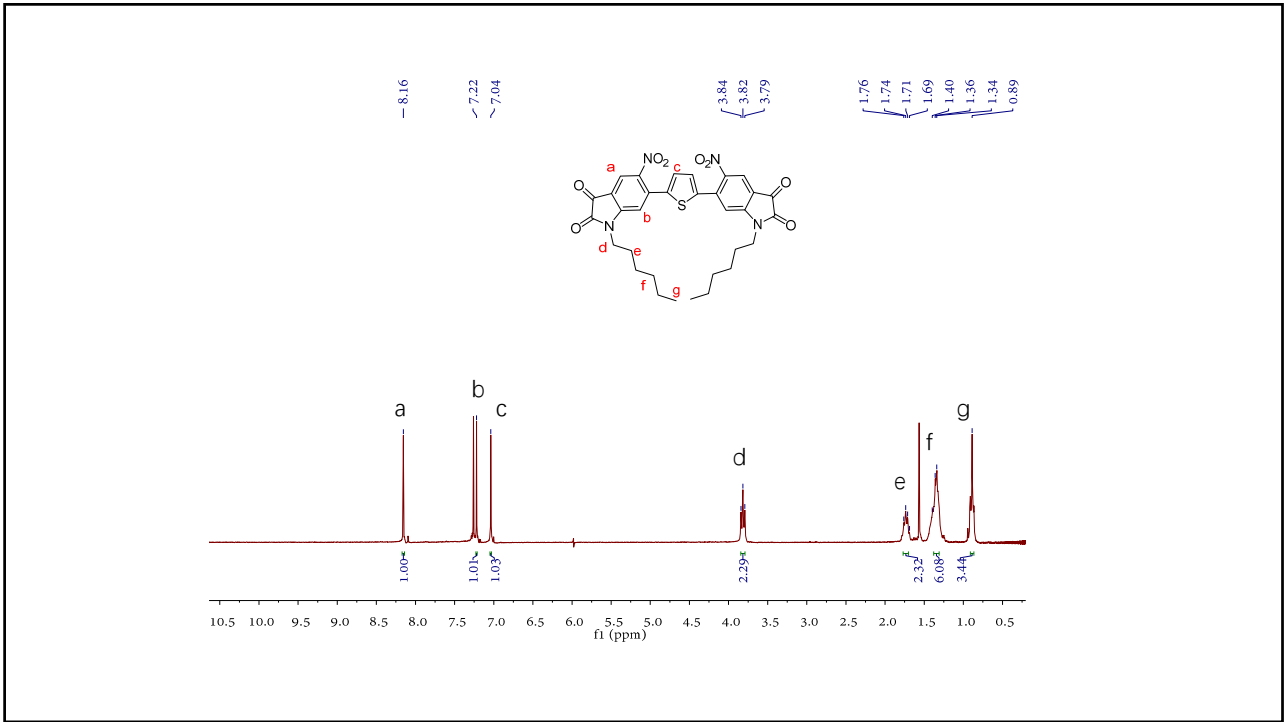
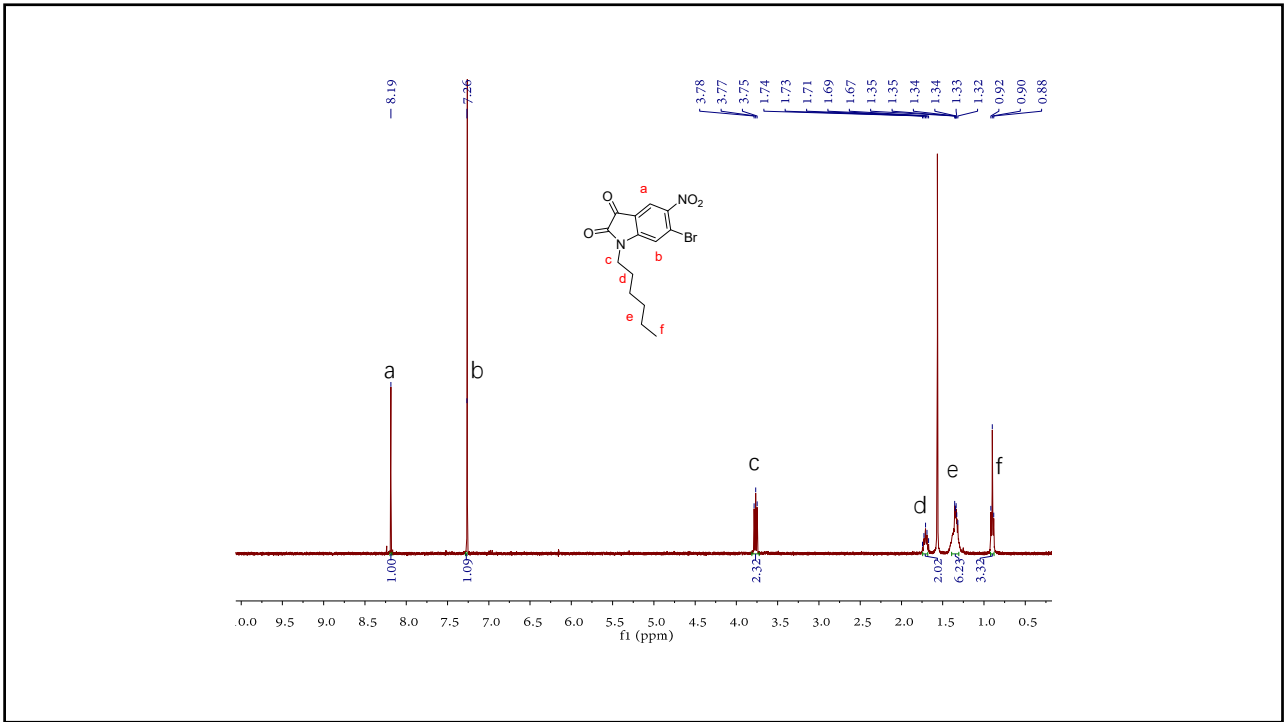


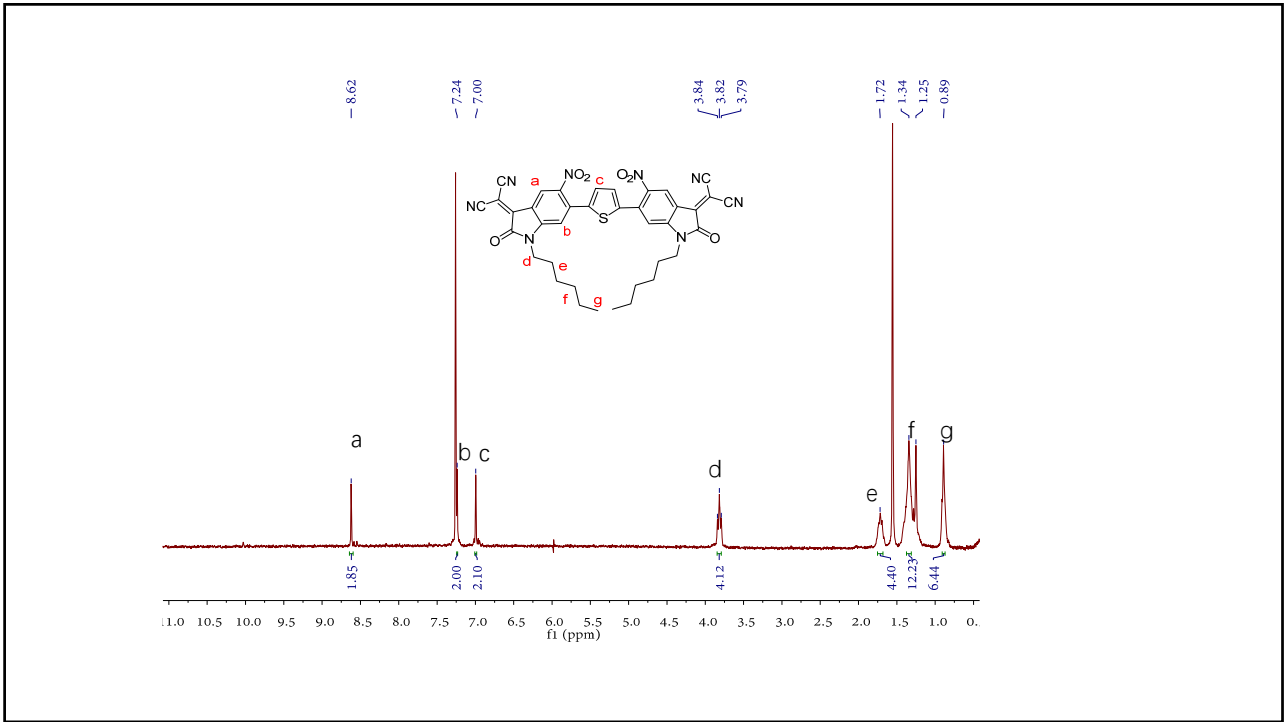
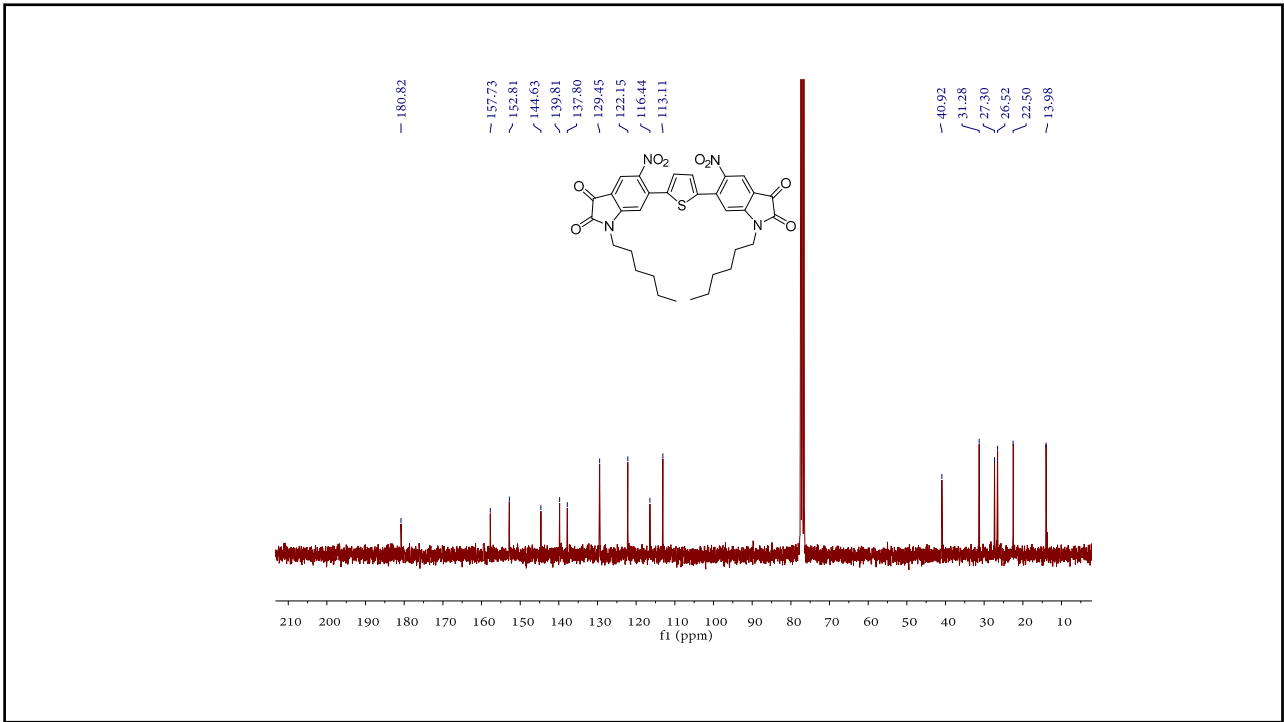


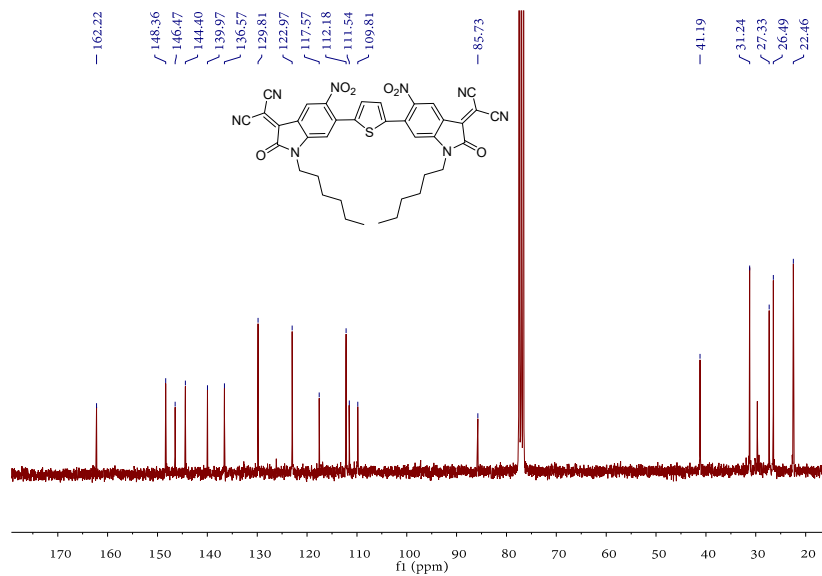




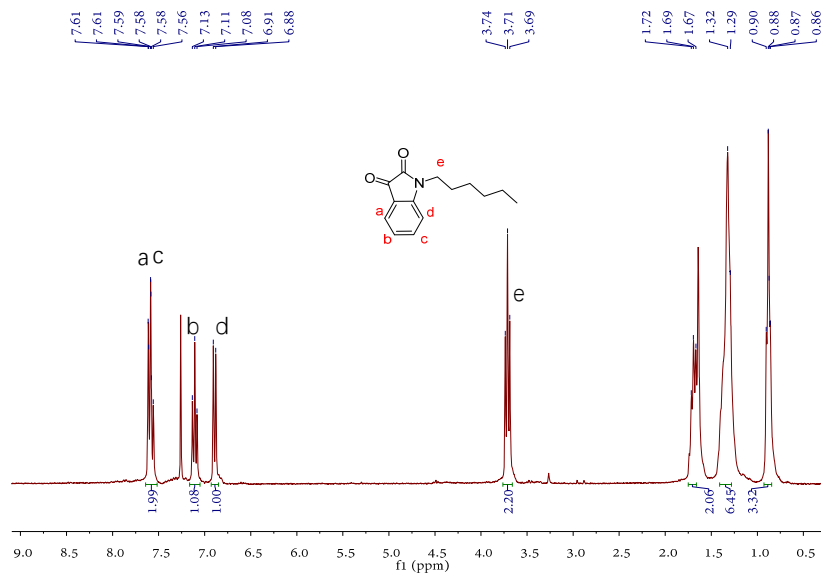
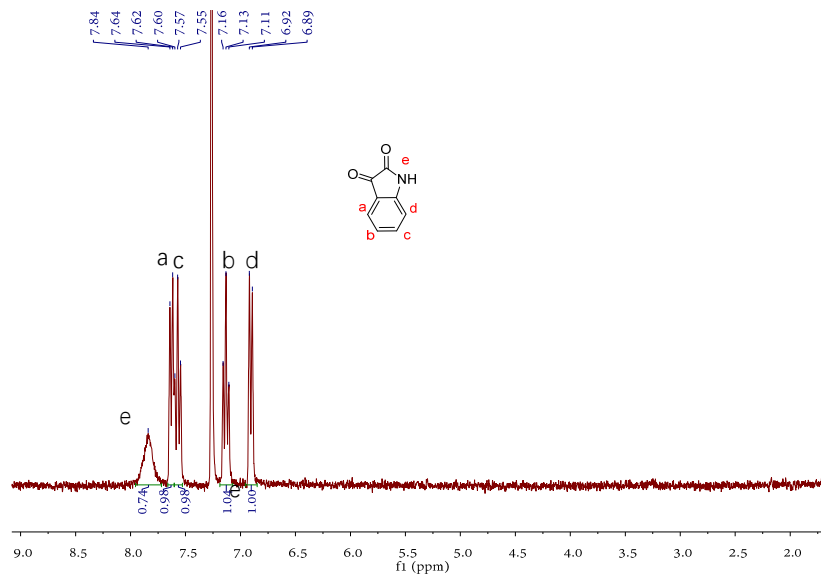


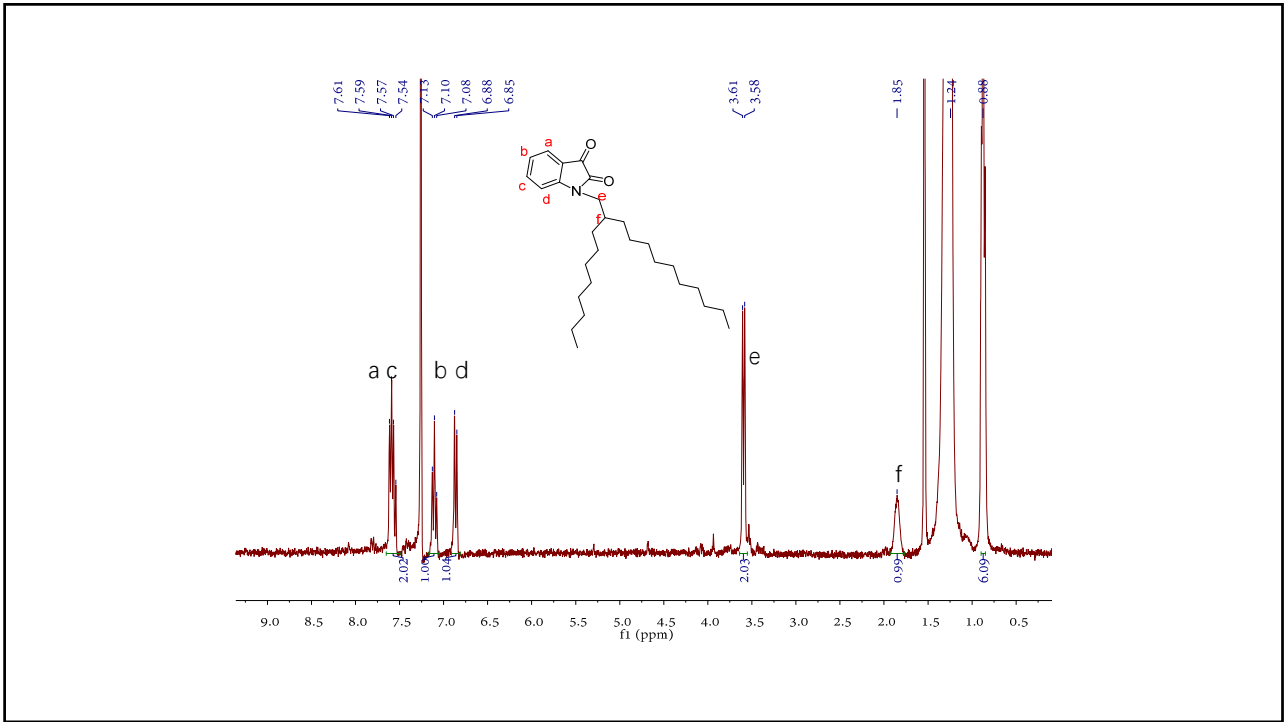
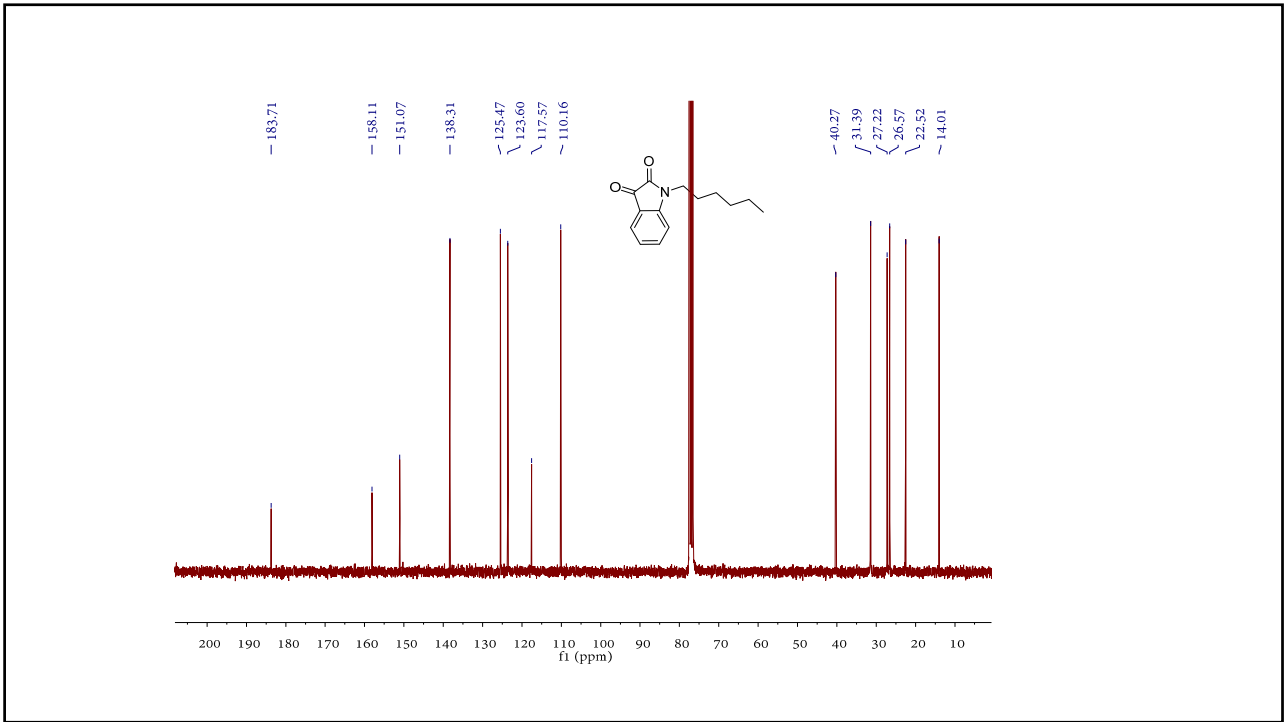


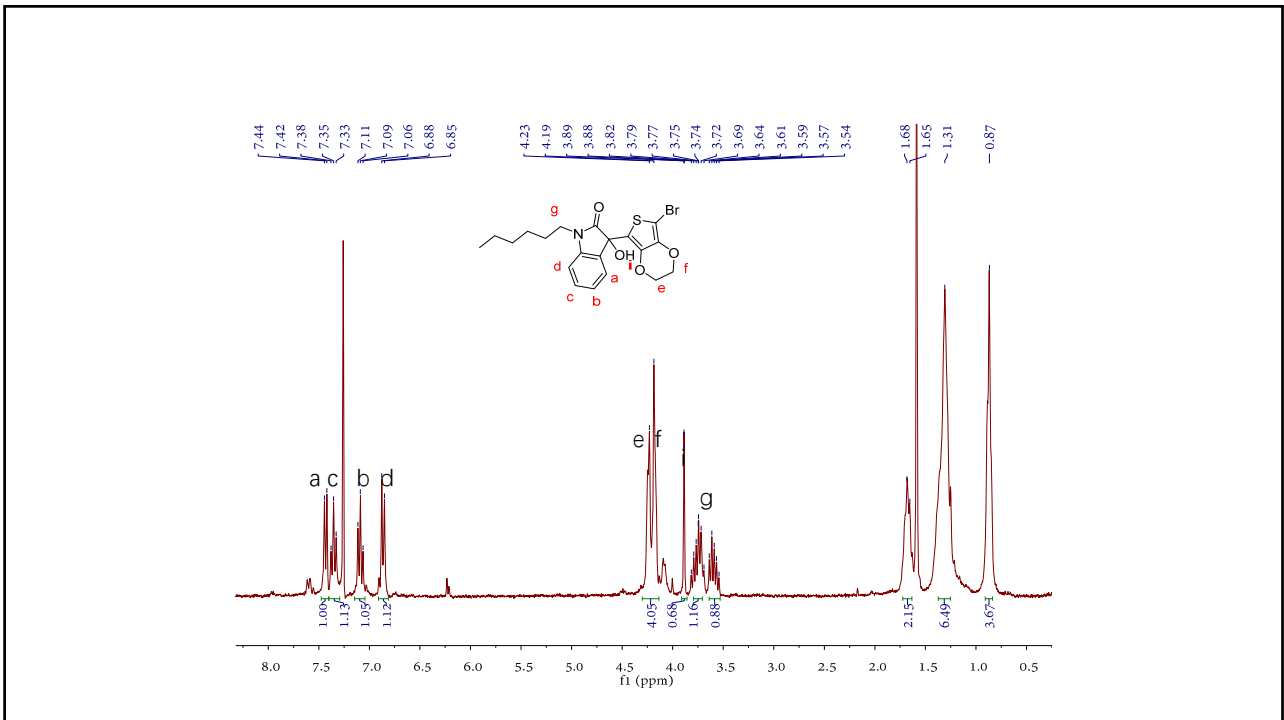
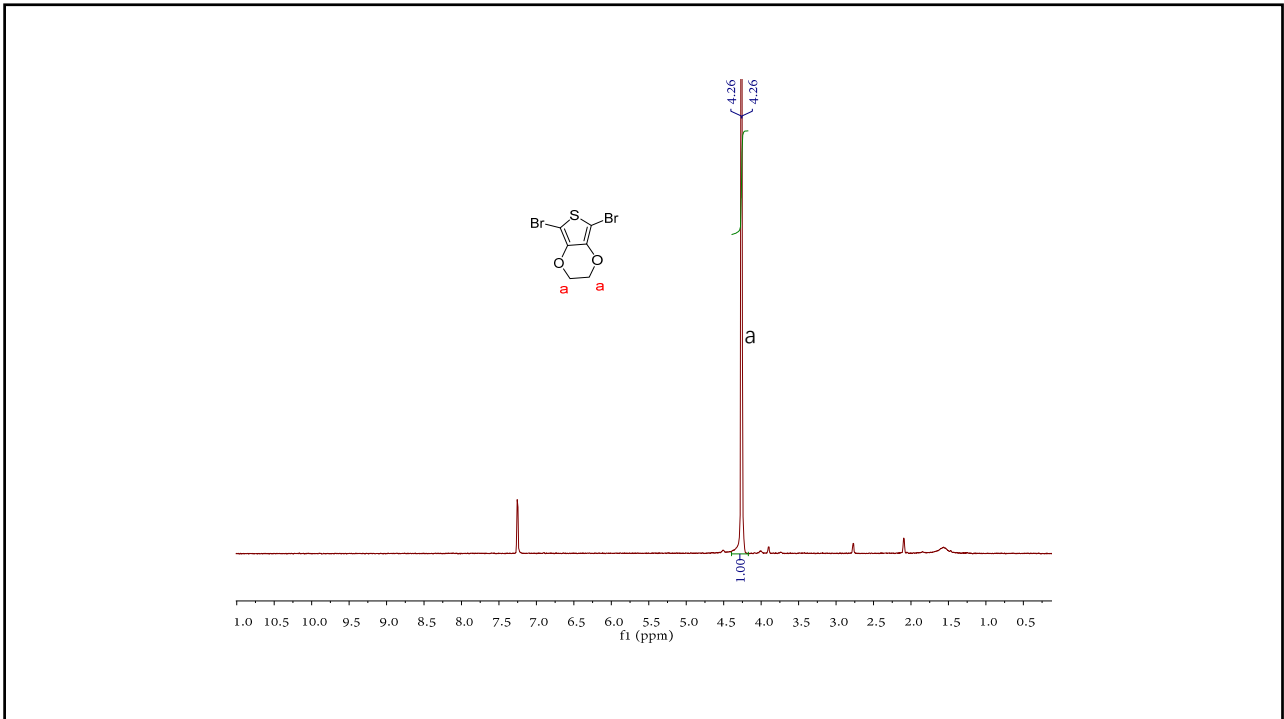


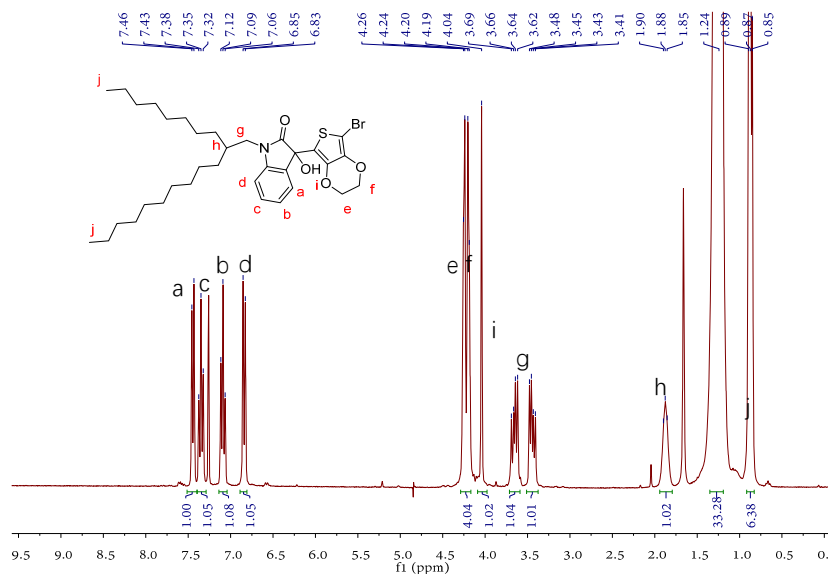
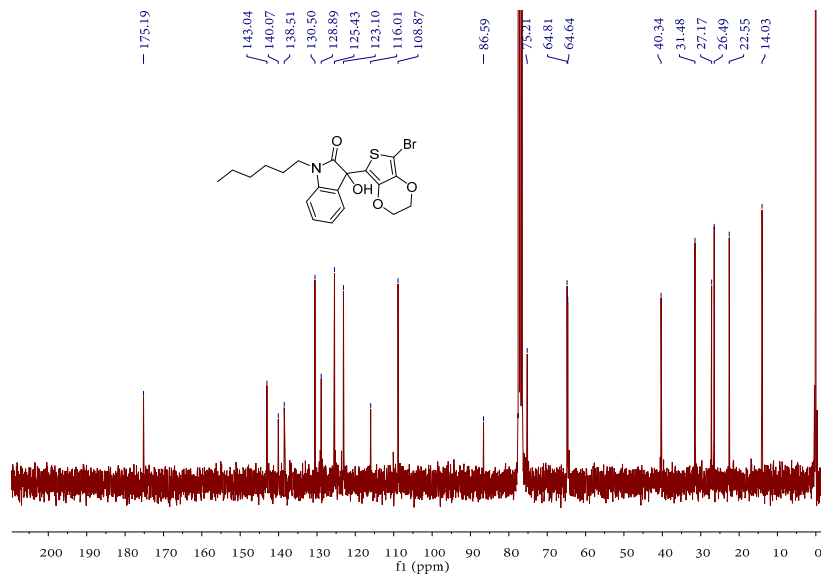


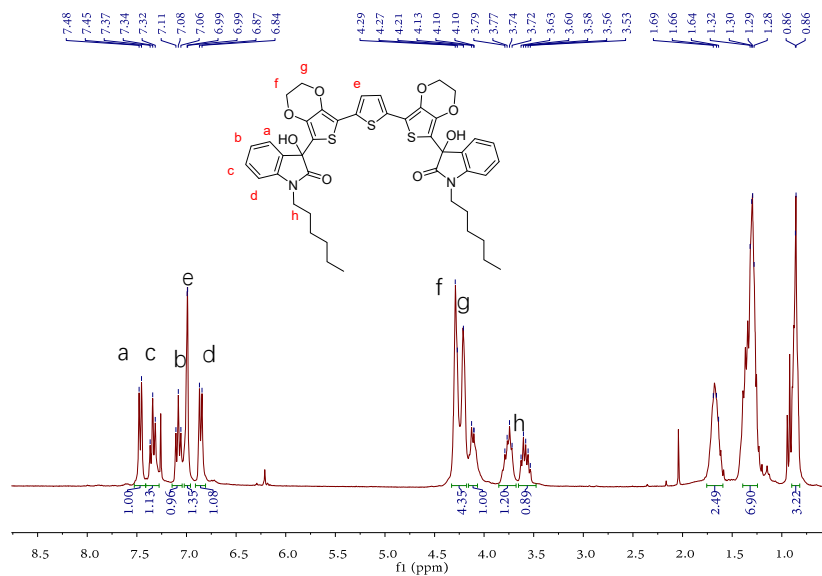
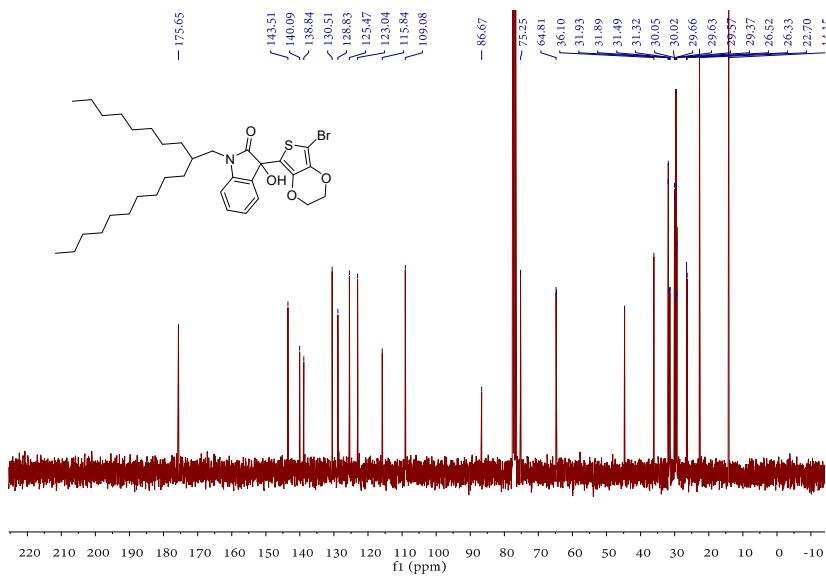
Chapter 4

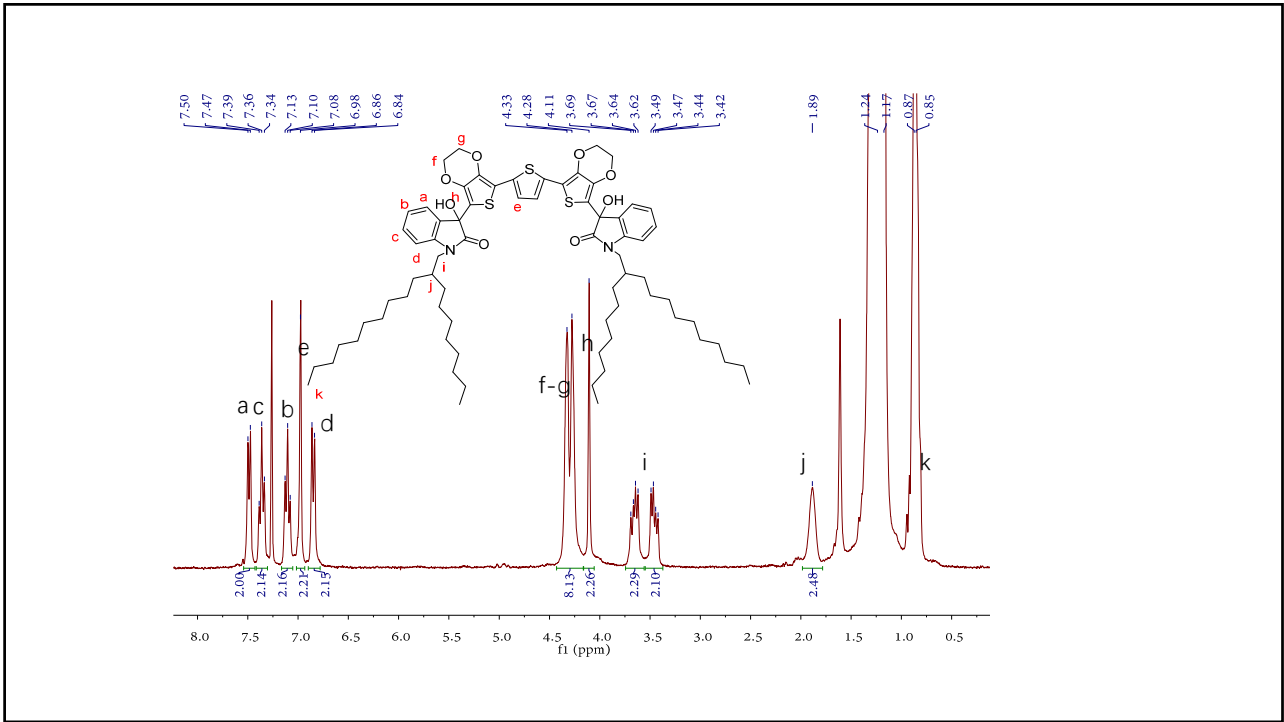
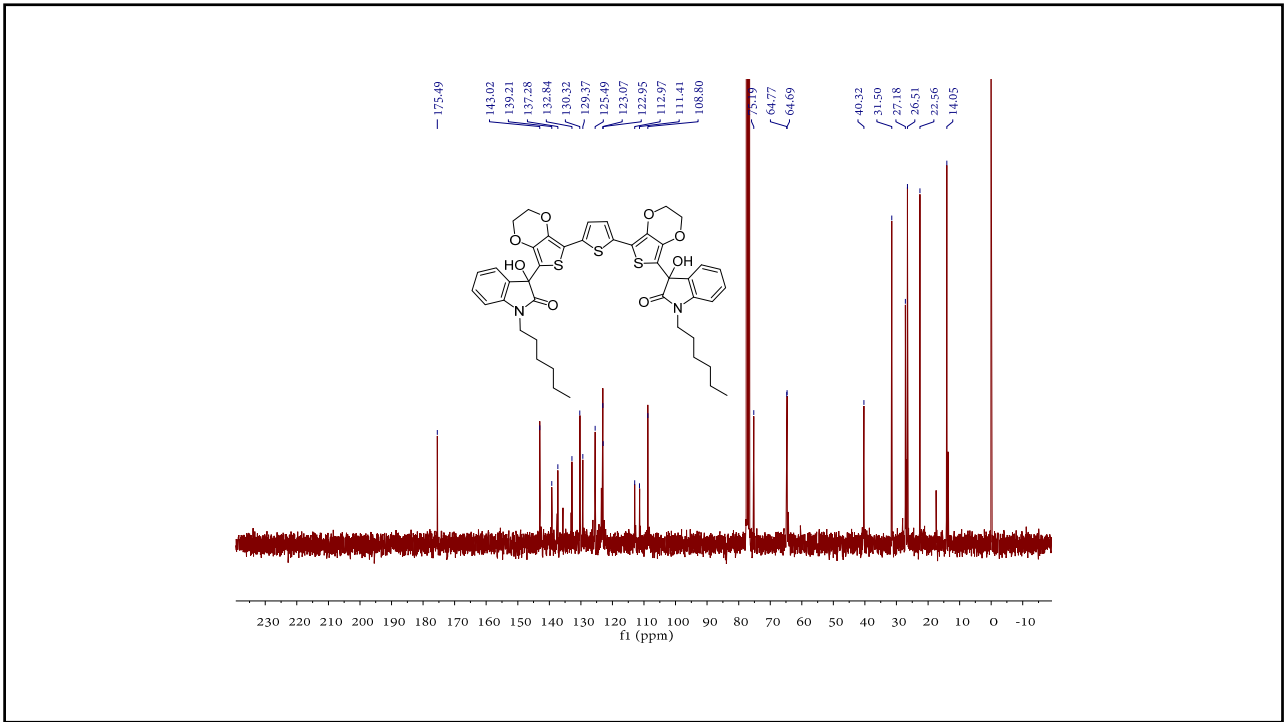


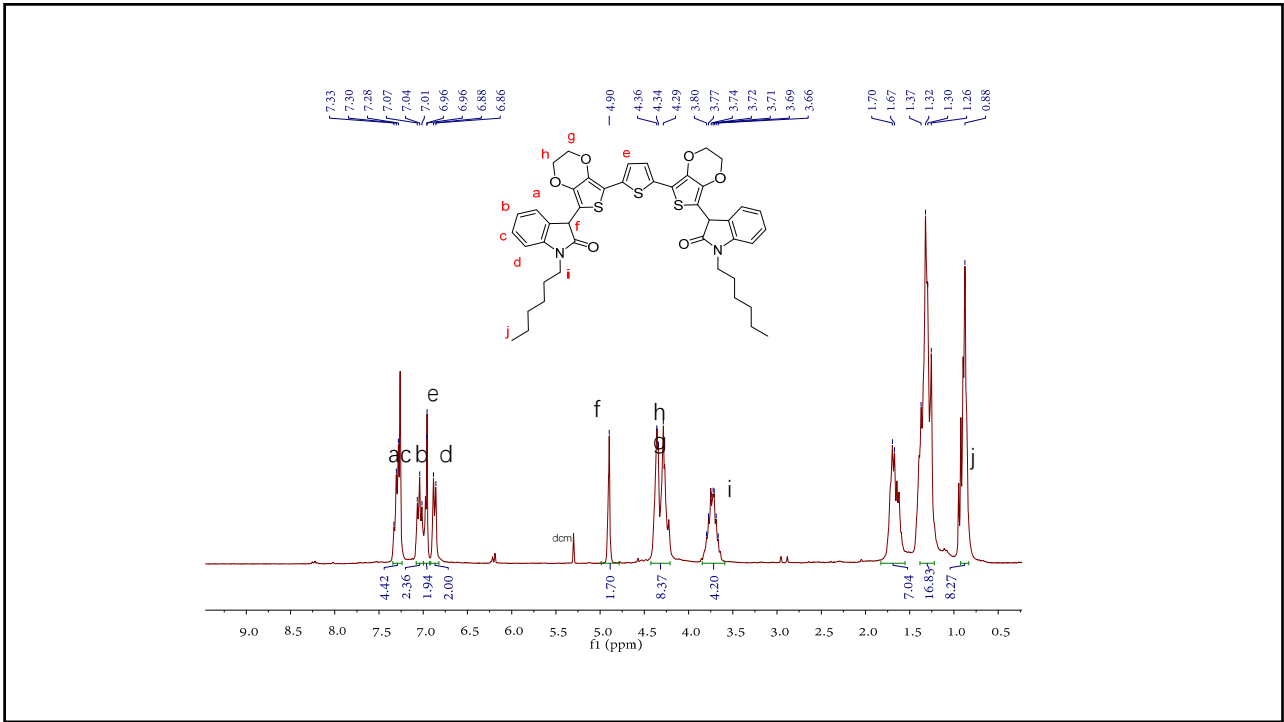
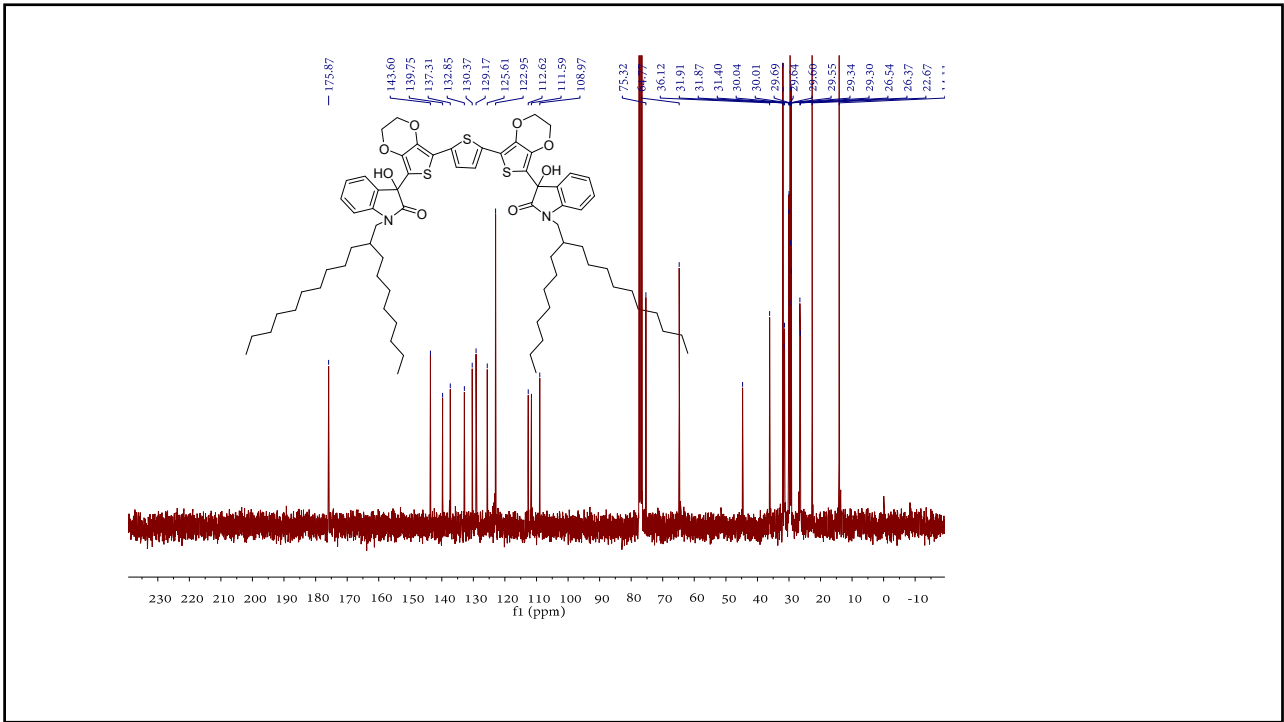


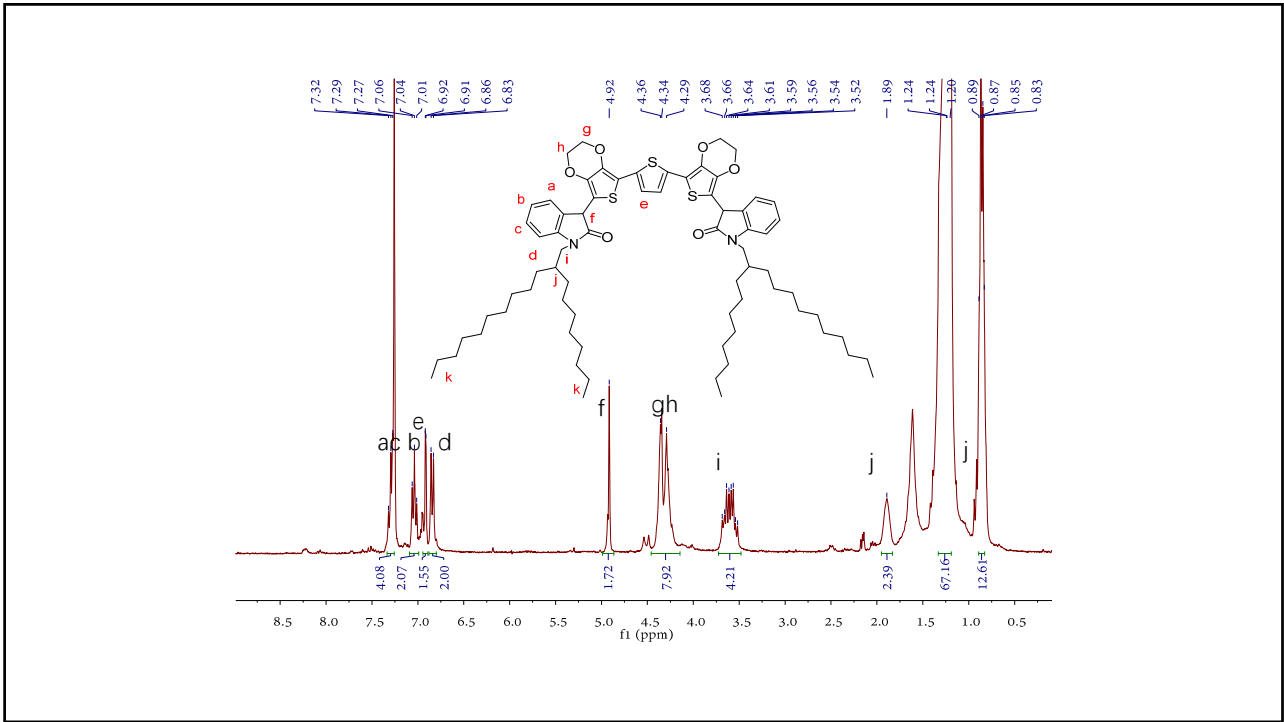
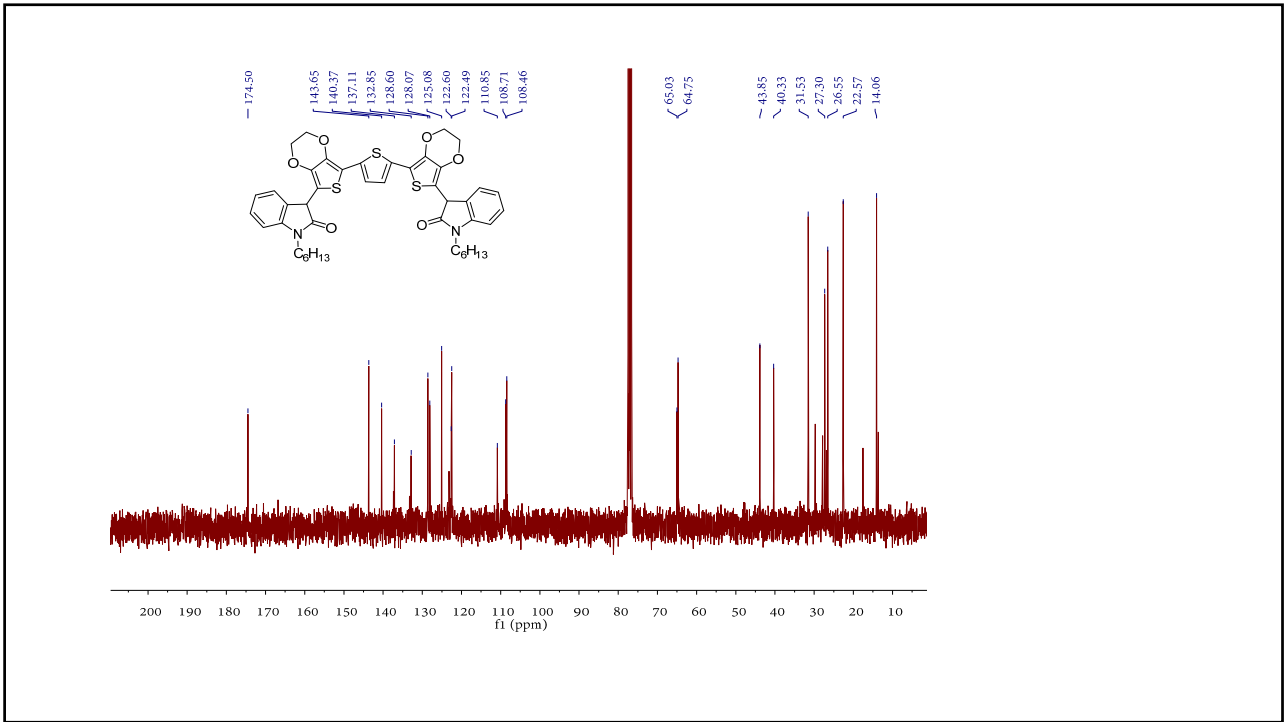


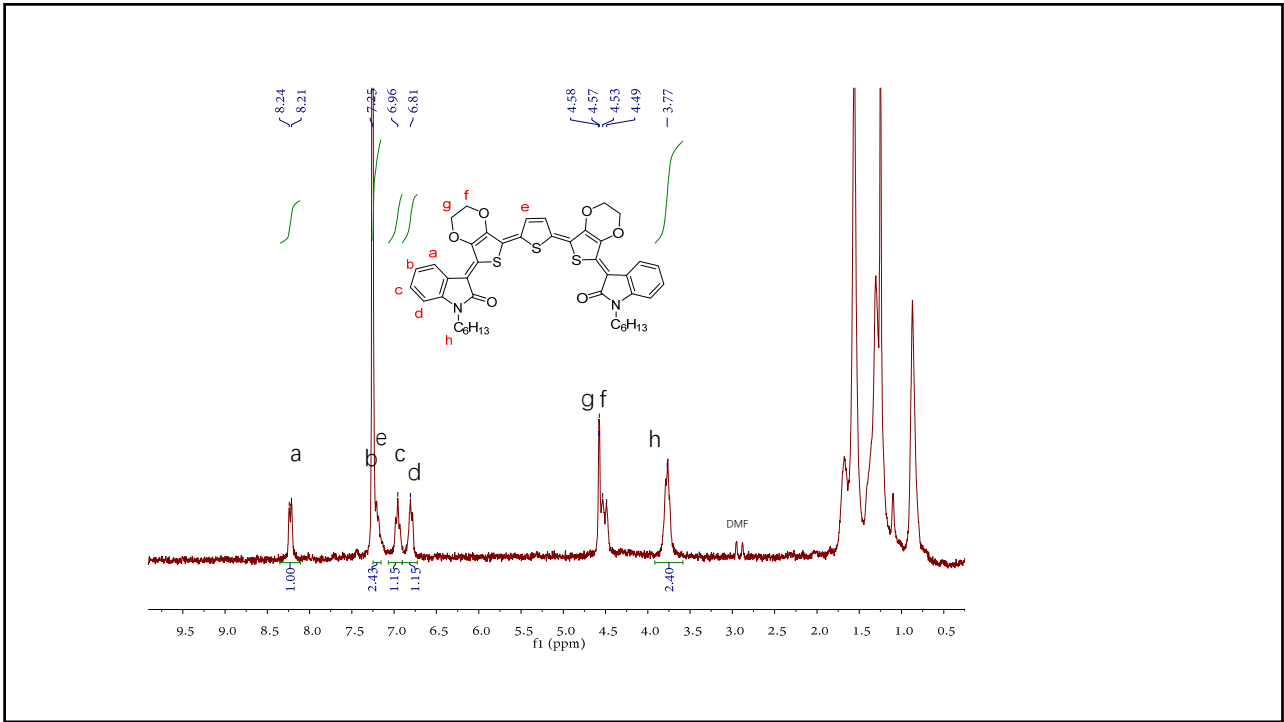
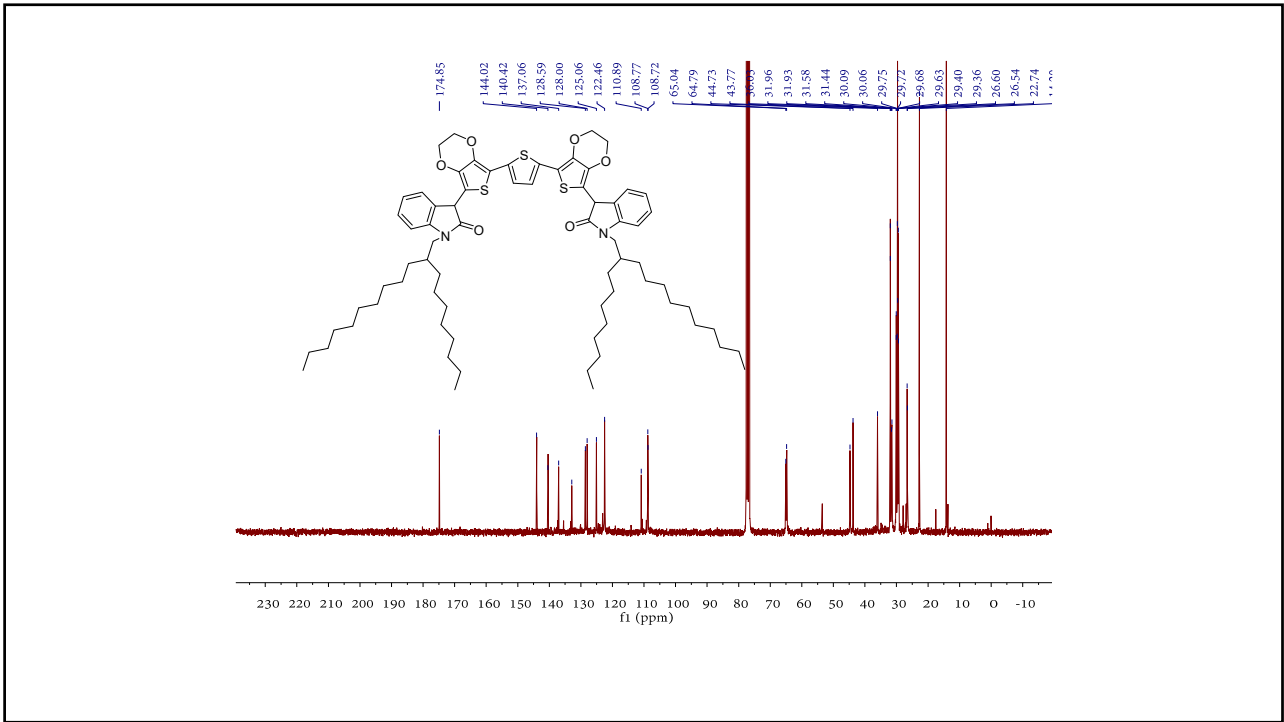


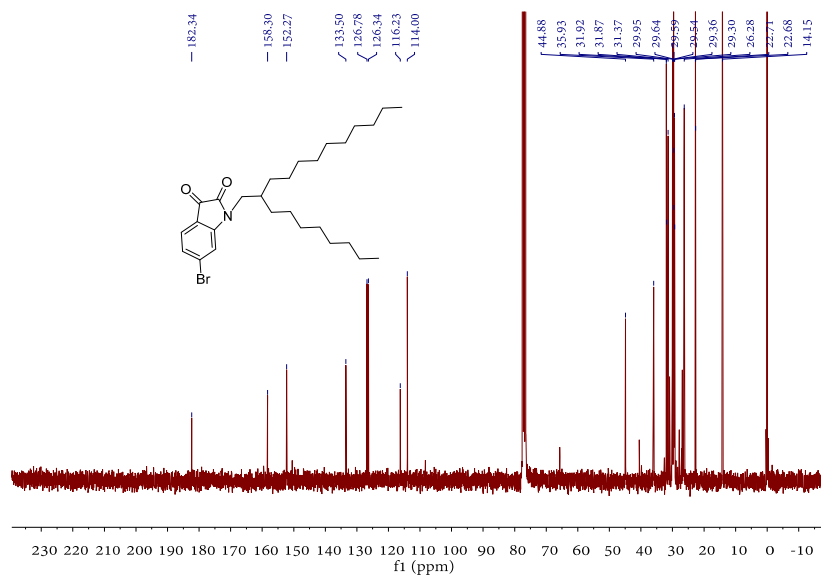
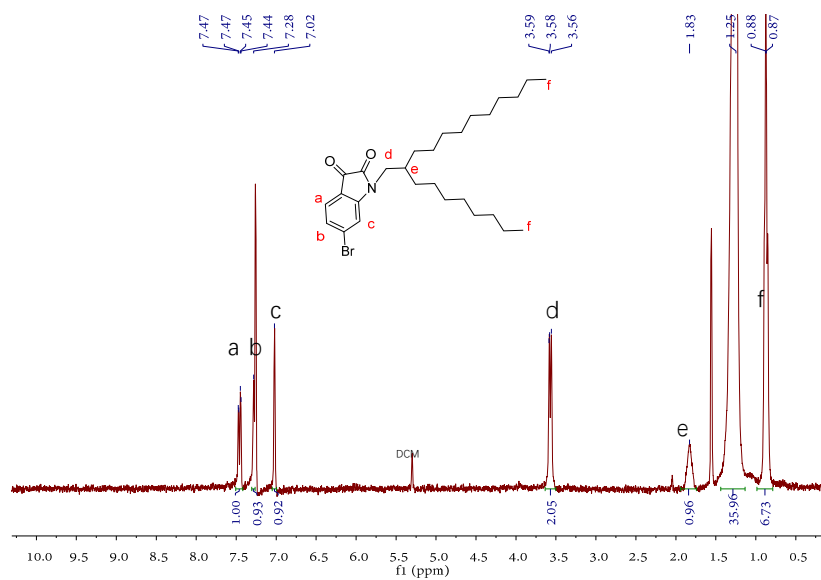


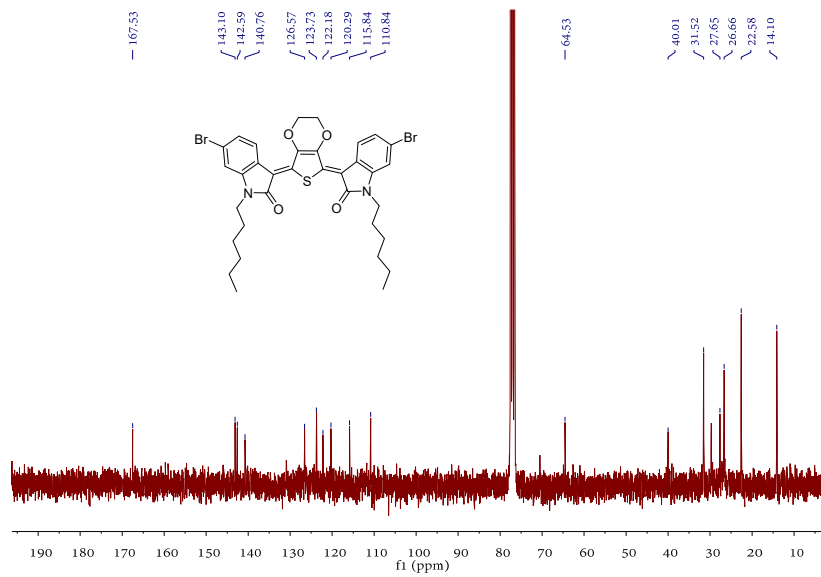
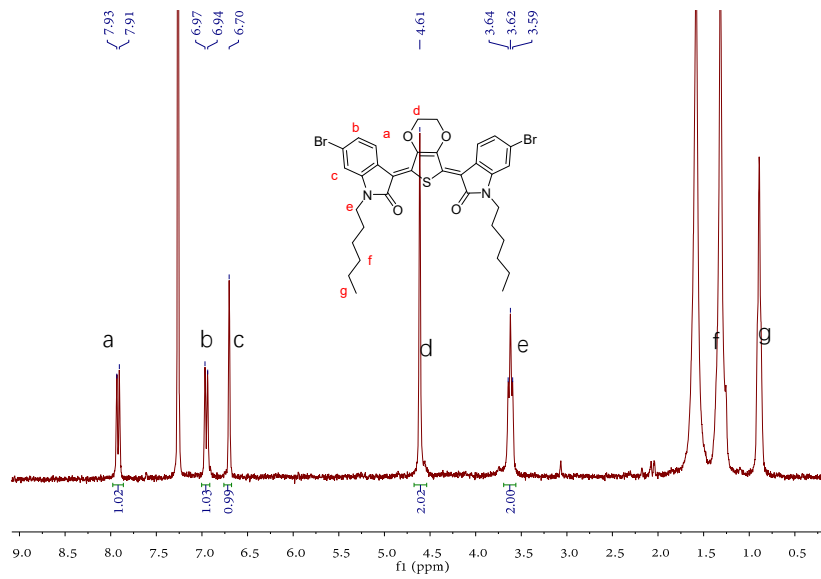


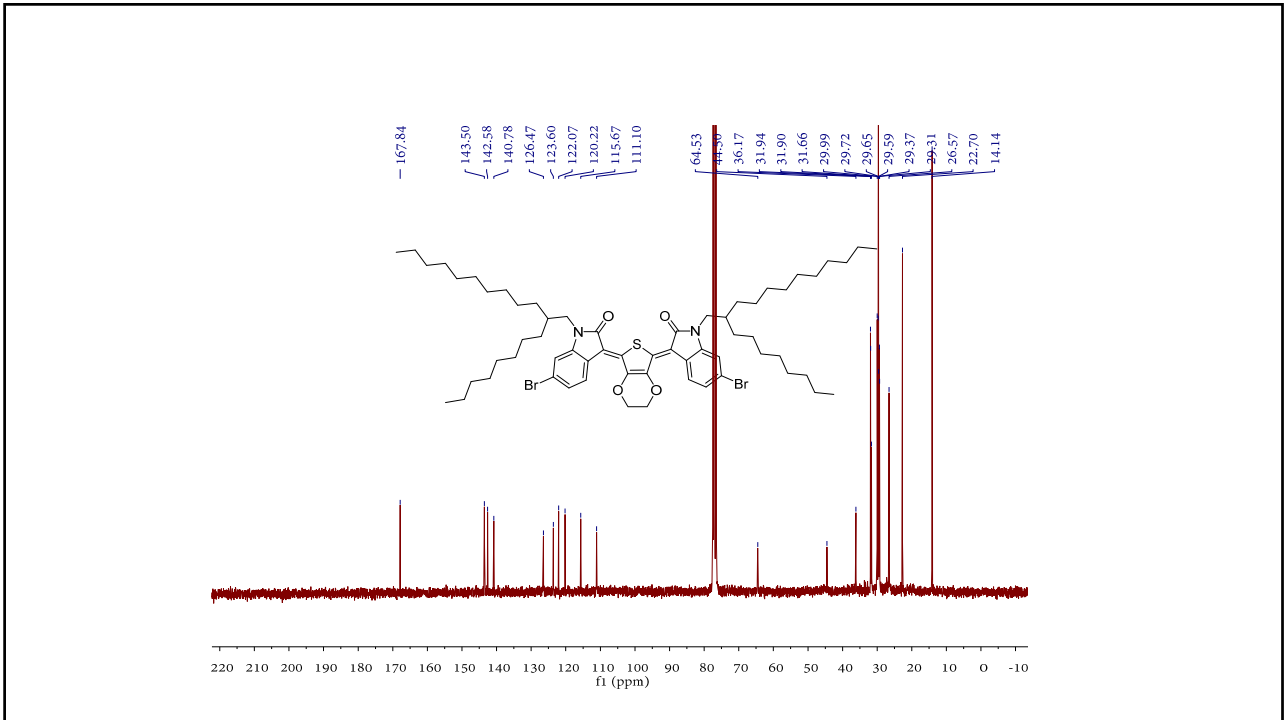
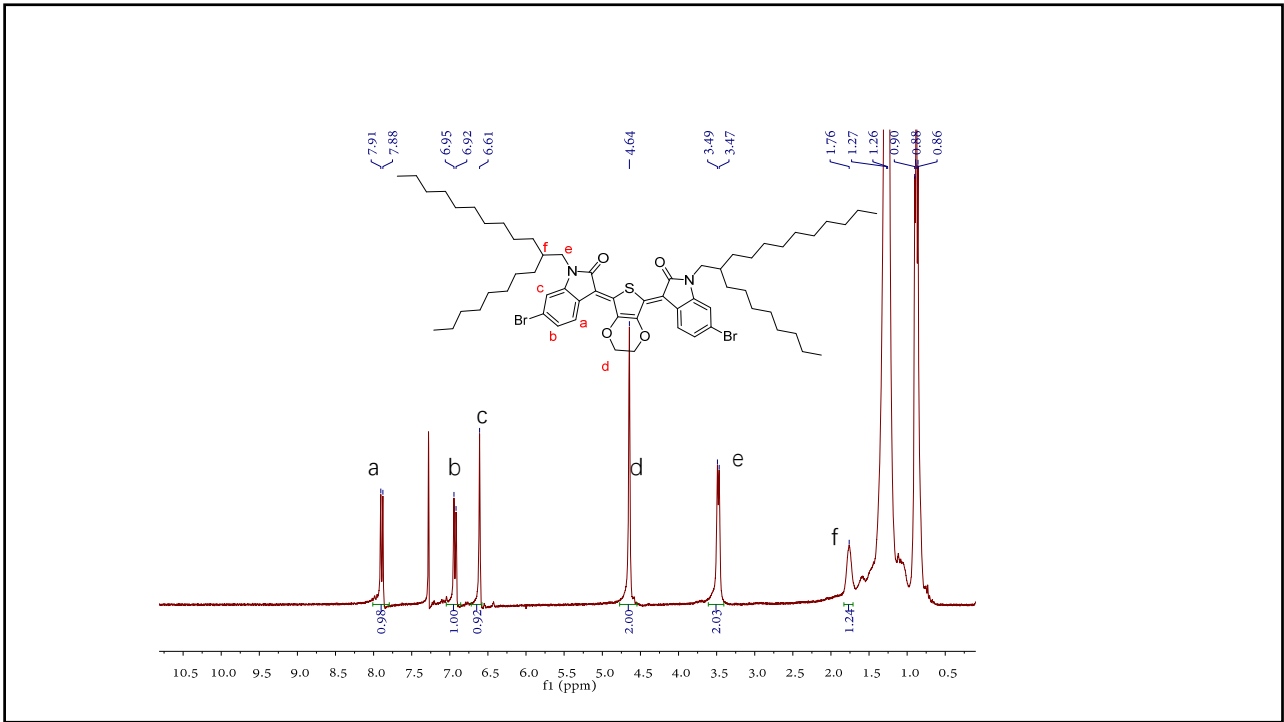


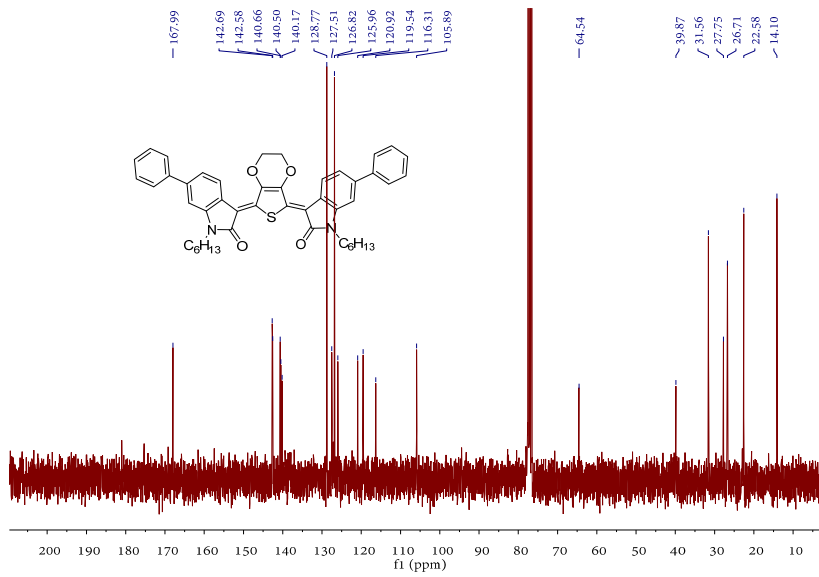
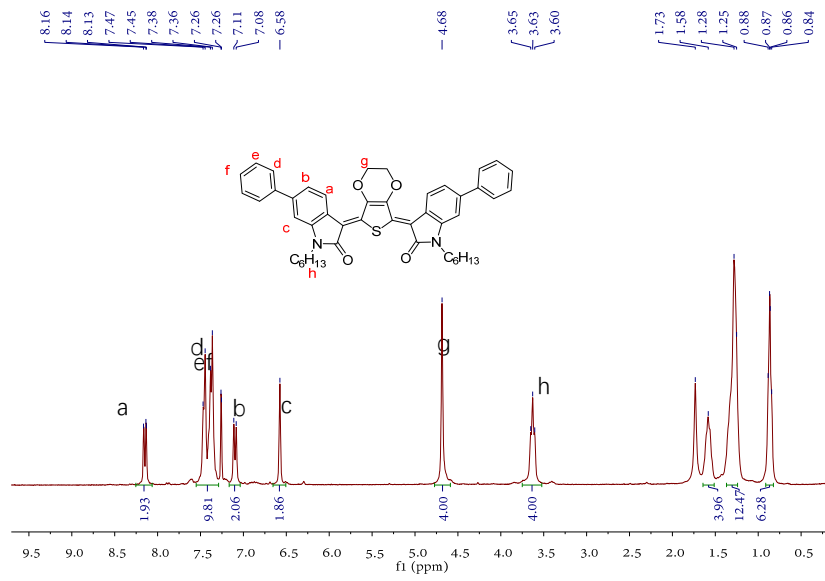


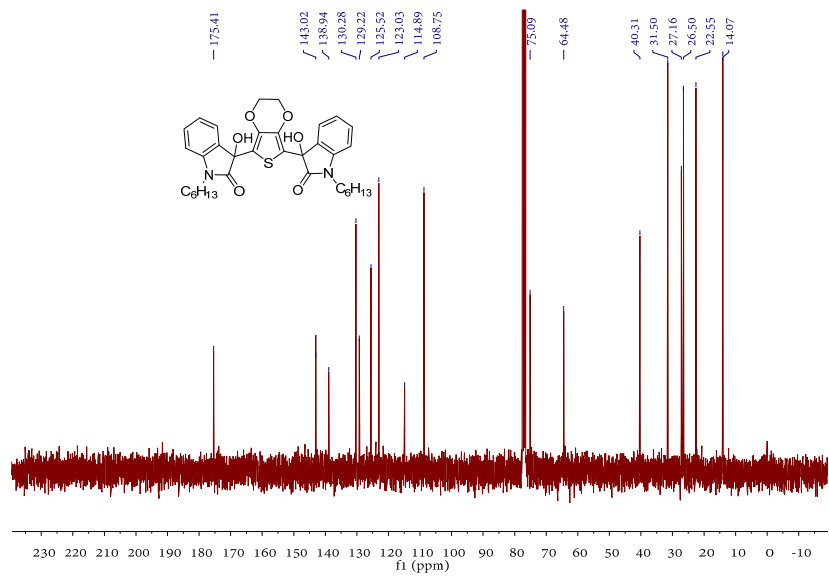
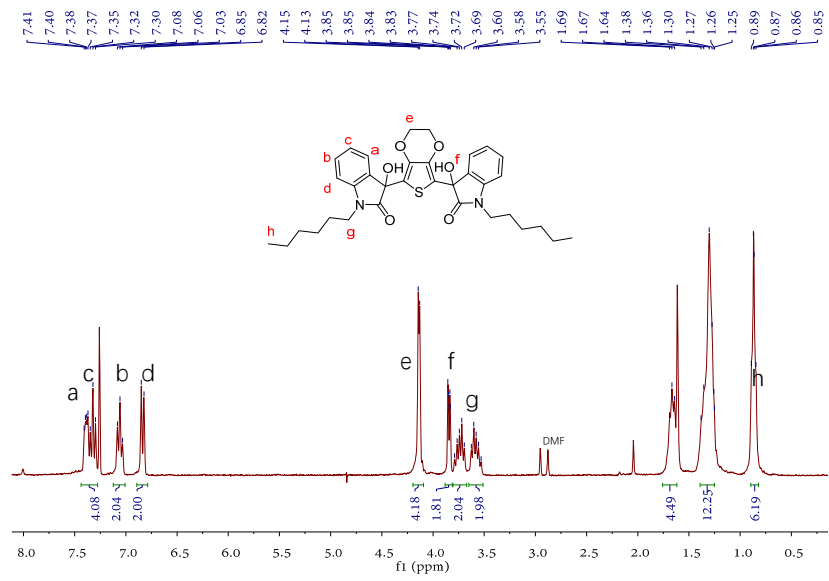


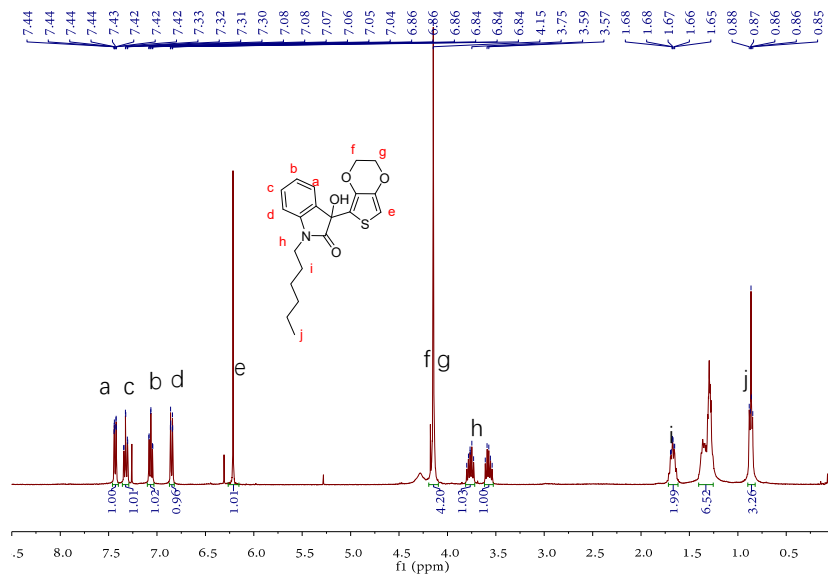
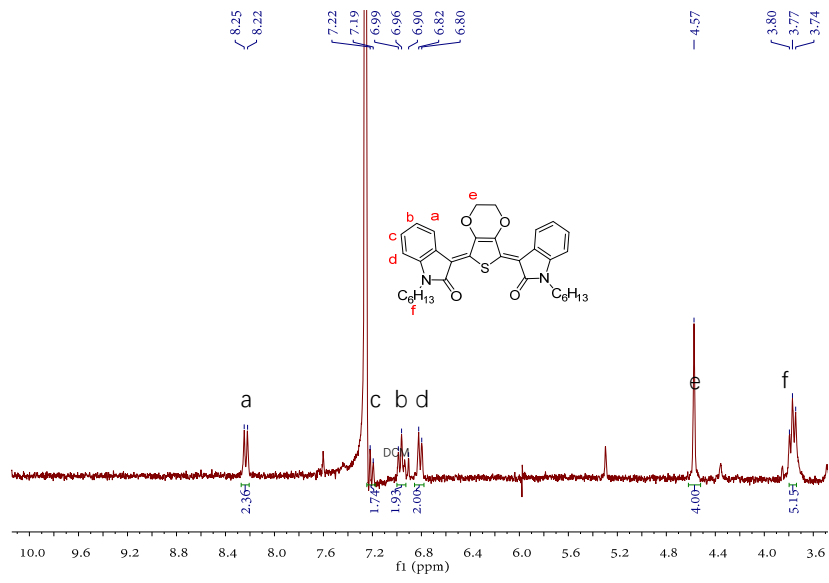


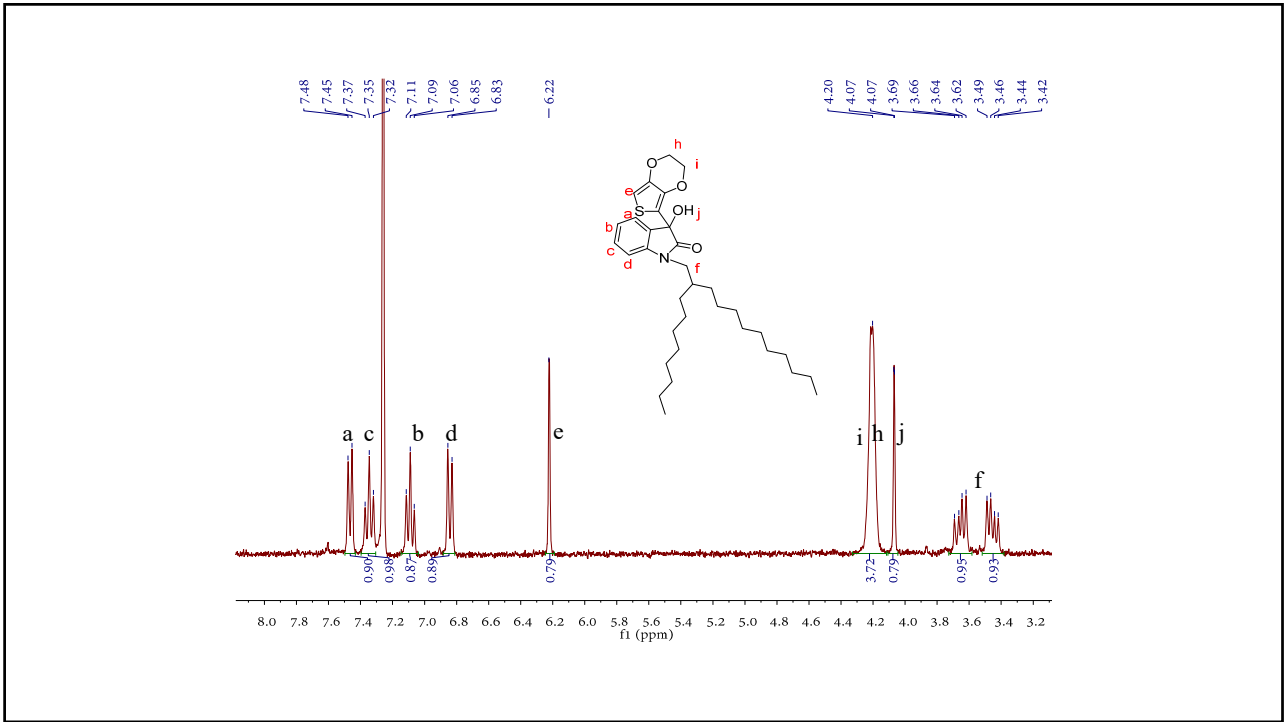
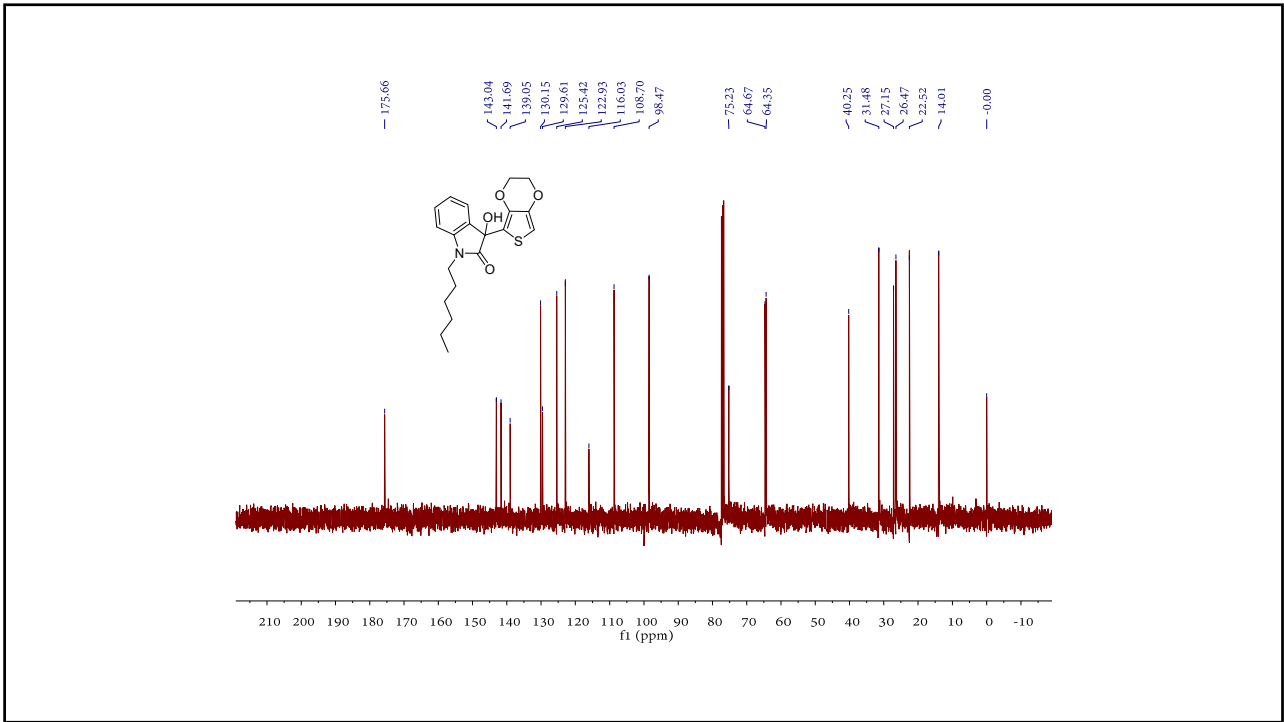


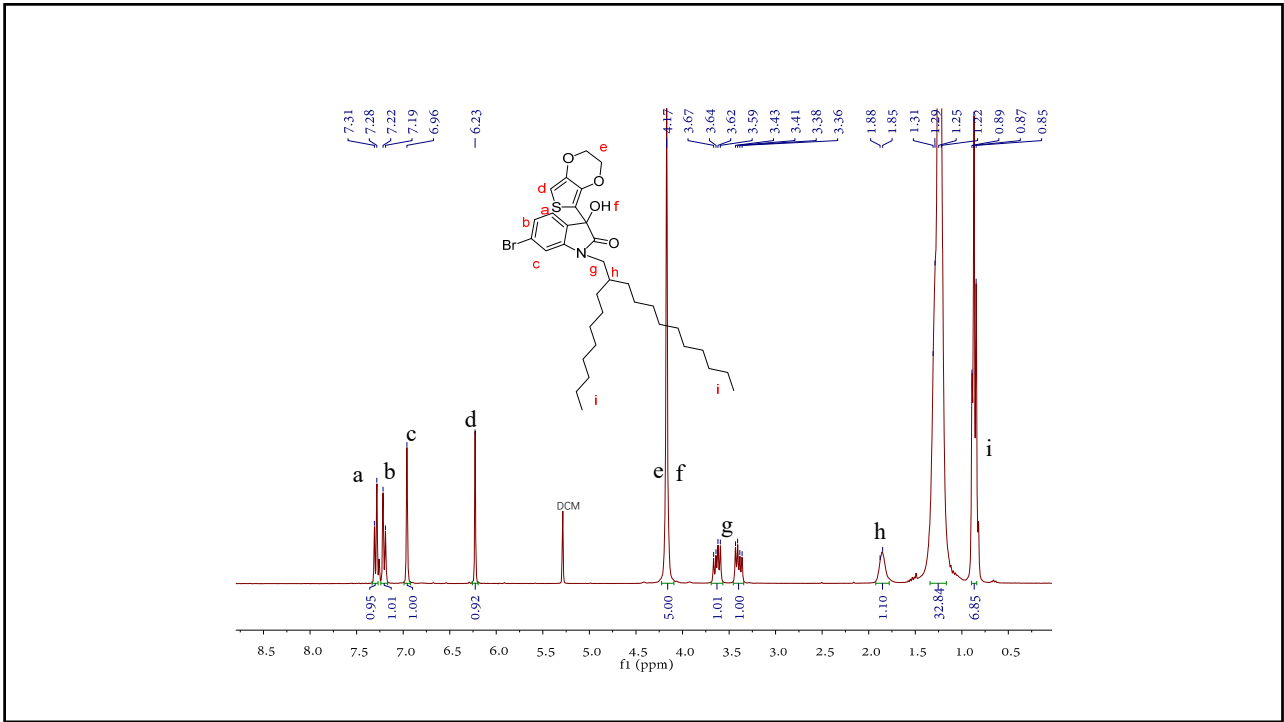
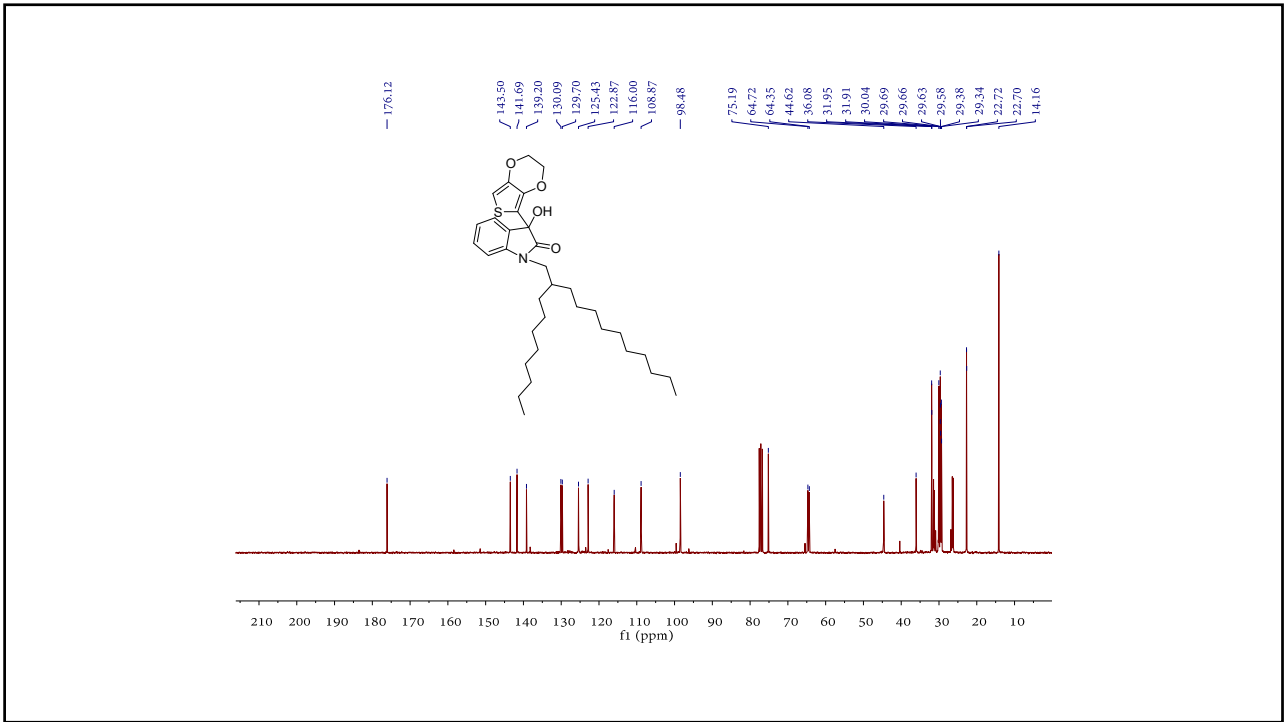


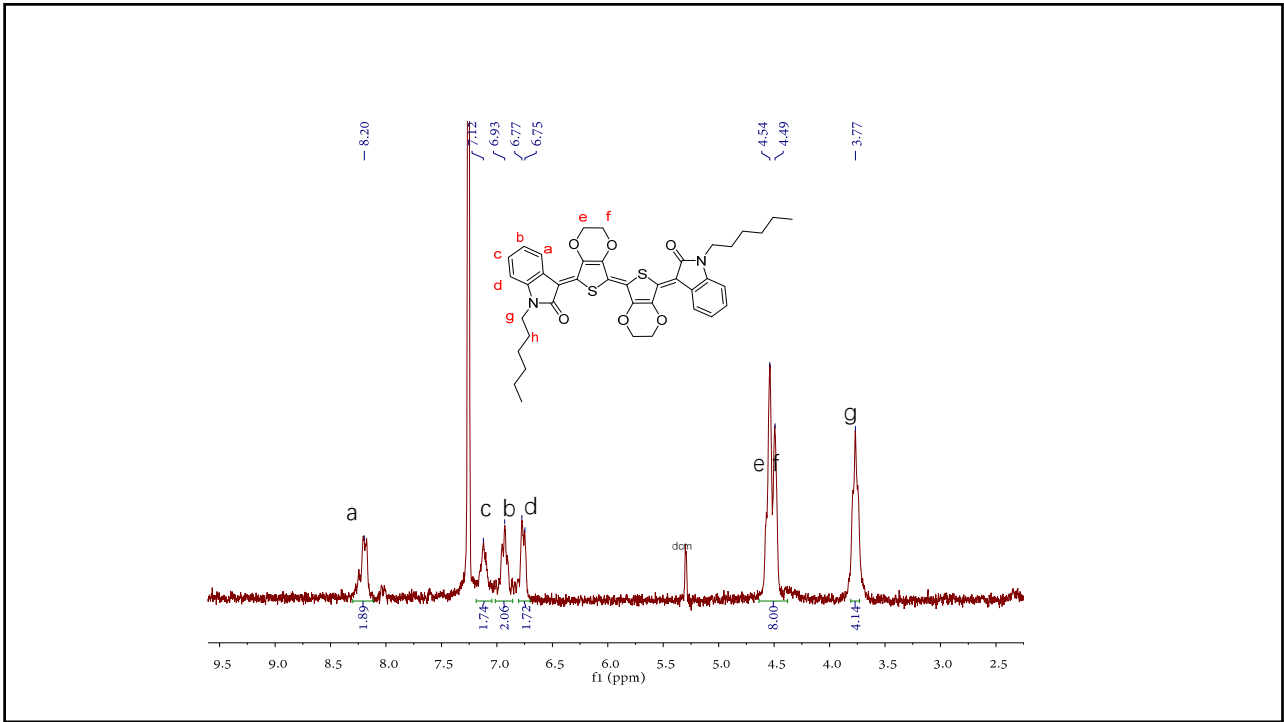
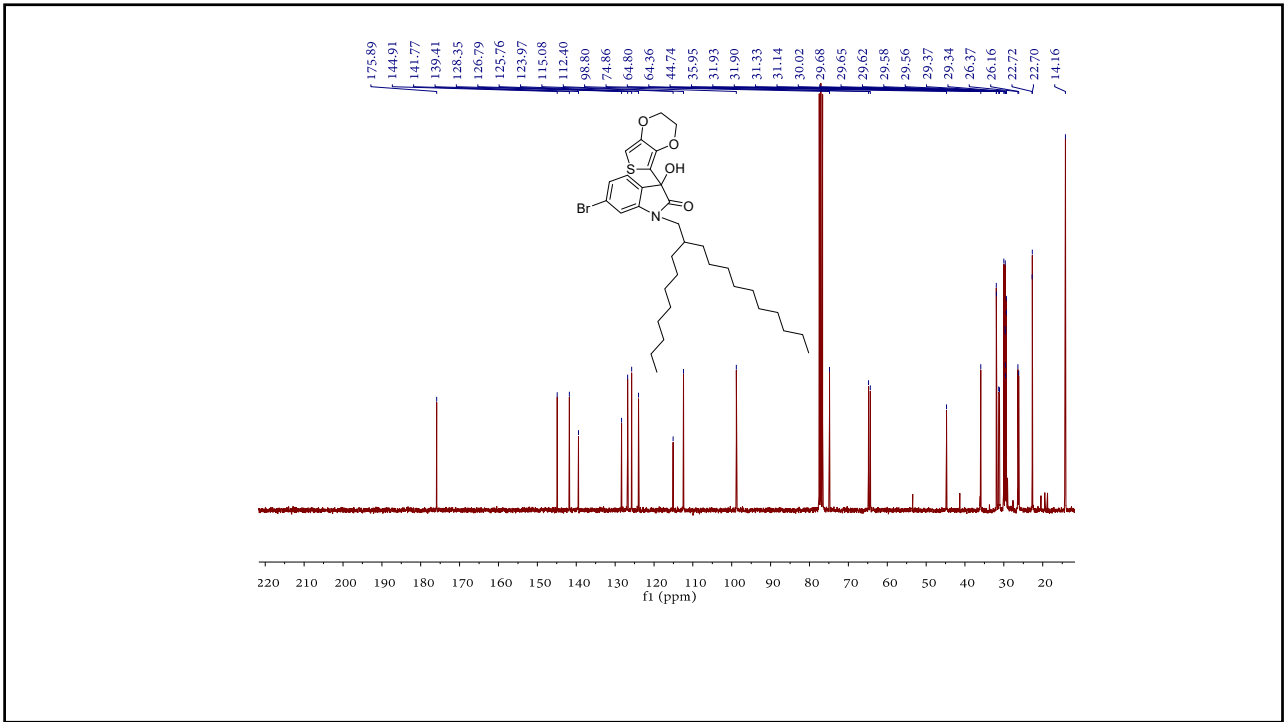


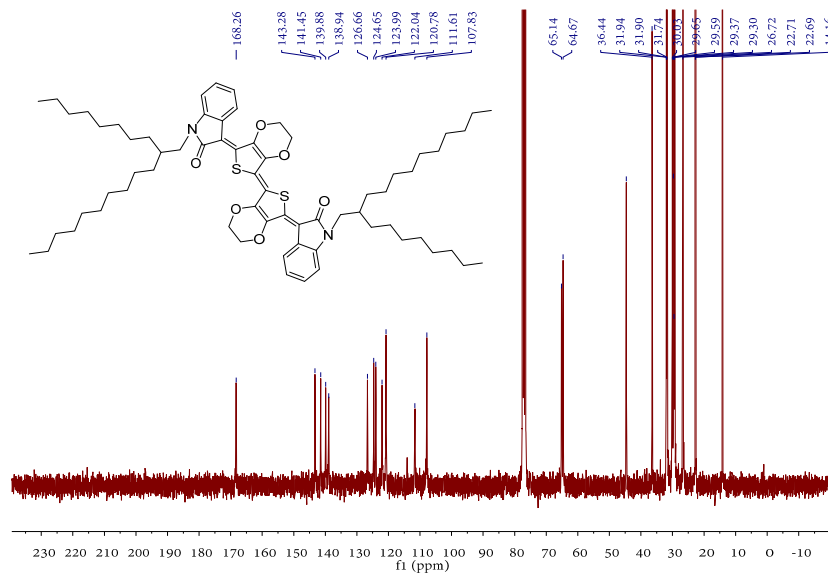
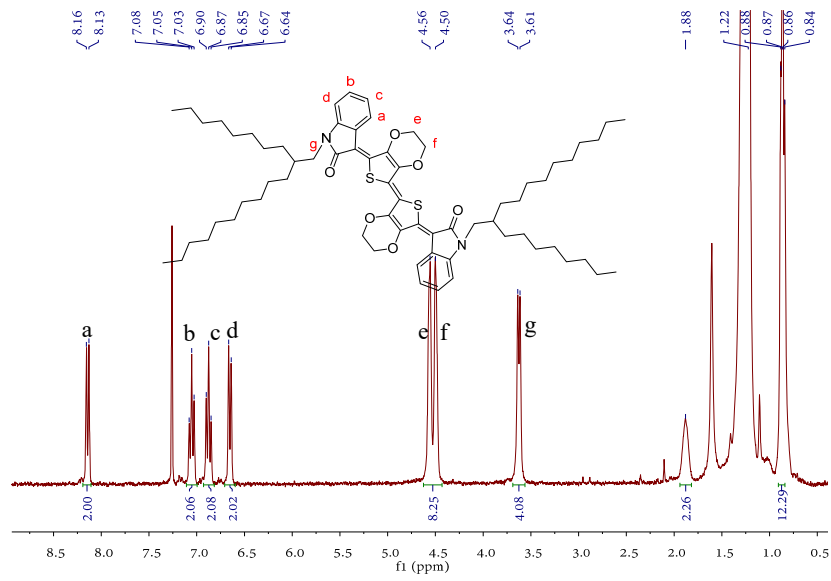


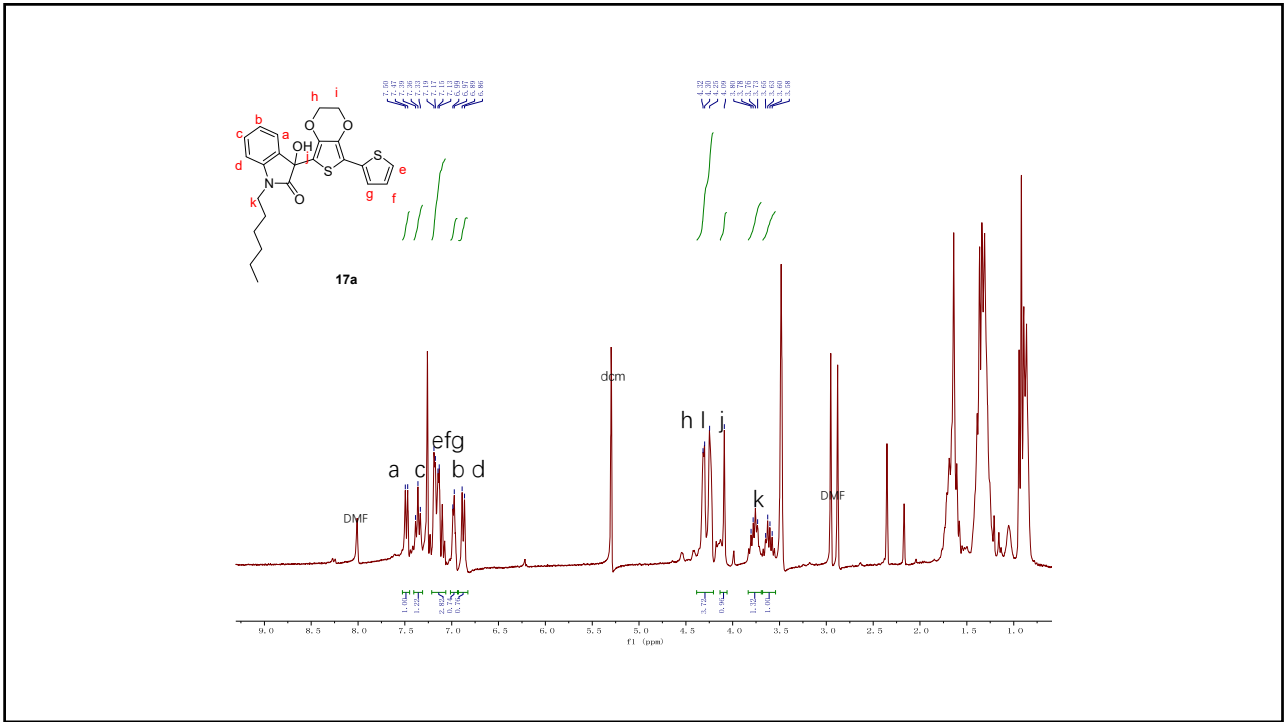
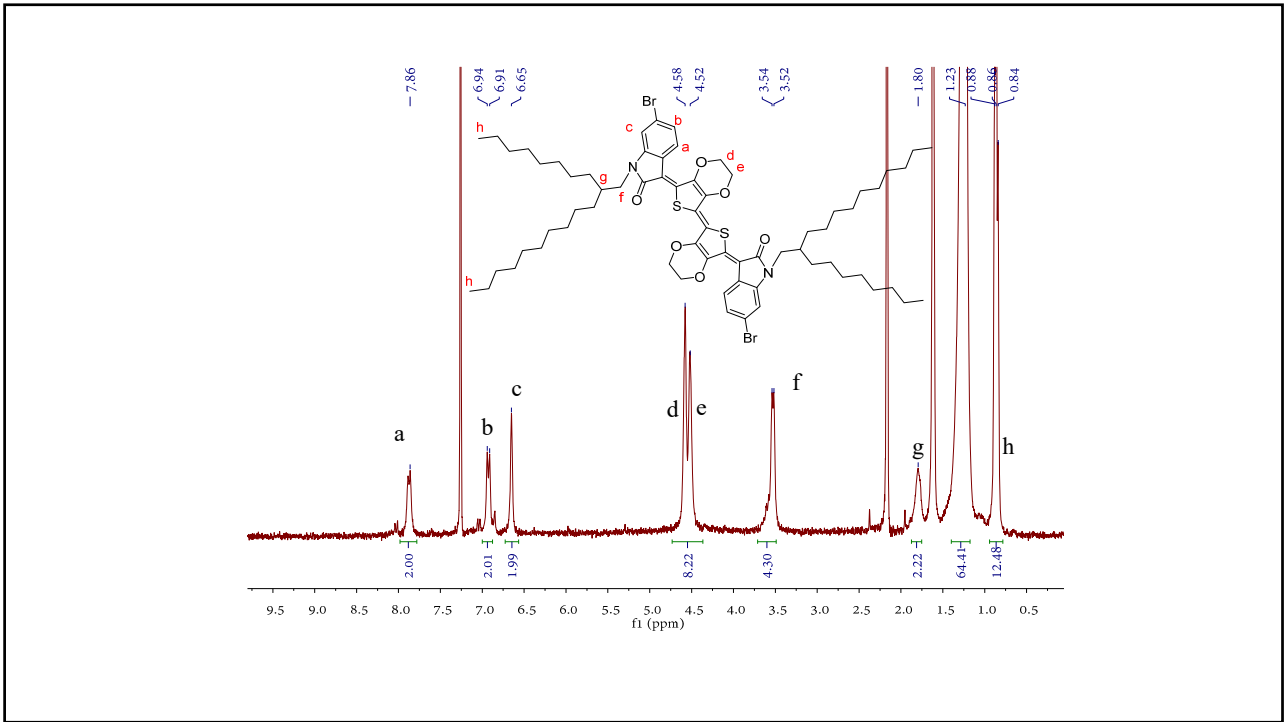


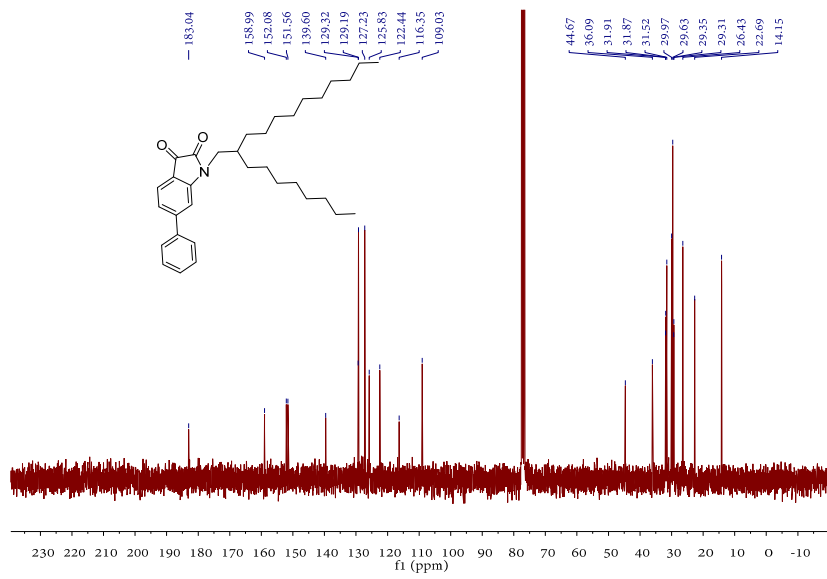
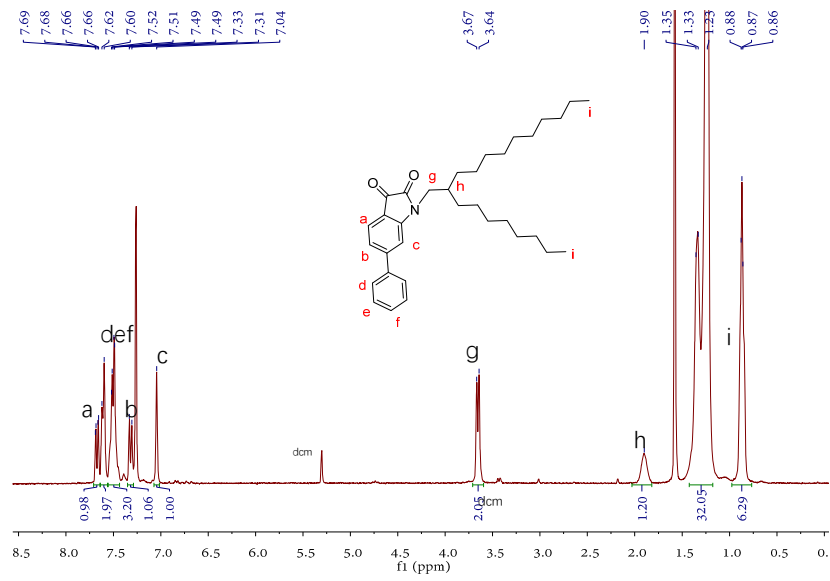


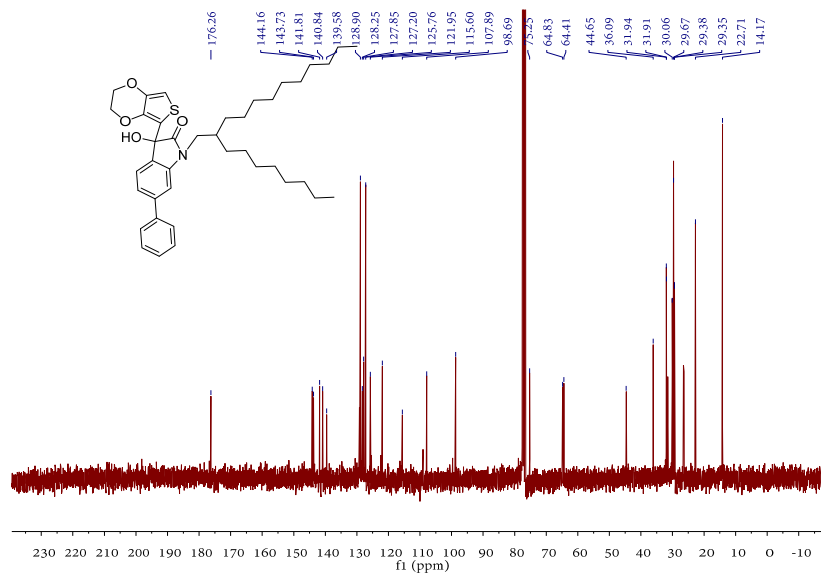
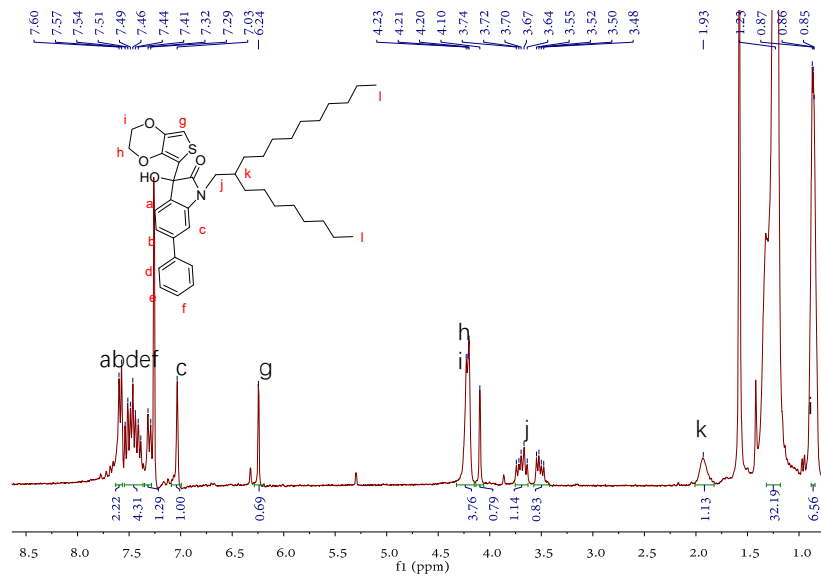


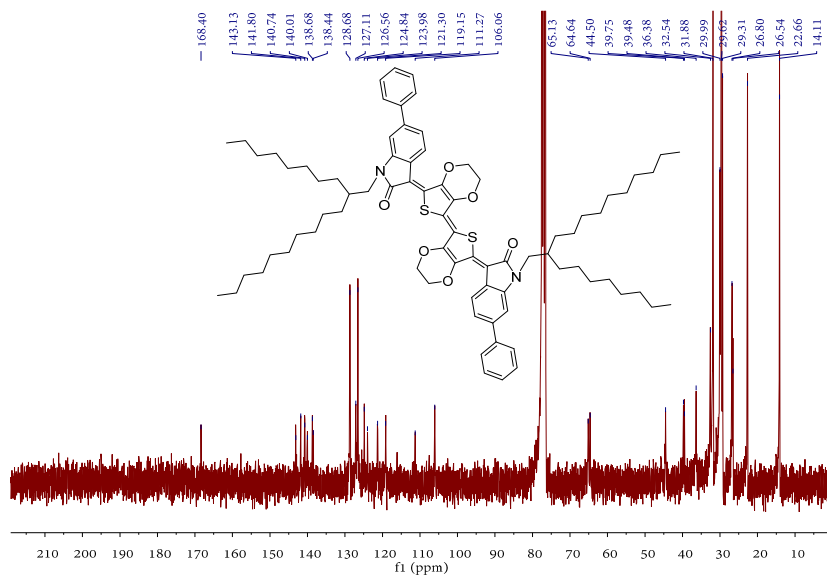
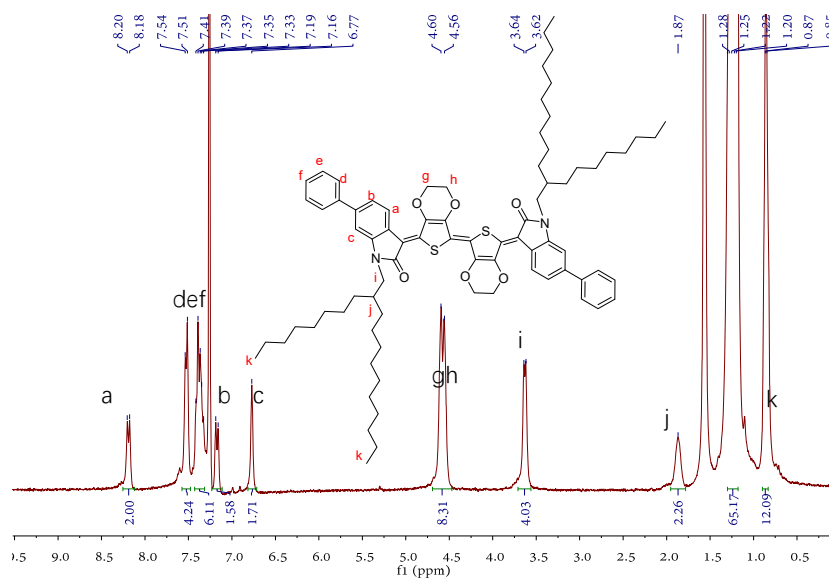


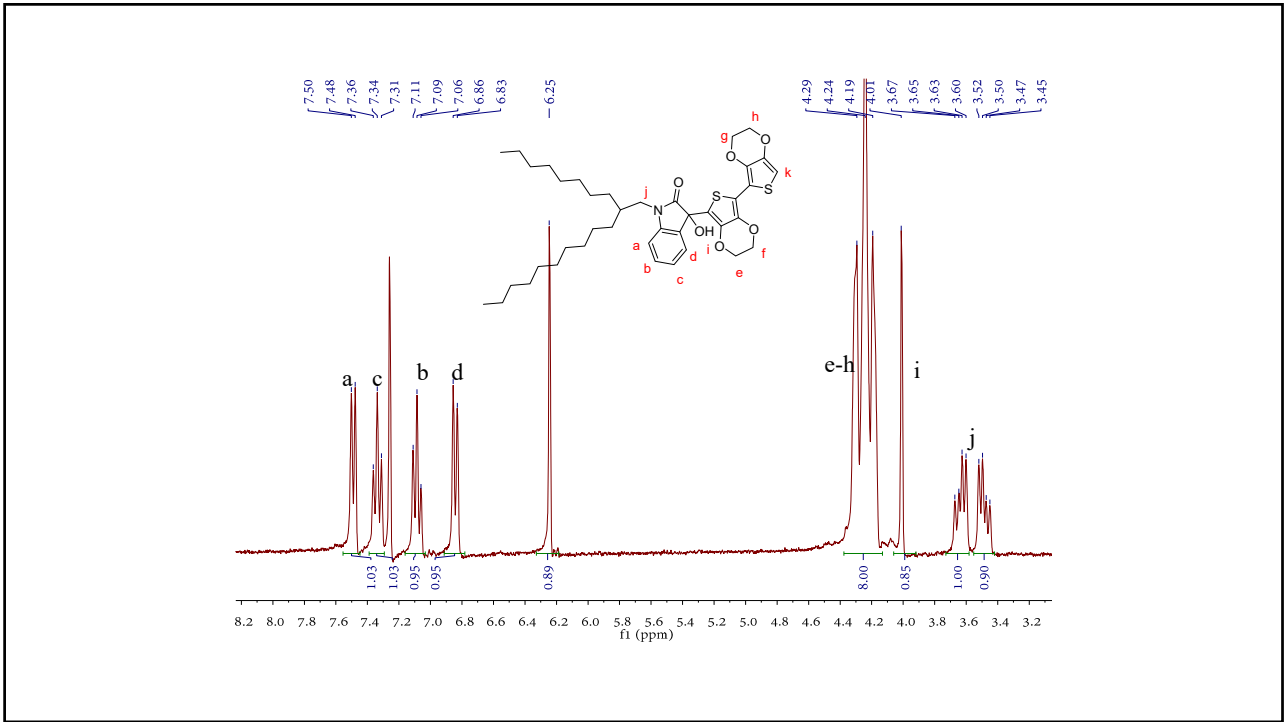
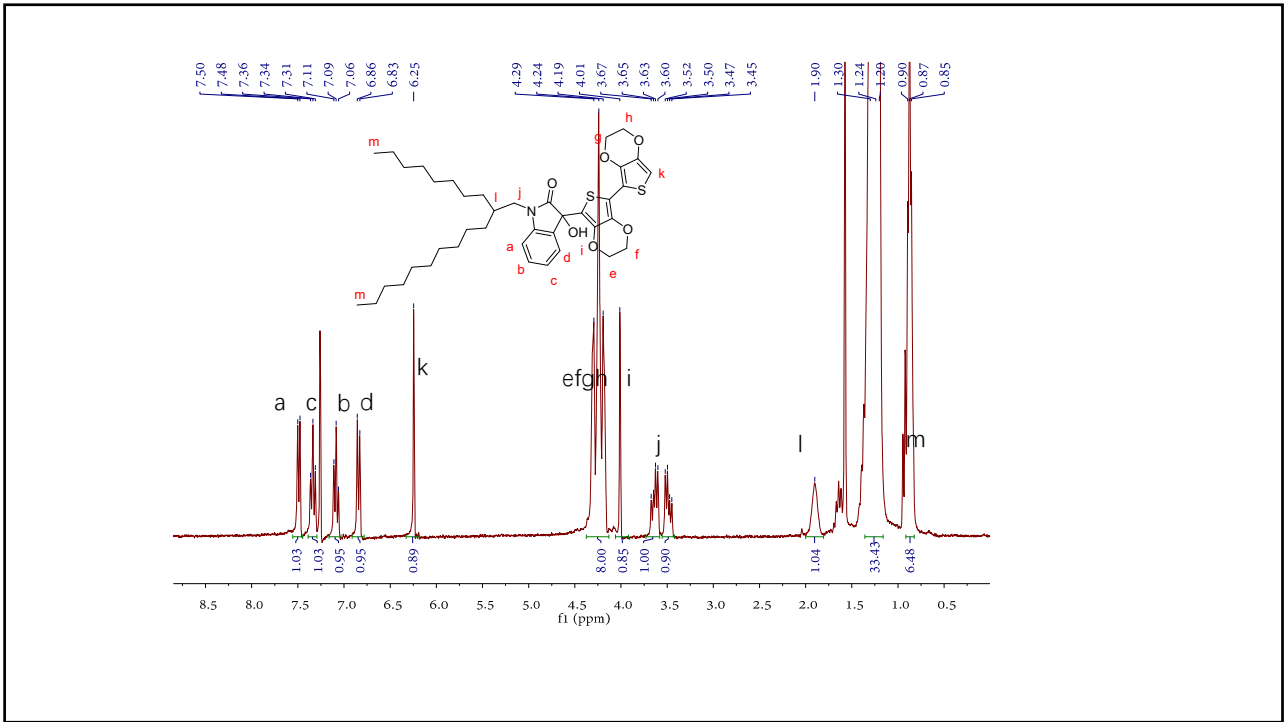


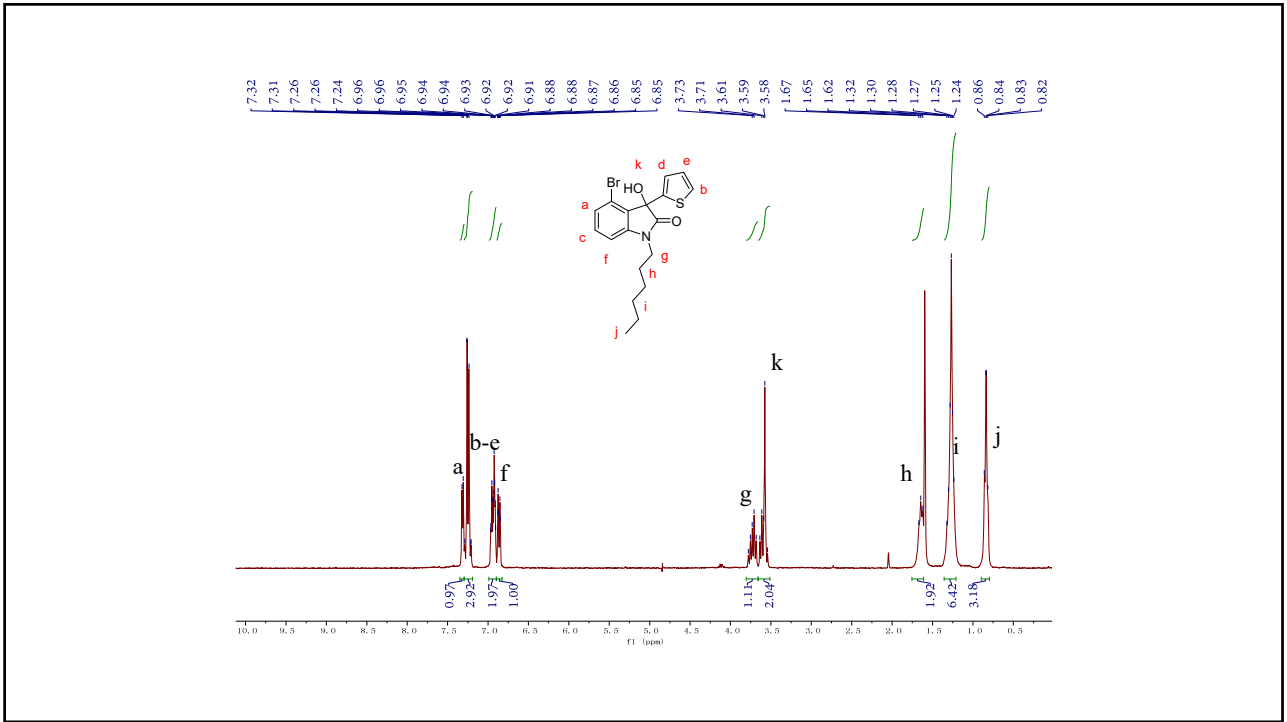
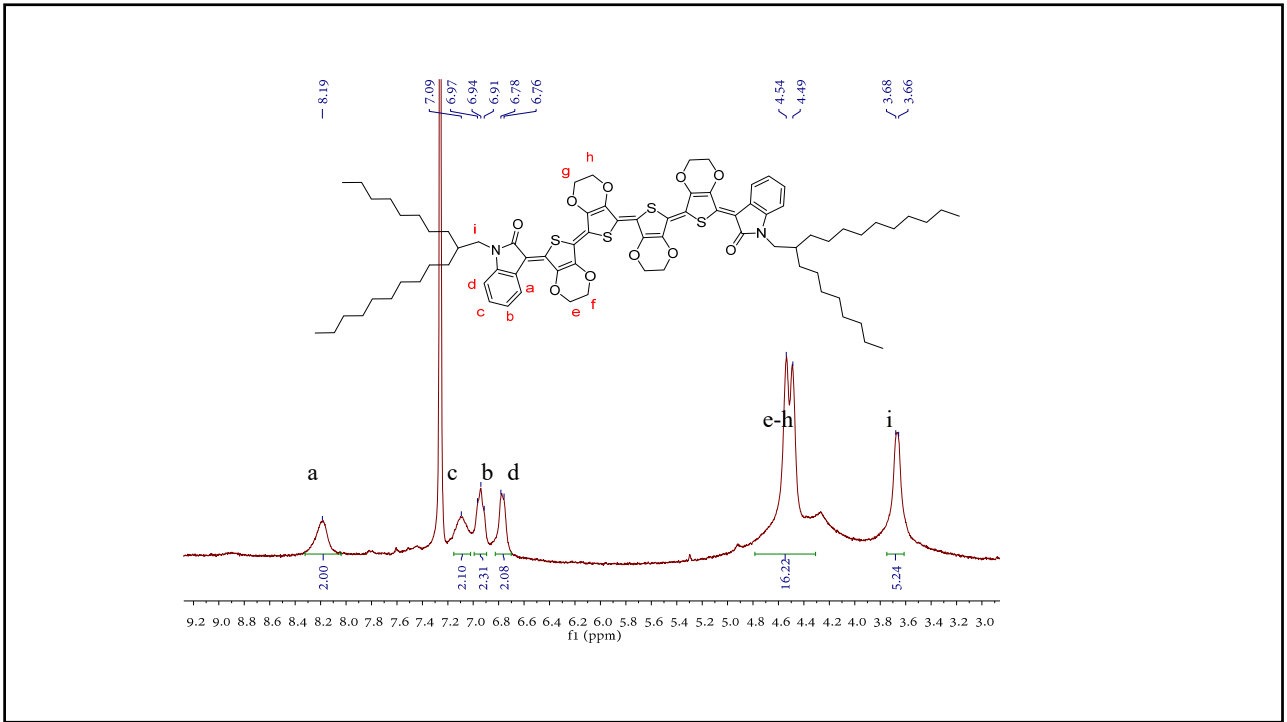


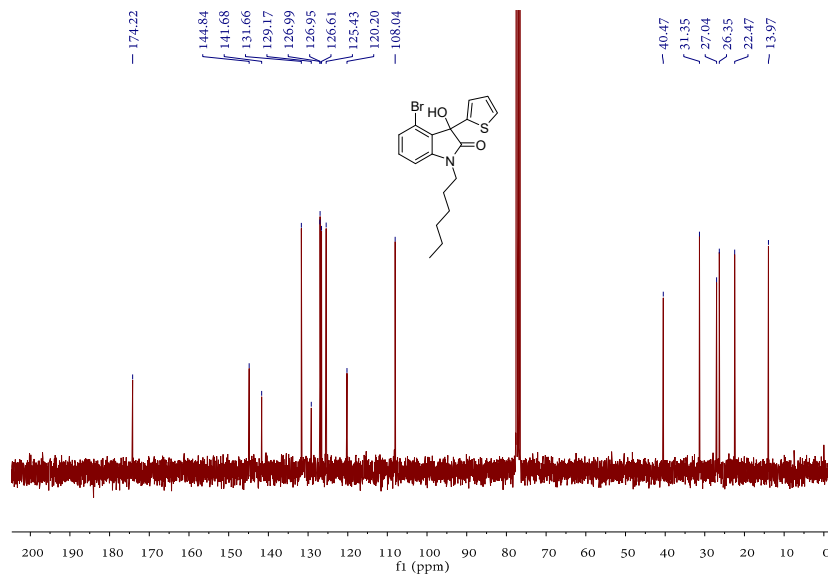




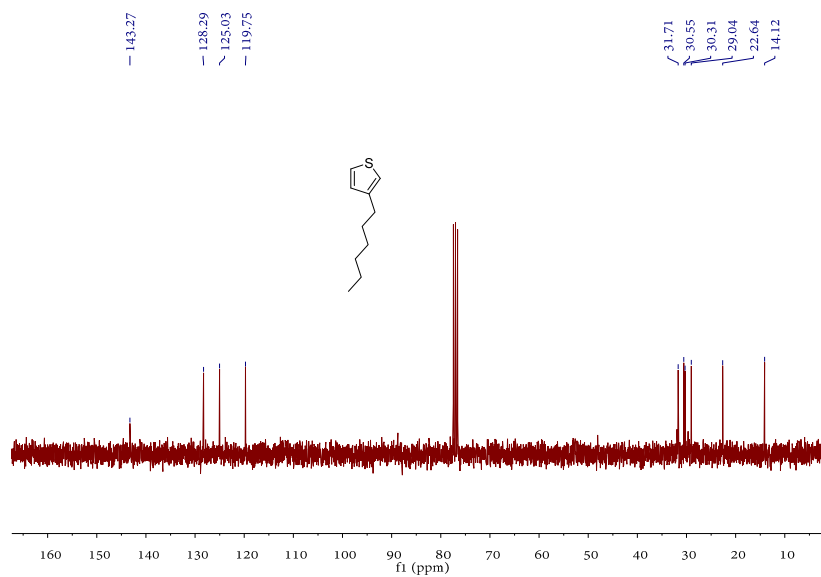
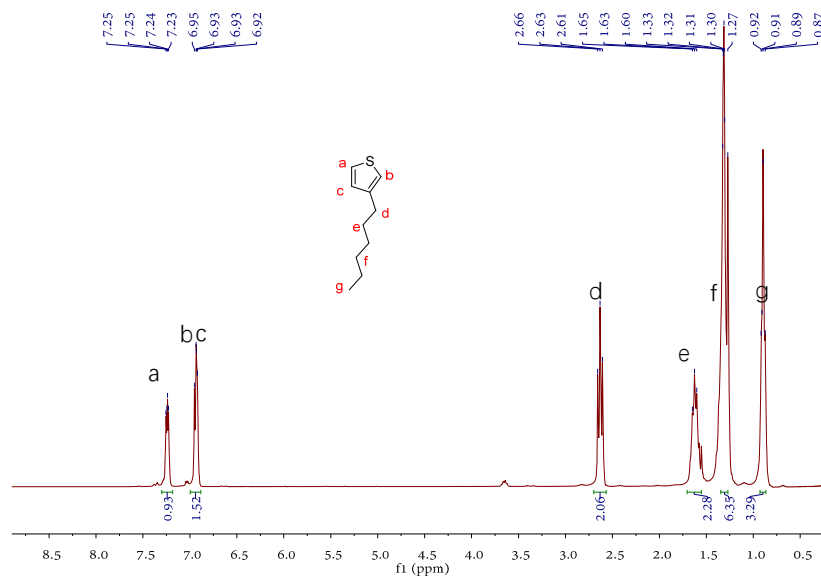


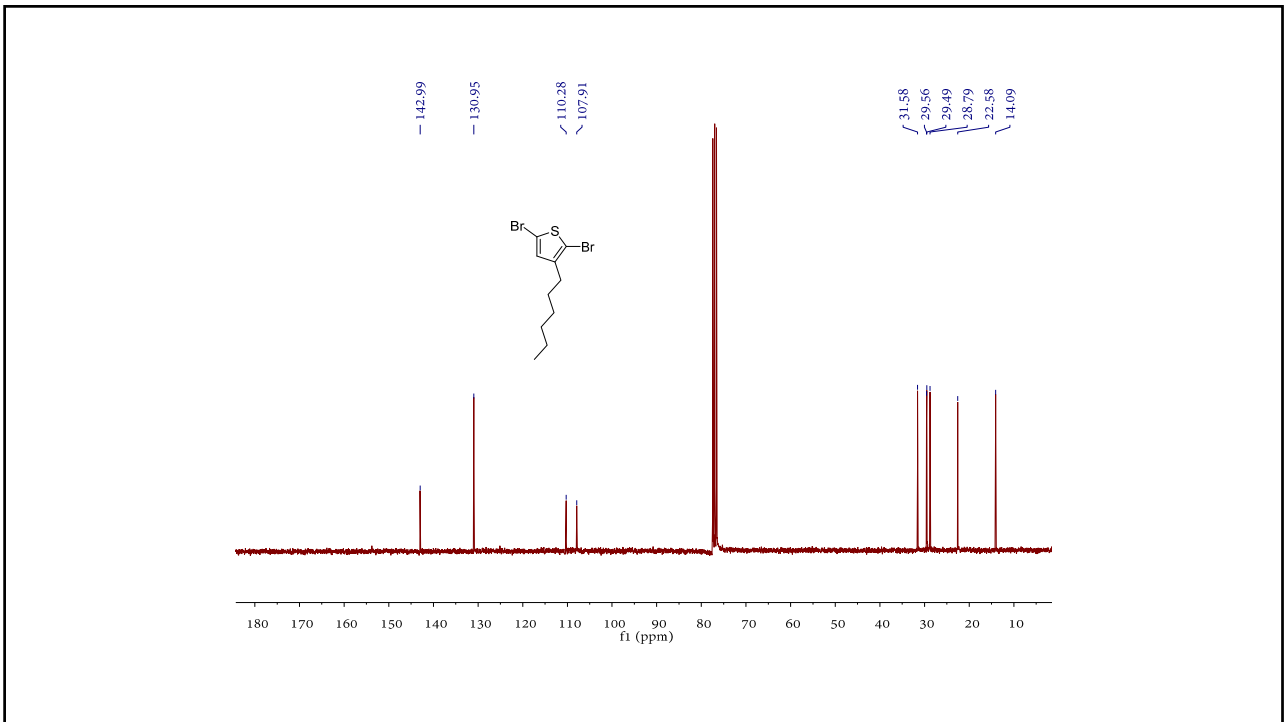
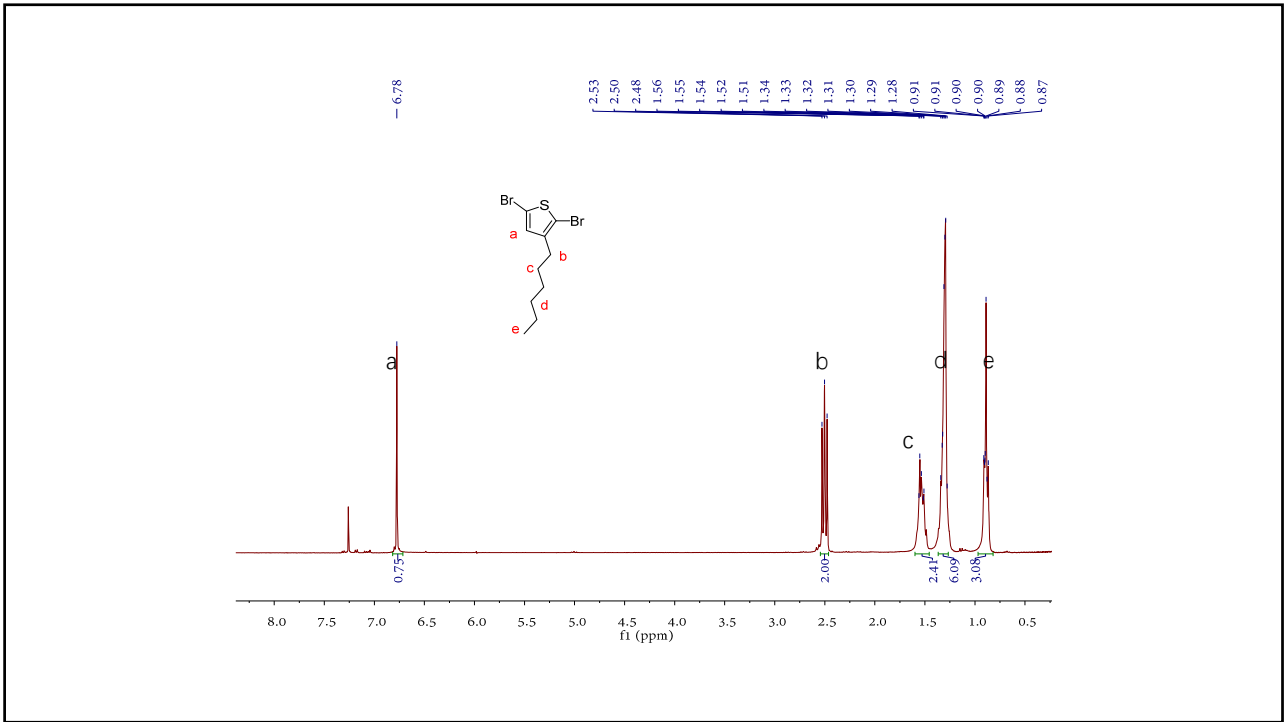


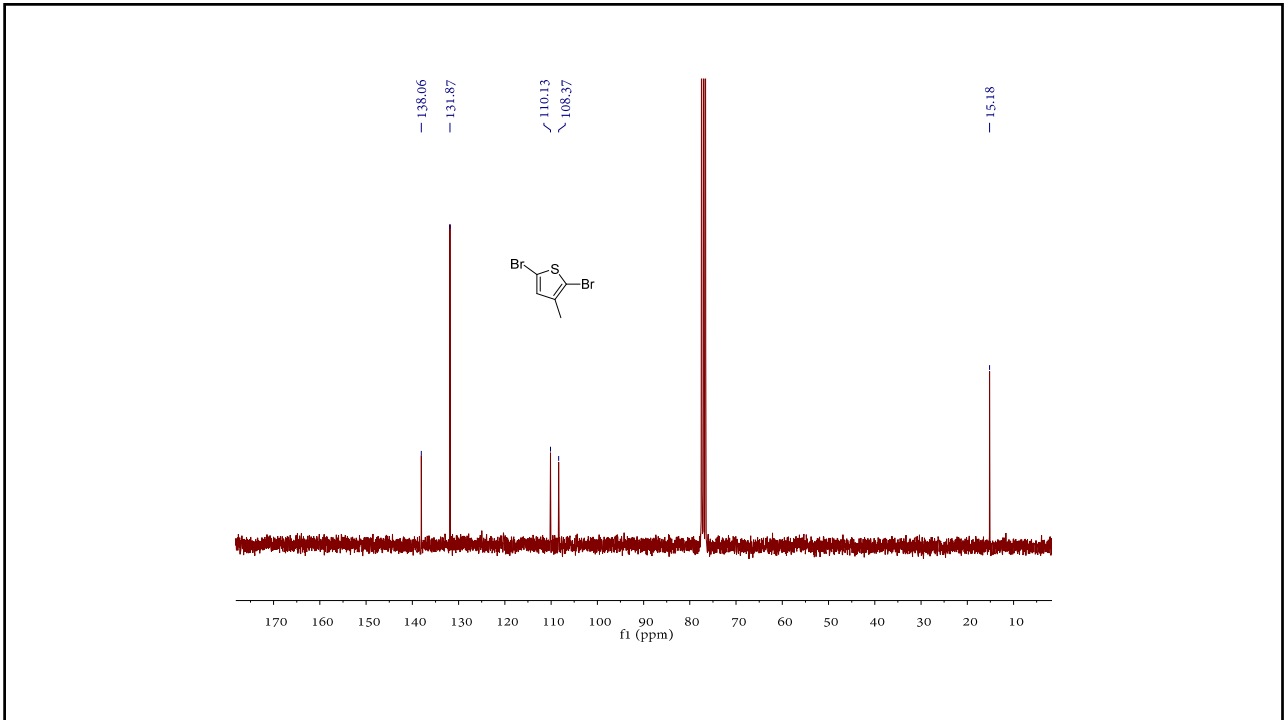
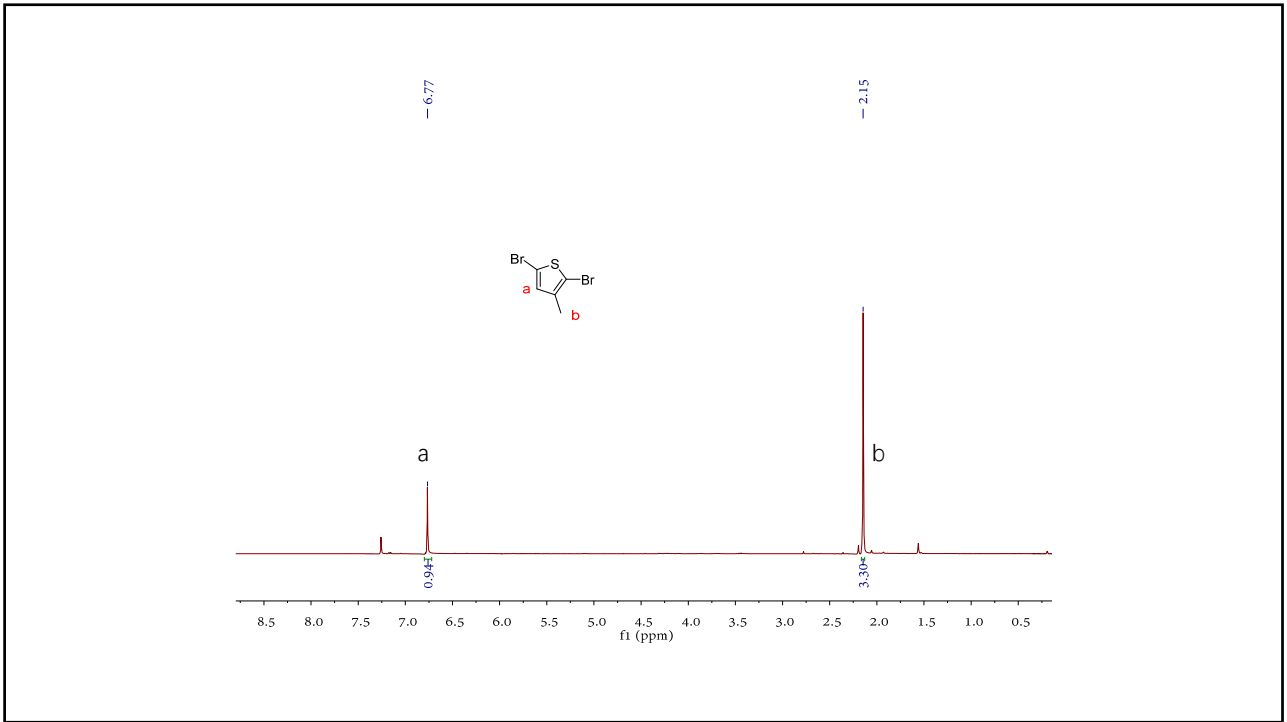


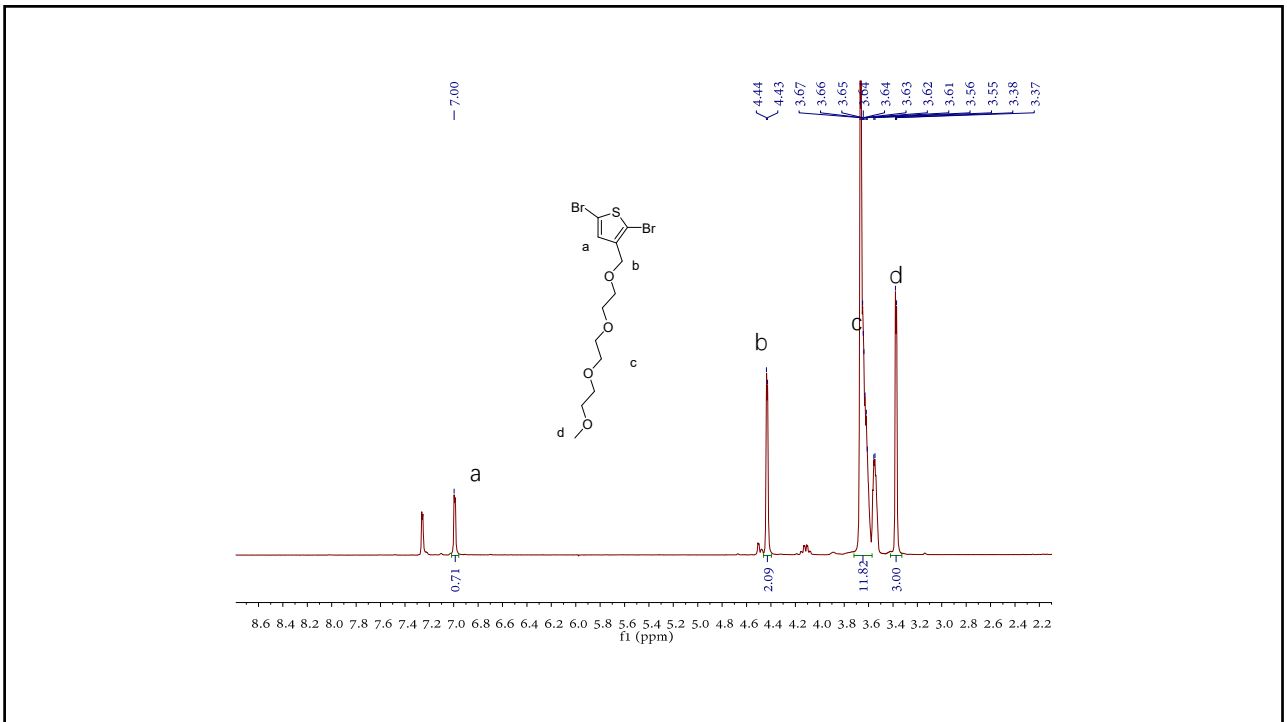
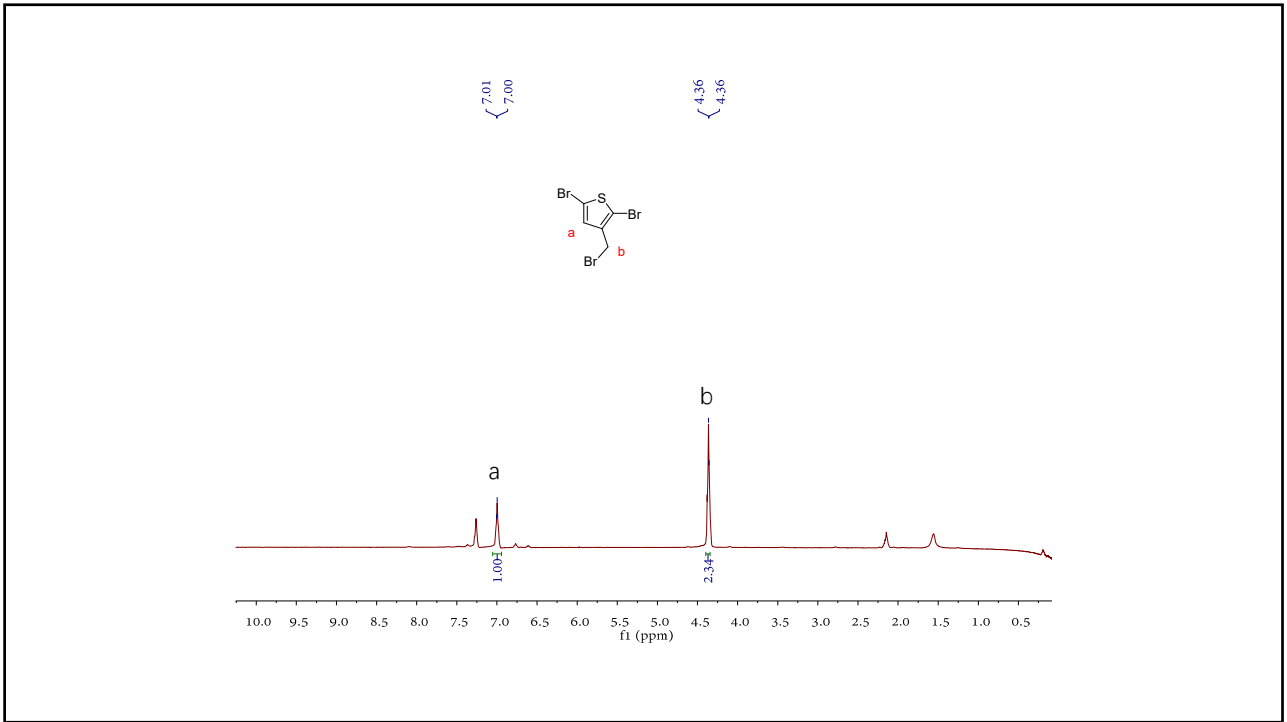


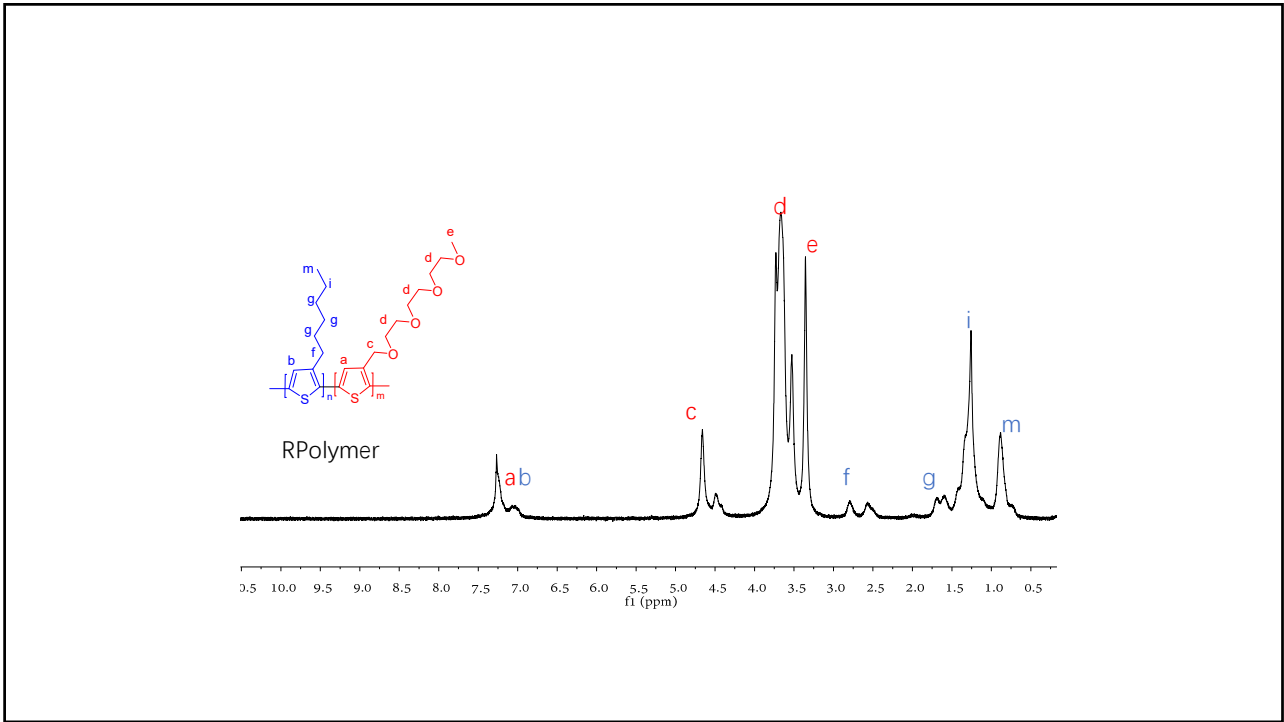
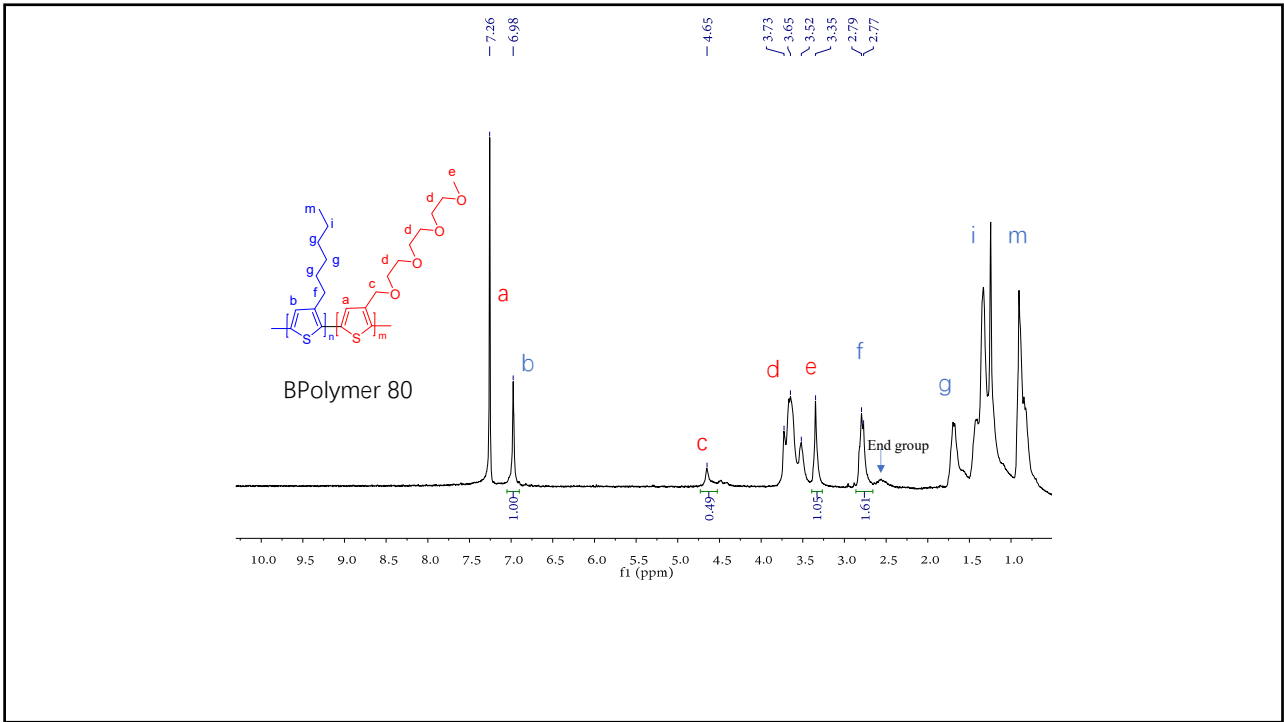
Chapter 5











Titre : synthèse de nouveaux semi-conducteurs organiques π -conjugués fonctionnels pour des applications en optoélectroniques

Mots clés : synthèse organique; semi-conducteur organique; propriétés optoélectroniques; molécules π -conjuguées.

Résumé : L'électronique organique est un domaine en plein essor, à l'interface de l'électronique, de la physique de la matière condensée, de la physico-chimie, et de la chimie organique. La découverte et le développement de nouveaux semi-conducteurs organiques ouvrent de nouvelles perspectives tant en sciences fondamentales qu'en termes d'applications.

Ce travail de thèse décrit la synthèse, l'étude physico-chimique et les propriétés optoélectroniques d'une série de nouvelles molécules π -conjuguées ayant la structure donneur-accepteur. Les variations structurales ont porté sur le groupement accepteur et le système π -conjugué. Les propriétés optiques et électrochimiques de ces nouvelles molécules ont été étudiées et ont permis d'établir quelques liens entre les énergies des orbitales frontières et certaines modifications structurales.

Title : synthesis of novel π -conjugated functional organic semiconductors for optoelectronic applications

Keywords : organic synthesis; organic semiconductors; optoelectronic properties; π -conjugated molecules.

Abstract : Organic electronics is an emerging field at the interface between electronics, materials science, physics, physical chemistry, and organic chemistry. The discovery and development of new organic semiconductors opens up new perspectives both in terms of fundamental science as well as their potential application in large area electronics.

This thesis describes the synthesis, physico-chemical studies and optoelectronic properties of a series of new π -conjugated molecules with donor-acceptor architecture. The structural variations have focused on the acceptor group and the π -conjugated system. The optical and electrochemical properties of these new molecules have been studied and analyzed to establish a correlation between molecular structure, physicochemical properties, molecular orbital energies and structural modifications.